Soft Volume Simulation using a Deformable Surface Model

by

Sylvester Arnab

A thesis submitted in partial fulfilment of the requirements for the degree of Doctor of Philosophy in Engineering

University of Warwick, School of Engineering

March 2009

In Loving Memory

of

Sama', Sumbu' Kadik and Sumbu' Katug

Table of Contents

List of Figures

List of Tables

Acknowledgements

I would like to acknowledge the following people for their direct and indirect contribution towards the completion of my doctorate research.

- Professor Vinesh Raja for his support and encouragement as my supervisor,
- Universiti Malaysia Sarawak (UNIMAS), The Malaysian Public Service Department (JPA) and the High Education Commission (KPT) for the Training Award that funded me during my first three years of research,
- The examiners who made the VIVA VOCE experience insightful,
- My family for their constant encouragement and love,
- Cliff Davies for his moral support and a shoulder to lean on,
- Dr. Kevin Neailey for his advices on various issues in relation to my doctorate research,
- Mitan Solanki for proof-reading some of my written work,
- Jacey-Lynn Minoi, Irine Runnie and Oak Phoomboplab for being in the same shoes,
- The Informatics and VR research group,
- Faculty and Staff of the Engineering Department, especially WMG
- Everyone who has kept me in their thoughts and prayers

But most of all, I would like to thank God for His divine intervention, unconditional love, wisdom, peace, joy, strength and grace.

DECLARATION

This thesis is presented in accordance with the regulations for the degree of Doctor of Philosophy. It has been composed by myself and has not been submitted in any previous application for any degree. The work in this thesis has been undertaken by me except where otherwise stated.

Abstract

The aim of the research is to contribute to the modelling of deformable objects, such as soft tissues in medical simulation. Interactive simulation for medical training is a concept undergoing rapid growth as the underlying technologies support the increasingly more realistic and functional training environments. The prominent issues in the deployment of such environments centre on a fine balance between the accuracy of the deformable model and real-time interactivity. Acknowledging the importance of interacting with non-rigid materials such as the palpation of a breast for breast assessment, this thesis has explored the physics-based modelling techniques for both volume and surface approach. This thesis identified that the surface approach based on the mass spring system (MSS) has the benefits of rapid prototyping, reduced mesh complexity, computational efficiency and the support for large material deformation compared to the continuum approach. However, accuracy relative to real material properties is often overlooked in the configuration of the resulting model.

This thesis has investigated the potential and the feasibility of surface modelling for simulating soft objects regardless of the design of the mesh topology and the non-existence of internal volume discretisation. The assumptions of the material parameters such as elasticity, homogeneity and incompressibility allow a reduced set of material values to be implemented in order to establish the association with the surface configuration. A framework for a deformable surface model was generated in accordance with the issues of the estimation of properties and volume behaviour corresponding to the material parameters.

The novel extension to the surface MSS enables the tensile properties of the material to be integrated into an enhanced configuration despite its lack of volume information. The benefits of the reduced complexity of a surface model are now correlated with the improved accuracy in the estimation of properties and volume behaviour. Despite the irregularity of the underlying mesh topology and the absence of volume, the model reflected the original material values and preserved volume with minimal deviations. Global deformation effect which is essential to emulate the runtime behaviour of a real soft material upon interaction, such as the palpation of a generic breast, was also demonstrated, thus indicating the potential of this novel technique in the application of soft tissue simulation.

List of Abbreviations

2D	Two Dimensional
3D	Three Dimensional
BEM	Boundary Element Method
CT	Computed Tomography
E	Elasticity Modulus
FEM	Finite Element Method
FPS	Frame perSecond
kPa	Kilo Pascal
LEM	Long Element Method
LOD	Level of Detail
MRI	Magnetic Resonance Image
MSS	Mass Spring Systems
PDE	Partial Differential Equation
REM	Radial Element Method
SMSS	Surface Mass Spring Systems
VDM	Volume Distribution Method
VMSS	Volume Mass Spring Systems
VP	Volume Penalty

Chapter 1
Introduction

1.1 Context and motivation

1.1.1 Context

The context of this research is within the framework of developing a computer-based simulation of soft objects. Soft objects refer to three-dimensional objects that are deformable upon interaction, such as soft furnishings, soft toys and human organs. The simulation of such entities has to be reflective of this behaviour.

The degree of accuracy and realism, however, is subjective to the domain of applications. The applications may range from scientific analysis to real-time training simulations. Scientific analysis, such as the investigation of the behaviour of human tissue for the design of new procedures or implants, demands accuracy of the deformation rather than a very short computation time. A training simulation, on the other hand, emphasises real-time interactivity rather than perfect accuracy. However, realism can be achieved by utilising a reduced set of behaviour parameters in the adoption of the appropriate assumptions for real-time simulation.

The requirement of a training simulation can generally be defined based on the user's role in the environment. Flight simulation, for instance, requires the pilot to react to the simulated environment and medical simulation expects the trainee doctor to interact with the simulated scenarios (Sundaraj 2004). Reacting excludes the importance of direct interactivity with deformable objects in the environment, which makes the development of a flight simulator simpler. The dissemination of a flight

simulator in the actual training settings is also faster. On the contrary, the necessity to interact with soft tissues in real-time medical simulation demands consideration of the computational power, accuracy and the algorithmic complexity. This substantially limits the development of a medical simulator.

1.1.2 Motivation

In the field of medical education, vast amounts of practical training are essential to broaden physiological knowledge of the anatomy as well as medical procedures. Novice physicians or surgeons have to be adequately trained before coming into contact with real patients. During the period of in-house training, “observe and repeat” is the key method in learning medical procedures by watching other certified practitioners performing on real patients (Sundaraj 2004). They will then be thrown into the deep end, where they have to repeat what they have observed during the training. This introduces the risk of making incorrect judgements due to the lack of hands-on training.

Great discomfort can also be imposed to real patients. For instance, the training of breast assessment requires a physician to palpate the breast in order to learn the appropriate techniques in tumour detection. Moreover, the scenarios of breast variations during the training are highly limited. For this reason, instead of using real patients, cadavers or animals in training, which impose cultural and ethical issues in most countries, a virtual approach to training can be a logical solution.

Real-time visual and behaviour replications of soft tissues in a training environment are of great importance. It is a plausible solution to avoid such undesirable risks and research studies indicate that simulation improves learning (Grantcharov et al. 2004). The motivation of the research is therefore, to contribute towards the development of

such an environment by investigating a new approach for soft objects simulation. The approach can be used to emulate deformable behaviour of soft objects such as a human breast. The implication of this is significant in the development of a training simulation that hones the skill in tumour detection through breast palpation.

Therefore, before dealing with a more specific training application, a deformable model that can support soft objects such as breasts is substantial. In this context, the dynamic behaviour of interest is confined within the definition of a deformable solid with a static global positioning, such as a deformable breast fixed on a static chest. Similar constraint is also true for most organs simulated for surgery training, where they are confined within the cavity of a human body. However, in this thesis, the breast is employed only as an illustration to substantiate the research implications as well as the scope of the proposed deformable model and its properties.

1.2 Description of the problem

Existing medical training simulations are generally based on geometric representations of the anatomical structures that take no account of their physical nature or the patient-specific properties. The issues in the deployment of such applications revolve around the accuracy of the employed deformable model as well as the need for real-time interactivity (Brown et al. 2001, Sundaraj 2004, Delingette & Ayache 2004; Mezger et al. 2008).

Many algorithms have been proposed for deformable models that promote and aspire to real-time computation but very often at the cost of overlooking the physics principles and bio-material properties. High-fidelity training simulators are possible if a physical, as opposed to a geometric, mathematical model of anatomical structures is exploited (Immersion 2008). For this reason, the two key requirements that influence

the quality of a training simulation are the accuracy of the virtual models and the real-time capability.

To achieve both accuracy and realism in the simulation of the dynamic behaviour of a soft object, it is of paramount importance that the resulting models are simulated based on its physical and material parameters. Representing the physical attributes and more specifically the realistic modelling of soft tissue will not only improve the existing training simulation but will also considerably extend the set of applications and the credibility of medical training simulation (Delingette 2000, Al-Khalifah & Roberts 2004; Grantcharov et al., 2004), from laparoscopic to open surgery simulation.

In order to include such properties in the configuration, volume datasets and the resulting volume model are commonly utilised. Volume models have been implemented to simulate deformable objects, such as human organs, due to their solid characteristics. The dynamic behaviour can then be configured using the physics-based methods such as the Finite Element Method (FEM) and the Mass Spring Systems (MSS), where it has to portray a deformable behaviour upon any user interaction.

The FEM method is, however, more suitable for scientific analysis and it is effective for small deformations (Dimaio & Salcudean 2005). This method is, thus, known to be computationally expensive (Batteau et al.,2004; Maciel 2005; Paloc et al. 2006). The optimised method based on FEM, such as the Boundary Element Method (Nealan et al. 2006), is limited by the pre-defined constraints that restrict its versatility. MSS, on the other hand, supports real-time and large deformations. The computational complexity is greatly reduced but the issue of accuracy limits the degree of confidence

in its configurations compared to FEM. MSS promotes faster prototyping and is more suitable for real-time simulation, where it puts more emphasis on the computation speed rather than perfect precision (Laugier et al. 2003).

Nevertheless, the accuracy of a volume model in general is substantially overshadowed by the latency of the simulation due to the complexity of the consequent geometrical mesh that imposes high computation and less usability in real-time applications (Delingette 1998; Al-Khalifah & Roberts 2004; Batteau et al. 2004). Thus, there is a great need for a deformable model that emulates real material properties of soft solid objects without sacrificing the computational efficiency. It is within this domain, this research work is proposed.

To address the issue of real-time interactivity, there has been a significant interest in employing a surface model as an alternative to the volume counterpart due to its simplicity and the possibility of reducing the computational cost (Aubel & Thalmann 2000; Brown et al. 2001; Vassilev & Spanlang 2002; Zhang et al. 2002; Mendoza et al. 2002; Laugier et al. 2003; Matyka & Ollila 2003; Sundaraj 2004; Choi et al. 2005; Marchal et al. 2005; Payandeh et al. 2005; Balaniuk et. al. 2006; Hong et al. 2006; Nealan et al. 2006). Rapid generation of highly detailed surface models is now possible by utilising 3D data acquisition devices such as the structured light scanners (Simple3D 2006, Mezger et al., 2008).

The complexity of a surface model is one order of magnitude lower than the volume models (Sundaraj 2004; Holbrey 2004). Even though, the dimension is reduced, the feasibility of utilising this approach is supported by the existence of the published assumptions of material properties. The assumptions include the parameters of elasticity, homogeneity and incompressibility listed in table 1.1. These parameters are

deemed feasible due to the limited visual and tactile perception of a human operator of a virtual environment (Wall & Harwin 1997; Bordegoni et al. 2001; Wade & Swanstons 2001; Batteau et al. 2004; Sur et al. 2004; Payandeh et al. 2005; Wuillemin et al. 2005). The scope of the deformable model (section 4.2.2) is based on these properties.

Table 1.1: *The assumptions of material properties to promote realism without sacrificing the computational efficiency (see section 2.2.1 and table 3.2)*

Parameters	References
Elasticity	Cotin et al. 1999; Tanner et al. 2001; Janssen and Vergeest 2002; Maciel et al. 2003; Maciel 2005; Etzmuss et al. 2003; Chui et al. 2007; Zhang et al. 2007.
Homogeneity	Koch et al. 2002; Basdogan et al. 2004; Roose et al. 2005; Balaniuk et al. 2006; Ruiter et al. 2006; Zhang et al. 2007 ; Rajagopal et al. 2008.
Incompressibility	Girod et al. 1996; Delingette 1998; Laugier et al. 2000; Picinbono et al. 2001; Azar et al. 2001; Delingette & Ayache 2004; Sundaraj 2004; Chui et al. 2007; Roan & Vemaganti 2007; Samani et al. 2007; Rajagopal et al. 2008.

Within the scope of a surface approach, it is of paramount interest to explore the key issues that influence the deployment of a deformable surface model in soft volume simulation. The main concerns in utilising a surface model are:

i) The complexity in estimating the properties based on the real material properties increases due to the absence of volume. To correctly emulate the volume behaviour of a real solid, the physical and material properties of the surface model have to be configured to promote realism.

ii) The complexity in estimating properties for surface elements is significantly magnified when the design of the mesh topology that defines the surface geometry is irregular or modified.

iii) The drawbacks in the absence of the internal volume also include the difficulty in conserving volume and solid behaviour during simulation.

Based on these concerns, the two key issues are the estimation of properties and volume behaviour.

The key parameters and issues are further established and discussed in Chapter 2 and 3. Figure 1.1 demonstrates the relationship between these parameters and issues in relation to the definition of the ensuing deformable surface model. This relationship compliments the proposed framework demonstrated later in figure 4.1.

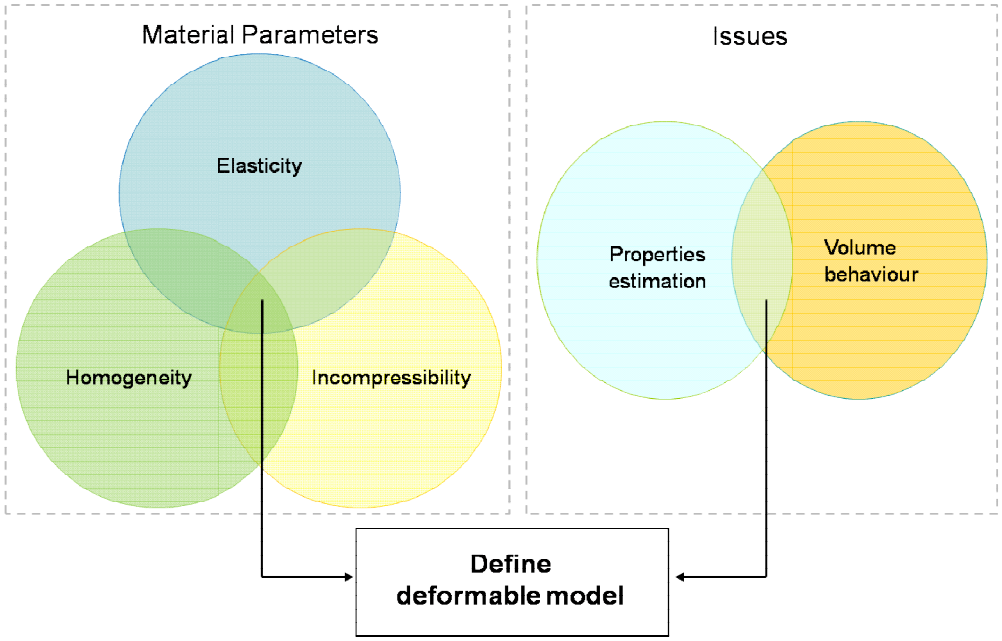

Figure 1.1: *The parameters and issues that influence the configuration of the deformable model (see figure 4.1)*

In reference to this relationship, the classic MSS is further explored. The proposed deformable model is specifically aimed at addressing these issues and parameters. They are further established in the background of this thesis and explored in the design and the evaluation of the deformable model. The evaluation hypotheses based on these issues and parameters are also discussed (see section 5.6.1).

1.3 Aim, objectives and contributions

1.3.1 Aim

The aim is to increase the accuracy of the configuration of a surface model towards simulating soft solid objects in terms of the estimation of properties and volume behaviour as well as in reference to the material parameters: elasticity, homogeneity and incompressibility.

1.3.2 Objectives

To achieve the aim, the research objectives are:

i) To investigate the surface approach in relation to the issues of properties estimation and volume behaviour

ii) To address the shortcomings of a surface model, which are the non-existence of internal volume and the design of the surface mesh topology

iii) To propose an enhancement to the surface model, which increases the accuracy by considering the real material properties in the novel extension to the configuration.

iv) The research incorporates a proof of concept by the means of empirical evaluations that leads to the justification of the novel contributions to knowledge.

Therefore, the objectives of this thesis are to:

i) Investigate the issues related to deformable modelling and the physics-based techniques in the volume approach,

ii) Explore the attempts in surface modelling in relation to the issues of properties estimation and volume behaviour,

iii) Propose an enhanced framework and configuration of a surface model,

iv) Evaluate the proposed model relative to the issues of properties estimation and volume behaviour, and the material parameters that include elasticity, homogeneity and incompressibility, and

v) Discuss the evaluation findings and the consequent contributions and implications.

1.3.3 Contributions

In relation to the aim and objectives, the thesis has contributed in terms of the following:

i) The review of volume and surface approach in modelling deformable solids and the identification of issues in this domain.

ii) A potential alternative to deformable modelling of soft objects in a real-time and interactive simulation. The thesis proposes a novel extension to the physics-based surface model that increases the accuracy of the configuration of the deformable objects.

iii) The implication of the proposed framework in the domain of medical training. Soft objects such as breast can be simulated based on their material properties. The potential is in the future work of breast assessment via haptic palpation towards the detection of tumours.

1.4 Thesis outline

According to the objectives, the main body of the thesis is organised into three main parts addressing correlated themes. Table 1.2 summarises the objectives in relation to the respective parts. Figure 1.2 illustrates the flow of the thesis, where each part sets the scene for the other.

Table 1.2: *The thesis*

Thesis Parts	Thesis objectives
Part 1: Background	i) Investigate the issues related to deformable modelling and the physics-based techniques in the volume approach,
	ii) Explore the attempts in surface modelling in relation to the issues of properties estimation and volume behaviour
Part II: The Proposed Deformable Model	iii) Propose an enhanced framework and configuration of a surface model
Part III: Evaluation Analysis and Discussion	iv) Evaluate the proposed model relative to the issues of properties estimation and volume behaviour, and the material parameters that include elasticity, homogeneity and incompressibility
	v) Discuss the evaluation findings and the consequent contributions and implications.

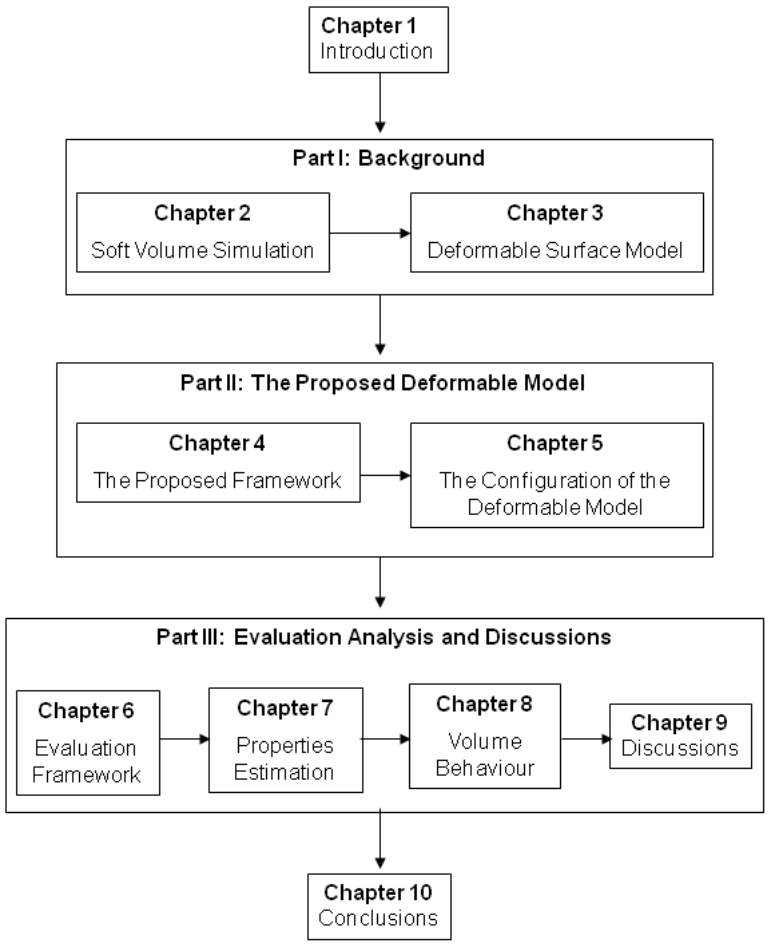

Figure 1.2: *The overview of the thesis structure*

Part I focuses on the background of soft volume simulation. This part begins with Chapter 2, where the important concepts and issues as well as the state of the art in soft volume simulation are reviewed. Soft assumptions employed for the material properties are also included in the discussion. Chapter 3 follows up from the key issues concluded in chapter 2, where the approaches and attempts specific to a surface model are discussed. This chapter establishes the scope and the goal of the proposed solution based on the correlated findings.

Based on the background discussed in Part I, Part II proposes a deformable surface model that addresses the considerations concluded in Chapter 3. Part II begins with Chapter 4, where the proposed simulation framework and the scope of the deformable model are introduced. The new deformable surface model is presented where achieving volume behaviour based on real material properties is of paramount importance.

Based on the relationship between the surface model and the object volume discussed in Chapter 4, Chapter 5 introduces the novel estimation technique for the model properties and its volume behaviour.

Part III discusses the empirical evaluation and the analysis of the ensuing findings based on the same key issues and material parameters explored in Part I and Part II. The first chapter in this part, Chapter 6, establishes the aim and objectives of the ensuing empirical evaluation to set the scene for the analysis and discussion in the following chapters. Chapter 7, addresses the evaluation of the estimation technique in consideration of the elasticity and homogeneity parameters. The findings extracted from the experiments are analysed and the hypotheses and the objectives are discussed and correlated with these findings. The hypotheses and objectives are all

met and the versatility of the estimation technique is demonstrated. The corresponding volume behaviour is evaluated in Chapter 8. This chapter not only describes the feasibility of the proposed model to emulate volume behaviour, but it also further establishes both the feasibility and the versatility of the proposed estimation technique in employing the soft assumptions of the material properties. Part III concludes with a discussion chapter, Chapter 9, where the major findings and knowledge contributions are correlated and summarised. The key research question and the objectives are also evaluated, where they are correlated with the analyses of the proposed model.

The thesis is finally concluded in Chapter 10, where the findings are summarised within the research aim, objectives and contributions. Further work and the future direction of this research are also discussed in this chapter in relation to the limitations of the proposed framework.

- PART I -

BACKGROUND

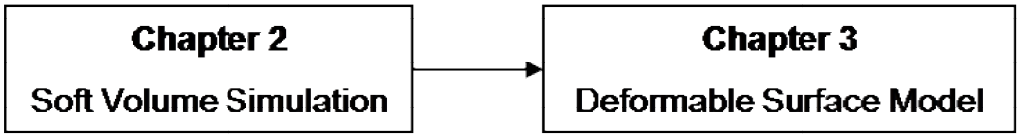

"A man travels the world over

in search of what he needs and returns home to find it."

George Moore (1873-1958)

Chapter 2

Soft Volume Simulation

2.1 Introduction

A solid object portrays volume behaviour that reflects the existence of the internal substance encapsulated by its exposed surface. The behaviour can either be rigid or non-rigid (figure 2.1). Non-rigid is also known as deformable or soft. Therefore, the obvious difference between a rigid and a deformable object is the latter allows internal position change, where the relative positions of two or more different nodes of the same object vary in response to external interventions such as gravity and interaction (Maciel 2005). Rigid objects such as metal could allow small if not negligible local deformation.

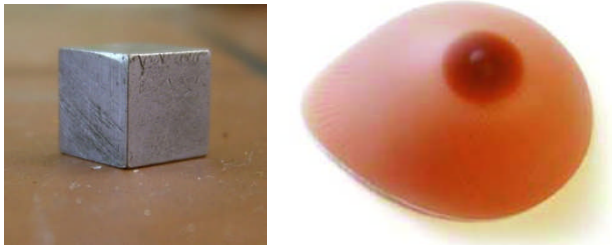

(a) (b)

Figure 2.1: *Solid bodies: (a) rigid metal (b) non-rigid prosthesis*

Global shape change is possible such as a metal rod bending upon the existence of external forces. Rigid models are the most widely used today, despite the fact that they cannot reproduce visible deformations and surface tractions. This is due to their apparent efficiency and relative simplicity. However, deformable models are increasingly employed in animation, edutainment and medical training due to the need to simulate soft objects.

In a virtual environment, a three dimensional (3D) model is manipulated to demonstrate such deformable behaviour. In the development of a medical simulation, for instance, 3D anatomical models are generated from scanned images such as from MRI and CT scans (NLM 2001; Al-Khalifah & Roberts 2004). To promote realism, the appropriate dynamic behaviour of the models has to be merged with the respective 3D visual representation. To achieve such configuration, techniques such as the physics-based modelling are commonly employed to define the dynamic and deformable behaviour of the model.

For such technique, volume dataset seems to be of utmost importance due to the co-existence of many entities within the same constrained space such as the various tissue types in an organ and the many organs contained in a human's body. The variation of materials within the solid object could be explored if volume data is employed as it holds some information about the internal anatomical structure of the tissues (Al-Khalifah & Roberts 2004). The main drawback of a volume method is that it significantly demands high storage space and high computational power to handle such massive data. Also, the necessity of such data has to be addressed.

The choice of the deformable models is governed by the computational power and accuracy. The nature of the applications that employ such models is also important. For instance, for pre-operative medical planning, accuracy is more important than speed. For intra-operative medical training, the simulation must be able to support the needs for real-time interactivity. Material homogeneity has often been assumed for the emulation of solid objects (Ruiter et al. 2006; Roose et al. 2005) to provide a simulation that is qualitatively effective with both real-time visual and interaction acuity.

The scope of this thesis includes the exploration of the non-rigid and dynamic solid models towards emulating real material properties as well as volumetric behaviour. Therefore, in this chapter, the concepts, assumptions, issues and methods engaged in simulating a deformable object are discussed.

2.2 Deformable Model

Most materials encountered in medical simulation can be regarded as deformable objects. In the scope of such simulator, it is not possible to model the complete biomechanical complexity of living soft tissue (Delingete 1998; Delingette & Ayache 2004; Dimaio & Salcudean 2005). Instead, most authors have resorted to simplified models to decrease the implementation complexity and to optimise computational efficiency (Tanner et al. 2001; Etzmuss et al. 2003; Roose at al. 2005; Ruiter et al. 2006; Zhang et al. 2007; Rajagopal et. al. 2008). Hence, to enable the design of the consequent partially generic framework for the deformable model, the parameters that influence the configuration of a deformable model has to be investigated. The relevant assumptions on how to effectively utilise these parameters are examined in the next subsections.

2.2.1 Material properties

This section discusses the three key parameters that define the material of deformable bodies, which are homogeneity, elasticity and compressibility.

2.2.1.1 Homogeneity

Homogeneity generally means the same all throughout. A material is homogenous if it is made of the same material as a whole. However, objects such as human organs can consist of various tissue types, which results in inhomogeneous material composition.

The respective properties are dissimilar for the different sections of each organ. A breast, for instance, is made up of various tissue types but mostly fatty (adipose) tissue confined within an elastic skin that gives breast its shape (figure 2.2).

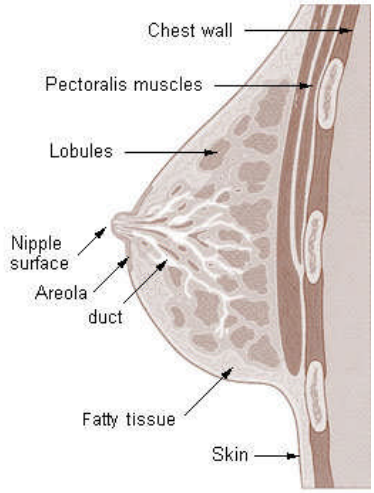

Figure 2.2: *The various tissue types consisted in a breast*

However, the tactile sensation produced from direct interaction with the skin surface demonstrates an assumption of a homogeneous material regardless of the different tissue types. For real-time simulation, such an assumption (Rajagopal et al. 2008) can be crucial in order to create a more simplified model. Ruiter et al. (2006) concluded that the material model with similar bio-tissue properties for a breast as a whole is sufficient and more complex inhomogeneous models do not increase simulation accuracy. Roose et al. (2005) supported the concept by stressing that the dependency of the overall deformation on the inhomogeneous nature can be avoided altogether by eliminating the need to model the variations in the substance composition.

An object material can display isotropic or anisotropic behaviours despite the level of material homogeneity. A material is isotropic if its properties are the same in any direction irrespective of the direction and orientation of internal or external forces, incidence to the radius of interaction. However, force orientation influences the surface response to external interaction, which indicates an anisotropic behaviour. The

surface behaviour reflects the accumulated behaviour of the internal volume composition.

2.2.1.2 Elasticity

Elasticity refers to the level of reversibility of the material to its original relaxed state when deformed, reflecting the conservation of shape as a response to a deforming force. Linear elasticity is perfectly reversible and such behaviour can be represented by the relationship of stress and strain of the material. It is based on Hooke's law where the stress and strain are proportional upon smaller deformation, conforming to the constraint that both yield and tensile (ultimate) stresses are not exceeded. This relationship is illustrated in figure 2.3.

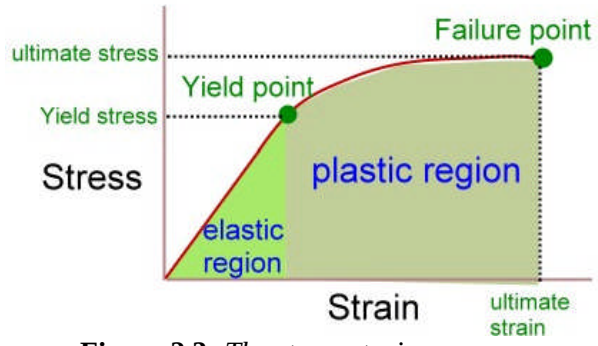

Figure 2.3: *The stress strain curve*

In general, most materials are linear up to a yield limit and translate to the non-linear mode or plasticity when deformed. The material will experience rupture when the tensile (ultimate) strength is exceeded. For non-invasive interaction, such as palpating a human breast, the yield and tensile limit of the material is never achieved. The published compression pressure of a mammography was claimed to be around 41 kPa (Russel &Ziewacz 1995; Ruiter et al. 2006). The advised palpation force is within the range of 1 to 2 Newton or 0.1 to 0.2 kg of weight (Patkin 1998), while a similar sensing range was concluded by McCreery et al. (2008) for tumour detection.

However, the palpation pressure has to be adapted to the attributes such as the size, shape and consistency of tissue (Saslow et. al 2004).

In physiological situations, biological tissues can be classed as viscoelastic. A material having this property is considered to combine the features of a perfectly elastic solid and a perfect fluid, such as living tissue, which is essentially made up of water (Picinbono et al. 2001). To replicate the behaviour, the material behaviour can be approximated from a reduced set of material values. One of these is the linear elastic deformation of soft bio-tissues and estimating the material properties as a whole, assuming a homogeneous set up. The assumption of homogeneity is demonstrated in the notion of fluid as the main material composition of a living tissue. Furthermore, to introduce viscosity to a linear system, the ambient approach has been employed which was based on the resistance to material movement within a medium of known density (Jansson & Vergeest 2002; Maciel et al. 2003; Maciel 2005).

Consequently, linear elasticity theory has often been utilised as a good approximation of the behaviour of a deformable body. It has also been claimed that linear elasticity provides the standard for simulations in science and engineering (Cotin et al. 1999; Etzmuss et al. 2003). Moreover, the influence of linear elastic tissues differs little from non-linear on the overall model. Modelled with the addition of linear elastic skin, non-rigid models such as breast models deform plausibly (Tanner et al. 2001; Zhang et al. 2007).

2.2.1.2.1 Elasticity Modulus

The elasticity of a material is described by the stress and strain relationship (figure 2.3) as well as the loading directions. This allows for many types of elastic modulus to be defined. The three principal ones are:

i) Young's Modulus

Young's Modulus is a measurement of material elasticity which is represented by the uni-axial tensile elasticity, or the tendency of an object to deform along an axis when opposing forces are applied along that axis. It is defined as the ratio of the tensile stress to the tensile strain. It is also often referred to simply as the elastic modulus. The modulus is derived from the stress-strain or force-elongation relationship as illustrated by figure 2.4.

$$\sigma = E\varepsilon \tag{2.1}$$

where, σ is the stress, ε is the strain and E is the Young's Modulus. Stress is defined as a pressure exerted on an object. It is calculated by dividing the force by its area of application. Strain in turn is the amount of deformation and it is derived by dividing the variation of the specimen length by its original rest length to give strain.

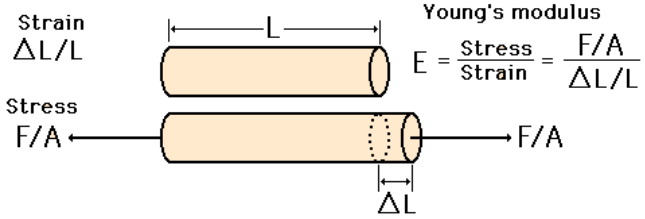

Figure 2.4: *Young's Modulus (E) extracted from the stress-strain relationship*

Where F is the force imposed on an area A, L is the rest length of the material and ΔL is the length variation in response to force F, the relation is:

$$\frac{F}{A} = E\frac{\Delta L}{L}$$

The linear relationship, which is employed to extract the modulus, is generally described as the engineering approach. The strain and stress can also be represented by the true approach which is illustrated in figure 2.5. In this approach, the significant change in the cross section of the material is taken into consideration.

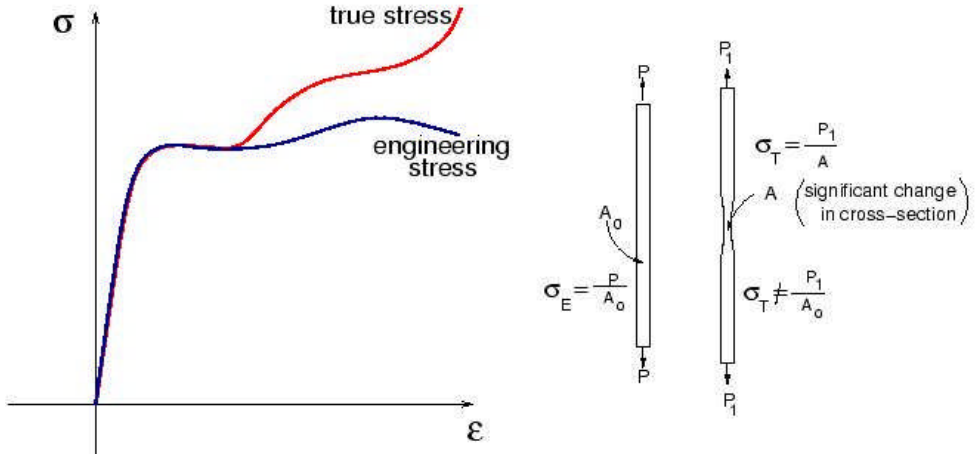

Figure 2.5: *Real stress-strain (in red) in response to the change in cross-section A*

For deformable model, elasticity is also associated with the level of stiffness of the model material. Based on the force-elongation relationship, stiffness constant can be defined by force divided by the elongation, or based on the engineering or linear stress-strain relationship for a Hookean material such as a spring with stiffness ***k***,

$$k = E\frac{A}{L} \qquad (2.2)$$

where, stress is proportional to the strain for all strains.

ii) Shear Modulus

The shear modulus (G) is also known as the rigidity modulus. The material displays shearing behaviour when the external force is perpendicular to the surface normal. G describes an object's tendency to shear when acted upon by the opposing forces, which is defined by shear stress over shear strain. When an object like a block (figure 2.6) of height *L* and cross section *A* experiences a force *F* perpendicular to the surface normal, the sheared surface will move a distance *Δx*. The shear stress is defined as the magnitude of the force per unit cross-sectional area of the face being sheared (*F/A*). The relative shear strain is defined as *Δx/L*.

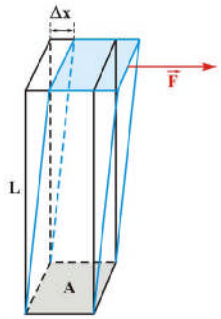

Figure 2.6: *Shear force acting perpendicularly to the top surface of the box*

The shear modulus denotes the material rigidity, where the relationship between the change in the horizontal distance (strain) and the amount of force (stress) is linear. Therefore, shear and rigidity are used interchangeably. This behaviour demonstrates that the elastic behaviour is influenced by the orientation of force. The resistance to this imposing force is different from the force that is imposed along the axis parallel to the surface normal as described by the E.

Assuming that the deformation does not exceed the yield limit, G can be expressed as a function of E and Poisson ratio (v) which is the ratio of radial strain to axial strain:

$$G = \frac{E}{2(1+v)} \tag{2.3}$$

Most materials have v between 0.0 and 0.5. Materials such as cork and sponge, show almost no Poisson contraction, meaning that they are compressible. Materials such as rubber and fluid have a Poisson ratio of nearly 0.5, which means that they are nearly incompressible. A perfectly incompressible material will have a Poisson's ratio of exactly 0.5 when deformed at small strains. However, most materials are nearly incompressible, where bulk modulus can be used to define their property.

iii) Bulk Modulus

The bulk modulus (B) is also known as the modulus of compression. Based on the characteristic of a solid object, B represents the object material reaction to volume

change. It also describes volumetric elasticity, or the tendency of an object's volume to deform when under pressure. Therefore, it is defined as volumetric stress over volumetric strain, and is the inverse of compressibility. Therefore, the larger the value, the more incompressible the material is.

B is an extension of E to three dimensions, where it influences the magnitude of pressure distributed to the surface of the volume object upon change of volume. Assuming that pressure does not cause the deformation to exceed the yield limit, B can also be expressed as a function of E and *v*:

$$B = \frac{E}{3(1-2v)} \tag{2.4}$$

It is a numerical constant that describes the elastic properties of a solid or fluid under pressure from all sides (figure 2.7). Consequently, it is actually the ratio of the tensile stress or compressive force per unit surface area to the change in volume (ΔV) per unit volume (V) (strain) of the solid or fluid. This relationship can be defined as:

$$P = B\frac{\Delta V}{V} \tag{2.5}$$

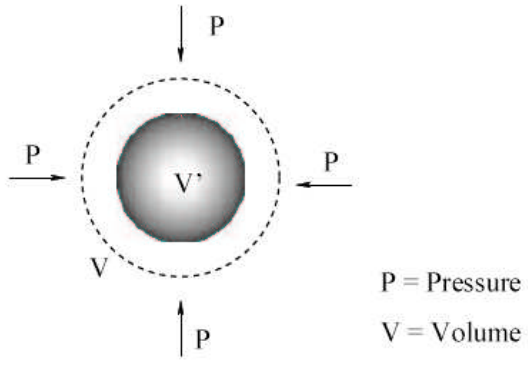

Figure 2.7: *Pressure causing change in volume from V to V' (Sundaraj, 2004)*

2.2.1.2.2 Young's modulus of soft tissues

There is a large bibliography on the study of soft tissue deformation in the domain of bio-mechanics. Levental et al. (2007) stated that the elastic moduli of biological

tissues range from the order of 100 Pa for the brain to 100 kPa for soft cartilage. However, there exists no property that is more accurate than another. These properties were extracted from small tissue samples and were influenced by the extraction method, device accuracy, the number of test samples and the origins of the samples. For example, the combination of various tissue types changes with various constraints, such as age. A younger person will have more glandular tissue in their breast than an older person. However, these estimations can be employed towards emulating the tissue behaviour in a virtual environment.

Table 2.1 summarises some of the values that describe the elasticity modulus of soft tissues. The values vary due to factors such as the initial pre-compression imposed on the tissue sample during the extraction of the elasticity modulus as well as the dissimilar samples of tissue and equipments employed by the authors. More values of similar tissue types published by different authors are illustrated in appendix A.

Table 2.1: *The modulus (E) values for various tissue types*

Tissue Type	**E (kPa)**	**Author(s)**
Breast adipose tissue	3.25 ± 0.91	Samani et al. (2007)
	18 ± 7 to 22 ± 12	Krouskop et al (1998)
	5 to 50	Saravazyan et al. (1994)
	15 to 25	Kruse et al. (2000)
Breast glandular tissue	3.24 ± 0.61	Samani et al. (2007)
	28 ± 14 to 35 ± 14	Krouskop et al (1998)
	5 to 50	Saravazyan et al. (1994)
	30 to 45	Kruse et al. (2000)
Prostate	1 to 5	Saravazyan et al. (1994)
Liver	0.64	Levental et. al (2007)
Intermediate grade carcinoma	19.99 ± 4.2	Samani et al. (2007)

2.2.1.3 Compressibility

Compressibility refers to the change of volume when deformed by stresses on the surface. Therefore, incompressible material reflects constant volume preservation when deformed. It is also independent of the shape preserving property of the object.

However, elastic and incompressible material resists both shape and volume change upon interaction.

The shape may change during deformation but volume will be preserved assuming that the tensile and yield strength have not been exceeded and density is constant. For instance, a constant change in pressure, exerted on a human breast, is transmitted undiminished throughout the breast tissue and constrained by the elastic skin. Volume compensation is achieved by the reaction displayed by the surface skin deformation. Figure 2.8 demonstrates image slices of a breast at different positions under the influence of gravity.

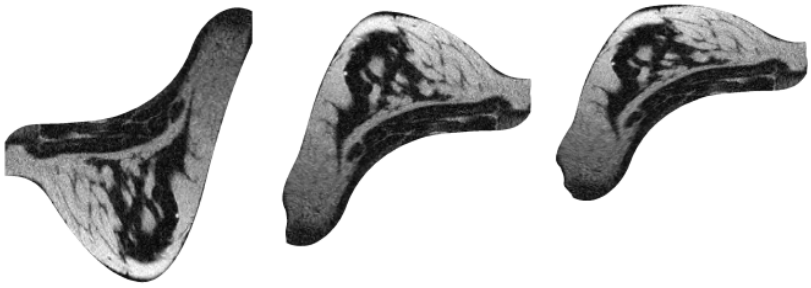

(a) (b) (c)

Figure 2.8: *MR image slices of a breast (Rajagopal et al. 2008) (a) prone gravity-loaded (b) predicted unloaded position (c) supine gravity loaded*

This is true to Pascal's Principle where it states that a change in pressure, exerted on an enclosed static fluid, is transmitted undiminished throughout this substance and acts perpendicularly on the surface of the container (figure 2.9).

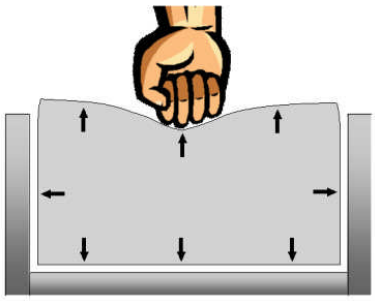

Figure 2.9: *Pressure distributed to promote incompressibility upon interaction*

Living tissue has been deemed incompressible due to being essentially made up of fluid (Picinbono et al. 2001; Delingette & Ayache 2004). The incompressibility of the fluid imposes the constraint that the volume of the deformable object is maintained at all times. In this case, it is actually nearly incompressible as its bulk modulus is a finite value. Soft tissues, such as breast and liver tissues can be considered as such (Girod et al. 1996; Laugier et al. 2003; Sundaraj 2004; Chui et al. 2007; Roan & Vemaganti 2007; Rajagopal et al. 2008).

As a further illustration, a liver consists of an elastic skin called Capsule of Glisson as the surface and the Parenchyma that includes a complex vascular network filled with 95 percent blood (Laugier et al. 2000; Sundaraj 2004). Due to the high content of fluid in the liver, it is possible to assume that the liver is incompressible and is of homogeneous material. The elastic capsule indicates a behaviour that obeys Hook's Law to some extent. Similar assumptions can be made for breast, where the skin is elastic and the internal material is made up of mainly adipose and glandular which have rather similar elasticity moduli (Aubel &Thalmann 2000; Samani et al. 2007).

2.2.2 Modelling

Such estimation in material properties has to be reflected by the visual responses of the solid model during simulation. Therefore, the visual representation of both static and dynamic behaviour has to be explored.

2.2.2.1 Visual representation

The visual or graphical representation of the deformable model has to support both static and dynamic behaviour. The geometry of the model is defined by the discretisation based on the existing datasets such as point clouds or pre-computed

polygon mesh. This section discusses the fundamentals that influence the modelling of the visual model as well as its dynamic behaviour.

2.2.2.1.1 Mesh topology

A polygon mesh or unstructured grid is an assortment of vertices, edges and faces that defines the shape of a polyhedral object in 3D computer graphics and solid modelling. The faces are usually defined as triangles, quadrilaterals, or other simple convex polygons. The different types of elements have to be stored to assist the need to access the respective geometrical information during modelling.

The polygonal mesh employed to define deformable models typically consists of triangular elements in 2D and tetrahedral elements in 3D. These elements are joined at discrete node points which are the smallest mesh element. The members of a mesh include the vertices (nodes), edges, faces, polygons and surfaces. Generally, only vertices, edges and faces are stored. Figure 2.10 illustrates a box object made up of the triangular mesh topology.

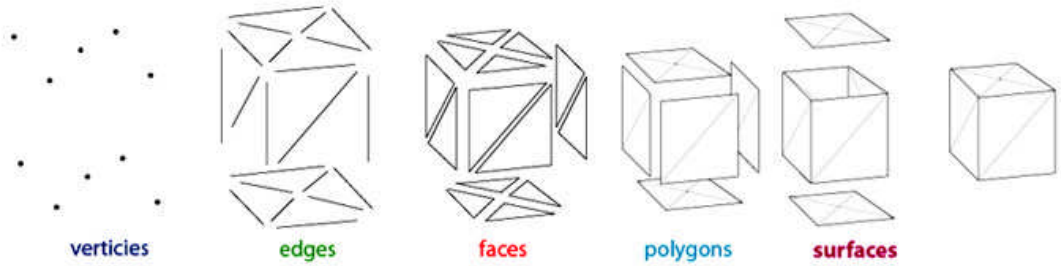

Figure 2.10: *A simplistic illustration of the creation of a hollow box model from the nodes (vertices from the point clouds) based on triangular mesh topology*

Once the object geometry and the required level of detail (LOD) of the surface topology are known, an appropriate set of elements and interpolation functions can be employed to create the mesh. The best choices of elements and their LOD depend on the object shape and trade-offs between the accuracy and computational requirements.

Some common two and three dimensional elements utilised in finite element are the triangular elements with three nodes, the rectangular elements with four nodes and the three dimensional tetrahedral elements with 4 nodes. These elements are used to define the surface and volume mesh of the object.

As demonstrated in figure 2.10, these elements when combined create a geometrical mesh of nodes and edges. The relationship of the elements of a mesh topology, which are faces and their respective edges and vertices (nodes), can be represented by the mesh data structure illustrated in figure 2.11. This promotes efficient traversing of mesh elements when employed in a simulation for rendering as well as for the definition of the properties of the deformable model. This data structure (Tobler & Maierhofer 2006) has been particularly optimised for real-time rendering based on the other data structures (Baumgart 1972; Campagna et al. 1998; Kettner 1998; Botsch et al. 2002).

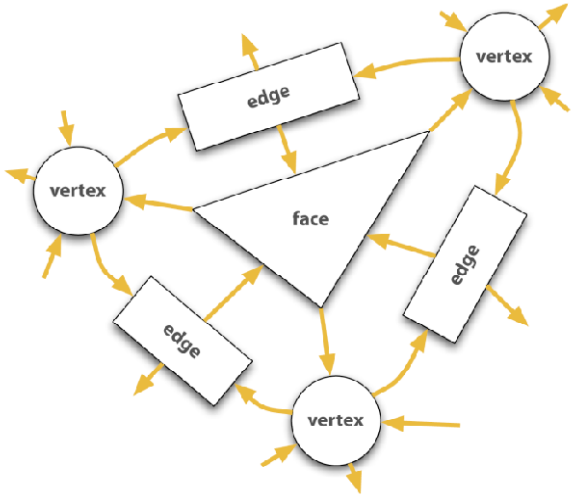

Figure 2.11: *Data structure for the mesh topology (Tobler and Maierhofer 2006)*

The face elements can be of dissimilar sizes depending on the concentration of the nodes. Hence, the characteristic of the mesh topology can either be regular or irregular. The topological design is very important as the numerical models for

deformable objects are highly topology-dependent (Bielser 2003). Figure 2.12 illustrates these characteristics.

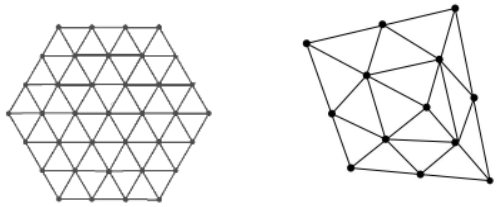

(a) (b)

Figure 2.12: *(a) Regular topology and (b) irregular mesh topology*

Furthermore, most objects are not of regular shape. Consequently, the surface topology also varies. Therefore, the regularity of a mesh topology has to support these characteristics. For example, some parts of the object may demand more refined mesh topology compared to others. This will consequently produce a more irregular mesh topology as a whole as illustrated by the wire mesh model in figure 2.13.

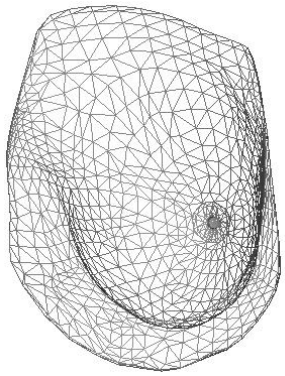

Figure 2.13: *The breast wireframe model with irregular mesh topology*

Figure 2.14 illustrates the different LOD of a hand model with irregular mesh topology. The analysis of the LOD methods is not a part of the research scope. However, topological refinement is widely employed to increase visual acuity (Zhang et al. 2002; Choi et al. 2005, Payandeh et al. 2005). For a deformable model, a topological refinement of a mesh requires the material properties to be re-approximated to define the behaviour of the new elements. Hence, the re-estimation has to be supported.

Figure 2.14: *The different LODs of a hand model (*Cacciola 2007)

For volume datasets, tetrahedral elements (figure 2.15) have been widely employed to represent the internal medium of the object. Furthermore, similar topology design and adaptive modification (Sifakis et al. 2007) can be imposed on the resulting internal mesh.

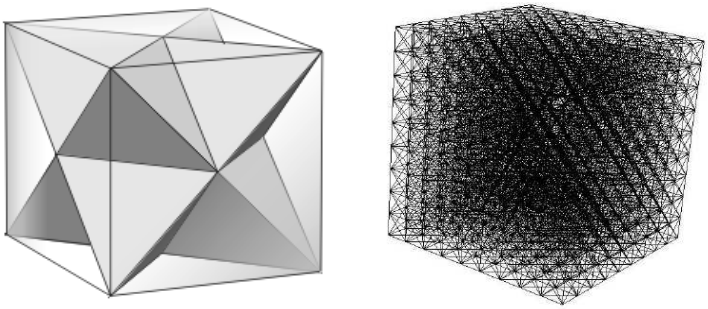

Figure 2.15: *Volume models with regular tetrahedral elements*

The complexity of a volume mesh is significantly larger than the surface mesh of the same object. The tetrahedral elements are employed to define the dynamic behaviour of the internal volume, which is visually reflected by the surface elements. Therefore, the visual rendering is carried out on the elements that are visible within the field of view at runtime.

2.2.2.1.2 Visual rendering

As shown in figure 2.13, the outline of the object is represented by the immediate wire mesh. When rendered using the Gouraud or Phong algorithm, the mesh elements and

their respective surface normals will be used to create the object surface as illustrated by figure 2.16. To improve realism, texture mapping can be employed.

Organs such as breasts have been investigated by researchers, where the assumptions include not only homogenous and incompressible properties but also of a convex shape (star-shaped object) (Vassilev & Spanlang 2002; Balaniuk & Salisbury 2003; Balaniuk et. al. 2006). Williams et al. (2003) even went to the extent of employing hemispheres to represent a simple breast model. The breast model, shown in figure 2.16, is convex and fixed on the chest geometry.

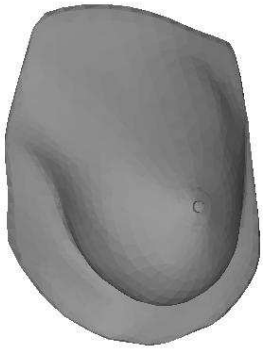

Figure 2.16: *The rendered surface of figure 2.13*

Liver has also been represented by a partially-convex shape topology such as illustrated by figure 2.17. Convex, in this case, refers to the direct internal connections between the nodes to the object centre (Vassilev & Spanlang 2002; Balaniuk & Salisbury 2003; Balaniuk et al. 2006).

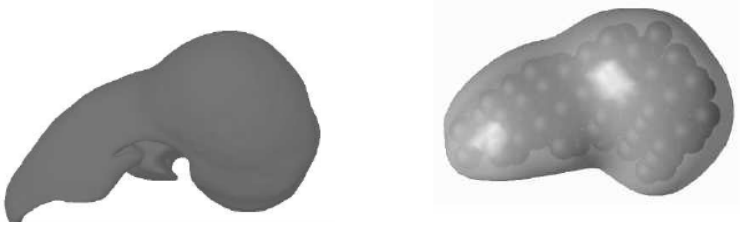

Figure 2.17: *Partially-convex approach employed to emulate liver simulation for training purposes (Hieber et al. 2004)*

The LOD of the simulated model can be changed at runtime in response to the change in shape topology when deformed to promote visual acuity. An adaptive method can

be employed to refine the operational area (Salisbury et al. 1995; Astley & Hayward 1998; Debunne et al. 2001; Zhang et al. 2002; Choi et al. 2005; Payandeh et al. 2005; Sifakis et al. 2007). This is also known as the area of interest, which defines the area within the immediate influence of interaction. Consequently, the mesh topology within this area can be more refined than within the non-operational area. The properties of the deformable model have to also reflect the correct material behaviour (static or dynamic) regardless of the irregularity of the resulting topology. When mapped with texture to increase realism, the texture may undergo distortion in response to surface deformation at runtime i.e. the movement of the nodes onto which the texture coordinates have been mapped. In the case of a homogeneous material, the distortion has to be uniform (Van Gelder & Wilhelms 1997; Van Gelder 1998; Zhang et al. 2002; Lloyd et al. 2007).

However, real-time topological modification is an issue if the dynamic behaviour of the model is based on real material and physical properties. The material properties of the pre- and post-refinement have to be preserved.

2.2.2.2 Dynamic behaviour

To increase realism in a virtual environment, the object has to emulate the behaviour of the material when deformed. Once rendered, it will be useful if the material properties can be used to define the dynamic behaviour upon external influences. For example, non-rigid solids should display a dynamic behaviour in terms of surface deformation upon interaction. Figure 2.18 shows an interaction with a deformable object. Besides being deformable, solid objects may also display positional dynamism, where the global position for the object changes significantly (figure 2.19).

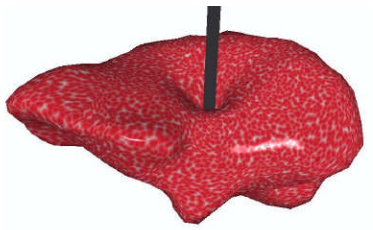

Figure 2.18: *Interacting with a soft solid, such as a liver, causes the local surface to deform (Debunne et al. 1999)*

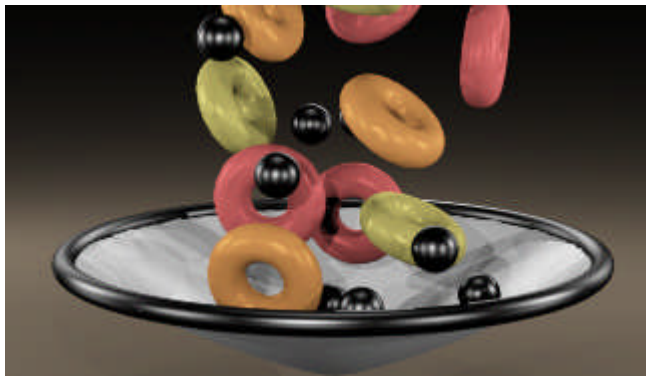

Figure 2.19: *Significant global positional dynamism of tori and balls in response to gravity (Shinar et al. 2008)*

However, for simulations such as employed by medical training, the organs are fundamentally deformable but constrained within a static global position, such as a deformable breast model fixed on a static chest frame or a prostate gland confined within a human body (figure 2.20). Therefore, the deformable behaviour is explored in this section, instead of the positional dynamism.

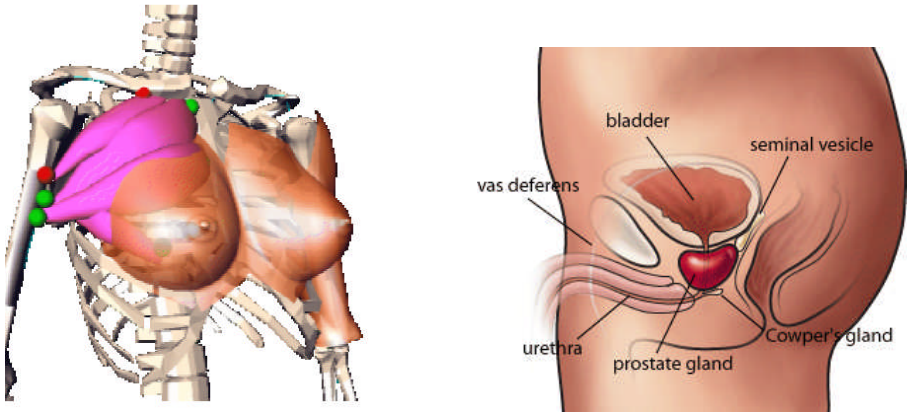

(a) (b)

Figure 2.20: *(a) Breast model fixed on a chest frame (Aubel & Thalmann 2000) (b) A prostate gland*

2.2.2.2.1 Local Deformation

Local deformation refers to the dynamic behaviour within the operational area which involves a relatively small region of the deformable object (Salisbury et al. 1995; Astley & Hayward 1998; Debunne et al. 2001; Zhang et al. 2002; Choi et al. 2005; Payandeh et al. 2005; Hong et al. 2006). The operational area can be the local area that is influenced by the interaction force as illustrated by the deformation within the yellow boundary in figure 2.21.

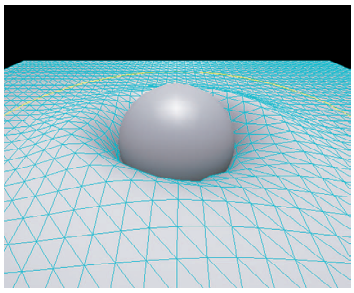

Figure 2.21: *A spherical probe interacting with the object surface (Hong et al. 2006)*

Thus, an interaction on a human body during surgery training will also concentrate on a local area within which the interactivity is prominent, such as probing the abdominal surface with a small device. Brown et al. (2001) assumed that most deformations are local to the operational area, where the motions of surgical instruments are relatively slow. Therefore any deformation will only be produced within the local area without affecting the global change of shape as illustrated in figure 2.22.

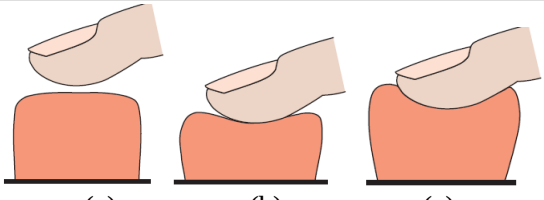

(a) (b) (c)

Figure 2.22: *Pressing an object in (a) can demonstrate (b) global and (c) local deformation (Hong et al. 2006)*

For a more realistic behaviour, global deformation can be displayed to complement the effect of the local deformation.

2.2.2.2.1 Global Deformation

Global deformation refers to deformations that involve the entire body (James & Pai 1999; Zhuang & Canny 1999), such as a solid tube bending due to an external force. Figure 2.23 demonstrates an object displaying local as well as global deformation in response to the direct interaction on the surface. The local deformation is displayed within the operational area while the global deformation is shown by the shape change.

Figure 2.23: *Local and global deformations upon an interaction (James & Pai 1999)*

2.2.3 Interactive Simulation

Training simulations differ from fixed graphical animations where the latter may not require any direct interactions and accuracy (Nealen et al. 2006). The dynamic behaviour of the deformable model should not be fixed as pre-computed animations but it should correspond with real-time influences such as the human-computer interactions.

The interactive capability can be enhanced by introducing appropriate tactile feedbacks. These feedbacks can be achieved with a haptic interface that produces relevant tactile sensation in response to the interaction (see appendix B for additional information on haptics). The general framework (figure 2.24) includes both visual and tactile feedbacks, where the LOD is constrained by the balance between realism and the computing power (Astley & Hayward, 2000). The respective performance is

measured by the update rate for both haptic and visual rendering, where the visual representation and accessing haptic information of the deformable model need to be updated at runtime (additional schematic diagram is illustrated in appendix B.1)

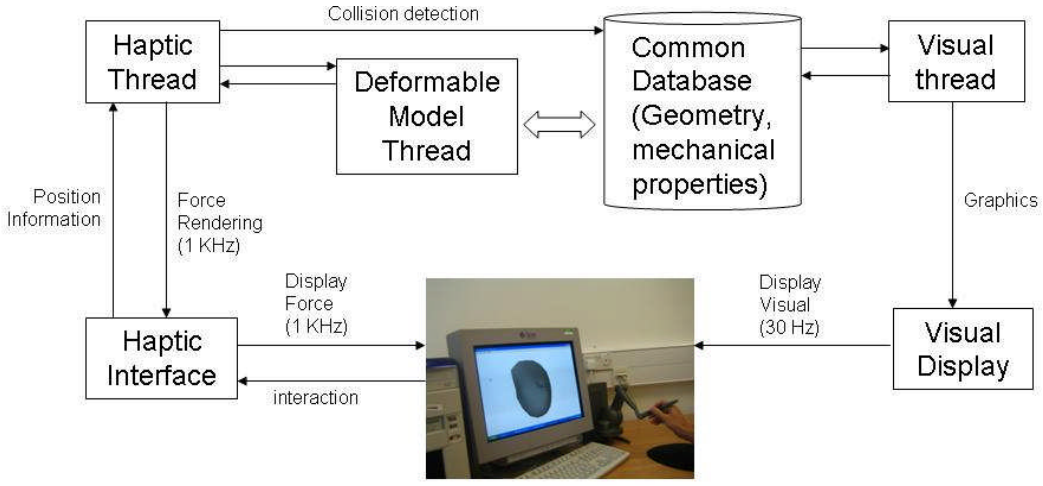

Figure 2.24: *The simulation framework adapted from (Hu et al. 2005)*

It has separate threads for visual and haptic, where each has to be maintained within the minimum update rate in the range of 20 to 30 Hz and 400 Hz to 1 kHz respectively (Sundaraj 2004). This means that visual and haptic feedback has to be produced at the correct frequency such that the user does not feel any uneasiness. These requirements thus, pose a constraint on how complex a virtual model should be.

Various deformable models have been employed for medical training simulations or pre-operative planning. Minimally invasive surgery simulation has been most popular due to the minimal dependency upon tactile realism and the constraint on the visual field of view. Furthermore, the behaviour of the tissue employed is based on fine-tuned properties. Karlsruhe (1997), Szekely et al. (2000), Kuehnapfel et al. (1999, 2001) and NLM (2001, 2003) attempted endoscopic simulation. Laparoscopic simulations, such as the Procedicus MIST (Mentice 2008) (figure 2.25), LapSim

(Surgical Science 2008) and the Laparoscopic VR (Immersion 2008) are currently available on the market. These products utilise their in-house haptic devices.

There are a few developments that attempted to manage the simulation data for surgery simulation. Applications such as LapSkill (Acosta & Temkin 2005a), G2H (Acosta & Temkin 2005b) and MVL (Kuroda et al 2005) have been introduced to provide libraries of visual and haptic data. However these studies focused mainly on the general mapping of fixed haptic values onto rigid organ models that are dependent on the experts to edit the haptic material data directly. Hence, the properties of the organ are dependent solely on the subjective fine-tuning of values.

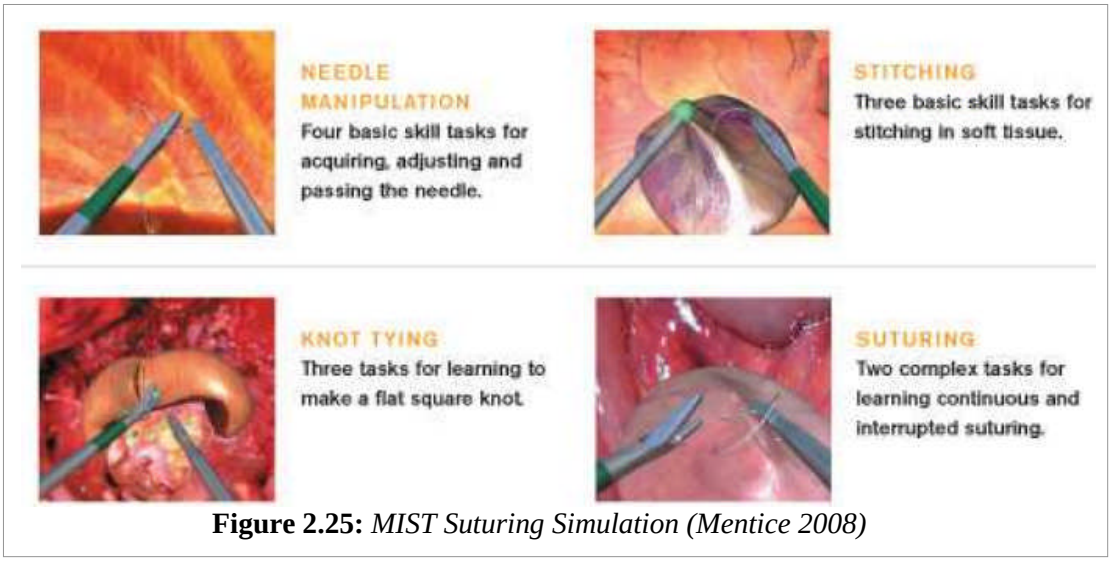

Figure 2.25: *MIST Suturing Simulation (Mentice 2008)*

The haptic properties are mostly modelled for each finite element or a group of finite elements without analysing the anatomical structure of the organ and the tissue members. The assumptions employed in training simulation are generally linear, homogeneous and isotropic behaviour (Koch et al. 2002; Basdogan et al. 2004). Burdea et al. (1998) used a simple deformable mesh to describe the prostate surface for the diagnosis of prostate cancer, and created an interactive palpation trainer using a haptic device. The model was not physics-based, but led to a computationally efficient palpation model.

On the other hand, further studies indicated a need for more realistic physics-based modelling based on material properties. Similar heuristic models were employed by Dinsmore et al. (1997) for the palpation of sub-surface tumours in the liver and by Langrana et al. (1994) for virtual knee palpation. Others studied the mechanics of palpation for the location of tumours in the lungs and breasts (McCreery et al. 2008), and reported tissue behaviour far more complex than those described by the above mentioned models. A deformable model for breast simulation was explored by Balaniuk et al. (2006), where a simplistic model was used to analyse the visual effect of using implants in breast augmentation. However, real material properties were not included in their interpretation of the model.

To promote real-time interactivity and the dynamic behaviour of the deformable model, both the visual and tactile realism have often been sacrificed. The availability of properties that define the object material has to be effectively utilised. However, embedding real material properties into a deformable model is a great challenge. Not only do the existing methods need to be explored, but the previously discussed assumptions on the properties have to be correlated.

2.3 Physics-based Methods

Terzopoulos (2003) defined the deformable models as a class of physics-based modelling methods, which have been extensively utilised in various research domains that include computer vision, medical imaging and computer graphics. However, the techniques for deformable modelling may range from non-physical methods, such as Splines (Bartels et. al. 1987; Dachille et al., 2001), Free-Form Deformation (Sederberg & Parry 1986), Chainmail (Gibson, 1997; Tanguy et al. 2007) and numerical (Botsch et al. 2007) to methods based on physical principles, which

account for the effects of material properties, external forces, environmental constraints and object deformation (Gibson & Mirtich 1997; Maciel et al. 2003; Maciel 2005, Delingette & Ayache 2004; Chen et al. 2007, Adam et al. 2008). New advances in hardware resources allow physically accurate graphical simulation at interactive rates. However, an effective compromise between realistic modelling and interactive speeds is yet to be achieved.

Deformable models that are utilised for simulation must be physically realistic and possess a relatively low computational complexity. It has been demonstrated that the physics-based models have an advantage over previous computation animation techniques (Sundaraj 2004). This invariably means numerically solving the partial differential equations (PDEs) that govern the evolving shape of the deformable objects instead of incorrectly assuming the behaviours. Furthermore, bio-material properties can be explored and included in the design of the behaviour.

Therefore, the investigation interest is on the state of the art of the physics-based techniques that have been employed to simulate soft volumetric solids. Particular attention is also given to the real-time characteristic and high deformation. The two main methods described in this section are the Finite Element Methods (FEM) and the Mass Spring Systems (MSS). MSS is generally more feasible for real-time simulations of highly deformable solids compared to FEM which is more suitable for pre-operative planning or scientific analysis, where accuracy is more important than speed. It is also known to support small deformation.

2.3.1 Finite Element Method (FEM)

Finite element method (Bathe 1996) is claimed to be the most accurate method for solving a deformation problem under certain boundary conditions, where it considers

continuum physics. Continuum means that the objects are solid models with mass and energies distributed throughout. The method used for solving the PDE is discrete, even though the employed models can be discrete or continuous (Maciel 2005).

The method is used to determine an approximation for a continuous function that satisfies some equilibrium expressions. It decomposes the deformable object into a polygonal mesh. A function that solves the equilibrium equation has to be extracted for each mesh element, which is represented by a polynomial interpolation (Tanguy et al. 2007). Consequently, continuous representations with varying levels of continuity may be produced (Delingette 1998).

In solid mechanics, this mesh is employed to provide the discretisation upon which the elastic material functions of stress and strain are integrated. This requires considerable computation, which for many engineering applications is usually important, but not critical. It has been widely employed in soft tissue modelling but the linear constitutive law for the tissue is used in the context of small strains. Consequently, the displacement of nodes is constrained to be small.

Earlier works on soft tissue include attempts on emulating and predicting the deformable behaviour of living muscles (Chen & Zeltzer 1992; Hong Zhu et al. 2001). Williams et al. (2003) analysed breast using a simple model based on hemispheres. FEM, however, can provide a level of realism but is computationally less efficient (Batteau et al. 2004; Paloc et al. 2006) compared to the mass-spring approach. The linear elastic theory can only support small deformations of an object which is true for rigid materials. However, soft volumes, such as biological material, can deform in large proportions. Consequently, the small deformation assumption can no longer hold. Due to this, the amount of computation required at each time greatly increases.

In order to reduce computing time, attempts such as the condensation technique (Bro-Nielsen and Cotin, 1996), hybrid method (Kuhnapfel & Maab 1999; Cotin et al. 2000; Kuhnapfel et al. 2001), tensor-mass model (Cotin et al. 1998), boundary formulation (James & Pai 1999) and banded-matrix methods (Berkley et al. 2004) have been introduced. The resulting model, such as proposed by Bro-Nielsen & Cotin (1996), displayed homogeneous elastic behaviour to reduce complexity. This means that real-time solutions become possible despite the substantial pre-processing steps that reduce the versatility of the model. Real-time interaction was constrained within the selected operational areas. Any modifications in the structure, such as the topology, induced a new computation of constraints such as the matrices of the system (Meseure & Chaillou 2000). Therefore, the constraints will need to be pre-computed to support the various possible operational areas. Moreover, the need for off-line and substantial pre-computation is also a significant limiting factor to the topological changes of the mesh, which might be required to represent cutting and adaptive refinement at runtime.

If there are no topology changes, it is possible to obtain real-time deformations by using pre-computation (Sundaraj 2004; Dimaio & Salcudean 2005). Nevertheless this is still limited to small deformations, which can be a handicap for soft tissue simulations. This is also a limitation of the more recent work on the FEM-based warped stiffness approach to accelerate computation (Garcia et al. 2006). To address this issue, Mendoza & Laugier (2003) earlier proposed an implementation of an explicit formulation of FEM taking into account large deformations and topology changes. They managed to perform cutting on a virtual human liver by considering constraints such as specific interaction behaviours and limited stress conditions. However, versatility was still sacrificed, where extensive pre-computation steps as

well as the definition of the operational area still had to be carried out to confine the dynamic behaviour of each movable node of the mesh. Furthermore, the update and the intermediate caching of stiffness matrices within the local operational area demanded large memory space. Consequently, this results in the interaction framework becoming less flexible. Therefore, a large dataset to support volume would incur significantly higher computational cost. To address real-time issue, Adam et al. (2008) implemented a mesh-less approach, where deformation was generated relative to the interconnecting key points on the geometry and according to the pre-planned motion between key-framed poses.

On the whole, FEM has too heavy a computation burden to achieve accurate and interactive-time results for both volume and surface approach. Generally, FEM is not suitable for interactive and real-time applications for the present processing capacity. Besides, for soft solid, large deformation is an important requirement.

2.3.2 Mass-Spring Systems (MSS)

Mass-spring network representations of non-rigid bodies are able to exhibit elementary physical properties and have been popular for animation and image synthesis (Holbrey 2004) due to their simplicity and scope for efficient computation. Instead of starting with a PDE and subsequently discretising the object in space, such as FEM, MSS begins with a discrete model (Nealen et al. 2006).

An MSS model consists of discreet point masses connected by elastic spring links. When the network is mapped against the polygonal mesh, such as in figures 2.26 and 2.27, the MSS mesh network is created, where masses are the vertices and the springs are the edges. The mechanical properties of the simulated body are represented by data stored in the nodes and the spring links, where mass is associated with each node

and spring constant is associated with the edges. Springs connecting point masses exert forces on the neighbouring nodes when a mass is displaced from its rest position.

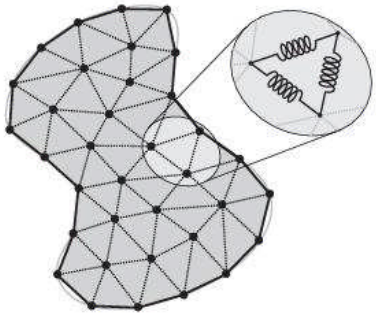

Figure 2.26: *MSS mesh network based on the triangular mesh*

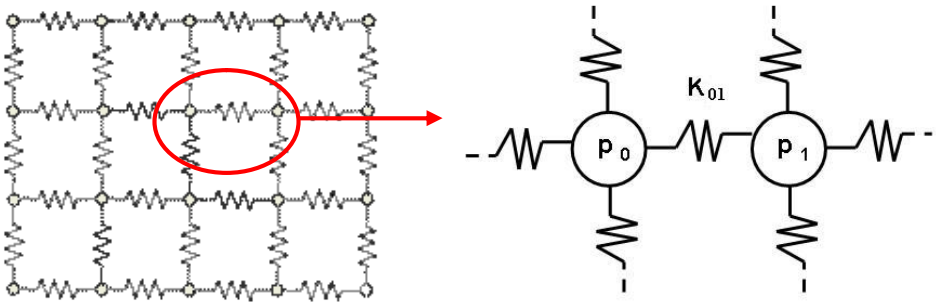

Figure 2.27: *A spring connection s with stiffness k_{01} between masses at nodes p_0 and p_1 based on the square elements of the mesh as an illustration of concept*

Hence, any change of length relative to a rest length will cause an internal force to occur between the spring nodes. The resulting force vector is calculated based on the stiffness constant and the damping constant ***b***. Each node in the mesh is subjected to the following equation with ***p*** being the coordinate vector of the node:

$$m\ p'' + b\ p' + \sum_s \vec{F}_s = \vec{F}_{ext} \qquad (2.6)$$

where, *p''*and *p'* are its respective velocity and acceleration, ***m*** is the mass at the node, b is the damping constant, $\vec{F}_s$ is the internal force along the spring connection ***s*** and $\vec{F}_{ext}$ is the total external force imposed on the node. The internal force $\vec{F}_s$ of the spring link ***s***:

$$F_s = k_{01}\left(\|p_0 - p_1\| - l_{01}\right)\frac{p_0 - p_1}{\|p_0 - p_1\|} \qquad (2.7)$$

where, $||p_0-p_1||$ is the magnitude of the displacement of the current state of the spring link $\boldsymbol{s}$ *(node pair* $\boldsymbol{p_0}$ *and* $\boldsymbol{p_1}$*)*, $\boldsymbol{l_{01}}$ is the rest length of the spring link, and $\boldsymbol{k_{01}}$ is the stiffness (spring) coefficient of the node pair. The resulting force is distributed to the both nodes in the opposite directions.

In the numerical integration techniques, either solved using explicit or implicit Euler[1], the spring constant determines the elasticity of the surface and mass plays an important role in determining the displacement of the nodes to produce dynamic behaviour of the simulated body. The acceleration of a node is extracted from its Newtonian relationship with the imposed force and mass, where it is next integrated with the time step to extract the current velocity, which in turn determines the displacement of the node at that time step.

This approach to modelling, which is also known as particle based, might best be described as "quasi-physical". Although the underlying mathematics has a basis in classical physics, it does not aim to represent material properties directly. Therefore, estimating the right properties is a great challenge. Instead, deformable bodies are approximated by a collection of point masses connected by weightless springs, which are usually damped to control vibration as described by equation 2.6. However, the employment of real material parameters have been explored in various works (Van Gelder 1998; Bruyns et al. 2002; Maciel et al. 2003; Mollemans et al. 2003; Chen et al. 2007; Llyod et al. 2007). However, these attempts are still not versatile and are constrained by the object shape and the tetrahedral mesh topology.

[1] Euler integration is a numerical integration for calculating trajectories from forces at discrete timesteps. Where first-order differential equations are solved with a given initial value.

MSS allows real-time computation and topological changes to be easily achieved for relatively large models, although subjective testing and an initial processing step is usually required to optimise the choice of properties for the elements (Hoppe et al. 1993; Eischen & Bigliani 2000; Radetzky et al. 2000; Maciel et al. 2003). Furthermore, the flexibility of the MSS is influenced by the following attributes:

i) The design of mesh topology

The regularity of the topology influences the way the MSS is configured. The number of springs per node conditions the global behaviour of the system. If the model is under-constrained, several equilibrium positions are possible and the model can exhibit incorrect behaviour (Delingette 1998). If the system is over-constrained (Bourguignon & Cani 2000), the range of deformation is restricted and the material properties are also modified (Hong et al. 2006).

ii) The deformation behaviour

Mass-spring models are not based on continuum mechanics (Holbrey 2004). However, for small deformations, a spring model behaves similarly to a linear elastic finite element model as verified by Keeve et al (1996) but the two methods cannot otherwise be easily compared. Even though methods based on the genetic algorithm (Joukhadar et al. 1997; Bianchi et al. 2004) have been introduced, the pre-computing requirement imposes constraints on the versatility of the model. The method involves pre-computing the MSS parameters for specific deformation behaviours. Consequently, real time activities such as adaptive mesh modification (Hutchinson et al. 1996; Bro-Nielsen & Cotin 1996; Choi et al. 2005, Sifakis et al. 2007) will be an issue. Furthermore, FEM models are commonly suitable for smaller deformations (Holbrey 2004), where MSS deals with highly deformable and elastic materials.

MSS is famously known for non-solid objects, such as cloth simulation (Lafleur et al. 1991; Carignan et al. 1992; Provot 1995; Volino et al. 1995; Baraff & Witkin 1998). Recent enhancement includes interactivity and real-time capability (Vasilev et al. 2001; Fuhrmann et al. 2003; Volino et al. 2005). The use of MSS for solid materials has been employed to animate face (Terzopoulos & Waters 1990; Parke & Walters 1996), which led to latter works on the simulation of bone and tissue interaction which were explored in various works such as (Lee et al. 1995; Teschner et al. 2000).

The trade-off between realism and efficiency was investigated by Teschner et al. (2004) where deformable tetrahedral and surface meshes were employed while preserving the volume and surface area. However, properties estimation based on real material properties was not explored. Eischen & Bigliani (2000) proposed rigorous comparisons between the FEM and the iteratively fine-tuned mesh properties, which resulted in similar results for small deformations. Maciel et al. (2003) attempted an extension to the MSS based on molecules system (as inspired by Jansson & Vergeest (2002)), which properties estimation depends on the corresponding mass-spring configuration and the original shape of the object.

Therefore, although suitability is high for real-time and large deformation compared to FEM, there is an obvious issue in properties approximation (Batteau et al. 2004). Incorrect estimation will produce properties such as large stiffness for the springs, which results in stiff rigid objects. This incurs poor stability that can cause slow simulation. Smaller time steps would be required by explicit solvers such as the explicit Euler method. However, for large deformation, stiff constants should be avoided to emulate soft solid behaviour.

To further enhance the real-time capability of the classical MSS, there has been an increase in the use of surface MSS for solid simulation, which utilises the assumptions of material properties. The surface approach is particularly popular in animations to reduce the computational complexity. Applications are such as suturing training (Promayon et al. 1996; Brown et al 2001), muscle deformation (Nedel & Thalmann 1998; Aubel & Thalmann 2000, Hong et al. 2006) and breast simulation (Aubel & Thalmann 2000; Vassilev & Spanlang 2002; Balaniuk et al. 2006). Not only was the mesh dimension reduced for the surface alternative but the computation efficiency was also improved. However, the issues in properties estimation and volume preservation are significantly magnified due to the non-existence of volume discretisation. Relevant attempts based on the surface approach are explored further in Chapter 3.

MSS, in general, has less computational complexity compared to FEM. However, there is a prominent challenge to parameterise its dynamic behaviour with real material properties and to promote volume preservation during simulation.

2.4 Issues

This section explores the attributes or issues that influence the characteristics of the deformable models employed in a simulation. It has been identified so far that the real material and physical properties have to be explored to define the behaviour of the deformable model. This motivates the natural inclination to the domain of the physics-based methods.

Nevertheless, there are issues such as the estimation of properties and the emulation of volume behaviour. Since real-time interactivity with deformable materials is a principal requirement for simulations such as for medical training, the following

discussion place special emphasis on the mass-spring systems. Other methods are also considered to provide a more general overview.

The issues general to simulation can include the trade-offs that are influenced by the type of simulation and the stability issues (Gibson & Mirtich 1998; Al-Khalifah & Roberts 2004). The latter is, however, less important due to the fact that the scope of the research emphasises highly deformable material. Therefore, the instability due to a stiff rigid system is not a foremost issue. On the other hand, stiff or rigid characteristics are directly instigated by the manner in which the properties are approximated.

For this reason, the next section discusses the key issues of immediate importance, where they directly influence the behaviour of the deformable models.

2.4.1 Types of Simulation

Generally, attributes such as the processing and storage capacity, influence the visual and tactile acuity of a simulation. However, the types of simulation and their respective requirements should play an important role in defining the trade-offs between the issues of realism and computational speed (Delingette 1998; Al-Khalifah & Roberts 2004). Furthermore, both visual and haptic perception of a human operator of a virtual environment is limited (Wall & Harwin 1997; Bordegoni et al. 2001; Batteau et al. 2004; Sur et al. 2004; Payandeh et al. 2005; Wuillemin et al. 2005). This provides the opportunity to explore the estimation of material behaviour from a reduced set of material values in the adoption of such assumptions for real-time and interactive simulation.

For a given surgical simulation, the two major constraints for the modelling of soft tissue are the deformation accuracy and the consequent computation time. Delingette (1998) summarised the different types of applications according to the two criteria as roughly demonstrated in figure 2.28.

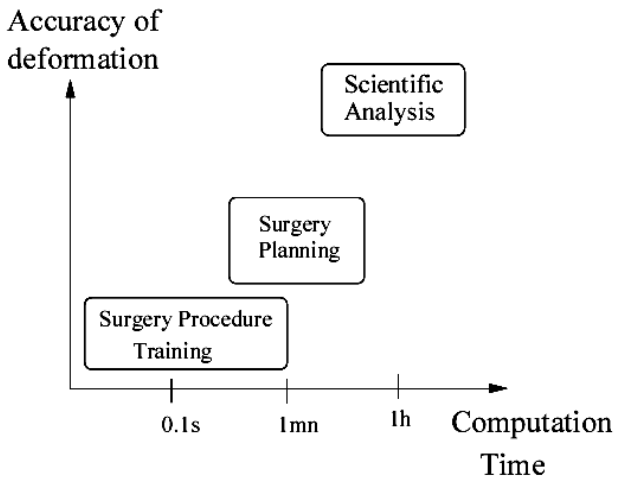

Figure 2.28: *The time versus accuracy requirements of the deformable model (Delingette 1998)*

These applications fall under two main categories as follows:

i) Pre- operative planning and analysis

Prior to a surgery, new procedures or surgical tools and materials can be evaluated and analysed. This includes both scientific analysis and surgery planning. Scientific analysis aims at validating the physical hypotheses of soft tissue for the design of new procedures or implants. In such cases, the accuracy of deformation is far more important than the computation time. Pre-operative planning involves effective evaluation and comparison of the possible outcomes of medical interventions and techniques. Consequently, the accuracy and fidelity of the employed model are of paramount importance. However, simulation time is secondary. Therefore real-time simulation is not particularly necessary and the dynamic behaviour at runtime is irrelevant (Williams et al. 2003).

ii) Intra-operative and real-time training

Surgical training requires real-time performance, where visual and haptic feedback can be produced at the correct frequency such that the user does not feel any discomfort (Sundaraj 2004). However, the accuracy and detail may be compromised to some degree. The extent of this compromise appears to vary from procedure to procedure. Assumptions on the physical and material properties have been employed such as discussed in section 2.2.1, where for training, a homogenous, linear and incompressible system can be employed to represent the global behaviour of soft tissues such as breast and liver. Existing commercial applications include the laparoscopic simulations as described in section 2.2.3, which rely less on the accuracy of the visual and haptic effect. Even though the accuracy is commonly sacrificed; new techniques to increase realism have to be explored.

Where accuracy is required, FEM can deliver at the cost of simulation speed and memory capacity. This is commonly required by pre-operative planning. The hybrid method and the adaptive meshing technique have been proposed to accelerate simulations, but these methods are not fast enough to achieve real-time interactivity. Pre-processing methods have also been extensively researched to overcome computational obstacles but they require an additional storage that depends on a pre-defined sampling space and behaviour. The operational area of the deformable model is also limited by these constraints.

For intra-operative training, speed is the main requirement and realism that is constrained by the limitation of human perceptual capabilities. Particle methods such as the MSS excel in this area, where it is simpler to implement and supports larger

deformations. On the other hand, although the MSS is simple and efficient, it is difficult to accurately model the behaviour of deformable objects because the elasticity is modelled only with compressible springs. The employment of material properties to define the behaviour of these springs has not been extensively explored.

For surgery training, for instance, realistic visual and haptic feedback is more important than the accuracy of deformation. However, if the difference of behaviour is too great under large deformations, it could result in learning inappropriate procedures. Therefore, real material properties are important in the definition of a deformable model.

2.4.2 Properties Estimation

Properties estimation is a great challenge for MSS. Since the model is tuned through its spring coefficients, good values for these constants are not always easy and straightforward to derive from material properties. Although most simulation systems opt for linear elasticity and homogeneous properties, the properties such as the spring constants and mass are a challenge to estimate (Bruyns et al. 2002). This is due to the fact that volume meshes can be irregular to meet the needs for various shape topologies as well as the need for a more refined LOD within the operational areas.

A volume model is commonly discretised into tetrahedral elements that can be used to determine properties such as the mass and spring constants represented by the resulting volume of each tetrahedron. Maciel et al. (2003) stated that to discretise an object by a set of springs, the stiffness of every spring must be proportional to the fraction of the volume of the object it represents. Previous works (Bielser 2003; Bourguignon & Cani 2000; Paloc et al. 2006) attempted to distribute mass to the

individual tetrahedral elements based on the volume of each element relative to the total object volume.

Since the tetrahedrons were deemed regular, the properties were also regularly distributed to the nodes. Bielser (2003) implemented an explicit FEM that utilised a regular method to distributing the properties to the respective tetrahedral nodes. His assumption was that the tetrahedron would always have identical faces. He assumed a fixed centre of gravity of the element in order to extract the barycentric relationship between the four nodes to the tetrahedral mass which led to the division of the tetrahedral mass by four. This assumption was also stated by Mollemans et al. (2003), Paloc et al. (2006) and Lloyd et al. (2007).

Based on the simplicity of distributing the same mass to the nodes and stiffness to springs and the assumption of regular tetrahedrons, many attempted to produce a mesh topology that is as regular as possible. Deussen et al. (1995) used simulated annealing to search for optimal parameters, where mesh nodes were re-positioned to produce regular mesh topology. The resulting uniform concentration of nodes led to the coefficients being distributed as regularly as possible. This significantly affects the versatility of the deformable model where such pre-computation has to be carried out upon any topological modifications. Furthermore, some irregular surface topologies require irregular mesh network. Morris (2006) implemented similar simulated annealing to calibrate the material parameters of his model.

Based on section 2.2.1.1 on homogeneity, an object with homogeneous material has the same behaviour in any of its part regardless of its mesh topology. For example, the object in figure 2.13 has irregular mesh topology but it should reflect homogeneous material behaviour irrespective of its nodes distribution. However, maintaining

material homogeneity is a challenge when the mesh topology is irregular. Distributing uniform values to this topology will result in inhomogeneous behaviour.

To address these issues, many researchers and developers opted for statistical or heuristic fine-tuning, where a variable was manipulated to map the properties such as the spring stiffness to the pre-calculated values or the pre-defined statistics. These approaches have been commonly employed by applications described in section 2.2.3. However, this method lacks versatility and requires costly pre-definition and re-definition when the model mesh is modified. This consequently requires properties to be re-established to preserve the model behaviour.

Eischen & Bigliani (2000) and Etzmuss et al. (2003) proposed a comparative method between the FEM and the iteratively fine-tuned MSS, which resulted in similar results for small deformations. Maciel et al. (2003) also proposed an iterative method, where the spring coefficients of the spring connections of the proposed molecules system, were fine-tuned by manipulating an unknown variable. The dynamics of the molecules system is represented by the corresponding volume MSS in figure 2.29.

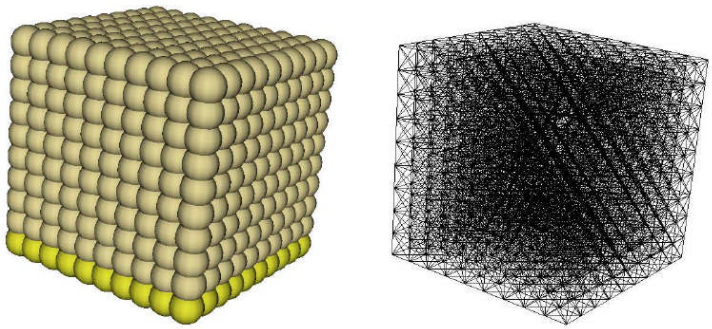

Figure 2.29: *Molecules system with 1000 molecules and 7560 spring connections (Maciel 2005)*

This variable was iteratively changed to modify the spring constants so that the elastic behaviour of the model reflected the original Young's modulus. However, this method can only be employed if the shape of the model is suitable for uni-axial tensile

analysis as discussed in section 2.2.1.2. The stress and strain relationship of the proposed model was used to derive the elastic modulus but other properties such as the shear and bulk moduli were not included in the estimation.

Expert fine-tuning has also been employed to modify the properties of the deformable model employed in training simulations (Radetzky &Nurnberger 2002; Brown et al. 2003), where the tactile feedback complements the visual feedback. Radetzky & Nurnberger (2002) obtained expert input assisted by a fuzzy-logic procedure, which employed a natural language. The terms employed to define the behaviour are solid, hard, soft, wobbly, doughy, and mushy (Holbrey 2004).

However, haptic recall is subjective and the consistency changes from one expert to another due to the limitation in the average visual and haptic perceptions of a human operator. A study undertaken by Sur et al. (2004) found that a small group of participants were reasonably sensitive to the changes in material properties such as the Young's modulus and the Poisson's ratio. But although most participants selected acceptable values for tissue parameters, opinion was observed to vary quite widely as to what realism really implied. The final simulation based on this technique was the correlation from the different perceptual inputs of the various experts as well as the developers' assumptions. As a result, the method of using expert opinion to fine-tune haptic feedback is not only rigorous but also unreliable and subjective.

A more sophisticated fine-tuning method was first introduced by Joukhadar et al. (1997). The method was called the genetic algorithm which was based on pre-computed constraints. Specific case scenarios or reference models were employed to design the constraints for the genetic estimation. They first used a numerical method to distribute the masses along the volume elements. The desired case specific

behaviour of the object was represented by a set of constraints, such as its position and orientation in the function of time, maximum deformation, velocity and acceleration.

Bianchi et al. (2004) employed a similar algorithm to identify spring coefficients as well as mesh topology in a volume MSS. The resulting mesh was compared to the FEM reference model. The method is computationally expensive and requires specific reference models. And the results may not hold for the different mesh resolutions as the method does not support real-time activities such as mesh topological refinement. Topological modification requires properties to be re-established in order to preserve the material and physical properties of the simulated model. Additionally, the internal volume mesh re-configuration was required to allow properties to be fine-tuned by the algorithm.

Instead of employing rigorous fine-tuning that takes away the versatility of the simulated model at real-time, a method to distribute properties to the deformable system has to consider the design of the mesh. Van Gelder (1998) introduced a method to calculate the stiffness for the elastic edges of the triangular and tetrahedral meshes in consideration of the regularity of the original mesh, where it has also been adopted by Bruyns et al. (2002), Mollemans et al. (2003) and Paloc et al. (2006) for regular tetrahedrons. Van Gelder's approach was based on the area of the triangles and the volume of the tetrahedrons formed by the edges. The elasticity modulus and the Poisson's ratio were included in the estimation. This method was then verified by the use of texture distortion to observe the surface homogeneous behaviour. However, the elasticity modulus of the resulting model was not compared to the original value.

Moreover, the estimation for volume mesh was dependent on the tetrahedral configuration.

2.4.3 Properties Re-estimation

In order to be versatile, the estimation technique has to support even the simplest topological modification. The most common modification employed in simulation is mesh refinement where the LOD of an operational area is improved. Methods, such as the adaptive refinement, have been employed by previous works (Debunne et al. 2001; Choi et al. 2005; Sifakis et al. 2007).

Issues include re-distributing the mass to the refined area, where the mass is either reduced or increased (Bielser 2003). The regular estimation employs the same barycentric method, where a quarter of the mass of the new tetrahedron is distributed to each of its four vertices. Other researchers opted for similar uniform distribution for their spring mesh but experimented on mass re-distribution to support the need for multi-resolution. Zhang et al. (2002) and Payandeh et al. (2005) proposed mass re-distribution after mesh refinement based on the ratio of the original total of nodes to the new total after refinement. Choi et al. (2005) varied mass per node of the new refined level based on the initial LOD, where the value of the new mass was calculated based on the average of the masses at the initial level and masses at the new refined level. However, the deformation patterns of the area before and after refinement showed that the consequent dynamic behaviour over time was dissimilar. Besides, the original mesh topology has to be regular for this calculation to be possible.

The estimation methods described in section 2.4.2 have to re-define the constraints. The statistical method, such as (Zhang et al. 2002; Payandeh et al. 2005), modifies the

spring constant for each spring based on the statistical comparisons. Other methods, such as: simulated annealing (Deussen et al. 1995; Morris 2006), iterative method (Eischen & Bigliani 2000; Etzmuss et. al 2003; Maciel et al. 2003; Pezzementi et al. 2008), genetic algorithm (Joukhadar et al. 1997; Bianchi at. Al 2004) and fuzzy-logic (Radetzky et al. 1998; Radetzky & Nurnberger 2002) require rigorous and complicated pre-computation. These methods are also infeasible for real-time topological modification.

2.4.4 Volume behaviour

Most volumetric objects are either incompressible or nearly incompressible. When deformed, the object preserves constant volume regardless of its elastic behaviour (Irving et al. 2007). Volume preservation can be independent of shape conservation, where the later indicates material elasticity.

The change in volume denotes the loss or increase that has to be compensated by manipulating the behaviour of the deformable model. Penalty force or pressure has commonly been applied to the mesh elements to offset these variations. Techniques vary from penalising the tetrahedral volume change (Picinbono et. al. 2001) to the global deformation manipulation (Hong et al. 2006). Irving et al. (2007) demonstrated 1 to 15 percent of volume losses for the proposed numerical method and the standard FEM (Poisson ratio in range of 0.45 to 0.499).

For volume methods, the change of volume of the individual tetrahedral element influences the volume penalty (VP) forces utilised by FEM and volumetric MSS (VMSS). In FEM, the VP method penalises volume variation by applying to each vertex of the tetrahedron a force directed along the normal of the opposite face (figure

2.30). This force introduces incompressibility to emulate the material resistance to the change in volume.

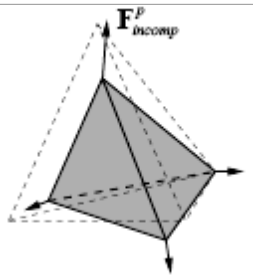

Figure 2.30: *Force penalty to compensate the volume variation (Picinbono et. al. 2001)*

The compensating force is calculated using the formula below:

$$\vec{F}^{P}_{incomp} = \left(\frac{V - V_0}{V_0} \right)^2 \vec{N}_P \qquad (2.8)$$

where, V is the current volume, V_0 is the relaxed volume and $\vec{N}_P$ is the normal of the opposite face. Coupled with FEM, the computational cost is very high but the volume as well as the shape of the object is preserved with minor variations. The force will always be positive, hence, the consistent pressure within the tetrahedron.

Bouguignon and Cani (2000) introduced a model, where the isotropic and anisotropic behaviour of the elastic material is controlled by the additional springs on top of the existing internal springs of the volume mesh. They were inspired by Promayon et al. (1996), where radial forces or displacements play an important role towards preserving a constant volume. The VMSS method is similar to VP for FEM where the tetrahedral elements will each have radial forces to compensate the variations of volume (Mollemans et al. 2003).

However, volume change is represented as a function of the total length of the nodes to the barycentre of the tetrahedron. The force direction is dictated by the unit vector of the current node from the barycentre (figure 2.31). Barycentre (B) is the average

position of the four nodes. The force (F) estimation is actually based on the MSS where the radial lines from the nodes to B are the barycentric springs.

For F_j of node j at position p_j is:

$$\vec{F}_j = -k_s \left[\sum_{i=0}^{3} \| \ p_i - B \ \| - \sum_{i=0}^{3} \| p_i - B \|_{t=0} \right] \frac{p_j - B}{\| p_j - B \|} \tag{2.9}$$

where, $\sum_{i=0}^{3} \| p_i - B \|_{t=0}$ is the total rest length of the barycentric springs, $\frac{p_j - B}{\| p_j - B \|}$ is the unit vector in the direction of the spring and k_s is the spring stiffness.

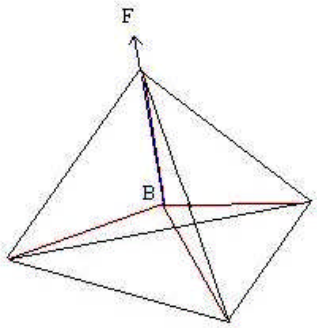

Figure 2.31: *Radial force F to preserve tetrahedral volume*

This method, however, introduces additional pressure on top of the complex network of internal springs (based on the tetrahedral elements). The object experiences stiffer behaviour as shown in figure 2.32 when a constant stretching force is imposed on a single surface node.

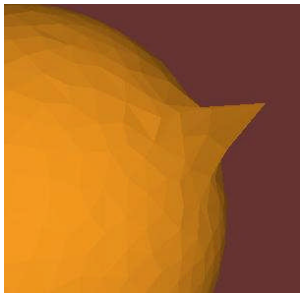

Figure 2.32: *A stiffer deformation produced by VP*

A similar technique was adopted by Vassilev & Spanlang (2002), where the penalty force was imposed radially to the surface nodes. Baudet et al. (2007) also employed

concentric pressure in order to promote volume conservation of the mesh elements (in the form of cuboids). Bulk modulus was employed to calculate the resulting pressure due to volume variation of these elements. The stiffness of the springs was extracted from the comparison to the imposed tensile parameters of the material. Nevertheless, the extraction method limits the feasibility to topologically modify the elements at runtime and the model is dependent upon the spring connection configured for each element.

The need to preserve volume should not compromise on the material properties of the object. The behaviour of the volume object should reflect the material properties with minimal discrepancies. Thus, the properties based on the real material attributes such as homogeneity, elasticity and incompressibility have to be sustained regardless of the design of the mass-spring topology.

Real-time volume preservation dependent on additional constraints that change the material properties is a challenge for VMSS. This requirement consequently influences the properties estimation technique.

2.5 Discussion

The scope of the research is specific to a material which is highly deformable, elastic, incompressible and homogeneous. It has been identified that the physics-based MSS promotes the benefits of rapid prototyping, computational efficiency and the support for large material deformation compared to FEM. These characteristics support the common generalisation in regards to the trade-off between speed and accuracy for training simulations (figure 2.28), where accuracy is overshadowed by the need for a more real-time and interactive environment. However, the efficiency is still restricted

by the mesh and computation complexity of the volume configuration employed by the classic MSS.

As an alternative to the VMSS, a surface approach (SMSS) promotes the same benefits as the volume counterpart but with lower mesh complexity. However, the difficulty in configuring the properties of the model is substantially increased. Consequently, the level of accuracy in terms of the material properties and volume behaviour is greatly reduced.

The ranking of the three approaches, namely FEM, VMSS and SMSS, is illustrated in table 2.2. The ranking is summarised based on the comparisons carried out by various authors, which reinforces the issue of accuracy in the employment of MSS in general and the surface alternative specifically. The implementation for the VMSS is more straightforward compared to the surface approach due to the existence of volume discretisation for the VMSS. However, the real-time computation of the surface model is more efficient. The accuracy, on the other hand, is an issue for both the MSS models.

Table 2.2: ***The ranking (worst (*)_to best (***)) of the common methods in deformable modelling***

	FEM	VMSS	SMSS	References
Implementation	*	***	**	Gibson & Mirtich 1997; Mendoza et al. 2002; Batteau et al. 2004; Delingette & Ayache 2004; Sundaraj 2004; Teschner et al. 2004; Maciel 2005; Choi et al. 2005; Dimaio & Salcudean 2005; Balaniuk et al. 2006; Hong et al. 2006
Speed	*	**	***	
Accuracy	***	**	*	

Even though accuracy is a great issue, a surface model is a potential alternative to its volume counterpart due to its simplicity and real-time interactivity. However, the fundamental issues that influence the implementation of a surface model are the same issues that influence the behaviour of a deformable model, which are estimation of the

properties and volume behaviour. The issue of the irregularity of a mass-spring topology is now magnified by the lack of volume information.

Acknowledging these concerns, the aim of the research is to address the issue of accuracy in the configuration of a surface model towards simulating soft solid objects in terms of the properties estimation and volume behaviour as well as in reference to the material parameters: elasticity, homogeneity and incompressibility. To achieve this aim, the objectives are:

i) To investigate the surface approach to address the issues of properties estimation and volume behaviour

ii) To address the shortcomings of a surface model, which are the non-existence of internal volume and the design of the surface mesh topology

iii) In accordance with the issues of properties estimation and volume behaviour, and with the consideration of the material parameters, an enhancement to the configuration of a surface model is to be proposed, which considers real material properties in the novel extension to the configuration.

iv) The research incorporates a proof of concept by the means of empirical evaluations that leads to the justification of the novel contributions to knowledge.

2.6 Conclusions

Volume objects such as biological tissues are materials of very complex behaviour. The non-linear properties vary from one sample to another and are dependent upon the structure and composition and are time and history dependent. As a consequence of such a wide set of variants, existing measured properties are not reliable and just barely describe the general behaviour of these materials. Despite that, specific situations can be delimited in which the behaviour can be established from a reduced

set of input material values. Linear elasticity of soft bio-tissues can be assumed for deformation that does not exceed the yield limit, such as breast palpation. The overall behaviour of the material can assume homogeneity and incompressibility. Such assumptions consequently increase the feasibility of a real-time simulation for intra-operative training.

Surface modelling has been identified as a potential approach in real-time simulation of deformable objects. The surface MSS has the same benefits as the classic MSS. However, the mesh complexity is lower, hence indicating a more efficient computational speed. However, the accuracy issue is magnified by the lack of volume and the characteristic of its mesh topology. Therefore, the same key issues such as the estimation of properties and volume behaviour influence the degree of effectiveness in modelling volume behaviour as well as the real material of the volume.

Acknowledging these issues, the next chapter explores the potential of employing a physics-based surface model towards emulating deformable volume behaviour, where the existing approaches and attempts within the scope of the issues are discussed.

Chapter 3
Deformable Surface Model

3.1 Introduction

A surface alternative to the volume method has been extensively employed in real-time simulations and animations within pre-defined constraints and fine-tuned properties. The capability of 3D scanners to contribute towards rapid generation of surface-based models also motivates this approach. The existing commercial products for intra-operative training simulation have employed surface models to promote real-time interactivity. However, the properties of the deformable model are not based on real material properties.

Furthermore, fine-tuning has been excessively employed before the final product was released. As discussed in chapter 2, this approach was not only rigorous but was also dependent upon the haptic recall capabilities of the experts. The issues that influence the deployment of such applications are the speed and the accuracy required by the types of simulation.

To capitalise on not only the large deformation and the computational efficiency promoted by a MSS but also the reduced complexity of a surface dataset, the surface MSS is of great interest instead of the more accurate but complex FEM. However, the issue with a surface model is the lack of volume. Without the internal meshing, a surface model is naturally unable to preserve shape and volume when deformed. Preserving the volume of a solid model involves manipulating the internal tetrahedral elements using either FEM or VMSS.

The internal network of springs as employed by the classical VMSS introduces high computational cost. Furthermore, animating constant volume deformations is not exactly straightforward (Bourguignon & Cani 2000). On the other hand, the surface alternative has no internal medium to preserve shape and volume. Therefore, without any internal support, the model will collapse under the influence of gravity (figure 3.1).

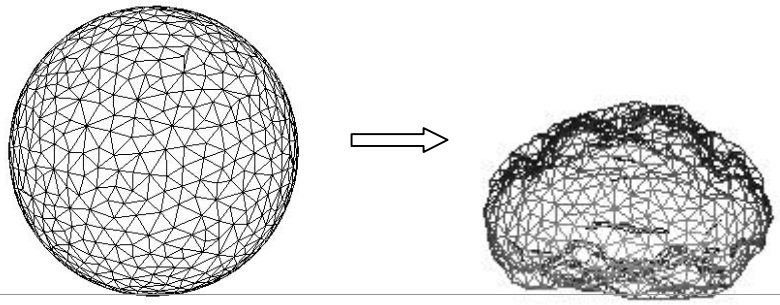

Figure 3.1: *The classic surface MSS collapses when gravity is switched on at runtime*

Not only will shape not be preserved during simulation, but the global deformation effect will also be incorrect upon interaction. For instance, as shown in figure 3.2, the interaction on the surface of a solid tube does not produce a global deformation effect on the opposite side of the interaction point.

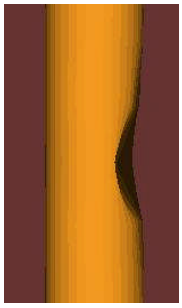

Figure 3.2: *Incorrect global deformation due to the absence of the internal volume*

The feasibility of employing a surface model depends on the properties defined for its material, which consequently establishes the deformable behaviour of the desired solid object at runtime. Hence, the physics-based techniques employed by a surface model in general have been explored to provide the overview within the scope of the

issues concluded in Chapter 2. These issues include properties estimation and the emulation of both local and global volume behaviour constrained by the design or the modification of the original mesh topology as well as the absence of internal volume.

3.2 State of the art

3.2.1 Volume Behaviour

Since there has been an increase in employing a surface model to emulate soft solid in real-time simulation, it is important to explore the existing techniques to manipulate the surface elements in order to achieve not only shape but also volume conservation during simulation. This supports the scope of a deformable model that is elastic, homogeneous and incompressible.

3.2.1.1 Re-meshing

To enable volume simulation, surface data can be manipulated to produce volume data. This approach formulates the internal definition of a surface model. In the Visible Human Project (NLM 2001, 2003), the geometrical dataset, normally a surface dataset, was extracted by segmenting the desired object from the scanned images, such as depicted in figure 3.3.

The flow illustrates the derivation of a volume mesh from a surface mesh. However, the re-meshing procedure was lengthy and the material properties would need to be re-distributed based on the new volume mesh topology (Hong et al. 2006). The re-meshing procedure was also dependent upon the constraints based on the specific scenarios. For example, how refined the internal volume should be and whether inhomogeneous material properties influence the discretisation.

Based on the example shown in figure 3.3, the complexity of the femur model was greatly increased (NLM 2001). The surface model originally had 2,482 nodes and 4,935 surface triangular elements. However, the complexity was increased to 20,689 nodes and 102,742 tetrahedral elements for the resulting volume model. Methods such as FEM and VMSS (section 2.4.4) utilise volume models to emulate solid behaviour. The resulting complexity significantly affects the computational speed if the model is to be deformable in response to real-time interactivity.

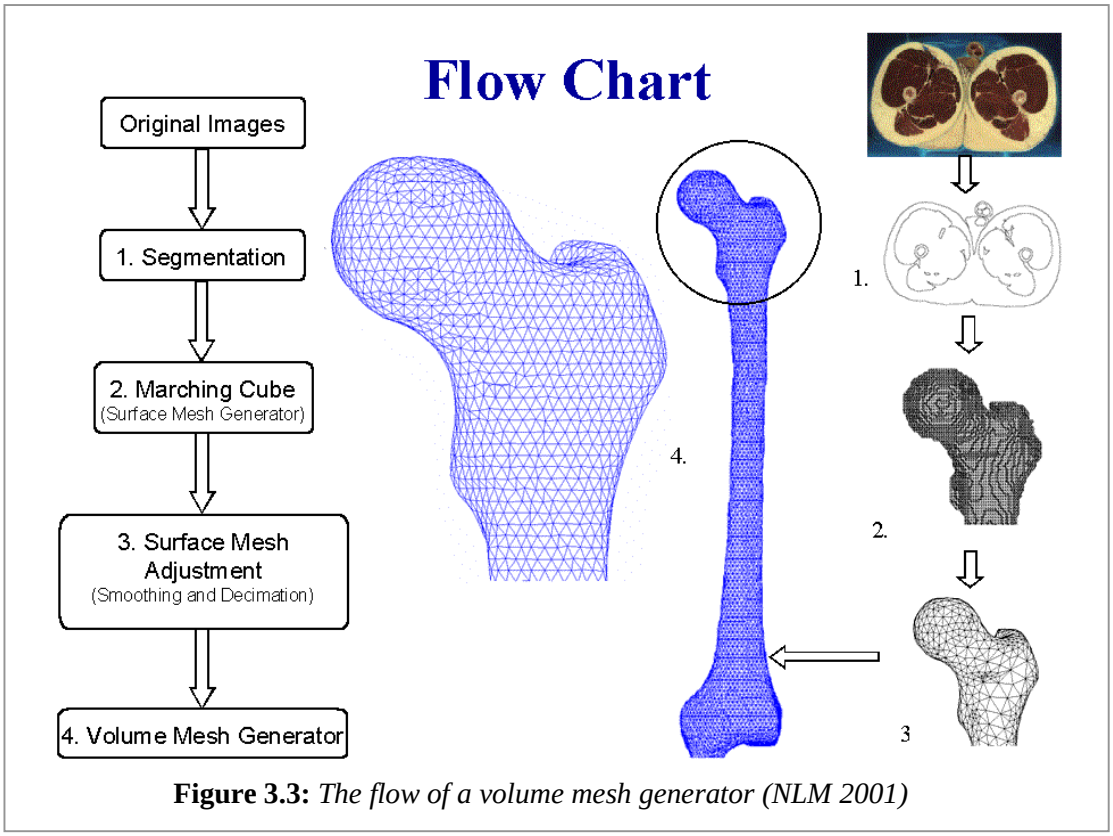

Figure 3.3: *The flow of a volume mesh generator (NLM 2001)*

In perspective, the benefits of a surface model that include lower mesh and computational complexity, establish the potential of the surface approach in the development of an interactive and real-time simulation of deformable objects. Moreover, a homogeneous and elastic setting that is often assumed by a surface model is justifiable by manipulating the flaws in human perceptual capabilities (Wall &

Harwin 1997; Bordegoni et al. 2001; Batteau et al. 2004; Sur et al. 2004; Payandeh et al. 2005; Wuillemin et al. 2005).

3.2.1.2 Virtual elements

As an alternative to creating physical elements such as the tetrahedral mesh to reflect solid behaviour, the surface model can be discretised into virtual elements in order to provide a conceptual framework for the internal definition. To fix the anomaly illustrated in figure 3.2, additional artificial springs that connect all the nodes to one another can be employed to emulate a more realistic deformation effect, where homogeneity is still promoted. In figure 3.4, Brown et al. (2001) connected the surface nodes to one another in a complex spring network in order to preserve volume and shape of a blood vessel model. The model was subjected to a much stiffer condition due to these additional elements (Bourguignon & Cani 2000; Hong et al. 2006). Moreover, the material properties were consequently modified (Hong et al. 2006). Thus, this approach is not versatile and the complexity increases with the number of mesh nodes.

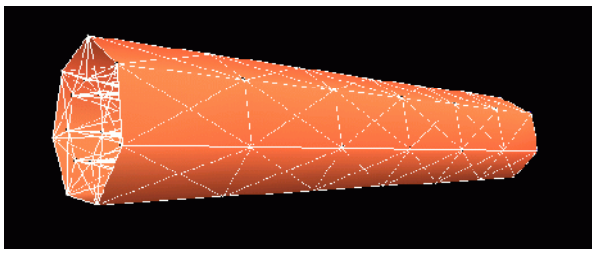

Figure 3.4: *A blood vessel is physically modelled by re-meshing the surface data to create a complex internal spring network (Brown et al., 2001)*

Vassilev & Spanlang (2002) introduced similar support springs based on the virtual discretisation in order to provide volume preservation during simulation. Assuming that the topology was regular, radial springs were implemented to connect the nodes to the object centre. The forces acting on the surface node were based on the overall

change in the total support spring length and the change in the individual spring length. The spring coefficients assumed a regular value, where it is similar to the stiff model utilised by Bourguignon & Cani (2000). Force penalty was determined based on the variation of the total lengths of the radial links within the individual tetrahedral element.

The Long Element Method (LEM), as illustrated by figure 3.5 (a), assumed an object as two-dimensional distributed elements filled with an incompressible fluid (Laugier et al. 2001; Costa & Balaniuk 2001; Balaniuk & Salisbury 2003; Balaniuk et. al. 2006). But at the same time, each element was also expected to obey Hooke's Law in the uni-axial direction. Pascal's principle and the law of conservation of volume served as boundary conditions to establish the state of equilibrium.

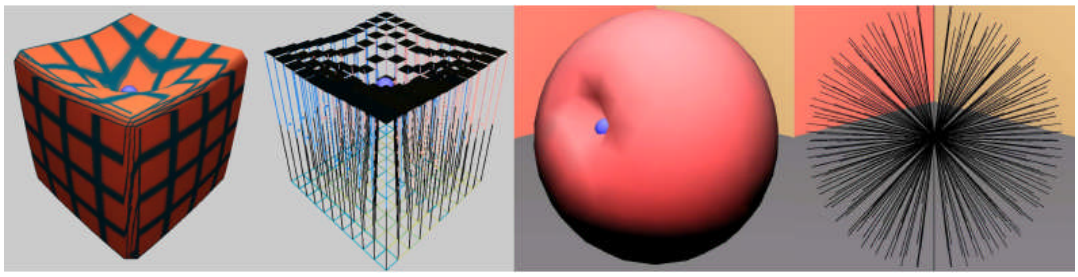

(a) (b)

Figure 3.5: *(a) LEM (b) REM (Balaniuk et. al., 2006)*

Error in the discretisation arose when the object experienced large deformation resulting in inconsistent outcomes and the absence of volume preservation. A straight-forward solution would be to discretise the object at each simulation interval. Nevertheless, this approach was not computationally efficient. Consequently, the validity of the LEM for interactive simulations is debatable although some of its assumptions, such as incompressibility are reasonable.

The Radial Element Method (REM) is a technique that was based on LEM (Balaniuk & Salisbury 2003; Balaniuk et. al. 2006). Instead of using long elements; radial elements were discretised for the internal volume, where links were created from the centre to the surface nodes (figure 3.5 (b)). The discretisation was similar to the technique described by Vassilev & Spanlang (2002), where the objects were deemed to be convex or star-shaped to allow these connections. This approach was motivated by the use of breast simulation for breast augmentation analysis. Real material properties were not included in the formulation of the boundary conditions that defined the dynamic behaviour of the breast model. This method was more applicable in the prediction of the breast shape after undergoing an augmentation with implants.

3.2.1.3 Pre-defined constraints

Constraints can be pre-defined to control the behaviour of the deformable object at runtime, such as the desired shape variations during deformation. For instance, the shape and motion of a deformable model were pre-planned relative to the key-frame poses and the geometry key-points as implemented by Adam et al. (2008). This method limits the behaviour of the model. Subsequently, it requires the estimation of boundary movements for different possible scenarios.

Boundary constraints have been employed to simplify the use of FEM (Nealan et al. 2006). The boundary element method (BEM) is a numerical computational method of solving linear PDEs which have been formulated as integral equations. The formulation of the boundary elements requires fully populated matrices. Consequently, the cost in storage and computational will also likely to increase. To address this issue, compression techniques have been introduced. However, the complexity increases with a success-rate that significantly depends on the nature of

the problem being solved and the geometry involved. The speed is unnecessarily sacrificed for the sake of realism even if complete accuracy is not crucial. Furthermore, it is not feasible when topological changes are likely (Delingette & Ayache 2004; Nealen et al. 2006). For that reason, although improvements have been proposed for FEM such as BEM, the computational complexity still increases substantially with the number of finite elements. This highlights that the drawbacks of FEM still prevail compared to MSS, especially for real-time simulation.

Based on MSS, there have been some attempts that addressed the shape conservation of a regular surface mesh. These attempts mostly revolved around simulating human muscles (figure 3.6). Human muscle simulation was attempted by combining a surface MSS with regular topology and an action line that either represented the force produced by the muscle on the bones (Nedel & Thalmann 1998; Aubel & Thalmann 2000) or a control line that was confined to a pre-defined behaviour. Nedel & Thalmann (1998) introduced angular springs to control the object surface shape during deformation, which consequently produced a stiffer model.

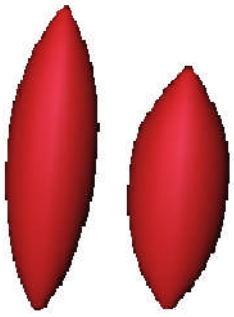

Figure 3.6: *Muscle contraction based on a surface mesh with near-exact volume preservation (Aubel & Thalmann 2000)*

Hong et al. (2006) extended these methods by introducing weighted constraints to dictate the deformation distribution of the muscle instead of using additional springs. They proposed a volume preservation technique using an implicit constraint

enforcement scheme and a deformation zone technique to achieve the local volume-preserved deformation by automatically distributing a weight vector to a closed surface model. As demonstrated by figure 3.7, the weighted constraints can be distributed based on the desired shape behaviour. Consequently, force penalty can be irregularly distributed to the surface mesh in response to volume variation, where the deformation effect is constrained by the boundary and volume constraints.

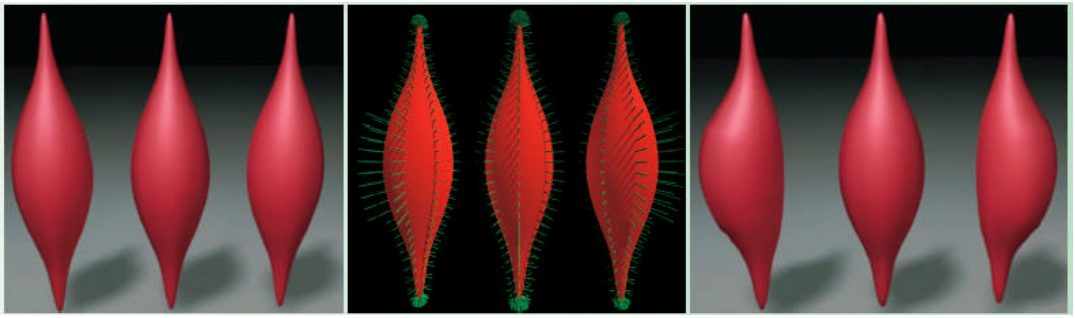

(a) (b) (c)

Figure 3.7: *Pre-computed weights to constrain deformation effect: (a) uniform weights (b) initial weights redistribution (c) effect of the weights (Hong et al. 2006)*

The resulting global effect reflected a deformation distribution based on the pre-defined behaviour and the relative volume conservation came close to the FEM volume penalty method. Even though the deformation effect adhered to the desired shape fixed by the initial weight distribution, this proof of concept has significantly illustrated the potential in manipulating a surface model to emulate a global deformable effect in response to the change of volume.

This concept was later extended to allow adaptive weight estimation for each node based on the local radius of influence of the interaction point. The consequent effect is illustrated in figure 2.21 when equation 3.1 was employed to manipulate the weights:

$$w_i = \left(\cos\left(\frac{\| p_i - p_f \|}{r} \right) + 1 \right) / 2 \qquad (3.1)$$

where, p_i is the position of node i, p_f is the position of interaction and r is the radius for the deformation zone within the user-specified threshold. The approximation only handled the immediate local deformation and was independent of the orientation of the interaction force.

This, therefore, restricts the flexibility of the model as the deformation behaviour will have to be defined for each possible interaction location. Additionally, to achieve both local and global deformation effects regardless of the absence of internal volume, the orientation of the interaction force relative to the surface normals has to also be considered at runtime.

3.2.1.4 Pressure model

Pre-defined constraints are not versatile for simulation that demands real-time interactivity. To conserve volume during real-time deformation, the consequent variations have to be compensated in order to maintain the original value. Most attempts in soft solid modelling assume the behaviour of an elastic surface that encapsulates incompressible fluid. Incompressibility is emulated, where the penalty pressure or force is distributed to the surface elements of the resulting deformable model in response to its volume variations. Such pressure models have been employed in works carried out by Costa & Balaniuk (2001), Matyka & Ollila (2003), Balaniuk & Salisbury (2003), Sundaraj (2004), and Balaniuk et al. (2006).

Matyka & Ollila (2003) achieved a soft solid effect by employing the thermodynamics concept for pressure calculation. A simple and regular surface MSS and the integration of the second Newton law provided the surface behaviour of a soft body with fixed or non-fixed internal air pressure. Pressure was also distributed radially that demonstrated a ballooning effect (figure 3.8). Properties, however, were

approximated as uniform based on the regular topology. Therefore the constraints had to be re-defined for different topologies. This method is particularly suitable for simple computer animations.

Figure 3.8: *The ballooning effect of pressure within a surface MSS (Matyka & Ollila 2003)*

Based on the radial discretisation technique, the REM technique (Costa & Balaniuk, 2001; Balaniuk & Salisbury 2003; Balaniuk et. al. 2006) is particularly well suited for simulating convex objects such as breasts. The breast was simulated as a surface skin filled with incompressible fluid. The radial elements were configured as mass-lesssprings, defined by their respective lengths, areas and elasticity coefficients. The mesh topology employed was regular to simplify the estimation of properties. The relationship between the stress (internal and external pressures) to the respective strain influenced the equilibrium equation defined for each radial element. The static equilibrium condition stated that the forces, or pressures, inside the element should be equal to the external forces, or pressures, applied externally. This equation was used to determine the change in length of the radial elements when a stress exists. The global conditions or constraints defined for this equation are the surface tension, the Pascal principle and volume conservation.

A similar approach was proposed by Sundaraj (2004), where pressure was an important parameter in conserving the volume of a surface model. The method, which

was called the Volume Distribution Method (VDM), was also based on LEM. However, the difference is that the surface was not discretised into virtual volume elements. VDM also used bulk variables such as pressure, volume and bulk modulus as the model parameters. To constrain the shape of the model in response to volume variation, Pascal's principle and volume conservation were used as boundary conditions. The limitation of this method is the distribution of pressure and volume, which was dependent on the area of each of the surface triangular elements that was deemed regular. This highlights the consequent issue in properties estimation, which will be discussed in section 3.2.2.

3.2.1.5 Shape preserving springs

To avoid a complex internal spring network, a more effective support springs method can be adopted into the MSS, where zero length springs were placed at the nodes (Laugier et al. 2000; Meseure & Chaillou 2000; Laugier et al. 2001; Mendoza et al. 2002; Laugier et al. 2003; Zhang et al. 2002; Choi et al. 2005; Payandeh et. al 2005). The additional complexity is only O(n), where it is proportional to the number of nodes instead of to the number of tetrahedrons for volume meshing. These springs are independent of one another to avoid the complex additional spring network employed by other methods. The method is also known as the shape memory springs (Promayon et al. 1996; Marchal et al. 2005), which was utilised to emulate elastic characteristics. A simple illustration of the surface and memory springs of an object is shown in figure 3.9.

These springs have been employed in various simulations such as the simulation of skin behaviour of a virtual thigh (Laugier et al. 2000; Mendoza et al. 2002; Laugier et al. 2003). Choi et al. (2005) implemented these springs to preserve the shape during

simulation to avoid surface collapse when a force was imposed on the nodes (figure 3.10). The stiffness of the springs was mostly fine-tuned based on pre-defined properties (Zhang et al. 2002; Payandeh et al. 2005) such as using pre-calculated and location specific values from a probing device (Laugier et al. 2000; Mendoza et al. 2002; Laugier et al. 2003). Choi et al. (2005) employed regular values for the springs prior to any topological modifications.

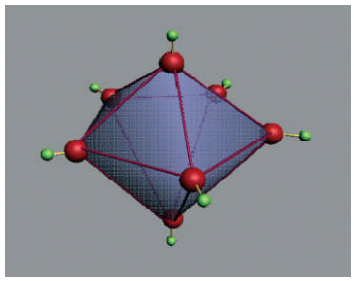

Figure 3.9: *Shape Preserving Springs (green memory springs) (Choi et al. 2005)*

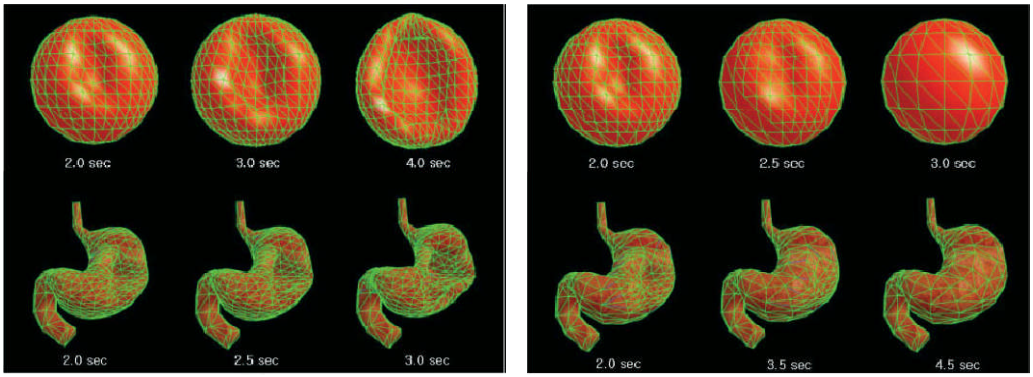

(a) (b)

Figure 3.10: *Deformation behaviour (a) without, and (b) with the shape memory springs (Choi et al. 2005)*

These springs, though, do not consider the volume preservation of the object and real material properties. The solid impression was achieved by opposing the shape change at runtime. There is a potential in this approach for a highly deformable object confined within a static global environment, due to the shape conserving capacity. However, these springs require an approximation of coefficient based on real material properties.

3.2.2 Properties Estimation

Conserving volume to reflect incompressibility is inadequate to reflect the true properties of a non-rigid solid. The deformable behaviour has to also reflect the material properties. Therefore, the estimation technique is crucial for the configuration of a deformable model.

As discussed in sections 2.4.2 and 2.4.3, the approximation of properties for MSS in general is a great challenge. Furthermore, any topological modifications require properties to be re-established to conserve the material behaviour. The complexity is increased as the dimension of the polygonal mesh is reduced for a surface model. This is due to the fact that the surface alternative does not have the internal discretisation to guide the determination of the appropriate material properties.

3.2.2.1 Properties Initialisation

Cignoni et al. (1999) and Villard & Borouchaki (2002) stated that the mass of a node element could be approximated proportionally to the area of the neighbouring faces (triangles) in order to preserve the total mass of the object. Based on the relationship described by Bourguignon & Cani (2000) and Bielser (2003), mass can be distributed to the surface triangular elements. Assuming the triangles are regular, a third of the mass of the triangle can be distributed to each mass.

VDM (Sundaraj 2004) implemented regular triangular elements assuming the barycentre as the centre of each triangle. Consequently, the area was distributed to the node elements based on the barycentric contributions from the neighbouring triangles as illustrated in figure 3.11. Volume compensation pressure was then distributed to the nodes based on their respective areas during deformation. As a result, the pressure distribution assumed that the triangular elements would remain regular despite the

possible irregular distortions during simulation. The volume represented by each node was extracted from the ratio of the area over the total area. This is, of course, infeasible as area is two dimensional. Hence, the surface area does not correctly represent the volume under the surface. Internal volume discretisation has to be considered in the properties extraction.

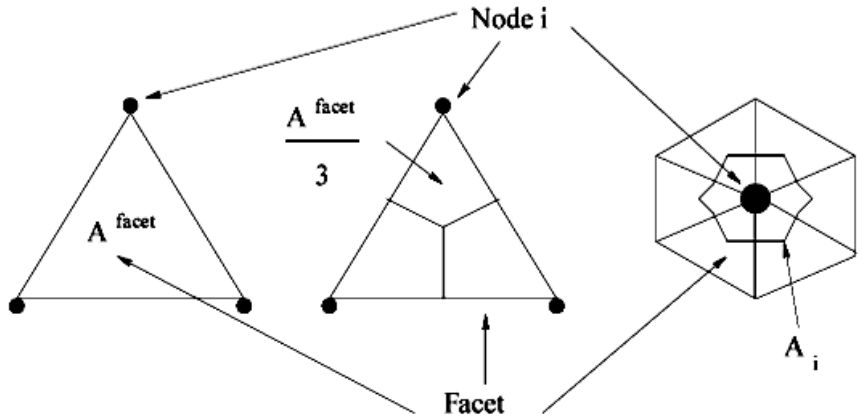

Figure 3.11: *(a) A regular triangle (facet) with 3 nodes (b) Regular area distribution based on the barycentre (c) The sum of area at node i from the neighbour contributions (Sundaraj 2004)*

To simplify properties distribution and to promote homogeneous material, mesh elements have commonly been arranged in a regular topology (figure 2.12(a)) (Delingette 1998; Van Gelder 1998; Bourguignon & Cani 2000; Brown et al. 2001). If the mesh topology is perfectly uniform, the simplest way to determine mass at each node is to divide the total mass with the total number of nodes. As discussed in section 2.4.2, Deussen et al. (1995) fine-tuned the topology by re-positioning the nodes to produce a more homogeneous topology and employed an annealing method to iteratively determine the mesh properties, which was also used by Bhat et al. (2003) and Morris (2006). Consequently, the regular concentration of nodes led to the masses being distributed as uniformly as possible. This method is not only computationally expensive but it is not versatile when it comes to the different mesh resolutions.

Moreover, regular topology is impractical for many deformable bodies as the surface of the simulated body may not necessarily have the same amount of node concentration as previously demonstrated in figure 2.13 and 2.14. The nature of the shape of an object should determine the node concentration based on the surface topology and curvature. In most simulation, the accurate visual effect is most important within the local area of interest. The area of interest is the radius of influence of the interaction point on the object surface, where visual acuity is predominantly focused (Zhang et al. 2002; Choi et al. 2005). To do the same amount of computation for the other areas would of course be less computationally effective. Any topological changes or deformation should be computed locally. Brown et al. (2001) stated that the system should effectively limit the computations to those portions of the object that undergo significant deformations.

Most simulations using a surface model employ the assumption of a homogeneous material. Thus, it is important at this stage to produce a homogeneous material despite the topology design. Distributing regular properties to an irregular mesh topology will produce an inhomogeneous material due to the different spatial concentration of nodes at the different parts of the surface. Bhat et al. (2003) and Bianchi et al. (2004) stressed that uniform elastic material cannot be determined by employing regular mass-spring properties, but irregular properties distribution is required to support the topology design.

As discussed in section 2.4.2, Van Gelder (1998) distributed properties to the spring elements based on the topology of a surface mesh. His surface method was plausible, where the distortion observation during deformation demonstrated that the proposed

estimation was more realistic compared to the regular approach. Figure 3.12 illustrates that the proposed method produced a more uniform distortion of circles on the texture.

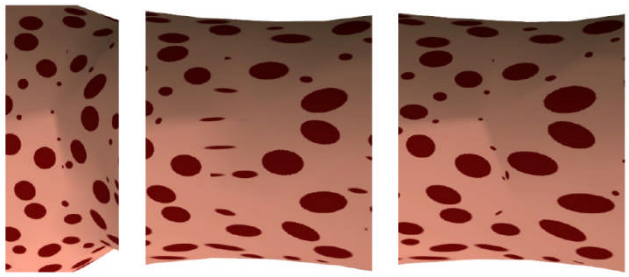

(a) (b) (c)

Figure 3.12: *Elastic surface membrane (a) unloaded (b) stretched (regular stiffness coefficients) (c) stretched (irregular spring stiffness) (Van Gelder 1998)*

On the other hand, solid behaviour is of interest in this thesis. Even though the estimation method is suitable for an elastic surface membrane, solid behaviour has to be reinforced. The three dimensional extension of this approach involves internal tetrahedral elements based on volume dataset. Consequently, it is not feasible to have a surface model without the existence of an internal mesh.

The attempt, however, highlights the feasibility of employing an irregular approach to support the realistic dynamic behaviour of both surface and solid by addressing the design of the mesh topology. The design of the topology directly influences the PDE employed to calculate the node displacement as imposed by force on the object. Mass embedded in each node directly affects the displacement of the nodes in response to the internal and external force distribution. Assuming that the properties, such as mass and spring constants have been irregularly distributed to each element, force dissemination should also be irregular respective of the topology (Bielser 2003). Most researchers opted for regular mass and stiffness distribution for even the irregular mesh topology. This causes an abnormal concentration of mass at different parts of

the body which produce stiffness anomalies. Therefore, properties have to be estimated based on the nodes concentrations.

3.2.2.2 Topological Refinement

Topological modification results in the re-approximation of properties. Properties should not only be correctly distributed but also preserved upon the modification of mesh topology. The topology can be altered to enhance visual acuity or to respond to virtual incision as employed in medical simulation. Both require properties to be re-distributed to preserve the material behaviour of the object.

To assess the versatility of an estimation method, the simplest topological modification, such as mesh refinement, has to be supported in order to address a more complicated requirement in the future. The multi-resolution technique has been widely employed to support the operational area (Zhang et al. 2002, Choi et al. 2005, Payandeh et al. 2005). The refinement for multi-resolution can be made adaptive depending on the force of interaction and surface curvatures as illustrated by Choi et al. (2005). This area of interest normally undergoes mesh subdivision to improve the concentration of nodes. The computational cost of both visual and haptic rendering can be optimised by concentrating any rendering within this area. Other areas outside of the zone of interest will undergo a less costly global simulation.

The material properties of the model should be preserved after subdivision. The degree of conservation is portrayed by the deformation behaviour within the area. The behaviour can be represented by the displacement patterns of the node elements. For instance, node C (figure 3.13) should reflect identical displacement patterns before and after subdivision with minimal deviation.

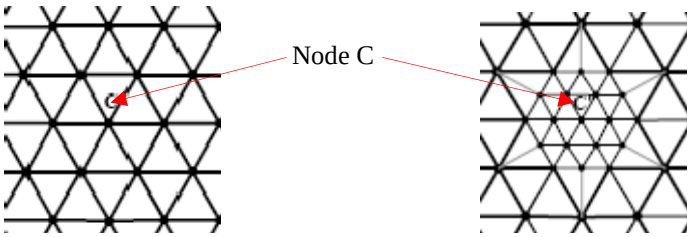

(a) (b)

Figure 3.13: *(a) Before refinement (b) after one-level refinement*

Zhang et al. (2002) and Payandeh et al. (2005) stressed that the surface should display the same deformation behaviour and tactile feedback before and after refinement. For this reason, the deformation behaviour has to be preserved but the visual effect should be effectively enhanced within the refined area (figure 3.14).

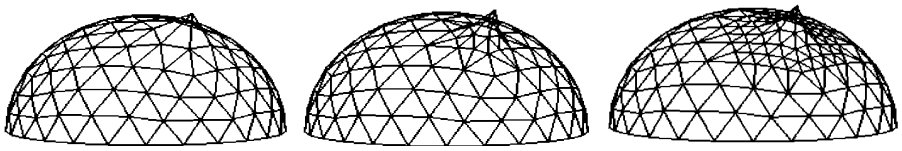

(a) (b) (c)

Figure 3.14: *Deformed (a) original mesh (b) one-level (one ring) mesh subdivision (c) two-level (two ring) mesh subdivision (Payandeh et al. 2005)*

For regular topology, re-estimation of properties was carried out based on the number of the new nodes within the refined area. Zhang et al. (2002) proposed mass and spring re-distribution after subdivision. The new mass and the inner spring coefficient for the nodes within the subdivided area, ***m'*** and ***k'*** were calculated as:

$$m' = \frac{m\ N}{N'} \qquad \text{and} \qquad k' = \frac{k\ N}{N'} \tag{3.2}$$

where, ***m*** and ***k*** are the regular mass and stiffness value at each node, ***N*** is the total number of nodes in the area prior to subdivision and ***N'*** is the number of nodes after subdivision. Payandeh et al. (2005) implemented a similar technique to initially determine the properties of the subdivided elements. Based on the offline node displacement analysis before and after subdivision, the values were statistically fine-tuned to preserve the displacement behaviour.

Choi et al. (2005) recommended an adjustment scheme to support multi-resolution. Regular mesh topology was initially assumed. Upon refinement based on the pre-defined criteria, they varied mass per node of the new refined level relative to the initial level. The value of the new mass is the average associated with the mass at initial level and mass at the new refined level. For instance, for node ***i*** (red triangle) in figure 3.15, the mass calculation for that node is as follows:

$$M_i = \frac{(Mass\ of\ zerolevel\ node * 2) + (mass\ of\ onelevel\ node * 3)}{5} \qquad (3.3)$$

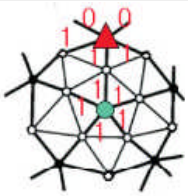

Figure 3.15: *Mass nodes in multiple details level (Choi et al., 2005)*

The consequent displacement pattern of the coarse (pre-refinement) mesh did not coincide with the refined mesh (figure 3.16). The patterns of pre- and post-refinement should be conserved with minimal deviation. This is to ensure that the material will display similar behaviour during deformation (Zhang et. al. 2002; Payandeh et al. 2005). Moreover, the existing estimation required the original mesh topology to be regular and an irregular original mesh was not explored.

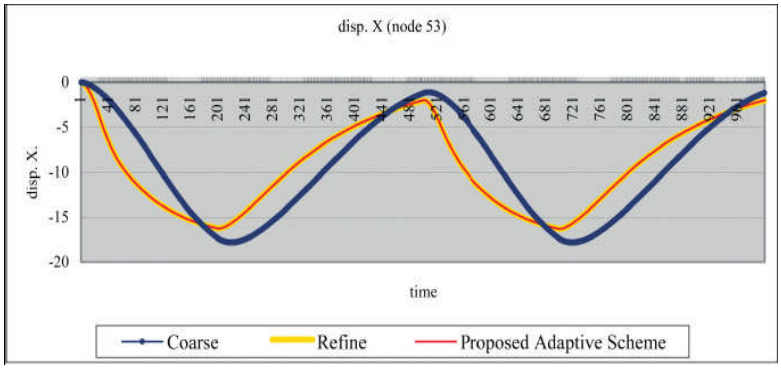

Figure 3.16: *Displacement Comparisons (Choi et al. 2005)*

There is clearly a gap in the domain of properties estimation and re-estimation within the scope of a surface model regardless of the mesh topology and the absence of internal volume.

3.3 Discussion

The analysis of the previous approaches in volume simulation recognises the advantage of a much smaller problem size by employing a surface MSS. The benefits of a surface model include rapid prototyping, less mesh and computational complexity as well as the support for large material deformation. Attempts to emulate solid behaviour by manipulating the surface models have been reported. However, these models were confined within the pre-defined constraints and properties which were fine-tuned. The main approaches that address the main issues are summarised in table 3.1.

It is acknowledged that the key issues include the configuration of properties and volume behaviour based on real material properties, which are constrained by the design of mesh topology and the non-existence of internal volume. The existing approaches fail to recommend a complete framework that addresses both issues. Nevertheless, the potential of a surface model towards emulating soft volume behaviour can be explored by correlating the techniques discussed in this chapter and chapter 2. These approaches include the adaptable discretisation employed by the shape preserving springs that promote elasticity and the impression of internal substance, the pressure model that responds to the volume variation at runtime, and the internal discretisation of virtual elements that can potentially assist in the configuration of properties. Particular interest is to explore the use of these techniques in an attempt to approximate the material properties of the internal substance in

relation to the tensile properties as well as the material parameters (table 3.2) as previously described in section 2.2.1.

Table 3.1: *Summary of main approaches discussed in various works*

Issues	**Approaches**	**Authors**
Properties estimation and re-estimation (volume and surface approach)	Regular distribution	Deussen et al. (1995), Delingette (1998), Bourguignon & Cani (2000), Brown et al. (2001), Paloc et al. (2002), Bielser (2003), Mollemans et al. (2003), Sundaraj (2004), Paloc et al. (2006), Lloyd et al. (2007)
	Fine-tuning (topology, coefficients)	Deussen et al. (1995), Joukhadar et al. (1997), Radetzky & Nurnberger (2002), Maciel et al. (2003), Brown et al. (2003), Sur et al. (2004), Morris (2006), Pezzementi et al. (2008)
	Irregular distribution	Van Gelder (1998), Bruyns et al. (2002), Mollemans et al. (2003), Paloc Et al. (2006), Lloyd et al. (2007)
Volume behaviour for surface model	Re-meshing	NLM (2001)
	Virtual elements	Brown et al. (2001), Costa and Balaniuk (2001), Vassilev & Spanlang (2002), Balaniuk & Salisbury (2003), Balaniuk et. al. (2006)
	Pre-defined constraints	Nedel & Thalmann (1998), Aubel & Thalmann (2000), Hong et al. (2006), Nealan et al. (2006)
	Pressure model	Costa and Balaniuk (2001), Balaniuk & Salisbury (2003), Balaniuk et. al. (2006), Matyka & Ollila (2003), Sundaraj (2004)
	Shape preserving springs	Laugier et al. (2000), Meseure & Chaillou (2000), Zhang et al. (2002), Mendoza et al. (2002), Laugier et al. (2003), Choi et al. (2005), Marchal et al. (2005), Payandeh et al. (2005)

Table 3.2: *Summary of the main soft assumptions on material properties*

Properties	**Authors**	**Assumptions**
Homogeneous	Koch et al. (2002), Basdogan et al. (2004), Dimaio & Salcudean (2005), Roose et al. (2005), Balaniuk et al. (2006), Ruiter et al. (2006), Zhang et al. (2007), Rajagopal et al. (2008)	An organ can be represented as homogenous because inhomogeneity does not increase real-time simulation accuracy. For instance, in a real time simulation, the overall deformation of a breast can be represented by a homogeneous material, such as the adipose tissue, where the overall deformation behaviour is independent of inhomogeneous nature. Model validation can be performed on homogeneous phantoms
Linear Elastic	Cotin et al. (1999), Cotin et al. (2000), Tanner et al. (2001), Janssen and Vergeest (2002), Maciel et al. (2003), Etzmuss et al. (2003), Dimaio & Salcudean (2005), Chui et al. (2007), Zhang et al. (2007)	Linear elasticity provides the standard for simulations in science and engineering. The influence of linear elastic tissues differs little from non-linear on the overall model. Modelled with the addition of linear elastic skin, the breast model deforms plausibly. Furthermore, soft tissues such as liver have been assumed isotropic in the extraction of its material properties. However, ambient viscosity and damping can be introduced to the linear system for each model elements based on the material density, volume, and the velocity of the elements at runtime.
Incompressible	Girod et al. (1996), Delingette (1998), Laugier et al. (2000), Picinbono et al. (2001), Azar et al. (2001), Delingette & Ayache (2004), Sundaraj (2004), Chui et al. (2007), Roan & Vemaganti (2007), Samani et al (2007), Rajagopal et al. (2008)	Living tissue is deemed incompressible as it is essentially made up of fluid. For example, liver is 95 percent blood and breast mostly consists of adipose tissue. Adipose and fibro glandular tissue of a breast can be considered to be incompressible. The incompressibility assumption furthers the characterisation of the mechanical behaviour of breast tissue.

These assumptions are feasible due to the limitation in visual and haptic perception in a virtual environment. The parameters, as briefly summarised in table 3.2, further justify the motivation behind the exploration of a surface MSS within the scope of a globally deformable solid confined within a static environment (static global position). The consideration of these attributes should dictate the manner by which the deformable model is configured in order to substantiate the rigour of properties estimation and volume effect.

3.3.1 Scope and goal

The scope of this current research involves the need to emulate soft solid objects such as a human breast, with the aim to improve the accuracy of the configuration of the deformable model. The work is thus within the domain of intra-operative training simulation. The increasing relevance of the use of a surface approach instead of the volume counterpart has also shaped the research direction. By employing a surface model, the benefit of lower mesh and computational complexities can be achieved. Furthermore, the availability of 3D scanning devices contributes towards the rapid generation of surface models.

Taking breast simulation as the real-time application, the potential of the shape preserving springs can be exploited. This is due to the constraint on the global positional dynamism of the model, where it has to be fixed. Additionally, this approach also supports the emulation of elastic material and avoids the complexity of the internal spring networks. The complete scope of the deformable model is elaborated upon in Part II.

The aim of the research has been to improve the accuracy of the configuration of a surface model towards simulating soft solid objects in terms of the estimation of

properties and volume behaviour as well as in reference to the material parameters: elasticity, homogeneity and incompressibility.

Acknowledging this issue, the main goal of the proposed framework in the following part (Part II) of the thesis is to generate a deformable surface model that:

i) adopts real material properties based on the assumptions of elasticity, homogeneity and incompressibility in the configuration of its properties,
ii) addresses the issue of the design of the mesh topology and its influence on the estimation of properties,
iii) establishes the relationship between the surface elements and volume,
iv) demonstrates the local and global deformation behaviour in response to external force influences regardless of the non-existence of volume.

Part II explores these considerations and consequently proposes a physics-based surface model parameterised with real material properties.

3.4 Conclusions

Both chapters in this part addressed the first two objectives of the thesis, where the existing techniques, the immediate issues and the assumptions that influence the emulation of deformable objects have been investigated. Based on the scope of a real-time simulation, a surface model imposes less complexity in terms of the finite elements and the subsequent computation involved in simulating their dynamic behaviour. The resulting deformable effect is supported by a surface MSS, where it supports the need for highly deformable material. However, to adhere to the assumption of elasticity, the yield limit is not to be exceeded. For this reason, simulations such as breast palpation can be supported in future applications.

Previous methods employed pre-defined constraints and pressure models in response to volume variation during deformation. Therefore, the motivations behind these methods are correlated to guide the configuration of a deformable model that not only conserves volume during simulation but also adopts the existing material properties such as the elasticity modulus, despite the absence of volume elements and the design of the mesh topology.

The proposed deformable model is discussed in Part II, where Chapter 4 introduces the scope of the simulation and the deformable model as well as the preliminary volume discretisation for the configuration of the model. Chapter 5 describes the ensuing techniques for the proposed estimation of material properties and volume behaviour as well as the relevant evaluation approach.

- PART II -

THE PROPOSED

DEFORMABLE MODEL

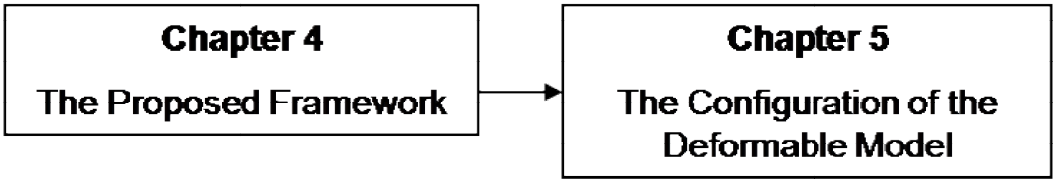

"Generosity is giving more than you can, and pride is taking less than you need."

Kahlil Gibran (1883-1931)

Chapter 4
The Proposed Framework

4.1 Introduction

Real-time simulation of a deformable solid is commonly constrained by the complexity of the classic model that is based on volume datasets. Volume datasets have been employed in models such as FEM that are particularly suitable for smaller deformations and are commonly employed in pre-operative analysis, where real-time requirement is unnecessary. Although the method has constantly undergone various modifications to enhance computational speed, versatility is still significantly sacrificed. This is due to its complete dependency upon pre-computed constraints which can be very case specific. The bigger the dataset, the more memory space it demands to store the immediate constraints.

For intra-operative simulation of soft solid entities such as human organs in medical training, it is important to support large deformations and interaction as well as possibly mesh modification at runtime. Since a homogeneous and linear system can be employed without affecting the realism of real-time simulations, a surface model is a potential alternative. The model is aimed at conceptual rapid prototyping where generality and simplicity are commonly more important than perfect precision. There is no deformable model that is perfectly accurate for soft volume simulation, not even theoretically. However, it is beneficial to explore the possibility of a full or partial generality which can be utilised within the scope of this current research.

Despite the fact that embedding real material properties in a MSS is a great challenge, the feasibility in utilising these properties is explored. This chapter introduces the framework for the deformable model according to the objectives in section 3.3.1. The properties of the model are further configured based on the techniques subsequently discussed in Chapter 5.

4.2 The Simulation Framework

4.2.1 General Overview

The current research involves the definition of the deformable model that can be adopted by the existing simulation framework (intra-operative), specifically the deformable model thread as described in figure 2.24. The configuration of the ensuing model sits within the extension established at the preliminary stage of the simulation flow as illustrated in figure 4.1. The scope also includes the runtime manipulation of the model in the deformable model thread according to the new configuration. The flow of the initialisation and the runtime activities are summarised in appendix C.

The geometrical data of the model is initially read into the system and stored in a binary space partitioning (BSP) tree to optimise the visual and haptic rendering of the model in real-time (figure 4.2). The mesh information that includes the vertices, faces, edges and the subsequent neighbour relationship (figure 2.11) is used to construct the deformable model and to define its physical and material properties. The research does not include the construction of mesh topology from the raw surface datasets but it rather employs the existing geometrical mesh to construct the deformable model. Consequently, the initial mesh extraction method as illustrated in figure 3.3 is excluded from the research scope.

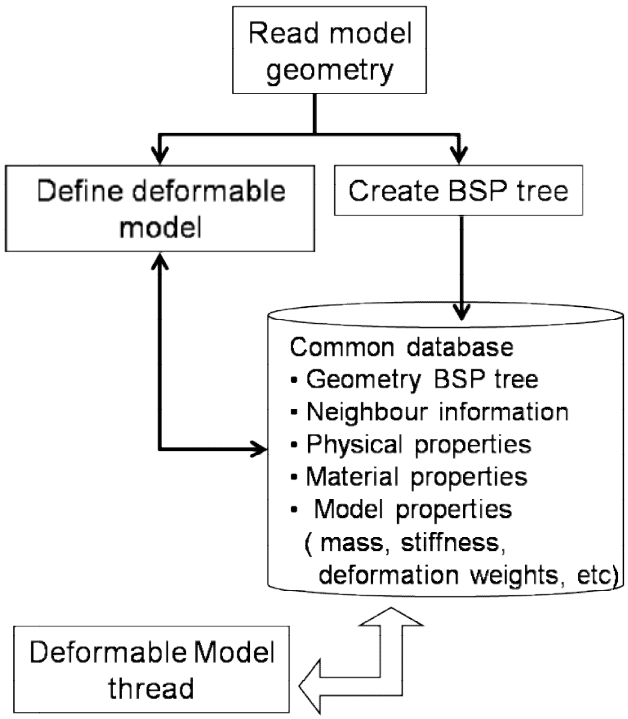

Figure 4.1: *The initialisation flow for the deformable model thread for the adopted framework in figure 2.24*

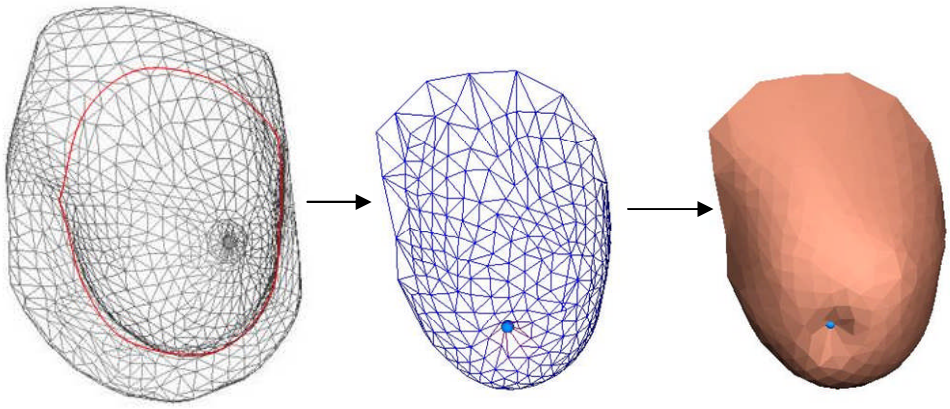

Figure 4.2: *Extracting a geometrical mesh for a breast to create the visual representation*

Within the deformable model thread, the virtual representation of the object can be interacted with by employing a desktop haptic device (figure 4.3). The mesh information is manipulated by both haptic and graphic rendering where the surface mesh is made up of triangular elements. For experimental purposes and proof of concept, the interaction is based on a point interaction and a penalty collision method.

Explicit Euler integrator is utilised to support large deformations as stiff or rigid solid systems are not within the scope.

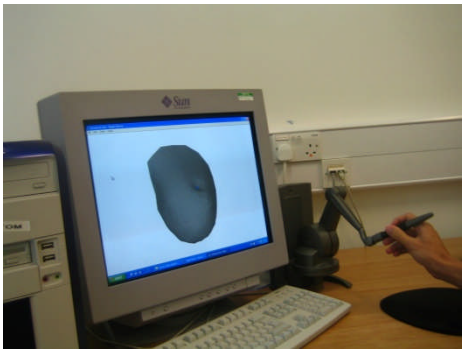

Figure 4.3: *A Haptic device (Phantom Desktop) used to interact with the virtual model*

The deformable behaviour of the soft body upon any external interaction is reflected by the haptic and visual feedback. Figure 4.4 illustrates the simulation achieved by the proposed framework. The soft solid should produce both local and global deformation in response to interaction.

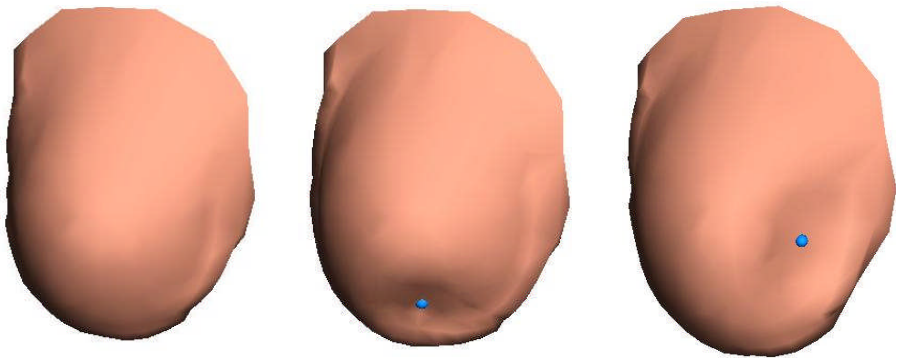

Figure 4.4: *A generalised deformable breast model interacted with a haptic probe (blue sphere)*

To enhance the accuracy of such behaviour, the deformable model has to be configured with real material properties. The implementation of the deformable behaviour correlates with the framework of the physics-based modelling technique, specifically the MSS. To facilitate the investigation and implementation, the scope of the model behaviour requires definition to establish the domain within which the

research is carried out. The proposed surface model will adhere to the scope definition in tackling the key issues discussed in Part I.

4.2.2 The Scope of the Deformable Model

Based on the scope and goal discussed in section 3.3, the research is interested in the dynamic behaviour of a soft solid with negligible global spatial movements, such as a breast on a static chest (figure 2.21, 4.2 and 4.4). A breast demonstrates a convex shape at rest positions (Vassilev & Spanlang 2002; Hieber et al. 2004; Balaniuk et al. 2006). These characteristics are thus considered in the modelling of a deformable body in this thesis.

The scope of the behaviour adheres to the parameters established throughout the thesis, which are homogeneity, elasticity and incompressibility (as summarised in table 3.2). By mitigating these assumptions, the surface approach has been explored as a possible alternative to the classic volume method due to it being computationally less-demanding and simpler to implement. Hence, by disregarding the dependency of the overall deformation on the inhomogeneous nature of an object such as a breast (Roose et al. 2005; Ruiter et al. 2006), the utilisation of surface formulations is possible.

The behaviour of the soft body as a whole upon interaction is more important than the reaction of the different tissue types. Moreover, the tissue location varies in cases. The non-linear properties vary from one sample to another and are dependent upon the structure composition, time and history. As a consequence of such a wide set of variants, existing measured properties are not reliable and just barely describe the general behaviour of these materials. On the other hand, specific situations can be

delimited in which the behaviour can be established from a reduced set of input material values. These values conform to the assumptions of the material behaviour.

In addition, the yield and tensile limits of the elastic material are not to be exceeded. This adheres to the assumptions for the amount of force proposed for breast in the application of tumour detection. The palpation force was advised to be within the range of 1 to 2 Newton (Patkin 1998). This will consequently produce a deformation that will not exceed the original size of the breast. However, for larger deformations, larger magnitudes of force will be explored.

Human tissue such as breast is deemed incompressible. Such soft body assumes an elastic skin as the surface, and is filled with an incompressible homogeneous material. The surface deformable model regards such assumptions. For instance, due to the high content of adipose in breast, it is possible to deduce that it is incompressible and of homogeneous material. Moreover, linear elasticity can be assumed since the yield limit of the material will not be exceeded during the simulation. An ambient influence of viscosity is also included in the configuration to emulate the viscosity of tissue.

The properties estimation based on these assumptions contributes towards realistic behaviour in real-time simulation. To address the issue of properties estimation as well as the non-existence of inner volume for the proposed surface model, the object's internal volume represented by the surface mesh elements has to be determined. To define the volume contribution to the approximation of properties, initial discretisation is required to extract the homogeneous volume distribution under the surface elements. The resulting definition will be utilised to establish the respective properties based on the real material properties.

The research is not directly within the domain of bio-mechanics or medicine. Consequently, the scope does not include the extraction of bio-material properties and the specific studies of such properties. However, a range of published material properties, as described in table 2.1 and 3.2, will be directly utilised to exemplify the proof of concept in implementing the assumptions of the behaviour of the deformable model.

4.3 The Surface Model

The configuration of the deformable model with the material properties is dependent upon its mesh topology and the physics-based method employed to emulate the ensuing dynamic behaviour. The surface mesh topology is enhanced in order to formulate a deformable model towards emulating soft solid behaviour. Regardless of the absence of internal volume, the surface model should not only retain its shape during simulation but also the object volume to promote incompressibility. The assumptions of linear and homogeneous material behaviour instigate the exploration of the classic surface MSS and the shape preserving springs. The subsequent enhancement is the core of the proposed deformable model.

4.3.1 Surface Springs Topology

The surface MSS is based on the surface mesh topology that consists of nodes and springs represented by the edges of the triangular elements (section 2.3.2). As illustrated in figure 4.5, nodes with mass $\mathbf{m_i}$ and $\mathbf{m_j}$ are linked by a spring with stiffness $\mathbf{k_{ij}}$. The surface behaviour is represented by this spring network. Instead of looking at the spring force described by equation 2.5, the individual contribution to node $\boldsymbol{i}$ is defined. The connection force at node $\boldsymbol{i}$ with coordinate $\boldsymbol{p_i}$ based on the spring link in figure 4.5(b) is:

$$\vec{F}_i = -k_{ij}\left(\left\|p_i - p_j\right\| - l_{ij}\right)\frac{p_i - p_j}{\left\|p_i - p_j\right\|} \tag{4.1}$$

where, $||p_i-p_j||$ is the magnitude of the displacement of the current state of the spring link, $\boldsymbol{l_{ij}}$ is the rest length of the spring link, and $\boldsymbol{k_{ij}}$ is the stiffness (spring) coefficient of the node pair.

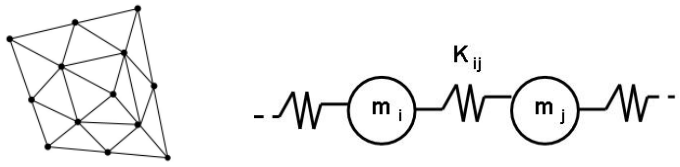

(a) (b)

Figure 4.5: *Surface mesh topology: (a) the nodes or vertices connected by edges (b) a pair of nodes (i and j) or masses (m_i and m_j) connected by a spring with stiffness k_{ij}*

The topology can be irregular to support the need for multi-resolution in haptic and graphics rendering. This spring network will not be able to preserve volume behaviour during deformation due to the absence of the inner spring mesh. The inner supports, which are initially based on the concept of the shape preserving or shape memory springs, are subsequently extended to provide the volumetric reinforcement.

4.3.2 Volume Springs Topology

In order to preserve the rest shape of the object; the inner springs have to be defined to provide support to the mass at the nodes (figure 4.6), where the concept of shape memory is adapted (section 3.2.1.5). The volume springs, also considered as the virtual elements, work in a similar way to the surface spring but the rest length of the spring is zero. Unlike the additional springs adopted as the virtual elements described in section 3.2.1.2, these springs are independent of the surface springs as well as of one another. The complexity is O(n), where n is the number of surface nodes. In consequence, the complexity of the internal spring network can be avoided.

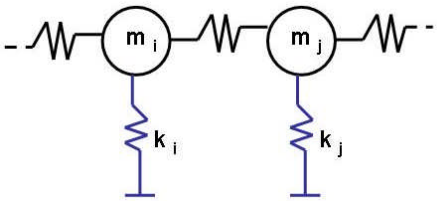

Figure 4.6: *The mass spring network with surface and volume springs*

Based on equation 4.1 and figure 4.7, but rest length is equal to zero, the reaction force at volume spring will only affect mass at node ***i***,

$$\vec{F}_i = -K_i\left(\left\|p'_i - p_i\right\|\right)\frac{p'_i - p_i}{\left\|p'_i - p_i\right\|} \tag{4.2}$$

where K_i is the stiffness of the inner spring at node ***i***, p'_i is the new position of node ***i*** at runtime and p_i is the anchored position of node ***i***.

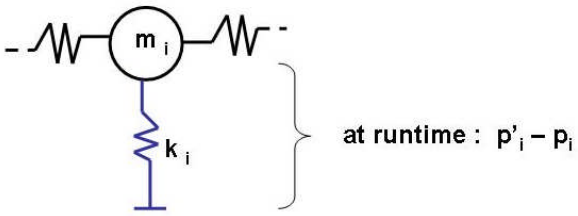

Figure 4.7: *An inner spring stretched during simulation*

The stiffness describes the level of elasticity of a virtual space or volume represented by the node. The stiffness coefficients are derived respective to the normal of the surface nodes in accordance with the uni-axial tensile analysis. Based on section 2.2.1.2, elasticity can be described by three main parameters which are the uni-axial, shear and bulk tensile properties. These characteristics are considered when the estimation method is derived in order to counter the issue of inflexibility in terms of the springs dimension and to extend its role from preserving the object shape at equilibrium to dynamically preserving the object volume during simulation. The spring coefficients can now be established with regards to real material properties. The proposed techniques are elaborated upon in Chapter 5.

4.3.3 The force model

Based on the proposed topology, this section summarises the force model that governs the mechanics of its dynamic behaviour. The model is described by two attributes, ***i*** and ***S***, as defined below:

- The index ***i*** of the surface nodes, where $0 \leq i < n$ and ***n*** is the total number of nodes. This index is used to identify the mass and the stiffness of the volume spring at each node.
- A set of the surface spring connections, $\boldsymbol{S} = \{S_{i1}, S_{i2}, \ldots S_{is}\}$, directly linked to each node ***i***, where $S_i = \{ S_0, S_1, \ldots S_{n-1}\}$ and ***s*** denotes the total number of connections.

The model behaviour is determined by the forces produced at each node ***i*** by each connection of ***S*** and some external forces. Hence, for all nodes (i = 0…n-1), the force contribution at node ***i***, $\boldsymbol{F_i}$ is:

$$\vec{F}_i = \vec{F}_C + \vec{F}_G + \vec{F}_L \tag{4.3}$$

where:

$\vec{F}_C$: The force contribution from the spring connections

$\vec{F}_G$: The global force contribution

$\vec{F}_L$: The local force contribution

4.3.3.1 The connection force

The force contributions, $\vec{F}_C$, from the spring connections to node ***i*** is defined by the following equation.

$$\vec{F}_C = \vec{F}_S + \vec{F}_V + \vec{F}_D \tag{4.4}$$

where:

$\vec{F}_S$: The force contribution from the surface spring connections local to the node. Based on equation 4.1, the force is defined as:

$$\vec{F}_S = \sum_{s=1}^{|S|} -k_{ij}\left(\|p_i - p_j\| - l_{ij}\right)\frac{p_i - p_j}{\|p_i - p_j\|} \tag{4.5}$$

where, $\boldsymbol{p_j}$ is the other member of the current spring connection in the calculation.

$\vec{F}_V$: The force contribution from the volume spring. Based on equation 4.2, the force is defined as:

$$\vec{F}_V = -k_i\left(\|p'_i - p_i\|\right)\frac{p'_i - p_i}{\|p'_i - p_i\|} \tag{4.6}$$

$\vec{F}_D$: The internal damping as illustrated by equation 4.7.

$$\vec{F}_D = \sum_{s=1}^{|S_i|} -b_{ij}\left(\vec{u}_i - \vec{u}_j\right) \tag{4.7}$$

where, $\boldsymbol{b_{ij}}$ is the damping coefficient. Vectors $\vec{u}_i$ and $\vec{u}_j$ are the velocity of the masses at node ***i*** and ***j*** respectively.

4.3.3.2 The global force

$\vec{F}_G$ includes the gravitational influence as well as the ambient friction. Furthermore, since the proposed model is a surface model without any internal volume, the penalising force to compensate the loss and increase in volume at runtime has to be imposed on the surface nodes. The volume compensation force or force penalty is discussed in chapter 5.

The global force influence is as described by equation 4.8.

$$\vec{F}_G = \vec{F}_g + \vec{F}_f + \vec{F}_P \tag{4.8}$$

where:

$\vec{F}_g$: The gravitation pull $\vec{g}$ imposed on mass $\boldsymbol{m_i}$, where,

$$\vec{F}_g = m_i\vec{g}$$

$\vec{F}_f$: The frictional force imposed on the whole object by the environment (global medium) opposing the individual mass movement (velocity). For

instance, the gravitational pull or any other external forces experienced by the mass. Where ***f*** is the frictional constant, the force is:

$$\vec{F}_f = -\vec{u}_i f$$

$\vec{F}_p$: The penalty force in response to the global volume change during simulation. Pascal's principle of incompressibility plays an important role where a change in pressure ΔP, exerted on a solid object, is transmitted undiminished throughout its incompressible medium and acts perpendicularly on its surface. The change in pressure consequently changes the volume. As a result, the volume compensation force has to be distributed to the surface nodes along the axis of their respective normals. The distribution method is described in section 5.3.2.

4.3.3.3 The local force

$\vec{F}_L$ is the force local to the volume discretisation at the node. Each volume spring is based on this internal volume. Therefore, ambient viscosity can be introduced to manipulate the movement relative to velocity and the medium density. Medium density ρ is mass *M* per-unit volume ***V.*** Therefore, based on the ambient viscosity:

$$\vec{F}_L = -v_i \rho \left\| \vec{u}_i \right\|^2 \frac{\vec{u}_i}{\left\| \vec{u}_i \right\|} \qquad (4.9)$$

4.4 Volume Discretisation

Explicit spatial discretisation allows the relationship between the surface elements and the respective internal volume to be defined. The existing methods are explored and the consequent evolution is carried out to address the relationship specific to the

aforementioned scope. This section establishes the ensuing innovation from these methods.

4.4.1 Surface Elements

Triangular elements have been employed to allow a surface mesh to be represented with more flexibility when it comes to irregular shapes and topologies. The basic components of these triangular elements are the nodes or vertices. These elements define the object surface, where the triangular elements can be rendered based on the respective normals (figure 4.8).

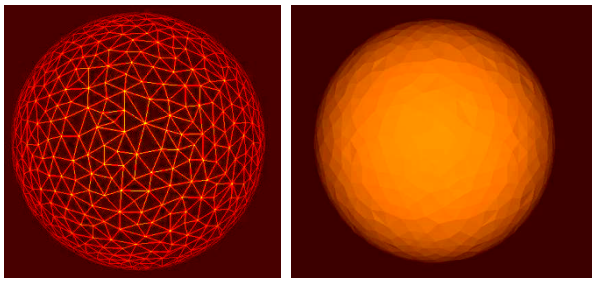

(a) (b)

Figure 4.8: *A sphere model made up of irregular surface mesh topology a) wireframe that shows the nodes and the resulting triangular elements (b) the rendered surface*

The relationship between the nodes and the surface triangles has to be defined to establish both physical and dynamic properties of the resulting 3D model. The spatial correlation stated by Cignono et al. (1999) and Villard & Borouchaki (2002) can be further extended to define the association of the area of the triangular elements A_t to the surface area A_S of the object mesh, which has also been employed by Sundaraj (2004) as discussed in section 3.2.2. Taking mass estimation as an illustration, mass can be determined corresponding to the surface area of the individual triangle. The total mass, M, of the object can be distributed to the triangular elements:

$$M_t = \frac{A_t}{A_s} M$$

where, M_t is the mass of the triangle.

However, as examined in chapters 2 and 3, the properties extraction should take into account the volume represented by these triangular surface areas. Bielser (2003) addressed the influence of the volume on the distribution of properties such as mass of:

$$M_t = \frac{V_t}{V} M \tag{4.10}$$

where, V is the total object volume and V_t is the volume of the tetrahedral discretisation to represent the inner volume. Maciel et al. (2003) stressed that the spring coefficients are proportional to the fraction of volume corresponding to the respective surface elements.

Since the surface model fundamentally consists of surface elements, it has to be virtually discretised into volume elements to reinforce this relationship. It is crucial to emphasise that the aim of this process is not to re-mesh the model into the volume discretisation as utilised by the VMSS but to act as a preliminary measure to coordinate properties distribution. The discretisation is initially based on the simplistic radial technique described in section 3.2.1.2, which is suitable for convex shaped models.

4.4.2 Radial Relationship

The volume discretisation is demonstrated by the explicit three-dimensional spatial approximation of the underlying surface mesh. The correlation of the surface elements to the global object properties is defined and exploited to establish the material properties for each of the surface elements of a mass spring mesh.

The radial link (figure 4.9) between the surface nodes to the object centre has been utilised by Promayon (1996), Vassilev & Spanlang (2002) and Balaniuk et al. (2006).

Bourguignon & Cani (2000) employed radial constraints to tetrahedral elements in order to provide force penalty to volume change as mentioned in section 2.4.4.

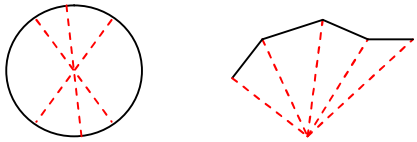

Figure 4.9: *Object surface with inner discretisation (based on figure 3.5 (b)) relative to the object centre: (a) Uniform shape (b) Non-uniform shape*

The object centre was employed as the common reference point, where the explicit discretisation attempts to define the local volume under the triangle. Generally, the centre of mass, *R*, of a system of particles is defined as the average of their positions, p_i, weighted by their masses m_i:

$$R = \frac{1}{M}\sum m_i p_i$$

where, M is the total mass of the system, equal to the sum of the particle masses.

In the case of an object with regular node distribution, the object centre is the average of the node positions assuming the object material is homogenous. For this assumption, mass at each node is deemed identical. However, if the topology is irregular, this method will be inaccurate as the mass at the nodes is unknown.

If the centre of the object is initially unknown, it should be derived based on the bounding box method. The bounding box can be constructed by extracting the minimum and the maximum value of x, y and z of the object assuming it is of a convex shape at rest. Subsequently, the centre will be the average of the corner coordinates of the box. Figure 4.10 illustrates a 2D representation of this concept. For the 2D object the centre is now the average of the extreme corner positions.

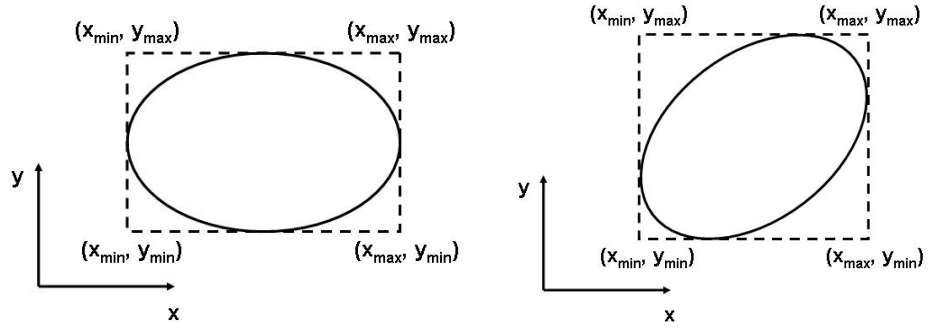

Figure 4.10: *Bounding box for a 2D object*

If the mesh is of irregular topology, the triangles are of different sizes. For this reason, different properties should be distributed to the individual triangles. The apparent issue is the need to correctly approximate the properties of the nodes in relation to the neighbouring triangles. For instance, mass at node **i** (figure 4.11) can be determined by manipulating the masses of the neighbouring triangles of which it is a member.

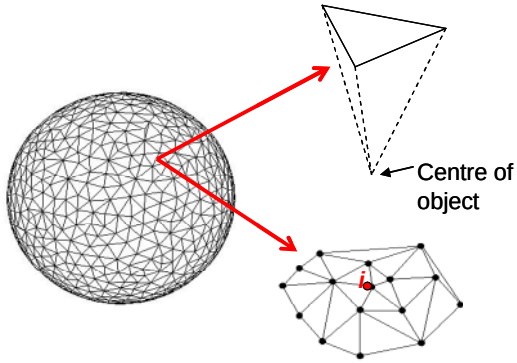

Figure 4.11: *Extracting individual mass for the triangle based on the tetrahedral discretisation*

Thus, the approximation method depends on the individual triangle and its local distribution before considering the global contributions from the other triangles. Previous attempts such as carried out by Bourguinon & Cani (2000), Bielser (2003), Sundaraj (2004) and Paloc et al. (2006) uniformly distributed properties to the respective nodes based on the barycentric relationship. In the case of a regular triangle, a third of the triangle mass is allocated to each of the nodes:

$$m_i = C_i \frac{V_t}{V} M$$

where, mass at ***i*** depends on the distribution coefficient, C_i = 1/3. For a regular tetrahedron, C_i = 1/4 (Bielser 2003; Paloc et al. 2006). Each node accumulates properties, such as mass, contributed by the neighbouring triangles.

The properties estimation is, however, sensitive to the distance of the mass nodes to the object centre. Since the mass at the nodes is not known, the barycentric position of the triangle is determined by assuming identical mass at the nodes. This is of course incorrect if the triangle is irregular (dissimilar edge lengths) and the nodes are of different individual distances to the object centre (figure 4.12).

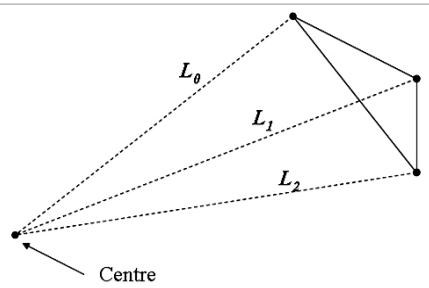

Figure 4.12: *The radial connection of the nodes to the object centre with dissimilar length L0, L1 and L2 respectively*

Consequently, the volume distribution for each node has to consider these lengths as they influence the properties estimation of the volume springs. Given that the properties have to be based on the real material, the stress and strain relationship of this material is to be defined within the volume specified for each node.

4.4.3 Uni-axial Tensile

As discussed in section 2.2.1.2, the stress and strain relationship employed to extract the elasticity modulus of a material is based on a force parallel to the normal of the surface area. In the first instance, the normal vector of each triangular element represents the axis of influence that guides the potential volume discretisation. Figure 4.13 shows the new volume discretisation (solid blue lines) relative to the original

radial discretisation in red dotted lines. It is a simple demonstration of the concept by reducing the dimension to two (cross-sectional). The black solid line represents the surface elements. In this case, it represents triangular surface elements. Two of the three nodes are shown here for illustration purposes. A similar illustration is repeated throughout this chapter.

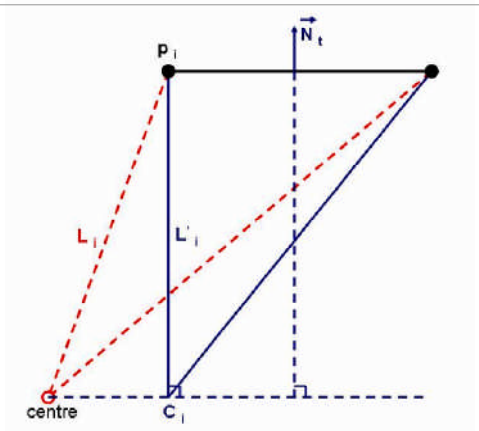

Figure 4.13: *Alternative discretisation based on the normal of the triangular surface element*

Since the nodes are the smallest element of a surface mesh, the new distance vector with length, L'_i, can be derived relative to the object centre and the surface normal. The length vector is an important parameter that defines the tensile axis along the surface normal of the consequent volume. The new volume is extracted by taking into account node p_i relative to the new centre point c_i and the remaining nodes of the triangular element.

At this point, it is established that the tensile axis is along the surface normal vector. However, the state of the surface triangles is dictated by the changes in the coordinates of the nodes over time. In MSS, the internal and external forces directly influence the dynamic behaviour of the nodes. Consequently, the deformable behaviour of the surface mesh is governed by these nodes as well as the volume springs attached to them. For this reason, volume has to be discretised in relation to

each node and its surface normal. The behaviour of the surrounding surface, of which a node is a member, depends on the properties along the axis of the node normal and not the normal of the surface triangle.

This approach supports the need for the volume springs at the nodes to be influenced by the orientation of force relative to the normal to create the impression of anisotropic behaviour. As demonstrated in figure 4.14, the normal at node **i** is the average of the normals of the surrounding surface areas, which has also been employed in Gouraud and Phong shading.

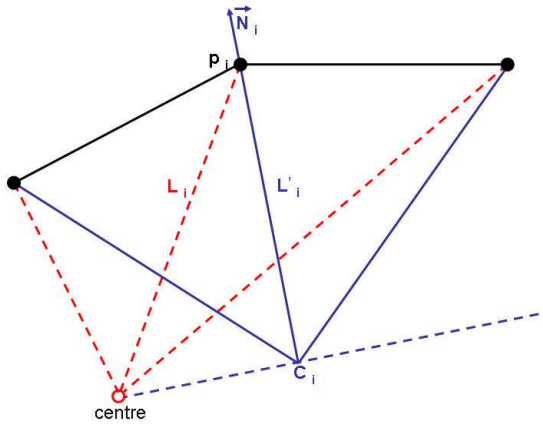

Figure 4.14: *The correct volume discretisation based on the normal at node p_i*

For a flat surface, the normal of the node is identical to the normals of the surrounding triangles as shown in figure 4.15. Thus, this discretisation will give a more relevant representation of the inner volume relative to the surface triangles compared to the radial method. For instance, in a case of a rectangular shaped solid, the relationship between the triangles and the inner volume is better represented.

As shown in figure 4.16, the nodes at the top part of the rectangular box are of regular concentrations. As a result, the properties of all the nodes minus the edge nodes should be similar. If the radial method (figure 4.16 (a)) is employed, the properties embedded at these nodes, such the coefficient of the volume springs, will vary due to

the dissimilarities in the axis length. This is caused by the tensile axis for each discretised volume that is not parallel to the surface normal at each node.

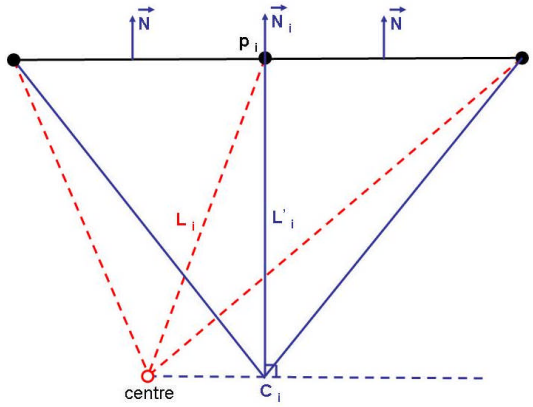

Figure 4.15: *Neighbouring surface elements with the same surface normal*

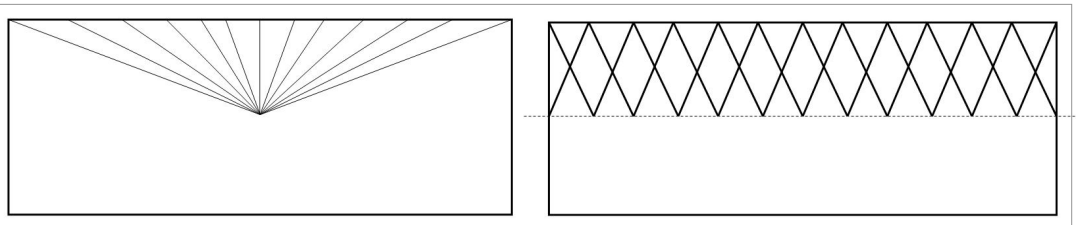

(a) (b)

Figure 4.16: *Explicit volumetric discretisation method based on (a) the radial method and (b) the proposed discretisation*

Figure 4.17 demonstrates the three-dimensional structure of one of the volumes that influences the properties at node p_i as previously illustrated in figure 4.14. The resulting tetrahedral volume can be calculated from the coordinates of the tetrahedral nodes. Therefore, the new centre point, $\mathbf{c_i}$, relative to the object **centre** and the new distance, $\mathbf{L'_i}$, have to be derived from the relationship. The new $\mathbf{L'_i}$ is the scalar projection of $\mathbf{L_i}$ onto the normal unit vector at point $\mathbf{p_i}$ as described in the following equations. Based on the surface normal at **i**, both $\mathbf{c_i}$ and $\mathbf{L'_i}$ can be extracted for all nodes (**i** = (0…n-1):

$$L'_i = \left(p_i - centre \right)_i \bullet \vec{N}_i$$

$$c_i = p_i - L'_i \vec{N}_i$$

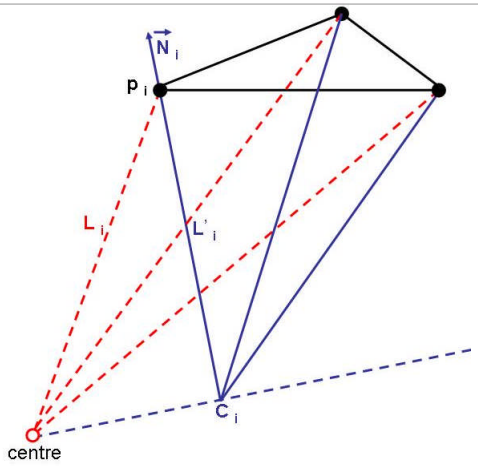

Figure 4.17: *Tetrahedral volume that influences the properties at p_i relative to its normal*

Similar discretisation as in figure 4.17 and the subsequent volume calculation will be carried out for other nodes relative to their normal and its neighbouring volume as illustrated in figure 4.18. The properties related to nodes $\mathbf{p_i}$ and $\mathbf{p_j}$ are influenced by the volume space discretised by the solid red and the blue lines respectively. The arrows denote the normal at the nodes.

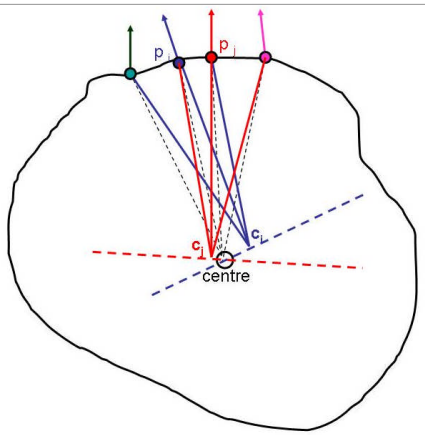

Figure 4.18: *Volumetric discretisation of an object*

4.4.4 The relationship with volume object

Figure 4.19 illustrates the neighbouring triangular elements with the resulting volumes of which node $\mathbf{p_i}$ is a member. It is an extension of figure 4.17. Similar discretisation and extraction are carried out for the other nodes.

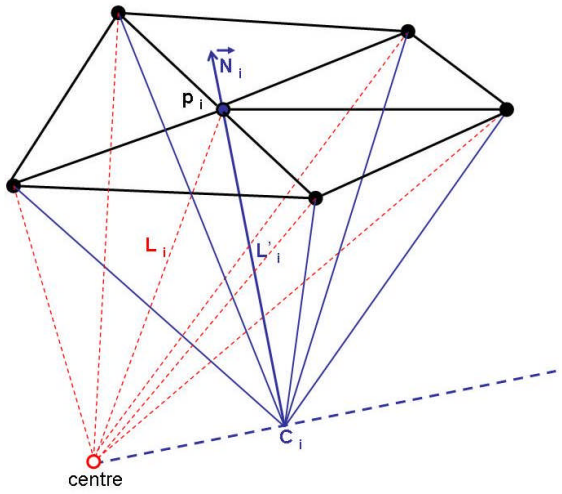

Figure 4.19: *Volume contribution from the neighbour triangles*

The method describes the relationship between each node with the surrounding volumes. Taking each individual node, the total volume represented by this node can be later utilised to estimate the properties. The algorithm includes:

```
For each node i (i = 0...n-1):
      Calculate L'i and ci
      For each neighbouring triangle t (i ∈ t):
            Volume vi + = volume vt
      End For
End For
```

4.4.5 Volume distribution

The volume distribution has to reflect the regularity of the surface triangles that consequently represent the volume discretisation. Taking a sphere model as an illustration, the volume distribution correlates with the mesh topology as demonstrated in figure 4.20. The inhomogeneity of the colour distribution indicates an irregular mesh topology. To reflect a homogeneous material, the deformable model has to include the design of the mesh topology in its properties estimation. Both spring and mass coefficients have to reflect the respective volume representations.

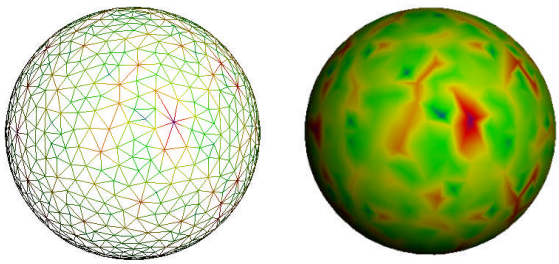

Figure 4.20: *The wire-mesh of a sphere and the respective volume distribution (max (red) to minimum (blue))*

4.5 Conclusions

This chapter has constructed the framework based on which the deformable model is configured. Despite the absence of internal volume, the surface model can be manipulated to provide an alternative approach to soft solid simulation.

The novelty of the volume discretisation is featured in this chapter, which subsequently assists in the estimation of properties. The unique contributions of this approach are:

i) The innovative enhancement of the classic shape preserving springs that not only considers shape preservation to promote elasticity but also takes volume conservation into account for the emulation of a solid behaviour.

ii) An original approach in adopting the tensile analysis of a material to establish the configuration of surface properties in terms of volume behaviour, which adheres to the standard practice in extracting the bio-material properties within the biomechanical research (see section 4.4). This relationship has not previously been established for a discreet surface model to address the absence of volume for the emulation of solid behaviour.

The properties of the nodes and the proposed volume springs are now based on the tensile properties of the material occupying the respective volumes. Therefore, based on this framework, the next chapter discusses the properties estimation technique within the scope of the deformable model. Volume behaviour for both local and global dynamic deformation is also explored.

Chapter 5

The Configuration of the Deformable Model

5.1 Introduction

This chapter discusses the configuration of the proposed deformable model taking into consideration the issues of properties estimation and volume behaviour.

The surface model, without the additional internal mesh (tetrahedral spring network), has been introduced. The only additional constraints to the surface springs are the versatile volume springs at the nodes to emulate volume behaviour. The behaviour of the volume springs is dependent on real material properties and sensitive to the orientation of force as well as the change of volume during simulation. The properties that govern the behaviour are established based on the explicit volume discretisation introduced in Chapter 4.

The main objective of properties estimation is to establish the physical properties of the MSS based on the material properties in consideration of the design of the mesh topology. The estimation scheme should thus support topological modification (multi-resolution) where the properties as well as the dynamic physical behaviour are preserved. The general proposition is that the properties estimation should promote the preservation of the material and deformation behaviour (local and global) of the soft volume with minimal deviation at runtime.

5.2 Spring Stiffness

5.2.1 Surface Springs

The surface behaves like an elastic membrane. To address the irregularity of mesh topology as employed by many models, the consequent spring stiffness is distributed based on Van Gelder's algorithm (Van Gelder & Wilhelms 1997; Van Gelder 1998). As discussed in Part II, this algorithm takes into account the design of the surface mesh topology as well as the elasticity modulus of the material. Consequently, it complements the proposed framework and the subsequent estimation technique for the volume springs.

5.2.2 Volume Springs

Even though the springs are of zero length, the coefficient can be preliminarily approximated relative to the tensile axis of the discretised volume discussed in section 4.4.4. The fraction of volume represented by each spring is an important parameter in the configuration of its stiffness instead of the shape of the respective spatial definition. In the case of the triangular surface elements, each element results in a tetrahedron as illustrated in Chapter 4.

In reference to the uni-axial tensile relationship of the volume contribution, equation 2.2 can be employed to extract the stiffness, *K*, of each spring:

$$K = E\frac{A}{L}$$

where, A is the area of the triangle. However, in terms of volume $\boldsymbol{V}$ and height, $\boldsymbol{L}$, the spring constant $\boldsymbol{K}$ at node $\boldsymbol{i}$ is:

$$K_i = E\frac{V_t}{L_i^2} \quad , \quad \boldsymbol{i \in t} \tag{5.1}$$

where, $\boldsymbol{t}$ is the triangle of which $\boldsymbol{i}$ is a member. The $\boldsymbol{K}$ extraction is now dependent on the volume under the surface triangular element. Based on figure 4.19, the equation

can be modified to consider the new length L'$_i$ which is along the normal axis from the new centre point $\mathbf{c_i}$:

$$K_i = E\frac{V_t}{L'^2_i} \quad , \quad \boldsymbol{i \in t} \tag{5.2}$$

Some objects have anisotropic behaviour depending on the orientation of the acting force. The subsequent volume spring can consider multiple parameters. The concept of elasticity, rigidity and bulk modulus of an object can be employed.

To illustrate this concept, another dimension is added to the spring stiffness. In this case, the shearing factor is considered. The shear modulus is concerned with the deformation of a volume when it experiences a force perpendicular to the surface normal. When the force is completely perpendicular to the normal at the node, the stiffness at that point refers to the shear modulus (equation 2.3) which can be extracted by manipulating the relationship between the shear modulus ***G***, elasticity modulus ***E*** and Poisson Ratio v:

$$K_i = G\frac{V_t}{L'^2_i} \text{ , where } G = \frac{E}{2(1+v)} \text{ , } \boldsymbol{i \in t} \tag{5.3}$$

In a global setting, the actual stiffness at node, ***i***, is the accumulation of stiffness contributed by the neighbouring triangles. Therefore, node, ***i,*** consequently has two stiffness parameters, which are the elastic stiffness, $\boldsymbol{K_E}$, and the shear stiffness, $\boldsymbol{K_G}$, as described by the following equation.

$$\begin{bmatrix} K_E \\ K_G \end{bmatrix}_i = E\sum_{i \in t} \frac{V_t}{L'^2_i} \begin{bmatrix} 1 \\ 1/2(1-v) \end{bmatrix} \tag{5.4}$$

5.2.3 Force Orientation

The dynamic nature of the nodes is dependent upon the orientation of force and the stiffness of the volume springs. Figure 5.1 illustrates the relationship between the normal and the force at a node. Based on this relationship, the inner stiffness at node,

i, depends on the orientation of the force, $F_{i,}$ relative to its normal N_i. When θ is 0°, the force is parallel to the normal at i. The stiffness will be the perfect elastic stiffness. But when θ is 90°, the stiffness refers to the shear stiffness.

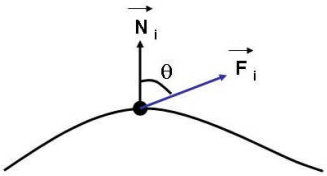

Figure 5.1: *Force vector relative to the node normal vector*

Figure 5.2 illustrates these extreme conditions when the force is perpendicular or completely parallel to the normal at the node.

(a) (b)

Figure 5.2: *Force orientation relative to the normal at the node (a) perpendicular (b) parallel*

The actual stiffness of the volume spring at ***i*** can be determined at runtime by manipulating the current dot product of the normal and the force unit vectors.

$$K_i = \left[\left\| \vec{N}_i \cdot \vec{F}_i \right\| \quad 1 - \left\| \vec{N}_i \cdot \vec{F}_i \right\| \right] \begin{bmatrix} K_E \\ K_G \end{bmatrix}_i \qquad (5.5)$$

This extraction method allows the anisotropic derivation of the stiffness at ***i*** based on the current force unit vector. A simple illustration of the solver algorithm for all springs is:

```
Function Spring Solver ():
      For all springs:
            If the rest length of current spring!= 0:
                  Solve current surface spring() (Eq. 4.5)
            Else If:
                  Solve current volume spring() (Eq. 4.6)
            End If
      End For
End Function
```

```
Function Solve current volume spring ():
      Calculate displacement ΔL
      Determine current k_i based on equation 5.5
      F_i += -k_i * ΔL    (Eq. 4.6)
      Add force contribution from ambient viscosity and damping
End Function
```

To solve the volume springs, equation 5.5 is employed. Ambient viscosity, as defined in section 4.3.3.3, is also included where it depends on the volume distribution at each node ***i***.

5.3 Volume Behaviour

The proposed estimation effectively considers volume represented at the nodes and in relation to the mesh topology and the material properties such as Young's Modulus and Poisson ratio. Once the properties have been configured, volume behaviour has to be demonstrated during simulation.

To reflect a solid behaviour, the model aims to maintain a constant volume during simulation. The deformable body should also portray shape conservation and realistic global deformation effects under the influence of gravity and interaction forces assuming linear elasticity, material homogeneity and incompressibility.

The proposition is that the combination of surface and volume springs based on the material properties provides the support to the mass nodes where:

i) volume is conserved with minimal deviation (nearly incompressible), where a constant deviation during simulation illustrates the feasibility in maintaining a constant volume during simulation

ii) global deformation effect is achieved despite the absence of internal volume

5.3.1 Shape Preservation

Linear elasticity indicates the ability to preserve the shape in response to deformation. The ordinary surface MSS will not be able to retain the original shape of the object as illustrated in section 3.1. This is the first requirement of volume behaviour with linearly elastic material. Figure 5.3 illustrates a sphere at different time steps during simulation. The object returns to the original rest shape at equilibrium.

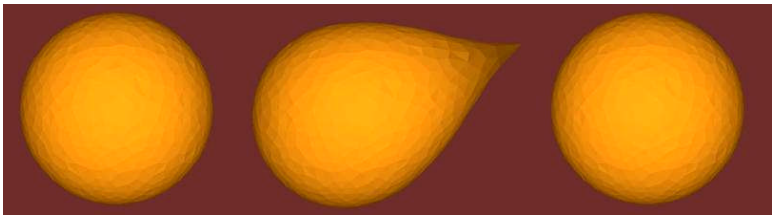

Figure 5.3: *A sphere at rest, under deformation and back to the original shape at equilibrium*

To emulate an incompressible material, restoring the material shape and volume at equilibrium is inadequate. The volume behaviour during the deformation is also important. It is crucial to preserve a constant total volume of the object during simulation. The proposed springs with two stiffness parameters provide the means for the surface to emulate volume behaviour when deformed but it does not take volume change during simulation into consideration. The next section addresses this limitation.

5.3.2 Volume Preservation

Volume variations can be calculated during simulation. Any compensation to the loss or increase in volume can be executed by manipulating the dynamic behaviour of the nodes. The dimension of the volume spring stiffness can be extended with the consideration of the modulus of compression. The corresponding bulk elasticity acts as a constraint against volume variation during simulation. Since the equivalent

Hookean relationship of **B** is a function of volume, which can be correlated from equations 2.4 and 2.5, the consequent bulk stiffness K_B at node i can be interpreted as:

$$K_{B\,i} = \frac{E}{3(1-2\nu)} \sum_{i \in t} \frac{A_t}{V_t} \tag{5.6}$$

In reference to the relationship in equation 2.5 and Pascal's principle, the penalty force at node i along its normal unit vector at a time step without any external force interaction on the surface is described by:

$$F_{i\,+=} -K_B \Delta V \; w_i \vec{N}_i \tag{5.7}$$

where, ΔV is the volume change and w_i is the weighted constraint factor that regulates the distribution of the penalty force. The factor is generally set to 1, which means that the volume change affects the different parts of the surface equally. However, the consequent penalty force at each node is influenced by its respective bulk stiffness. The force is imposed on the nodes along the surface normal. This is true to Pascal's principal that states that a change in pressure, exerted on an enclosed static fluid, is transmitted undiminished throughout the medium and acts perpendicularly on the surface of the container, hence preserving the volume of the material (section 2.2.1.3). This arrangement should produce global deformation as previously illustrated in figure 2.9.

To avoid incorrect volume calculation of the surface mesh during deformation, a more accurate volume calculation based on the surface node vectors and their respective normal can be employed. Current volume based on the positions of the nodes can be extracted at runtime using equation 5.8:

$$V_{\,=} \frac{1}{3} \sum_{i=1}^{n} \frac{A_i}{3} \left(N_x (x_1 + x_2 + x_3) + N_y (y_1 + y_2 + y_3) + N_z (z_1 + z_2 + z_3) \right) \tag{5.8}$$

where, volume ***V*** is the accumulation of the volume based on the individual triangle nodes relative to its normal and ***A*** is the area of the triangle. This supports both concave and convex object shapes.

The weighted factors can be manipulated to create a specific deformation effect as described in section 3.2.1.3. The shape of the object will deform according to the factors and the volume penalty force. In order to correctly distribute the interaction force effect to the object surface, the weighted factors have to be approximated in a way that it will consider both the orientation and the radius of force influence.

5.3.3 Local and Global Deformation

Upon an external interaction onto the surface, the constraint factors can be manipulated to control the local and global deformation effect of the object relative to the point of interaction and the orientation of the force. This section introduces the radius of influence and force orientation in order to address the need to manipulate both global and local deformations. The concept on the radius of influence or deformation zone (figure 5.4) has been explored by Hong et al. (2006). This operational area has been used to display local deformation effect as a response to the force as demonstrated by figure 2.21.

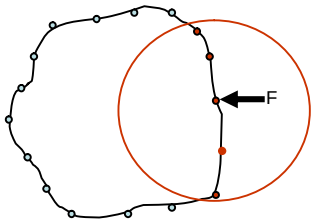

Figure 5.4: *Radius of Influence: The red nodes are within the radius*

To complement the proposed framework, this relationship (equation 3.1) has been modified. The area of influence is re-defined based on the cosine function as shown in

figure 5.5. Consequently, for a radius ***r***, the force will only influence the nodes within the resulting area. The constraint area is now described by:

$$COS\left(\frac{\|p_i - p_f\|}{r*2} * \Pi\right)$$

where, $\boldsymbol{p_i}$ and $\boldsymbol{p_f}$ are the position of node ***i*** and the point of interaction respectively.

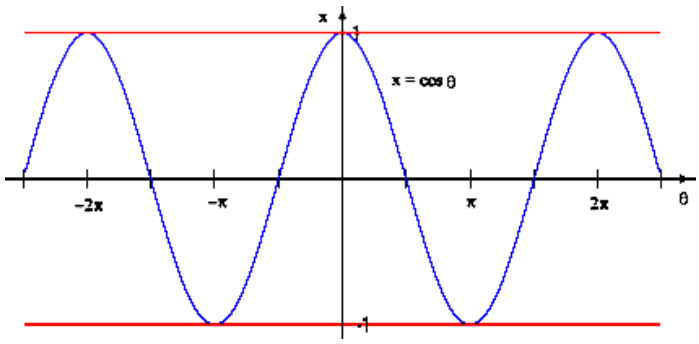

Figure 5.5: *Cosine function*

The radius of influence is insufficient to constrain the penalty force imposed by the volume variations. The orientation of force relative to the nodes is also crucial to control the resulting global deformation. It denotes the angle between the force unit vector and the distance unit vector of the point of interaction to the other surface nodes. The interaction force orientation (figure 5.6) is introduced as the additional correction factor.

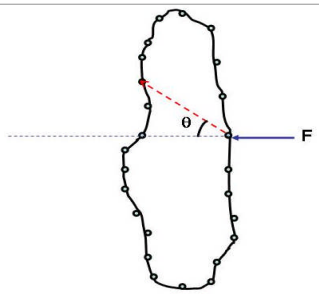

Figure 5.6: *The orientation of influence: the angle θ of the force relative to the distance unit vector of the point of interaction to the other nodes*

The influence of the orientation is extracted by solving a dot product between the force and the distance unit vectors:

$$\frac{p_i - p_f}{\|p_i - p_f\|} \bullet \vec{F}_f$$

Taking both the radius of influence and the orientation of force into consideration, the weighted factor at node ***i*** is:

$$w_i = \left(\frac{p_i - p_f}{\|p_i - p_f\|} \bullet \vec{F}_f \right) \left(COS \left(\frac{\|p_i - p_f\|}{r * 2} * \Pi \right) \right) \quad (5.9)$$

where, the node is within the radius of influence ***r***, and $\boldsymbol{F_f}$ is the force imposed at the interaction point. The value can be manipulated during simulation based on the angle of influence. The sum of the weights is equal to the total number of surface nodes as each force penalty at the nodes is based on their respective bulk stiffness and the reaction to the global volume change. The accumulation of these penalty forces represents the concentric global response to the total volume change.

To promote versatility in supporting various deformation behaviours, these weights can be re-approximated at runtime depending on the orientation of the interaction force. The estimation is confined within the radius of influence to avoid calculating weights for unaffected nodes. Hence, the estimation algorithm for the weighted factors is:

```
For (all nodes i= 0...n-1)
      If (the node is within the radius)
            Weighted factor at node i is derived using equation 5.9
      Else If
            Weighted factor at node i = 0;
      End If
End For
Normalise the weighted factors to the number of nodes n
```

These weights define the affected surface nodes and the respective magnitude of influence as a response to the volume variations caused by the interacting force. The volume penalty force acts perpendicularly to the surface of the object i.e. along the normal axis of each surface node (equation 5.7).

5.4 Mass Estimation

5.4.1 Mass Preservation

The aim of mass estimation is to distribute mass to the nodes. The total mass of the virtual model has to replicate the total mass of the real object. Therefore, the estimation method has to take mass preservation into account. This has to be true even when the mesh topology is modified.

Based on the previous relationship described by equation 4.10, mass can be distributed to the triangular elements relative to the inner volume subjected under each one as previously discretised. Mass is embedded at the nodes and not the triangular elements. However, mass at each node is influenced by the initial mass contributions from the surrounding triangular elements of which it is a member.

5.4.2 Estimation based on volume distribution

As volume has been initially discretised for each node, the volume ratio relative to the total volume approximated for the node can be determined. The volume ratios can then be employed to determine the mass that should be embedded at the nodes. Therefore, in a simplistic form, mass ***m*** at ***i*** is

$$m_i = \frac{\sum_{i \in t} v_t}{\sum_{j=0}^{n} v_j} M \qquad (5.10)$$

where, $\sum_{i \in t} v_t$ is the accumulation of volume under the neighbouring triangular elements ***t*** of which node ***i*** is a member, $\sum_{j=0}^{n} v_j$ is the accumulation of volume estimated for all ***n*** nodes, and ***M*** is the object mass.

Mass distribution correlates with the volume discretisation based on the mesh topology (figure 5.7). Mass at *i* is proportional to the spring stiffness. In order to produce a homogeneous behaviour when deformed, the volume spring stiffness at

each node must complement the mass it is supporting. For instance, based on figure 4.6, if $\mathbf{m_i}$ is larger than $\mathbf{m_j}$, the respective stiffness of $\mathbf{k_i}$ will be larger than $\mathbf{k_j}$. Figure 5.7 shows that the green plots denote larger mass distribution corresponding to the larger surface elements.

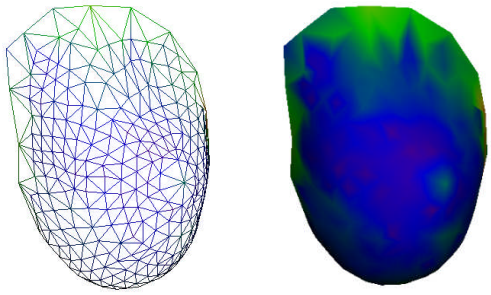

Figure 5.7: *Mass distribution of a breast model based on the respective mesh topology*

5.5 Properties Re-estimation

As discussed in Part I, multi-resolution is required by both graphics and haptics rendering in order to gain more accurate surface representation. Moreover, an operational area can be selected within which high computation can be constrained. Subsequently, this area can undergo further modification.

Topological modification consequently requires properties to be re-approximated. The issue is the preservation of the local behaviour, where the deformation behaviour should be maintained despite the modification of the surface topology. For instance, figure 5.8 displays a mesh topology before and after refinement.

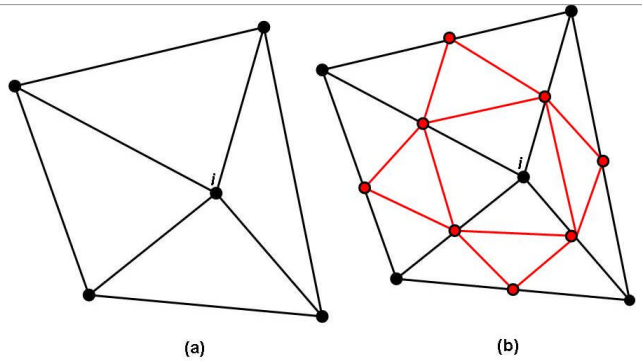

Figure 5.8: *Topological refinement (a) Pre-refinement (b) Post-refinement*

Figure 5.8 (b) contains new nodes and edges. As a result, the properties of the original nodes have to be preserved to avoid modifying the dynamic behaviour of the surface during simulation. As an example, when a force is imposed on node ***i***, the displacement pattern before and after refinement should coincide. The level of coincidence denotes the level of similarity in the dynamic behaviour which was not demonstrated by the re-estimation method introduced by Choi et al. (2005) as previously emphasised in section 3.2.2.2.

Upon any topological modifications, the same properties estimation can be repeated for all the mesh elements. However, to reduce the number of calculations, the re-estimation can be done locally. The properties for the nodes within the area of interest will undergo re-estimation based on the modified volumetric discretisation.

For mass estimation, the total mass will be equal to the total mass of the original nodes within the area before refinement. The previous equation for mass estimation can be re-used:

$$m_i = \frac{\sum_{i \in t} v_t}{\sum_{j=0}^{n} v_j} M \qquad (5.11)$$

where, $\sum_{i \in t} v_t$ is the accumulation of volume under the neighbouring triangular elements ***t*** of which node ***i*** is a member, $\sum_{j=0}^{n} v_j$ is the total volume estimated for all ***n*** nodes (the original and the new nodes within the refined area) , and ***M*** is the total mass of the original nodes before the refinement. The coefficients of the surface and volume springs will also be re-established based on the new volume discretisation of the nodes within the refined area. The same spring stiffness estimation will be carried out as described in section 5.2.

5.6 Conclusions

The enhancement of the configuration of the proposed deformable model is critical in achieving the aim to increase the accuracy of the resulting properties. The novel extension allows the tensile properties of the desired material to be integrated with the configuration. This extension addresses the issue of properties estimation and volume behaviour in reference to the objectives established in section 3.3.1.

The proposed method has evolved from simple shape anchors to volume springs that emulate volume material properties. These springs are sensitive to the change in volume and the orientation of force. By employing this surface alternative, the problem complexity imposed by the volume counterpart can be avoided while maintaining similar volume behaviour. The properties estimation takes the mesh topology into consideration. It involves volume discretisation that evolved from the initial radial method. The proposed framework, consequently, is able to include the real properties of the object as described by the stress and strain relationship of the object material.

Therefore, the novelty of this extension includes the following attributes:

i) The adoption of tensile analysis in establishing the configuration of surface properties in terms of volume behaviour, which adheres to the standard practice in extracting bio-material properties within the biomechanical research (see section 4.4). This relationship has not previously been established for a discreet surface model in order to resolve the absence of volume for the emulation of solid behaviour.

ii) The parameterisation of the coefficient of the volume springs is based on the quantitative measurement of bio-material properties, such as the Young's, Shear

and Bulk moduli as well as the Poisson ratio (see section 5.2 and 5.3). The state-of-the-art techniques that utilise similar springs rely heavily on the fine-tuning of properties with random values or an assumption of a regular topology that promotes uniform properties distribution. More sophisticated methods only consider a single modulus to describe the material behaviour. Hence, the novel extension provides a more accurate representation of the properties by considering more than one quantitative measurement.

iii) The consideration of runtime properties of the intended material, where the stiffness of the volume springs is dependent on the elasticity and shear stiffness in response to the orientation of force (see section 5.2.3). This adheres to the real behaviour of a material under properties extraction, where both Young's and Shear moduli address the uniaxial and shear tensile respectively.

iv) The deformation effects are manipulated at runtime to emulate solid behaviour despite the absence of volume (see section 5.3.3). Other researchers opt for pre-defined deformation effects or key-framed animations which limit the versatility of the deformation effect at runtime.

The next part of the thesis, Part III, aims to document the evaluation of this extension.

- PART III -

EVALUATION ANALYSIS
&
DISCUSSION

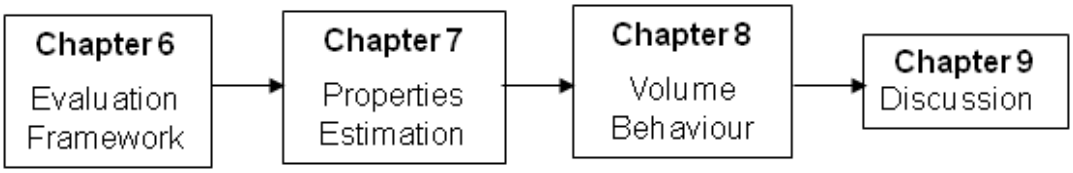

"We make our world significant by the courage of our questions and by the depth of our answers."

Carl Sagan (1934-1996)

Chapter 6
Evaluation Framework

6.1 Introduction

To verify the feasibility and the versatility of the proposed model towards simulating soft deformable solids within the prescribed scope, the simulation framework is implemented as the platform on which the behaviour of the model is observed and analysed at runtime.

The simulation framework as described in section 4.2.1 was developed on top of the Microsoft Visual C++, OpenGL and OpenHaptics platform. A Phantom Desktop haptic device (figure 4.3) was employed to provide interaction. The desktop PC had the specification of Intel Pentium 4, 2.40 GHz and 1 G RAM. This experiment setting was implemented for the evaluation. The findings are described and analysed in Part III of the thesis. To set the scene for the evaluation, the next subsections establish the aim, approaches and materials.

6.2 The evaluation aim

The aim of the evaluation is to validate the enhanced configuration of a surface model corresponding to the issues of properties estimation and volume behaviour; and with the consideration of the scope of the deformable model that includes the material parameters: elasticity, homogeneity and incompressibility; in hope to demonstrate accuracy in the resulting properties.

6.3 The evaluation hypotheses, objectives and techniques

The evaluation method is empirical where it is observatory and descriptive in the approach to the analysis and discussion of the behaviour of the proposed model. Consistent with the evaluation aim, the approach is classified into two key criteria

according to the main issues addressed throughout this thesis. The hypotheses and the objectives of the evaluation are established based on these criteria.

6.3.1 Properties estimation

The core component of the deformable model is the configuration of its properties. The rigour of this activity influences the consequent dynamic and volume behaviour. For this reason, the evaluation of the estimation technique is substantial.

The two key hypotheses are:

i) The proposed model is parameterised with real material properties. Thus, irrespective of its mesh topology, the resulting dynamic behaviour should reflect elastic and homogeneous material.

ii) Irrespective of topological refinement, the behaviour of the altered area should be maintained. This further verifies the versatility of the estimation technique, where homogeneity is still preserved despite the change.

To validate these hypotheses, the objectives of the evaluation are to:

i) Demonstrate the elastic behaviour of the model by observing the ability to conserve shape during simulation

ii) Validate the resulting elasticity modulus of the simulated model by analysing the stress and strain relationship

iii) Compare the model against a reference model with the consideration of identical physical and material properties

iv) Illustrate material homogeneity by analysing the relationship of the distribution of mass and spring coefficients

v) Highlight the flexibility of the estimation technique in supporting topological modification while preserving the homogeneity of the deformation behaviour

vi) Emphasise material homogeneity despite the design of the topology by observing texture distortions during deformation

Table 6.1 summarises the evaluation methods to achieve these objectives. Figure 6.1 demonstrates the rigour of the evaluation.

6.3.2 Volume behaviour

Once the configuration of the model has been evaluated, the corresponding volume behaviour is to be assessed. The hypotheses of the volume behaviour of the proposed surface model despite the absence of internal volume are:

i) The principal characteristic of an incompressible solid is to preserve a constant volume during simulation. For an elastic and incompressible material, the original shape at rest as well as volume during deformation should be conserved. Since materials such as soft tissues are not perfectly incompressible, minor discrepancy in volume preservation is expected.

ii) Despite the absence of internal discretisation, the global deformation effect of the surface is possible to reflect the assumption of an incompressible volume.

iii) As the surface method is a dimensional departure from the volume counterpart, the computational complexity is also reduced. When compared to a VMSS with similar mass-spring complexity, the proposed surface model is expected to be more efficient.

To validate these hypotheses, the objectives of the evaluation are to:

i) Analyse the volume variations of the model under the influence of the gravitational pull and the interaction force.

ii) Observe the visual effect of the local and global deformation under the different conditions

iii) Investigate the feasibility of the runtime manipulation of the global deformation effect in relation to the change of volume as well as the orientation and the radius of influence of the interaction force.

iv) Investigate the frame rate of the proposed surface model in comparison to the volume counterpart, where the same shape and MSS complexities are employed.

In order to achieve these objectives, the experiments described in table 6.2 are proposed to address incompressibility as well as the performance. Figure 6.2 illustrates the rigour of the evaluation.

Table 6.1: *Experiments to assess elasticity and homogeneity*

i) Elasticity
• **Shape preservation:** Elasticity denotes the ability to retain shape in response to any external intervention. The proposed model enhances the original concept of shape memory springs. Therefore, shape has to be conserved at equilibrium. • **Stress and strain analysis**: The deformable model should produce a behaviour that reflects its material properties. Based on the stress and strain relationship when the model is stretched, the elasticity modulus is derived. The deviation from the original value is analysed. Similar evaluation has been employed by Maciel (2005). • **Comparison with a reference model:** The shape of the model is observed at runtime and compared to the FE model analysed using SolidWorks and Cosmos FEA.
ii) Homogeneity
• **The distribution of mass and spring coefficients:** The springs provide support to the mass at the nodes. Subsequently, the relationship is illustrated by the surface behaviour during simulation. When imposed under the influence of gravity, no anomalies or irregularities should appear. • **Local behaviour analysis after topological modification:** The experiment is based on the pattern comparison carried out by Choi et al. (2005). The behaviour of the node displacement in response to the imposing force is observed at runtime. The patterns of these displacements can be compared to evaluate whether the local behaviour is preserved within the modified mesh area. • **Distortion test:** Texture will distort when the surface mesh deforms. To promote material homogeneity, the distortion has to be as uniform as possible as discussed by Van Gelder (1998).

Table 6.2: *Experiments based on the parameters*

i)	**Incompressibility**
•	**The analysis of volume variations during simulation:** This experiment involves imposing various conditions on the model where it is deformed by the gravitational pull or the external force interaction. Volume change is analysed over time to evaluate volume preservation.
•	**Deformation effect:** The visual response to the external force and the gravitational pull can be observed where both local and global deformation effects are evaluated. The proof of concept of the ability to produce a global deformation effect regardless of the hollow nature of a surface model is presented in the analysis.
ii)	**Performance**
•	**Comparison with a VMSS:** The previous section has described the comparisons that can be done against the FEM in terms of the visual behaviour as well as the elasticity modulus. It was recognised that VMSS fairs much better when it comes to real time simulation compared to FEM (Chapter 2). In addition, FEM is biased towards small deformation. Therefore, in this evaluation the surface mass spring model will be evaluated against the volume counterpart. Similar shape and initial mesh complexities will be employed to stress the versatility of the proposed model in terms of the frame rate.

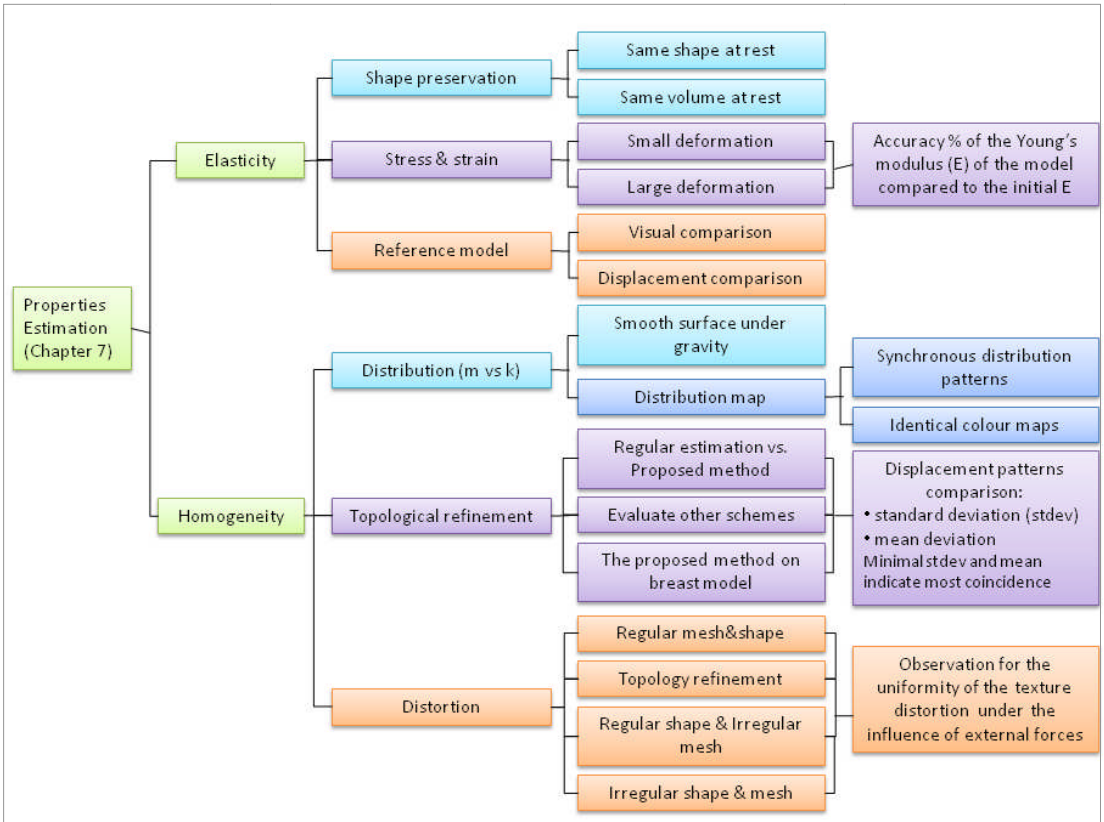

Figure 6.1: The evaluation taxonomy of properties estimation

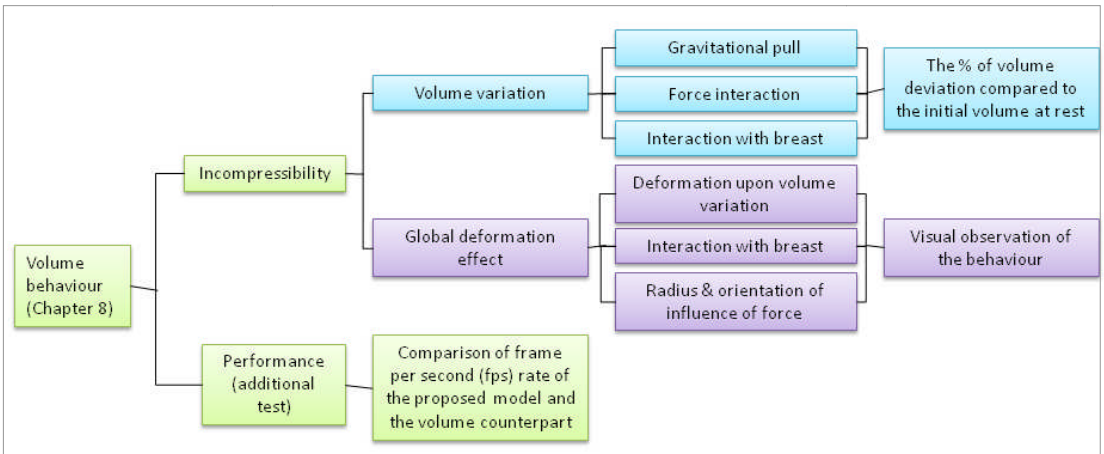

Figure 6.2: The evaluation taxonomy of volume behaviour

6.4 The Materials

The proposed model is deterministic by nature, though flexible and versatile in the approach to the different constraints such as volume constraints and properties estimation. Being deterministic, it thus produces the same output for a given starting condition or constraint when simulated (Origlio 2008). This means that the confidence level is high for all of the redundant experiment samples under the repeated constraints. This therefore, guides the choice of experiment samples.

6.4.1 Experiment samples

The sample models utilised in the evaluation are categorised based on these parameters:

i) shape
ii) mesh topology
iii) mesh complexity

As illustrated in figure 6.3, the shape and mesh topology can be regular or irregular while the mesh complexity depends on the number of surface elements. The five main ones are further summarised in figure 6.4.

The three cubes (6.3(a), (b) and (c)) have uniform mesh and shape topology but different mesh complexities. The sphere is an example of a uniform shaped model with irregular mesh topology. Finally, the breast model is an instance of an object with irregular shape and mesh topology. Additionally, the breast model is an open surface model.

In conjunction with the scope of a constraint environment, the open edge of the breast is fixed as is a real breast tissue to the chest bone. The bottom face of the cube is also

fixed to allow experiments such as the tensile analysis to be carried out. In the stress and strain analysis of human tissue and any other soft object, a small dimension has been considered and not the whole organ. In the following experiments, this is taken into consideration. A Poisson ratio of 0.4 (nearly-incompressible) and the Young's modulus (see table 7.1) are implemented in the configuration of properties.

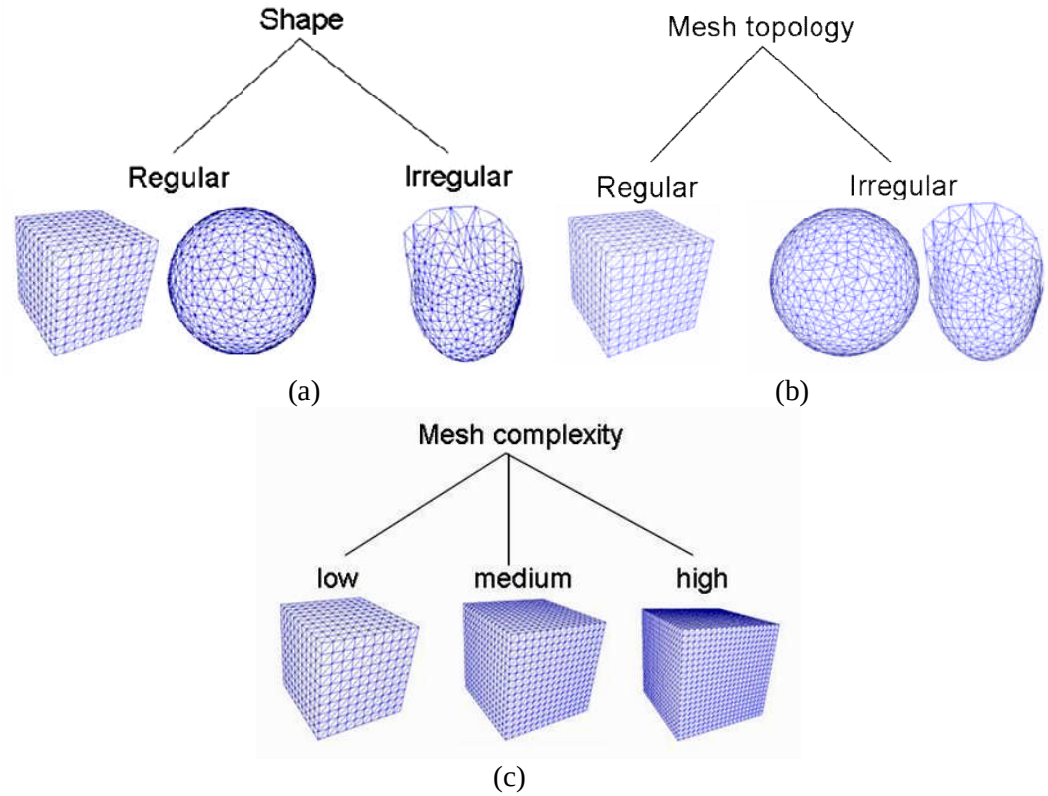

Figure 6.3: *Models based on the parameters: (a) Shape (b) Mesh topology (c) Mesh complexity*

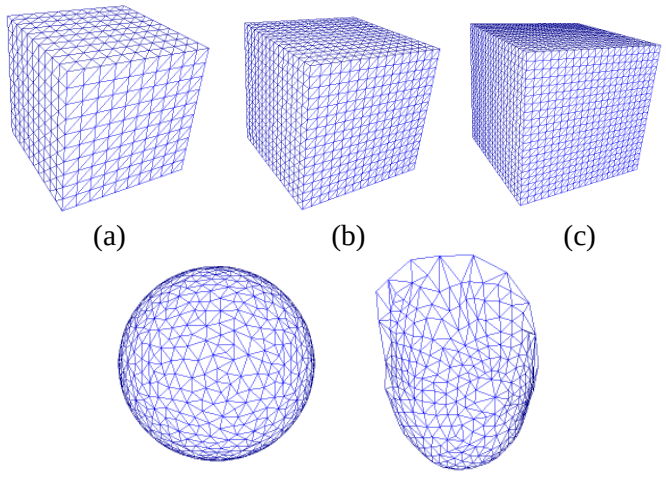

Figure 6.4: *Surface geometries: a) Cube (602 nodes) b) Cube (1352 nodes) c) Cube (2402 nodes) d) Sphere (1000 nodes) e) Breast (276 nodes)*

6.4.2 The configuration schemes

The proposed model features enhancements to the configuration of the classical surface MSS and the shape preserving springs. Consequently, the model will be compared against other state-of-the-art configuration schemes relevant to the employed framework. The comparison aims to highlight the feasibility and versatility of the proposed framework, where the novel configuration features:

- the initial volume discretisation based on the concept of uni-axial tensile and the consideration of the design of the mesh topology,
- the parameterisation of the coefficient of the subsequent volume springs with real material properties,
- the runtime derivation of the volume spring coefficients relative to the orientation of force, and
- the runtime manipulation of the deformation effect relative to the orientation of force and volume variations.

The resulting analysis endeavours to substantiate the overall evaluation aim, hypotheses and methods established for the proposed deformable model.

For a comparative analysis against the existing approaches, three relevant schemes based on the current techniques are implemented. The schemes are:

i) **Scheme A:** This is the original configuration which is based on the ordinary shape preserving springs (Laugier et al. 2003; Choi et al. 2005; Payandeh et al. 2005) as discussed in section 3.2.1.5. Uniform coefficients are defined for mass and springs. Upon any mesh refinement, the properties are re-established based on the refinement method discussed in section 3.2.2.2 (Zhang et al. 2002; Choi et al. 2005).

ii) **Scheme B:** A configuration which is based on radial discretisation (Vassilev & Spanlang 2002; Balaniuk et al. 2006) and the volume penalty method (Bourguignon & Cani 2000; Vassilev & Spanlang 2002). Bulk properties and the pressure model are considered when estimating the volume behaviour. This scheme represents the volume approach.

iii) **Scheme C:** This configuration includes the shape preserving springs parameterised with the uni-axial elasticity modulus. This means that the stiffness of the springs remains unchanged at runtime. This method has been employed by Van Gelder (1998) and Mollemans et al. (2003) for the triangular and tetrahedral elements. Moreover, it only preserves shape and does not take the change of volume into account. This is similar to Scheme A but the properties of the springs are established based on the design of the mesh topology and the consideration of the elasticity modulus.

These schemes only consider a single stiffness coefficient. They are compared with the proposed configuration (see chapter 4 and 5) that features more than one stiffness coefficient. The proposed configuration is referred to as **Scheme D** to simplify the ensuing analysis in the following chapters**.**

As described in part II, Scheme D features a novel configuration proposed for the deformable model. The significant characteristic of the estimation method is the inclusion of three parameters in the configuration of the proposed volume springs. The behaviour of the springs is dependent on the orientation of force as well as volume variations at runtime. The main considerations taken by all the schemes are summarised in table 6.3. The comparisons are in accordance with the key issues established in the evaluation approach (section 6.3).

Table 6.3: *The summary of the considerations taken by the schemes*

	Properties Estimation				Volume Behaviour	
Scheme	MSS Topology	Volume Discretisation	Material properties	Force orientation	Shape preserving springs	Volume Variation at runtime
A	Surface	No	No	No	Yes	No
B	Surface and radial	Radial based on REM	Single parameter for spring coefficients	No	Radial Springs	Yes
C	Surface	Based on tensile axis	Single parameter for spring coefficients	No	Yes	No
D (the proposed method)	**Surface**	**Based on tensile axis**	**Three parameters (uni-axial, shear and bulk tensile)**	**Yes**	**Volume Springs**	**Yes**

The estimation method (Van Gelder 1998) for the surface springs is standardised for all schemes. The significance of this is to eliminate the influence of the surface springs on the evaluation of the volume springs contribution to the behaviour of the deformable model. The resulting comparisons highlight the feasibility of the novel improvement to the shape preserving springs that are now defined based on the volume and the respective material properties. The coefficient for each inner spring for Scheme A was estimated based on the average of the total value of the stiffness of the volume springs in Scheme D (the coefficient in reference to the uni-axial tensile only) over the number of nodes. The significance of this is to standardise the total stiffness value of the inner springs to allow Scheme A to be compared with the proposed Scheme D.

The evaluation criteria established in section 6.3 are implemented to evaluate the behaviour of the proposed model and its configuration (Scheme D). Some of the relevant experiments identified for the parameters will be carried out to aid the comparative analysis of the main schemes. The key quantitative evaluations for each parameter (elasticity, homogeneity and incompressibility respectively) are summarised in table 6.4.

Table 6.4: *The key evaluations employed for the scheme comparison*

Parameters	Evaluation
Elasticity	The stress and strain analysis (Tensile analysis)
Homogeneity	Local behaviour analysis after topological refinement
Incompressibility	The analysis of volume variation during simulation

The ranking of the schemes will be concluded based on these key quantitative evaluations, where table 6.5 will be populated using the star system. One star (*) represents the worst scheme and four stars (****) indicate the best scheme. The grey shading indicates the columns which are not addressed in the current chapter. Any additional schemes that will further aid the analysis will be specified separately in the chapters in Part III.

Table 6.5: *Ranking table in reference to the key experiments for the evaluation parameters (elasticity, homogeneity and incompressibility respectively)*

Scheme	Stress and Strain	Topology Refinement	Volume Preservation
A			
B			
C			
D			

6.5 Conclusions

The deformable model has to be evaluated to validate the proposed configuration discussed in Part II. Prior to assessing the volume behaviour, it is important to evaluate the accuracy of the properties estimation. Chapters 7 and 8 (table 6.6) discuss the evaluation of these two key issues in accordance with the material attributes identified in sections 6.3.1 and 6.3.2 respectively. The evaluation techniques are elaborated upon in these chapters.

Table 6.6: *The main attributes of the evaluation analysis in Part III*

Part III	Elasticity	Homogeneity	Incompressibility
Chapter 7: Properties Estimation	√	√	
Chapter 8: Volume Behaviour			√

Chapter 7

Properties estimation

7.1 Introduction

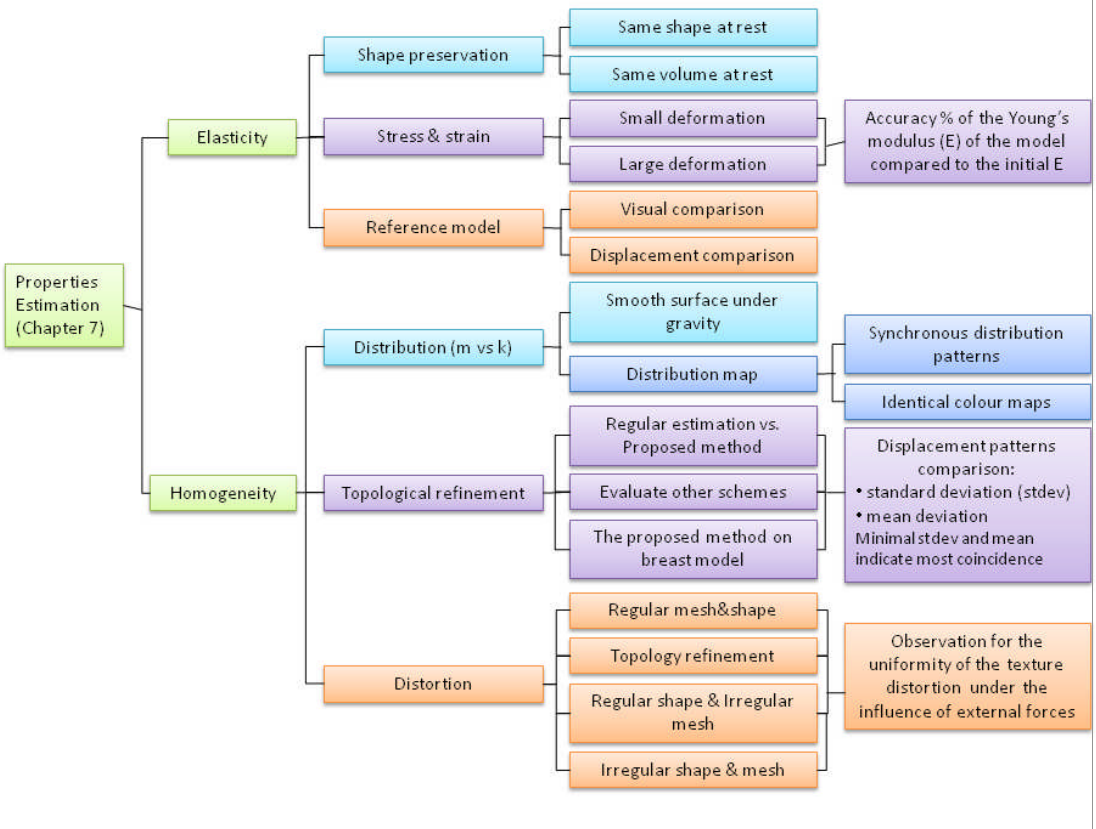

Figure 7.1: The evaluation of properties estimation

Verification and evaluation of the proposed technique is highly significant to ensure that the resulting model reproduces the original material properties employed in the estimation. The evaluation aim and the subsequent criteria have been established in chapter 6 based on the key hypotheses, which are formulated in consideration of the issues of the estimation of properties and volume behaviour of the proposed model.

This chapter aims to highlight the findings based on the evaluation methods established for the issue of properties estimation. The taxonomy in figure 7.1

summarises the respective experiments. The parameters, which are the elasticity and homogeneity attributes of the simulated material, are addressed in this part of the evaluation. To further complement the investigation, the novel extension to the configuration (Scheme D) was compared with the other configuration schemes (Scheme A, B and C) as described in section 6.4.2.

7.2 Evaluation Objectives

The two key hypotheses relevant to the issue of properties estimation are:

i) The proposed model is parameterised with real material properties. Thus, irrespective of its mesh topology, the resulting dynamic behaviour should reflect the assumption of homogeneity and elasticity of the real material.

ii) Irrespective of topological refinement, the behaviour of the altered area should be similar. This further verifies the versatility of the estimation technique, where homogeneity is still preserved despite the change.

In reference to these hypotheses and the evaluation taxonomy, the objectives of the evaluation are to:

i) Demonstrate the elastic behaviour of the model by observing the ability to conserve shape during simulation

ii) Validate the resulting elasticity modulus of the simulated model by analysing the stress and strain relationship

iii) Compare the model against a reference model with the consideration of identical physical and material properties

iv) Illustrate material homogeneity by analysing the relationship of the distribution of mass and spring coefficients

v) Highlight the flexibility of the estimation technique in supporting topological modification while preserving the homogeneity of the deformation behaviour

vi) Emphasise material homogeneity despite the design of the topology by observing texture distortions during deformation

The first three objectives can be classified as the assessment of the elastic behaviour of the model and the other three concern the homogeneity. The following sections discuss these assessments based on the respective experiments established in table 6.1.

7.3 Elasticity

7.3.1 Shape preservation

The ability to preserve shape denotes the elastic characteristic. Since the proposed model is initially based on the shape preserving springs topology, the resulting model has to demonstrate such behaviour. Considering the three-dimensionality of the model, the assumption for the shape preserving behaviour is to maintain the same volume at equilibrium (rest state).

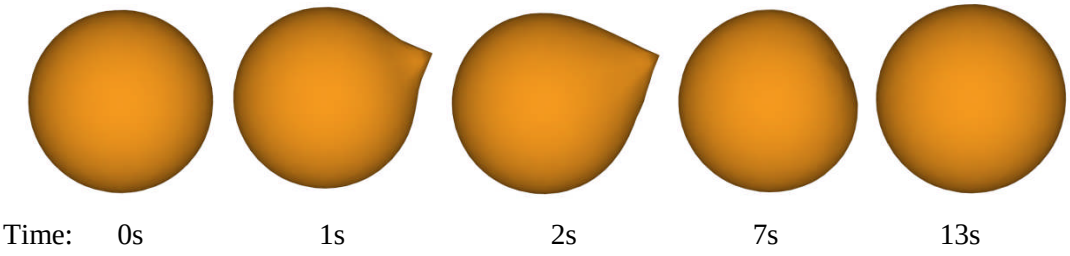

Figure 7.2: *Snapshots of the deformation of a sphere from the initial state to the final rest state after deformation*

A force was imposed along the normal of node of interest and the consequent deformation effects were observed over time. The initial and the end shape of the object were identical as illustrated in figure 7.2. The corresponding volume at

equilibrium substantiates the conservation of shape, where volume at the initial and end states were equal.

7.3.2 Stress and Strain Relationship

The ability to conserve shape does not necessarily substantiate the accuracy of the stress and strain relationship of the intended material in relation to the elastic behaviour. The configuration of the springs has to support this relationship in order to emulate the properties of the real material. Thus, to evaluate the estimation technique, the measurable behaviour of the surface model such as the stress and strain analysis was observed.

The proposed estimation considers the tensile analysis of the initial volume discretisation. The eventual stiffness of each of the volume springs was determined at runtime depending on the orientation of the force, either internal or external. In order to evaluate if the proposed estimation method preserves similar properties during simulation, the stress and strain relationship was re-analysed at runtime.

7.3.2.1 Elasticity Modulus

The elasticity modulus (E) or Young's Modulus can be re-extracted and matched against the E employed at the initialisation stage. The resulting percentage accuracy determines the feasibility of the proposed estimation technique. The initial E employed in this evaluation are summarised in table 7.1.

The E value for the adipose tissue as published by Samani et al. (2007) was claimed to be within 28 percent bigger or smaller than the proposed elasticity modulus. Other values such as Krouskoup's are within a huge range of values which were based on pre-compression. Therefore, the error should be within the range as depicted in table

7.1. The reason for using glandular and adipose is that as age increases, the ratio of adipose over glandular increases. A younger breast contains less adipose tissue. Therefore, the overall homogeneity will change proportionally.

Table 7.1: *The Young's Modulus of tissues (as correlated from Table 2.1)*

Material	E (kPa)	Description(s)
Breast adipose and glandular tissue	3.25	3.25 ± 0.91 and 3.24 ± 0.61 kPa for adipose and glandular respectively (Samani et al. 2007) based on 169 samples
	22.5	Mean for adipose (18±7 to 22±12 kPa) under 5% pre-compression (Krouskop et al. 1998) , which is within the range for Saravazyan et al. (1994): 5 to 50 kPa, and Kruse et al. (2000): 15 to 25 kPa.
	31.5	Mean for glandular (28±14 to 35±14 kPa) under 5% pre-compression (Krouskop et al. 1998), which is within the range for Saravazyan et al. (1998): 5 to 50 kPa, and Kruse et al. (2000): 30 to 45 kPa
Prostate	5	Maximum value for prostate based on Saravazyan et al. (1994): 1 to 5 kPa
Liver	0.64	Levental et. al (2007)
Intermediate grade carcinoma	19.99	19.99 ± 4.2 kPa for tumour (Samani et al. 2007)

7.3.2.2 Re-extraction of E

The tensile relationship can be analysed based on the engineering measurement or true measurement that considers the significant change in the model cross-section during large deformation. Assuming a linear relationship, both the engineering and true stress-strain relationship were analysed.

A cube model with a mass of 0.7 Kg was used to extract the relationship. A constant force (F) of 0.5 N was imposed on the upper surface of the cube and the bottom surface was fixed. The same experiment was repeated to consider the different surface

mesh complexities. The cubes in this chapter are referred to as Cube A, Cube B and Cube C corresponding to the cubes illustrated in ascending order of mesh complexity in figure 6.4.

Table 7.2: *Extraction of Young's Modulus (E) in relation to the breast adipose, liver and prostate tissue*

Breast adipose: original E = 3.25 kPa

Model	Cube A		Cube B		Cube C		Mean
Scheme	E	Error %	E	Error %	E	Error %	Error %
A	4.38	35	4.25	31	4.17	28	31
B	4.38	35	4.25	31	4.17	28	31
C	4.11	26	4.06	25	4.04	24	25
D	3.43	5	3.31	2	3.24	0.2	**2**

Liver: original E = 0.64 kPa

Model	Cube A		Cube B		Cube C		Mean
Scheme	E	Error %	E	Error %	E	Error %	Error %
A	0.85	31	0.82	29	0.81	27	30
B	0.85	33	0.82	29	0.82	28	30
C	0.79	24	0.79	23	0.79	23	23
D	0.65	1	0.64	0.3	0.63	1	**0.9**

Prostate: original E = 5 kPa

Model	Cube A		Cube B		Cube C		Mean
Scheme	E	Error %	E	Error %	E	Error %	Error %
A	6.67	33	6.48	30	6.37	27	30
B	6.67	33	6.48	30	6.37	27	30
C	6.22	24	6.18	23	6.15	23	24
D	5.11	2	5.03	0.5	4.98	0.5	**1**

The E value extracted from the four schemes identified in section 6.4.2 were compared. The re-extraction exercise utilised E values from as low as 0.64 to as high as 31.5 kPa. For the adipose modulus of 3.25 kPa, the possible values will be within the range of ± 0.91 (Samani et al. 2007). This means that the percentage error should be significantly less than 28 percent. Table 7.2 illustrates that Scheme D resulted in

around 2.5 percent deviation in relation to this E value, which indicates high accuracy in the estimation of properties compared to the other schemes.

Further analysis using the engineering stress and strain was carried out for the proposed model (Scheme D). The percentage accuracies are summarised in Table 6.3. The average of around 98 percent highlights the feasibility of the proposed approximation method which did not resort to the rigorous fine-tuning attempted by other researchers.

Table 7.3: *Percentage accuracy of the proposed Scheme D*

Model	Cube A		Cube B		Cube C		Mean
Original E (kPa)	E	Accuracy %	E	Accuracy %	E	Accuracy %	Accuracy %
0.64	0.65	99	0.64	100	0.63	99	99
3.25	3.43	94	3.31	98	3.24	99	97
5	5.11	98	4.92	98	4.84	97	98
19.99	20.11	99	19.55	98	19.24	96	98
22.5	22.63	99	22.03	98	21.68	96	98
31.5	31.63	99	30.89	98	30.45	97	98
					Mean Accuracy		**98**

7.3.2.3 Larger Deformation

The previous extraction was based on deformations which were assumed to be less than 50 percent extension of the original length (Figure 7.3). Larger deformation was produced by larger stress that results in an extension of more than 50 percent which is larger than the normal palpation stress imposed on a breast. In reality, large force intervention might result in the yield and tensile limits being exceeded. This will also normally result in an extreme change in cross-section.

Based on Cube B and E = 31.5 kPa, the stress and strain relationship for Scheme D is as illustrated in figure 7.4. Figure 7.4 (a) shows the relationship of a much smaller

stress compared to the resulting strain which is also illustrated by the deformation in figure 7.3. The true strain increases faster than the engineering strain with stress which is true to the concept illustrated in figure 2.5. Figure 7.4 (b) demonstrates a more significant increase in the real stress against strain, which was due to a more significant reduction in the body's cross sectional area during stretching.

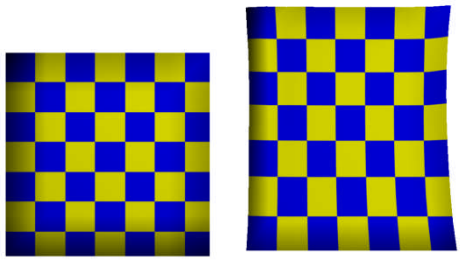

(a) (b)

Figure 7.3: *The change in cross section in response to a stretching force (Scheme D): (a) Unloaded (b) Stretched*

The palpation force for breast was advised to be around 1 to 2 Newton (Patkin, 1998). Russell & Ziewacz (1995) and Ruiter et al. (2006) claimed that mammography stress was around 41 kPa. Both claims resulted in large deformation. Consequently, E values were also re-extracted based on large deformation.

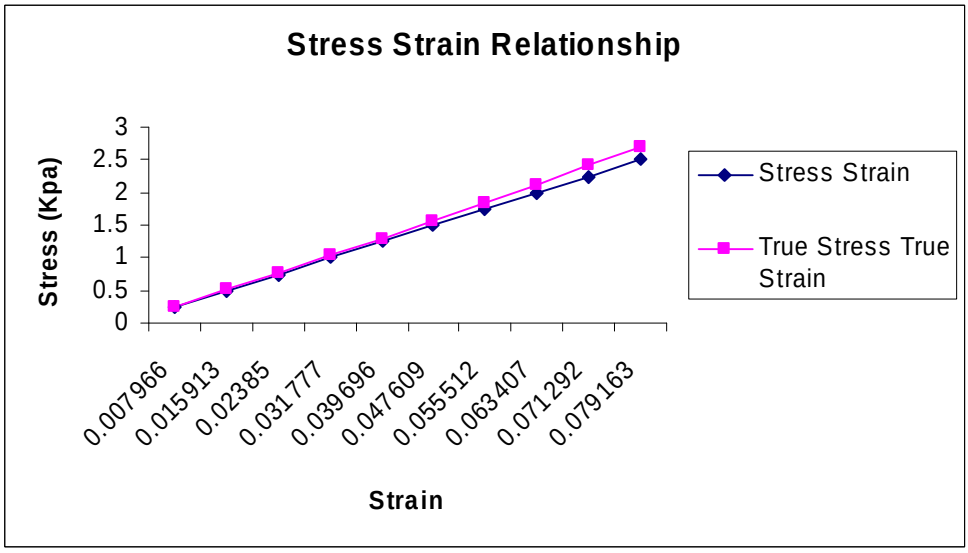

(a)

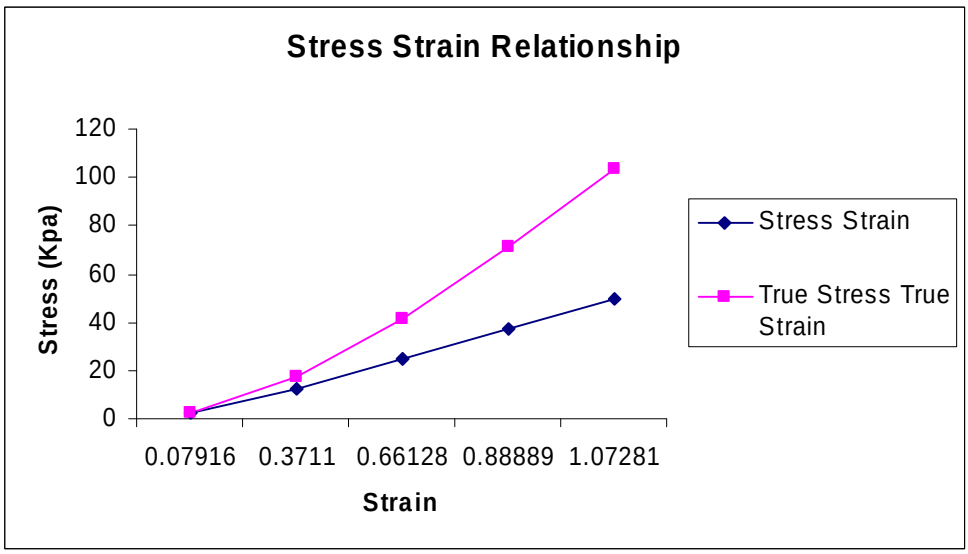

(b)

Figure 7.4: *Stress and Strain Relationship of Scheme D (E = 3.25 kPa) (a) Force magnitude between 0.1 to 1 N (b) Force magnitude between 1 to 10 N*

Table 7.4: *E-extraction for adipose and glandular tissue for the stress which is more than the proposed palpation stress (Scheme D)*

Method	Original E(KPa)	Cube A		Cube B		Cube C		Mean Error %
		E	Error %	E	Error %	E	Error %	
D (True)	3.25	8.20	152	8.10	149	8.04	147	149
D (Eng)	**3.25**	**3.80**	**17**	**3.68**	**13**	**3.61**	**11**	**14**
D (True)	22.5	68.85	206	68.19	203	67.86	202	203
D (Eng)	**22.5**	**28.05**	**25**	**27.19**	**21**	**26.74**	**19**	**21**
D (True)	31.5	75.57	140	74.53	137	74.00	135	137
D (Eng)	**31.5**	**36.30**	**15**	**35.09**	**11**	**34.46**	**9**	**12**
Mean error for engineering								**15**
Accuracy								**84**

When the interaction force was large, the property was still maintained within the range of possible values as shown by the engineering relationship, assuming that there was no significant cross-sectional area change. The true relationship demonstrates that the material's elasticity values increased as it exceeded the possible yield limit. This is due to the possible change in circumference upon reaching or on exceeding the yield limit. However, the engineering relationship has been employed to extract the original material properties. For this reason, the linear engineering estimation reinforces that

the material retained acceptable elasticity values at an average of 84 percent accuracy when subjected to a high external force.

These values conclude that regardless of the size of the deformation, the proposed Scheme D produced behaviour which was more similar to the original properties compared to the other methods. Scheme D consistently generated the least percentage error. It was also observed that the percentage accuracy was proportional to the increase in mesh complexity.

7.3.3 Displacement Comparison

The cube models were compared with the identical FEM models as analysed using SolidWorks and Cosmos platforms. Even though the FEM model is not perfectly accurate, it is a model that is based on volume data and real material properties. Each model was stretched by applying a constant force on the upper surface of the object. The resulting displacement analysis is depicted in figure 7.5. The displacement value of the model at equilibrium was compared with the proposed deformable model as summarised in table 7.5.

Table 7.5: *Comparison when the model is stretched (Force = 0.5 N)*

E (KPa)	Model	Displacement	
		cm	Deviation
3.25	FEM	0.8	
	Scheme D	0.7	5%
22.5	FEM	0.1	
	Scheme D	0.1	0.6 %
33.5	FEM	0.1	
	Scheme D	0.1	0.4 %

A shear force was also imposed on the top surface while the opposite surface is fixed. When compared with FEM, the visual representation (figure 7.6) indicates deviation in terms of the surface displacement analysis and the resulting shape at equilibrium.

This is a limitation of the shape preserving springs in the event of global positional dynamism. However, the impression of a sheared solid was demonstrated.

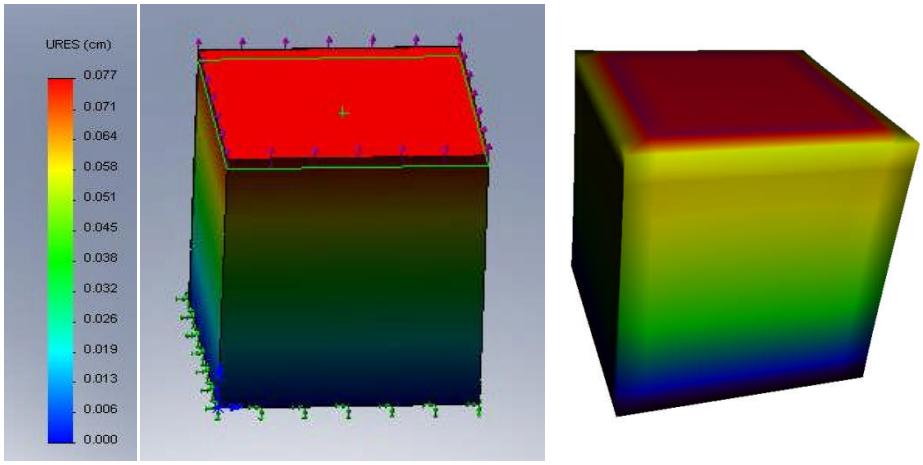

FEM Scheme D

Figure 7.5: *Stretching Displacement Analysis (3.25 kPa) of FEM and Scheme D*

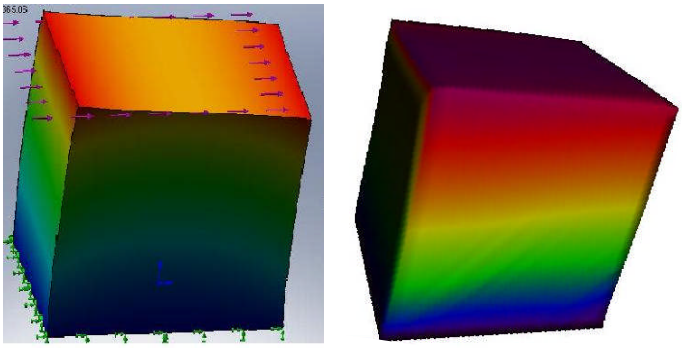

FEM Scheme D

Figure 7.6: *Shape comparison of FEM and Scheme D*

7.3.4 Summary

This section endeavoured to evaluate the elastic behaviour of the deformable model to accomplish the first three objectives established in section 7.2. It was demonstrated that the proposed Scheme D produced elastic behaviour in response to deformation, where the accuracy was substantiated by the elastic modulus extracted through the tensile analysis of the model. When compared against a reference model, the visual assessment indicated shape and displacement deviations. The model however

produced a more accurate displacement analysis when stretched compared to when sheared.

7.4 Homogeneity

Irrespective of the design of mesh topology, material homogeneity has to be reflected by the distribution of the coefficient of mass and volume springs at the nodes. This distribution has to be conserved upon any topological modification. For instance, the local behaviour of the refined area of interest should be preserved even if it requires properties to be re-estimated. Moreover, the nodes dynamic behaviour at runtime influences the resulting distortion behaviour of the surface texture.

7.4.1 Properties Distribution

In order to support homogeneity despite the possible irregularity of the mesh topology, the key nature of the volume springs is to provide the appropriate support to the mass at the nodes. For example, if the gravitational force is imposed on these masses, the springs will have to provide enough support for smooth realistic surface contours.

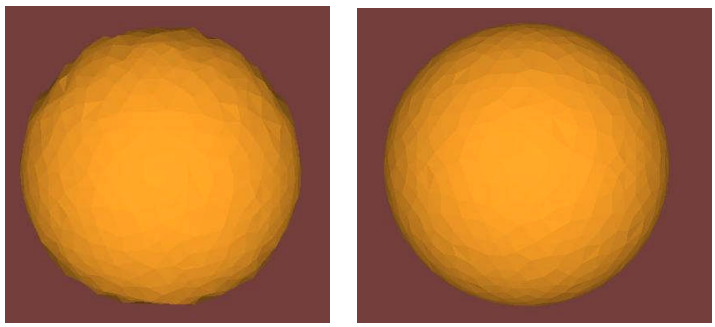

Scheme E Scheme D

Figure 7.7: *Gravity test*

To visually illustrate the importance of establishing the appropriate properties, a sphere model with irregular mesh topology was simulated under the influence of

gravity. The proposed estimation technique of Scheme D was compared with another scheme to highlight the significance. Scheme E was additionally implemented where it distributed mass in consideration of the mesh topology. However, the volume spring coefficients were uniform. Figure 7.7 illustrates that compared to Scheme D, Scheme E did not provide suitable distribution of mass and spring coefficients.

Based on the visual observation for Scheme D, the stiffness and mass in regards to the mesh topology were complementary at each node. The observation for Scheme C and Scheme D provided the same visual result at equilibrium due to the same fundamental estimation for a single stiffness parameter. However, for softer material, Scheme D demonstrated realistic reaction to the gravitational force during simulation as depicted by the snapshots in figure 7.8. The impression of compression was made possible by determining the runtime stiffness of the volume springs relative to the orientation of force.

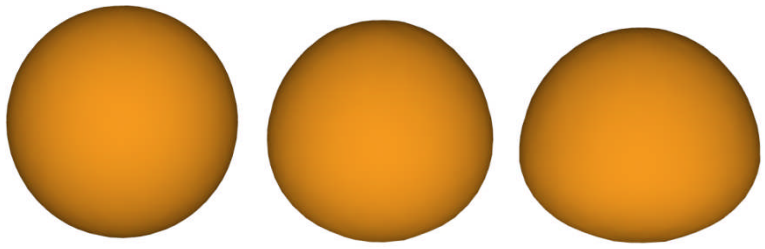

The changes in shape influenced by the force orientation, where the surface normal perpendicular to the vertical force displayed shear behaviour

Figure 7.8: *Snapshots of soft material deformation with anisotropic inner stiffness under gravity (Scheme D)*

The stiffness (k) of the volume springs would have to be proportional to the amount of mass (m) at the nodes in order to retain the material homogeneity. Based on the values approximated for the breast and the sphere model (figure 7.9), it can be concluded that the estimation scheme supports this hypothesis, where the peaks and troughs of the patterns are in sync.

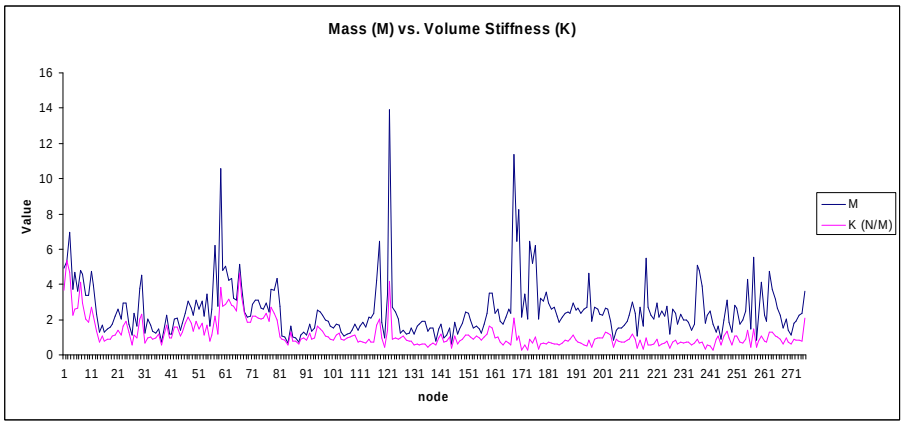

(a)

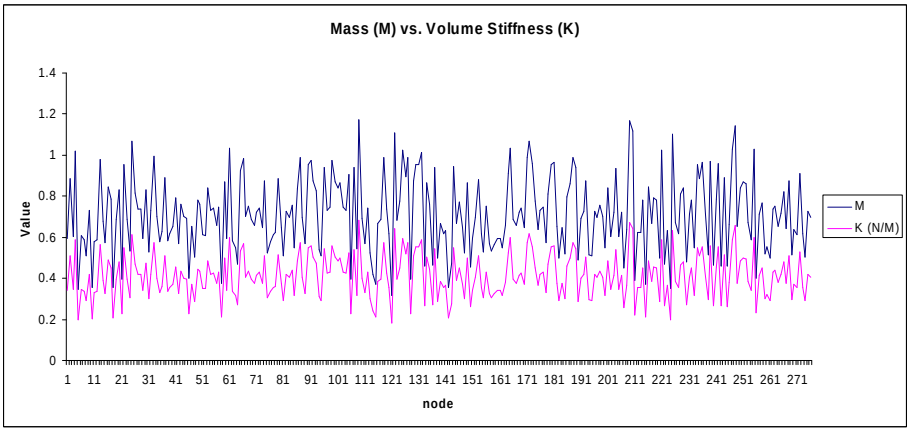

(b)

Figure 7.9: *Pattern comparison a) Breast model b) Sphere model (Note: values for stiffness have been scaled to be compared to the mass patterns (gram vs. N/m))*

The values of mass and the stiffness of the volume spring at each node reflect the respective volume represented by that node. To further illustrate the relationship, the distribution of the mass and stiffness coefficients are demonstrated in figure 7.10. Both distributions reflect the volume distributions shown in section 4.4.5.

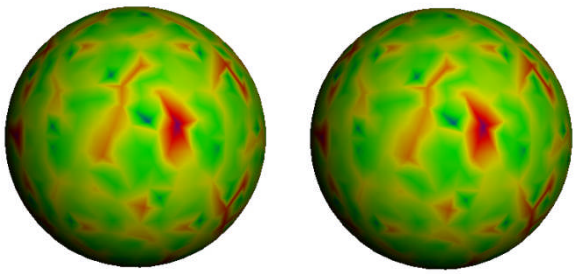

(a) (b)

Figure 7.10: *The distribution of (a) mass and (b) stiffness*

This relationship was also reflected by the regularity of the distortion for the texture as the homogeneous material, on which it was mapped, deformed under the influence of external forces (see section 7.3.4).

7.4.2 Properties Re-estimation

To further evaluate the versatility of the estimation method, it is important to consider topological modification. This is in line with the rising need for high visual acuity, such as the need for high definition graphics and deformation to promote realism. As discussed in Part 1, mesh refinement is normally executed local to the operational area to support selective rendering. The consequent topological modification requires the properties to be re-estimated within the area to preserve the properties as well as the dynamic behaviour of the material. The degree of the preservation of the local behaviour within the area before and after refinement reflects the level of accuracy.

7.4.2.1 Area of interest

To effectively evaluate the estimation scheme, a local area of interest has been chosen to compare the pre- and post-refinement behaviour. To illustrate the concept of multi-resolution, a simple loop or polyhedral subdivision technique (Shinya, 2005) was employed as shown in figure 7.11. Consequently, the properties of the volume springs and the mass at each of the mesh nodes were re-calculated at runtime.

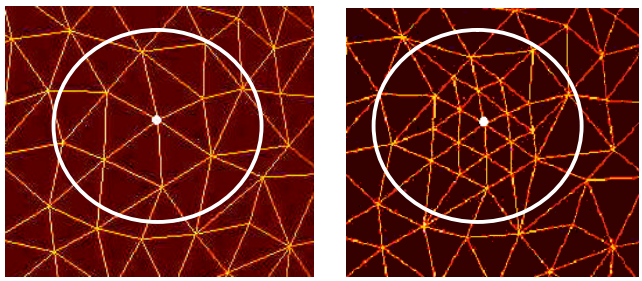

(a) (b)

Figure 7.11: *Loop subdivision of irregular mesh topology (a) Pre- refinement (coarse) (b) Post-refinement (a single level refinement)*

The subsequent re-estimation can be confined within the local area of interest without affecting the global property of the object. This promotes localised computation and cost effectiveness. The mesh shown in figure 7.11 (b) is the refined mesh (greater node concentration) of the original coarser mesh in (a).

7.4.2.2 The parameters of patterns comparison

The accuracy of the stress and strain relationship of the proposed model was approximated at around 98 percent. To validate the versatility of this model upon mesh refinement, the re-estimation evaluation has to be carried out. The evaluation focuses on discovering if the method supports mesh of any topology regularity and whether the behaviour will be preserved after refinement.

The experiment involved refining a local surface area and re-estimating the properties. A constant force was imposed on a node along its normal; $\vec{N}_i$ to the surface tangent at the node (figure 7.12). The displacement data was collected based on the selected nodes.

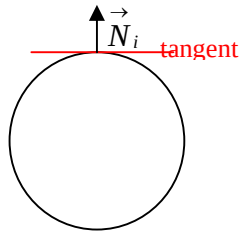

Figure 7.12: *The direction of force along the normal at the node*

The surface was deformed until it reached equilibrium. The displacement patterns within the coarse and the refined area were compared. Identical patterns indicate that the deformation behaviour was consequently preserved despite the change in the mesh topology. Two parameters were analysed to describe the displacement behaviour:

i) **The standard deviation** between the two patterns determines their level of co-incidence. The smaller the standard deviation, the more identical the patterns are.

ii) **The mean deviation** of the patterns represents the error in behaviour after refinement. The least value indicates the least deviation from the original behaviour.

The standard deviations and the mean displacement of all the schemes in response to various forces were collected and compared to evaluate whether the deviation increases or is maintained with increasing magnitudes. Both parameters are complementary. For instance, the behaviour is only preserved if both the parameters indicate small values. If the standard deviation is small but the mean deviation is significantly large, the deformation behaviour of the area is not identical.

Since the simulation model is a deterministic model, any repetition based on the same constraints, such as the same external force imposed on the same model, will produce the same displacement values over time. This means that the confidence level is high for all of the experiment samples. To increase the validity of the comparative analysis, the evaluation was repeated with other models with different mesh and shape complexities as well as the various external force magnitudes.

7.4.2.3 Estimation based on Mesh Topology

This section emphasises the importance of taking the mesh topology into consideration when estimating properties for the individual nodes and springs. The behaviour of the local area has been analysed based on the attributes of the displacement patterns. To carry out the analysis, a sphere model was chosen for its irregular mesh topology. Small forces were imposed on the selected nodes on the model. The model mass was 500 g, the elasticity modulus was 100 Pa and data was collected every 0.01 s. Scheme A, C and D were employed in the experiment to highlight the influence of the mesh topology in the properties estimation. Scheme B was not necessary as this part of the evaluation concerned with showing that the mesh

topology design is important. An additional scheme (Scheme E in section 7.4.1), which distributed regular volume spring stiffness but irregular mass at the nodes, was included to emphasise the relationship between properties and the mesh topology. Figure 7.13 illustrates the findings.

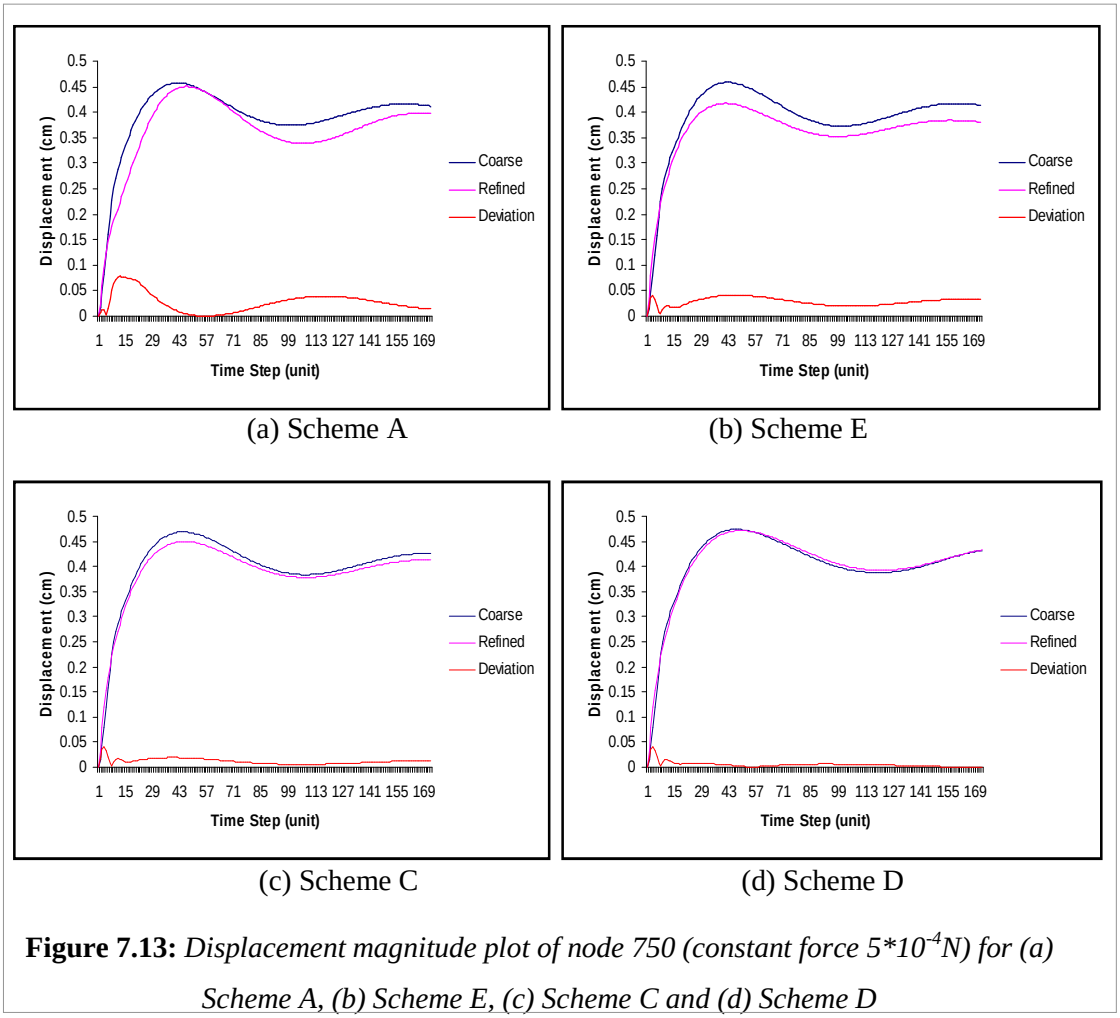

Figure 7.13: *Displacement magnitude plot of node 750 (constant force 5*10^{-4}N) for (a) Scheme A, (b) Scheme E, (c) Scheme C and (d) Scheme D*

The analysis discovered that the two proposed irregular schemes (C and D) preserved the surface dynamic behaviour with minimal standard deviation when the surface was refined. The patterns shown by Scheme D have the most identical behaviour compared to the other schemes.

The analysis was repeated for different forces and the standard deviations calculated denoted the level of similarity of the patterns. In figure 7.14(b), both scheme C and D produced small standard deviations which reflected the highest level of similarity

between the displacement patterns (coarse and refined). However, scheme D maintained a minimal displacement deviation under 0.006 cm for any amount of force compared to scheme C where its deviation increased with force (figure 7.14 (b)).

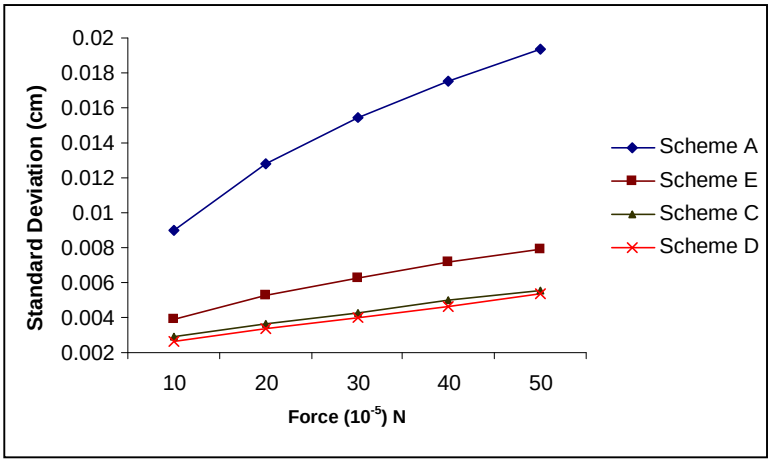

(a)

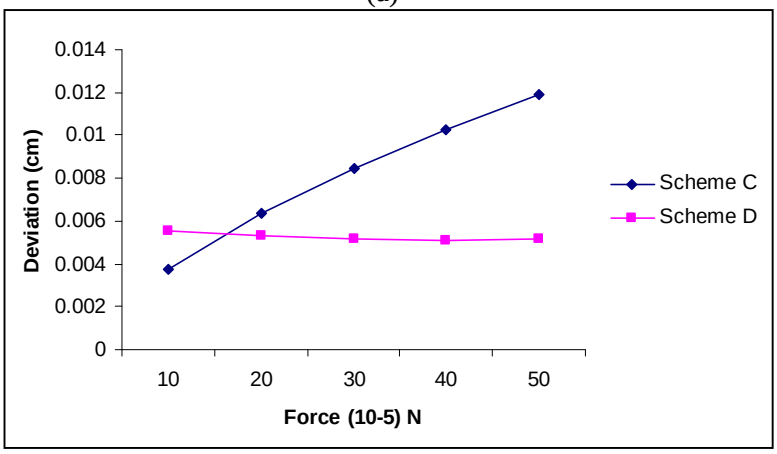

(b)

Figure 7.14: *Properties re-distribution after refinement: (a) The standard deviation of the displacement patterns for the different force amounts (b) Average displacement deviation comparison*

Based on this experiment, it has been demonstrated that it is important to preserve the homogeneity of the behaviour regardless of the design of the mesh topology that includes the event of topological modification. The feasibility of the method can be further explored by looking at the different mesh and shape complexities as well as the different material properties.

7.4.2.4 Re-estimation Evaluation

7.4.4.1 Local Behaviour Evaluation

Even if the standard deviation is low but the mean error is high, it is still not plausible. Both have to be low. Figure 7.15 illustrates the relationship achieved by the different schemes summarised in table 7.6. The proposed Scheme D achieved the lowest combination of standard deviation and mean error indicating behaviour preservation.

Table 7.6: *The mean and standard deviation (in millimetres (mm)) of the displacement patterns for the different schemes*

Scheme	Cube A		Sphere		Breast		Average	
	mean	stdev	mean	Stdev	mean	stdev	mean	stdev
A	0..07	0.03	0.04	0.02	0.05	0.04	0.05	0.03
B	0.08	0.05	0.06	0.03	0.08	0.05	0.07	0.04
C	0.04	0.03	0.03	0.02	0.04	0.03	0.04	0.02
D	0.03	0.02	0.02	0.01	0.04	0.02	**0.03**	**0.01**

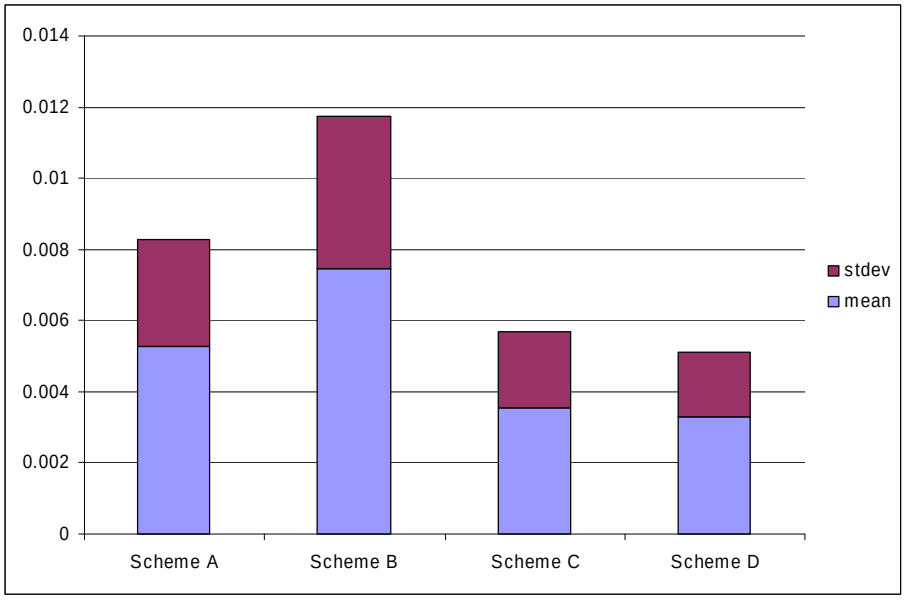

Figure 7.15: *The relationship between the standard deviation and the mean deviation from the pre-refinement displacement behaviour*

The sphere model was the most refined with 1000 nodes compared to breast that had about 276 nodes. Hence, the sphere displayed the lowest values for both standard

deviation and mean error. This was also due to the regular shape compared to breast. However, breast also showed low standard deviation and mean error as illustrated by one of the pattern comparisons in figure 7.16. This indicates a better behaviour preservation achieved by Scheme D compared to Choi et al. (2005) (Figure 3.16). Scheme A is based on the technique discussed by Choi et al. (2005), where it demonstrated inaccuracy in the behaviour preservation.

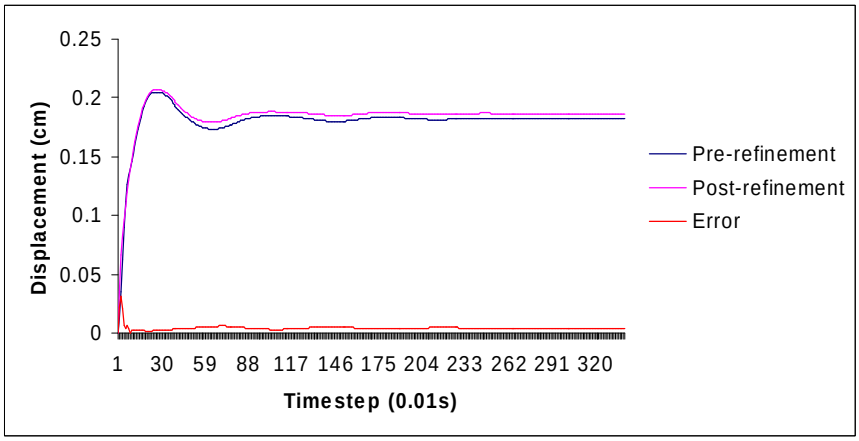

Figure 7.16: *Patterns for the pre- and post-refinement of breast model based on Scheme D nearly coincides*

7.4.4.2 Interacting with a breast model

The E value of the breast material employed in this evaluation was 3.25 kPa. Forces ranging from 0.5 to 1 N were imposed on the model. This section summarises the pattern comparisons achieved by the different schemes, where Scheme D surpassed all other methods in the preservation performance as illustrated in figure 7.17.

Even though Scheme B also produced a small combination of the standard and mean deviation (Figure 7.17), the patterns were more dissimilar especially at the initial stage before reaching equilibrium as illustrated in Figure 7.18. Furthermore, Scheme B did not produce correct E (Table 7.2) during the estimation testing and the

performance was inconsistent in reference to the overall analysis compared to the other schemes.

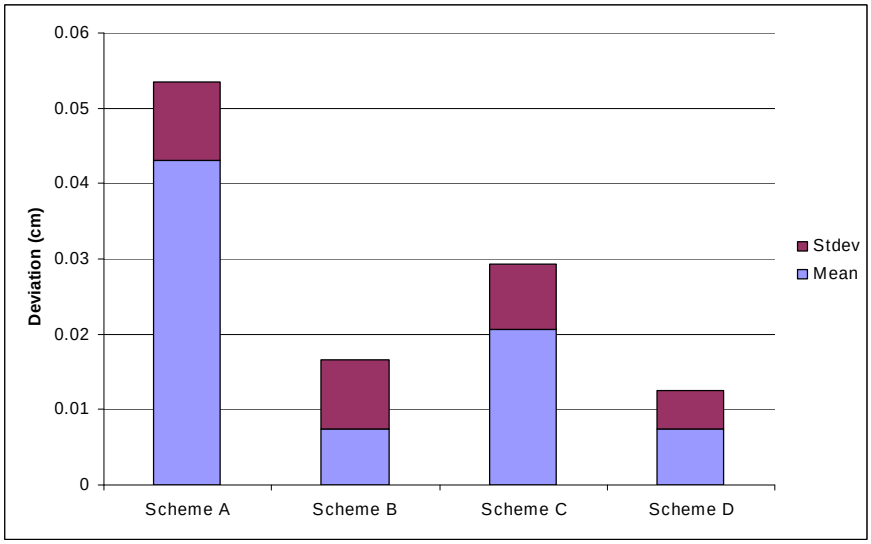

Figure 7.17: *The relationship between the mean and the standard deviation based on the displacement patterns comparison (overall analysis)*

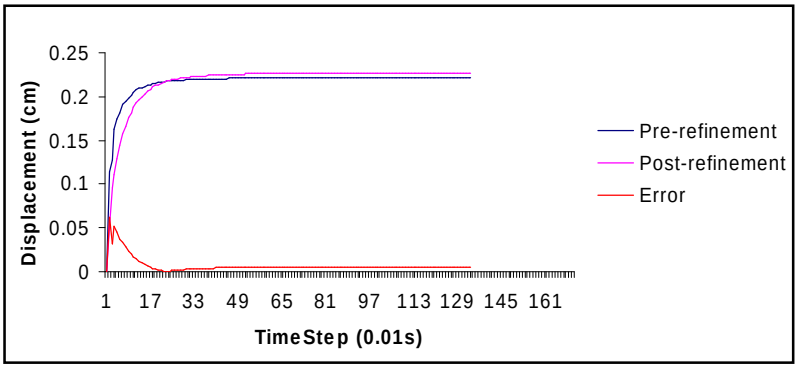

Scheme B

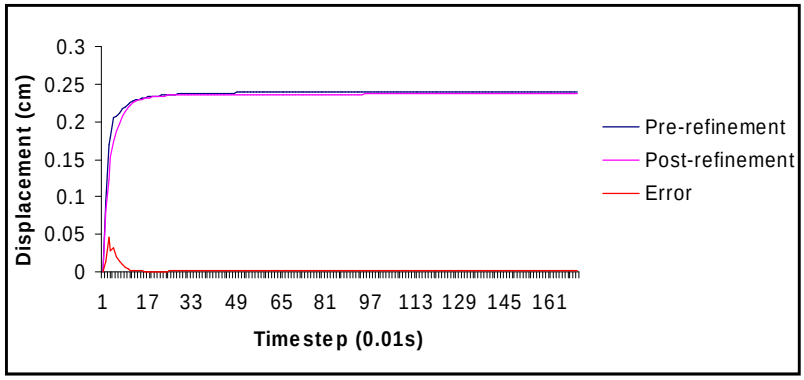

Scheme D

Figure 7.18: *Displacement patterns of Scheme B and D*

When the deformation was large (section 7.3.2.3), the accuracy of the extracted E value was around 84 percent of the initial E value. When the topology was refined, Figure 7.18 and 7.19 illustrate that the behaviour of the displacement was still preserved with minor deviation for large deformation (forces ranging from 1 to 5 N).

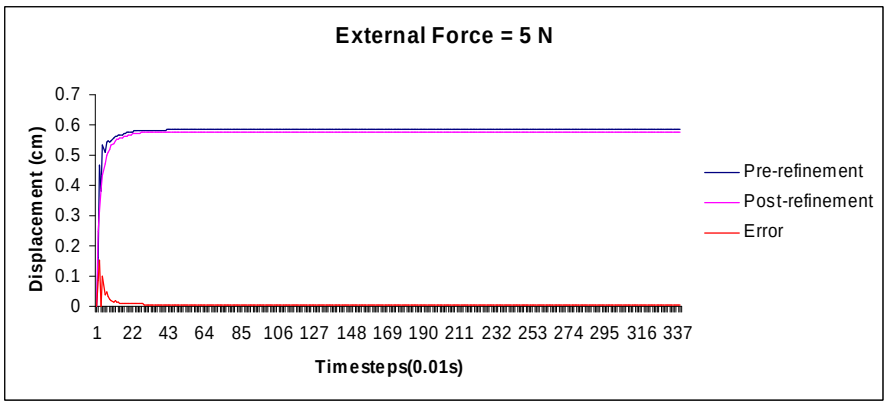

Figure 7.19: *Displacement patterns based on higher external force that produces larger deformation of Scheme D*

Even though the force was 5 Newtons, which is larger than the palpation force (1 to 2 N) of a breast model, the displacement patterns coincided with minor deviation. The summary of the relationship between the standard and mean deviation of the patterns is shown in figure 7.20.

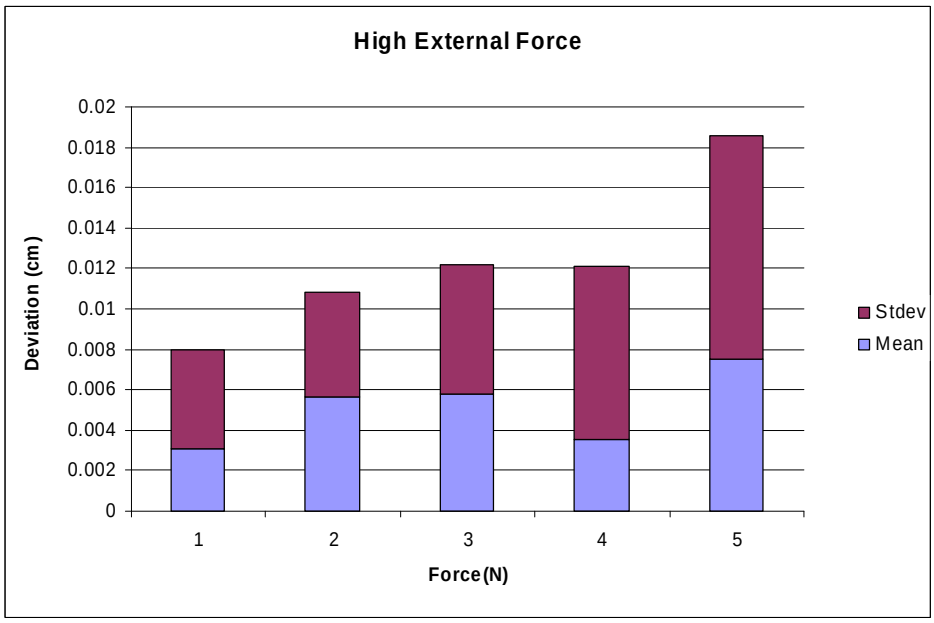

Figure 7.20: *A summary of the standard and the mean deviation over force (Scheme D)*

7.4.3 Distortion

Texture mapping is a technique to create a more realistic visual representation of an object. However, distortion is an issue when the object is deformed at runtime. The texture should display a more regular distortion when deformed regardless of the mesh topology onto which it is mapped. Uniform distortion indicates homogeneity. Van Gelder (1998) employed this method to evaluate his estimation method for a 2D membrane as shown in figure 3.12.

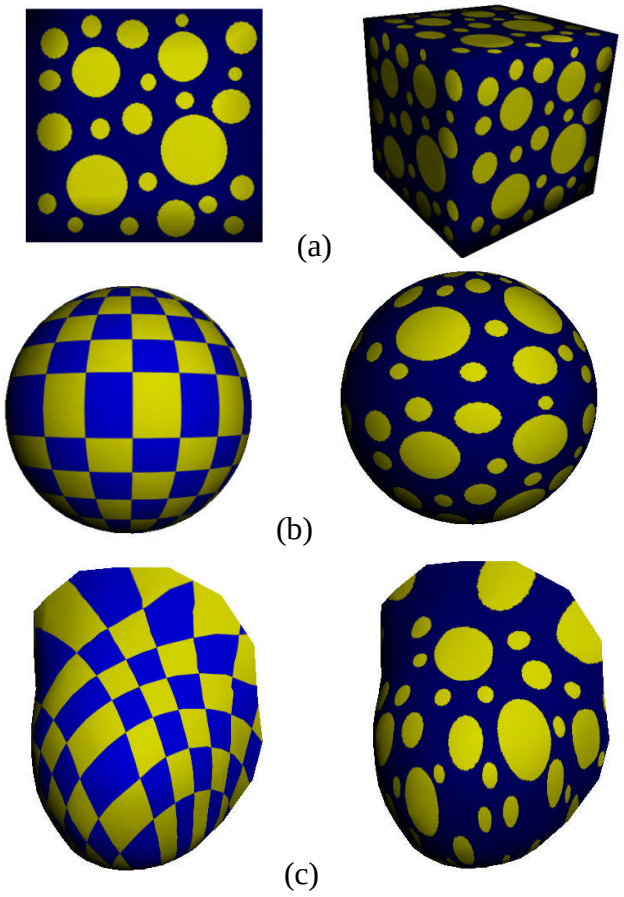

Figure 7:21: *Rest (unloaded) state of (a) cube (b) sphere and (c) breast*

The goal of this evaluation is to assess the feasibility of the estimation method in distributing the correct properties based on how the mesh elements are dynamically positioned. As discussed in section 2.2.2.1, the distortion of a surface texture is influenced by the dynamic behaviour of these elements. The significant characteristic

that was analysed is the uniformity of the distortion as the surface deforms. Even though the previous experiments emphasised that Scheme D emulated material properties more accurately compared to the other schemes, the local behaviour of the mesh elements should also be evaluated in terms of the behaviour of the texture distortion.

The evaluation was structured in a way that the complexity of the mesh and shape could be addressed by visual comparisons. The three main models at their rest states are as shown in figure 7.21. The criteria for the evaluation in the following sections were according to the sample parameters in figure 6.3.

7.4.3.1 Regular mesh topology

To additionally verify the consideration of the mesh topology in estimating the coefficient of the volume springs, the proposed Scheme D was compared with the original Scheme A (regular properties distribution for the shape preserving springs). Scheme C was also included in the distortion evaluation to reinforce the feasibility of determining the coefficients of the volume springs at runtime. The same cube of regular topology (figure 7.21 (a)) was employed in all of the schemes.

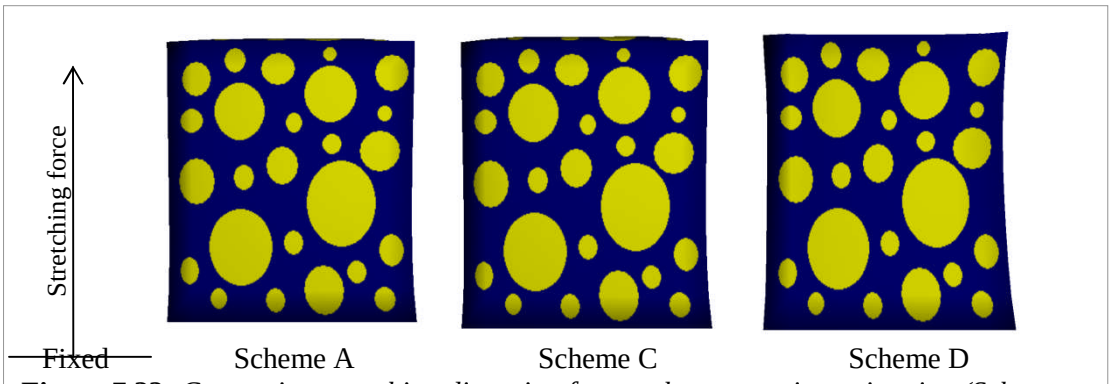

Figure 7.22: *Comparing stretching distortion for regular properties estimation (Scheme A) against the new schemes (C and D)*

The distortion of texture was nearly similar for all three schemes when a stretching force was imposed on the upper surface while the bottom surface was fixed (Figure

7.22), where all three corresponded to the direction of force. This is due to the mesh topology and the shape which was regular. Consequently, the properties at the node were all nearly identical. However, as established in section 7.3, Scheme A and C failed to reproduce the same elasticity modulus as the original.

Figure 7.23 illustrates that Scheme D produced a much more regular distortion compared to Scheme C, where the distortion of the squares (blue and yellow) was more evenly distributed. This is because in Scheme D, the stiffness of the volume spring at the node was determined at runtime based on the force orientation. Consequently, Scheme D produced a much more realistic shape, where the behaviour also responded to the change of volume to compensate loss or increase in volume.

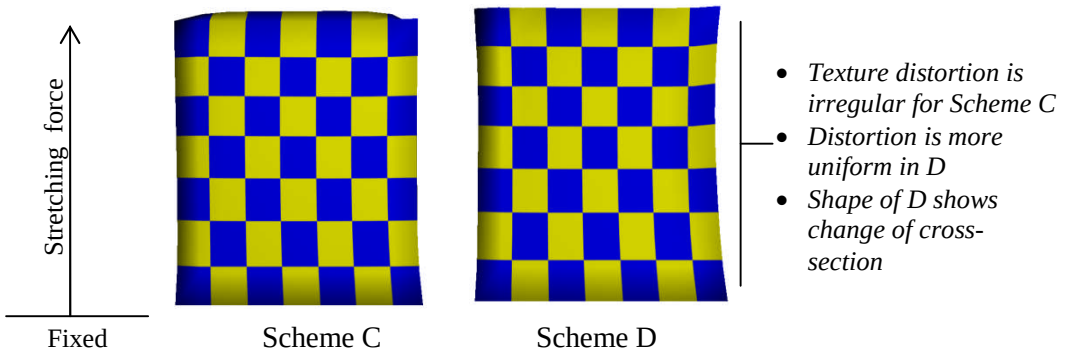

Figure 7.23: *Stretching distortion for Scheme C and D*

The versatility of determining the spring stiffness at runtime was further elaborated on by analysing the wireframe model of a regular cylinder. When the cylinder was suspended with the top surface fixed, the behaviour of the mesh topology was observed as shown in figure 7.24. The significance of this evaluation is to illustrate the feasibility of considering both uni-axial and shear spring parameters based on the orientation of force imposed on the masses. The mesh behaviour of Scheme C was stiff and it produced irregular distortion of the wireframe. Scheme D on the other hand

produced more uniform distortion for the surface mesh topology throughout the simulation. Thus, this illustrates homogeneity.

The stiffness of the volume springs in Scheme D produces deformation in response to the orientation of the acting gravitational and the resulting internal forces. Therefore, the deformation produced uniform distortion compared to the isotropic scheme C. The object under Scheme C has isotropic spring stiffness in response to the mass at the nodes in order to support the homogeneity of the material. Hence, it resulted in a much stiffer behaviour. Consequently, if a texture was to be mapped on the surface based on the mesh topology, it would experience irregular distortion.

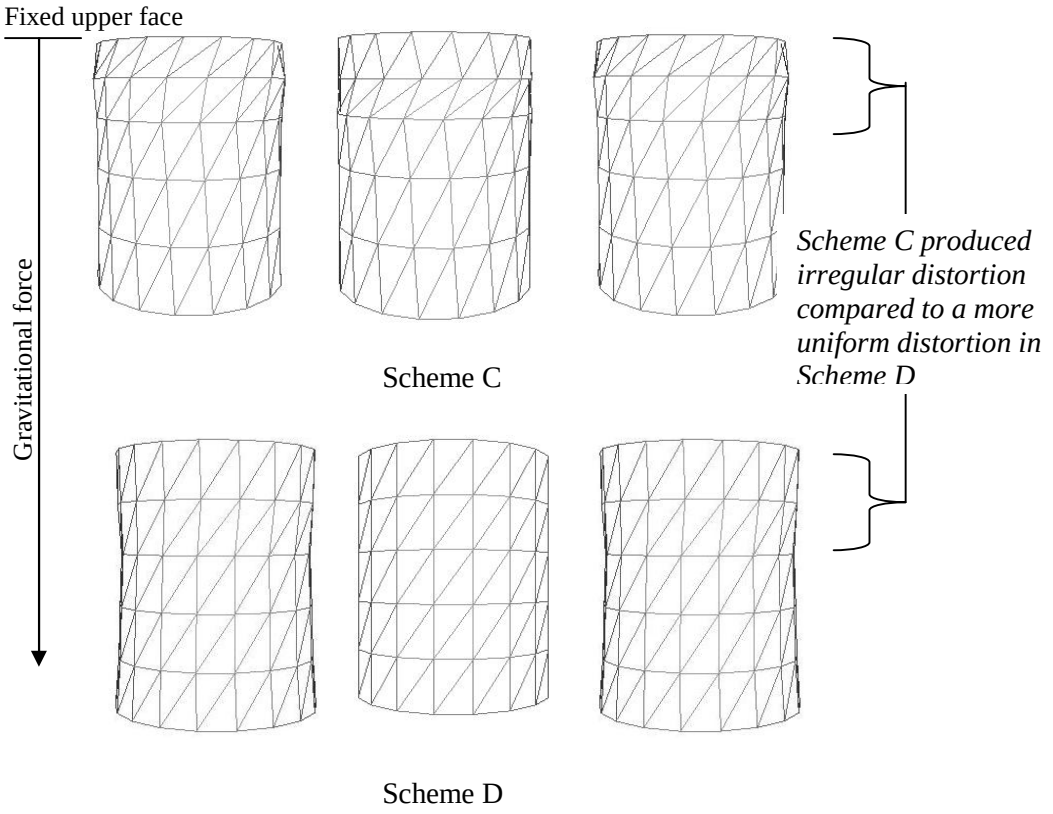

Figure 7.24: *Snapshots of the deformation under gravity with the top surface fixed (fully stretched by the gravitational force and back towards the fixed position during oscillation before reaching equilibrium)*

For shearing (figure 7.25), Scheme D displayed a more uniform distortion of the circles on the texture compared to Scheme A. This is due to the consideration of the

orientation of force at runtime. When compressed (figure 7.26), Scheme D still maintained a more uniform distortion behaviour as well as the shape. This reinforces the versatility of the complete configuration that considers the three parameters for the spring coefficients, force orientation and volume variation.

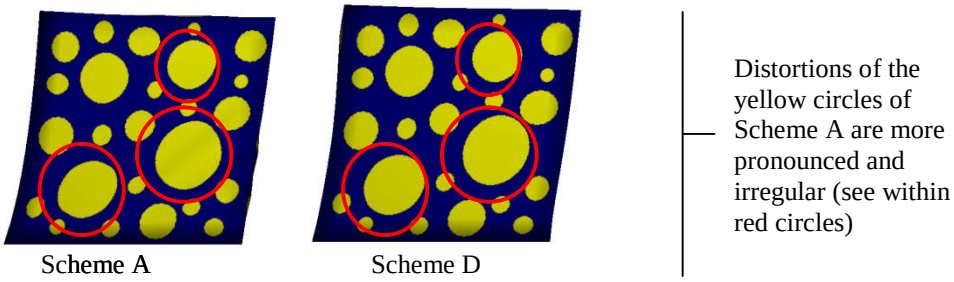

Figure 7.25: *Comparing shearing distortion for Scheme A against Scheme D*

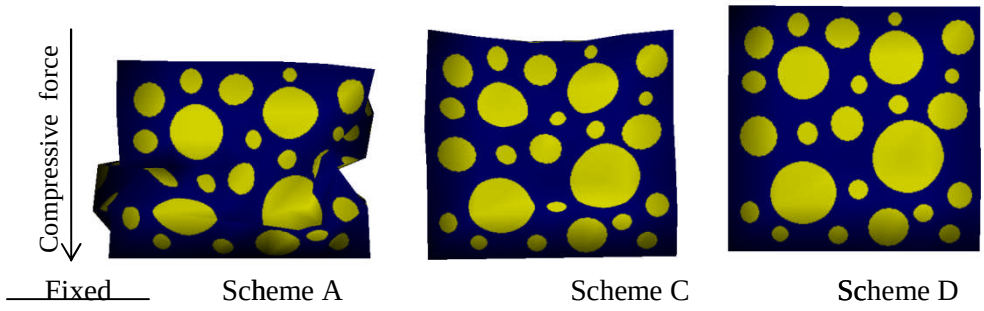

Figure 7.26: *Compressed*

7.4.3.2 Irregular mesh topology

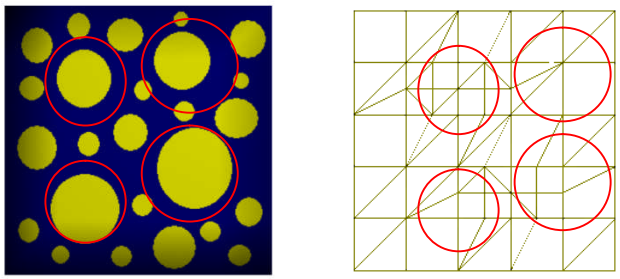

Figure 7.27: *Rest state of a cube with irregular mesh topology (Red circles denote the refined areas)*

The subsequent question is whether the same distortion behaviour will be produced when topological refinement is imposed on the surface. In reference to the evaluation in section 7.4.2 on properties re-estimation, the distortion exercise was carried out to

compare the local behaviours pre- and post-refinement. As illustrated in figure 7.27, four separate areas on the surface mesh were refined.

Figure 7.28 compares the stretching distortion before and after refinement for each scheme in reference to figure 7.22. The distortion was along the same axis for most of the circles on the texture for Scheme C and D. The behaviour of pre- and post-refinement was best preserved by these schemes as both are based on the same fundamental estimation technique. This behaviour verifies the material homogeneity irrespective of the change of topology. Distortion for Scheme A was highly irregular and differed from the distortion prior to refinement.

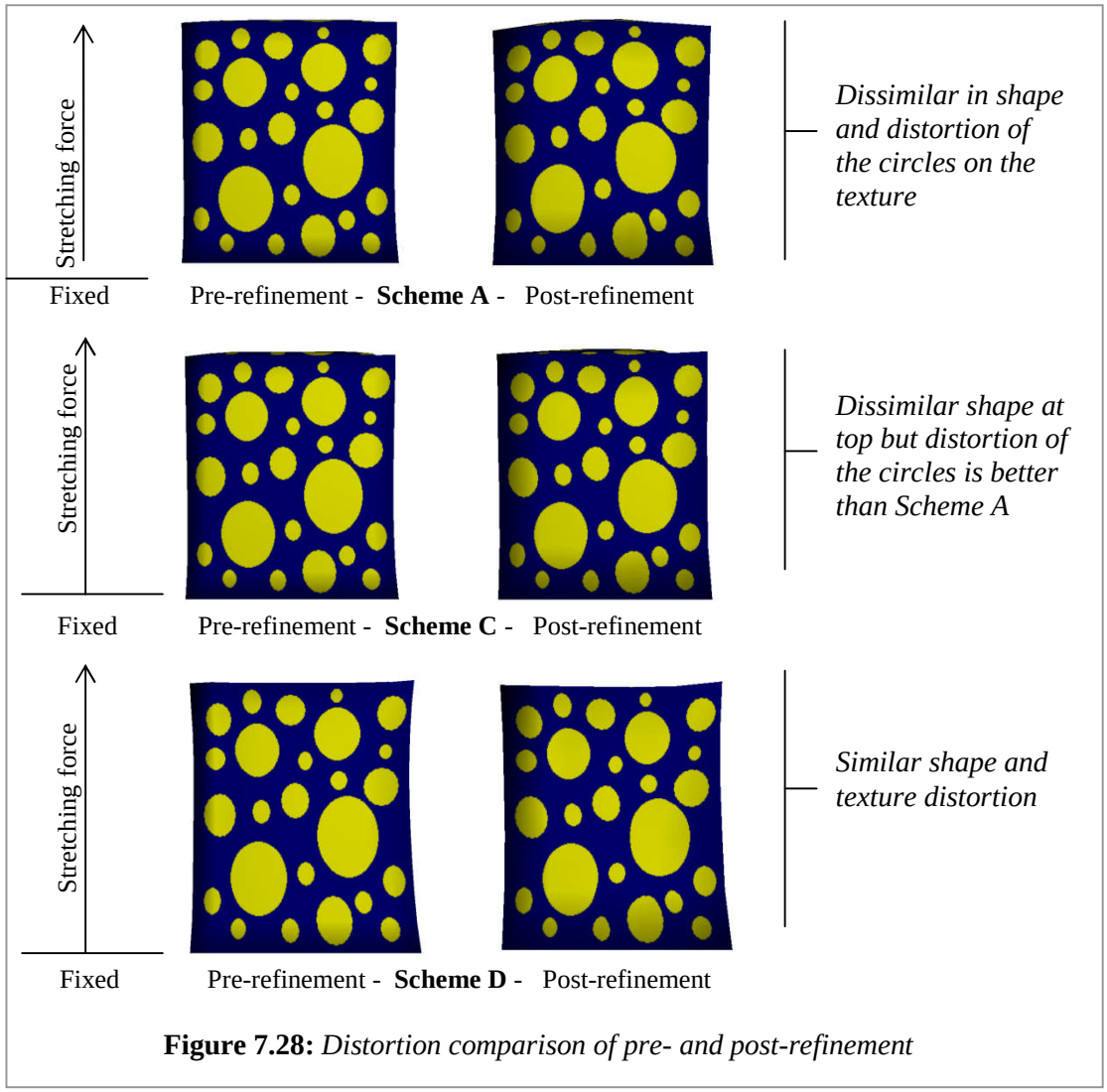

Figure 7.28: *Distortion comparison of pre- and post-refinement*

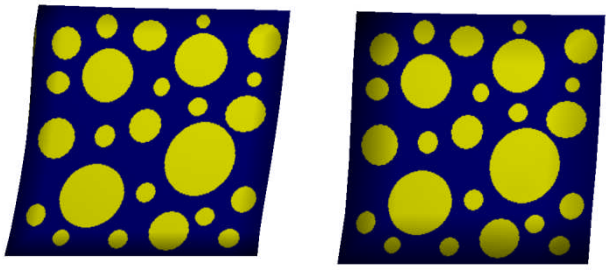

Pre-refinement Post-refinement

Figure 7.29: *Shearing distortion for Scheme D*

To further illustrate the high level of uniformity for Scheme D, the distortion in response to shearing was observed. Figure 7.29 demonstrates that the homogeneity of the texture behaviour was maintained. Additional evaluations have been conducted on models with regular and irregular shapes to reinforce the versatility of the configuration technique for Scheme D.

7.4.3.3 Regular shape with irregular mesh topology

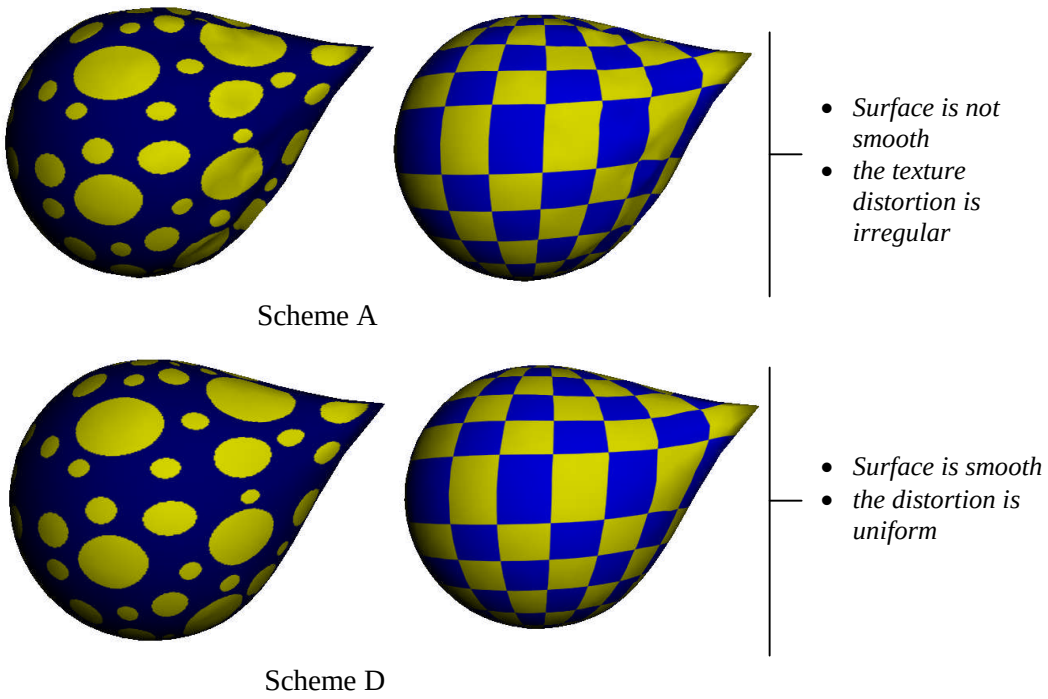

Figure 7.30: *The sphere deformed in response to an outward force imposed on the surface*

Since the shape of a sphere is regular, the distortion when stretched should be uniform. Figure 7.30 further illustrates that scheme D consistently maintained a more regular texture distortion despite the irregularity of the mesh topology.

7.4.3.4 Irregular shape and mesh topology

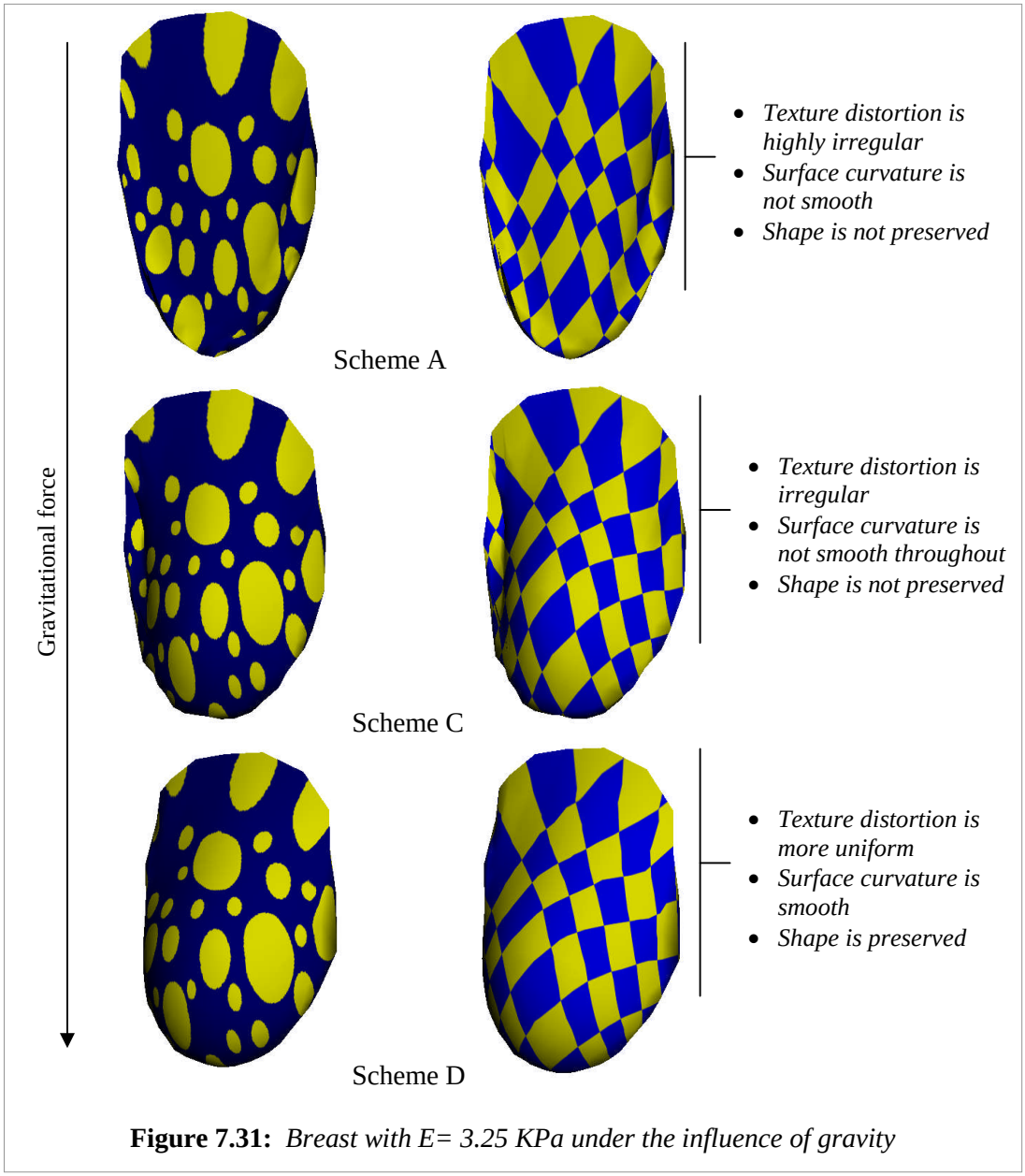

Figure 7.31: *Breast with E= 3.25 KPa under the influence of gravity*

The second shape employed was a breast model, which is not only of an irregular shape, but is also an open surface model. In figure 7.31, Scheme A produced a highly inconsistent texture distortion. The shape topology was also not preserved under the

gravitational pull. Scheme D consistently displayed regular texture distortion over the shape topology so as to emulate breast deformation under gravity.

This demonstrates that anomalies in the texture distortion were induced by the stiffness distribution in both Scheme A and C. The distortion in Scheme C was more inhomogeneous compared to Scheme D due to the spring stiffness being independent of the shear coefficient in response to the orientation of the force, which was considered by Scheme D.

7.4.5 Summary

The last three objectives established in this chapter were achieved in accordance with the evaluation findings analysed in this section. By analysing the distribution of mass and spring coefficients, the significance of properties approximation was demonstrated, where the proposed model (Scheme D) induced homogeneous behaviour during simulation. The flexibility of the estimation technique was also highlighted in terms of the preservation of local behaviour in response to the topological modifications. Homogeneity preservation was further demonstrated by the uniform texture distortion during deformation despite the design of the topology.

7.5 Conclusions

The configuration of the deformable model parameterised with real material properties is the core contribution to the feasibility of employing a surface model. The main objective of this chapter was thus to highlight the versatility and the feasibility of the proposed model concerning the estimation of properties in order to emulate elasticity and to maintain homogeneity. This chapter has not only illustrated the feasibility of embedding real material properties to a surface mass spring system but

also the feasibility of determining the spring properties at runtime based on the orientation of external and internal forces.

To further verify the findings, relevant experiments that compare the proposed configuration (Scheme D) against the other existing schemes (Schemes A, B, C) have been carried out. A ranking (out of 4 stars) based on the key quantitative findings is summarised in Table 7.7. Since the third parameter is not addressed in this chapter, the column of table 7.7 is not filled. This will be populated in the next chapter.

Table 7.7: *Ranking of the schemes (out of 4 stars) in reference to the first two key experiments for the evaluation parameters (elasticity & homogeneity)*

Scheme	Stress and Strain	Topology Refinement	Volume Preservation
A	*	*	
B	**	**	
C	***	***	
D	****	****	

In reference to the analyses and summaries for both section 7.3 and 7.4, elasticity and homogeneity were maintained irrespective of the design of the mesh topology and the refinement of the topology. Therefore, the hypotheses and the objectives of the evaluation have been met.

Not only is it vital to include real material properties in the configuration of the deformable model, but it is also important to achieve volume effects. The next chapter focuses on evaluating the volume behaviour of the proposed deformable model within the scope defined in Part II. The third column in table 7.7 will also be explored, where the incompressible behaviour of the model is addressed.

Chapter 8

Volume Behaviour

8.1 Introduction

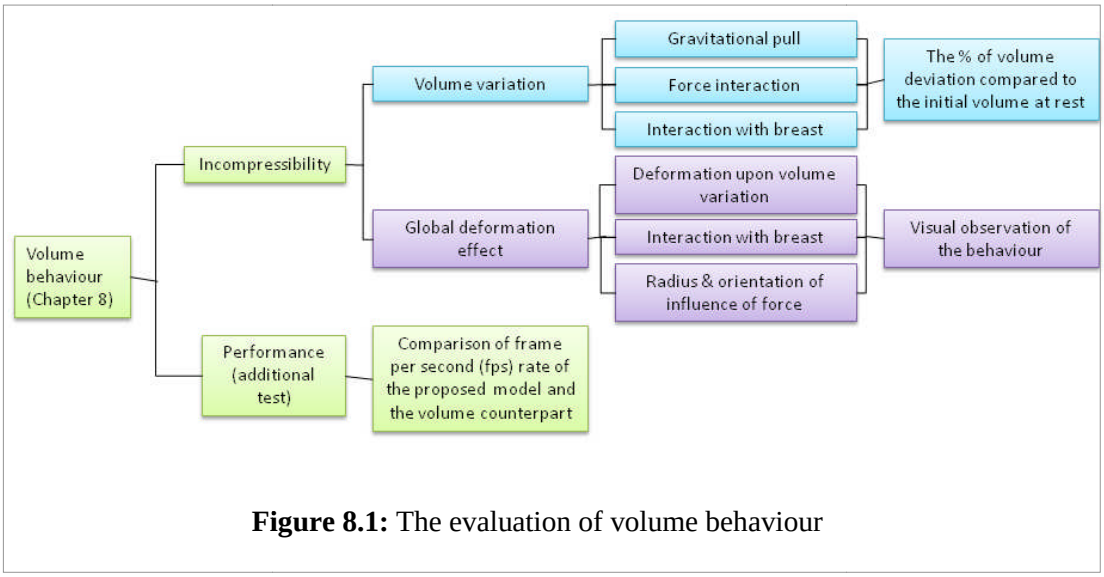

Figure 8.1: The evaluation of volume behaviour

Chapter 7 has concluded that the proposed configuration, with key features such as those listed in section 6.3.2, are feasible for a surface mesh of any irregularity. Besides material elasticity and homogeneity, incompressibility is another assumption adopted by the proposed model. In order to emulate such material, the model endeavours to not only preserve the shape but to also maintain the volume during simulation. However, near incompressibility is expected (Poisson ratio of below 0.5).

This chapter highlights the findings based on the evaluation approach established for the issue of volume behaviour in relation to incompressibility. The taxonomy illustrated in figure 8.1 summarises the respective experiments. An additional experiment that evaluates performance is also described in this chapter.

8.2 Evaluation Objectives

As described in the evaluation framework (see Chapter 6), the three key hypotheses relevant to the issue of volume behaviour are:

i) The principal characteristic of an incompressible solid is to preserve a constant volume during simulation. For an elastic and incompressible material, the original shape at rest as well as volume during deformation should be conserved. Since materials such as soft tissues are not perfectly incompressible, minor discrepancy in volume preservation is expected.

ii) Despite the absence of internal discretisation, the global deformation effect of the surface model reflects the assumption of an incompressible volume.

iii) As the surface method is a dimensional departure from the volume counterpart, the computational complexity is also reduced. When compared to a VMSS with similar mass-spring complexity, the proposed surface model is expected to be more efficient.

In reference to the above hypotheses, the objectives are to:

i) Analyse the volume variations of the model under the influence of the gravitational pull and the interaction force.

ii) Observe the visual effect of the local and global deformation under the different conditions

iii) Investigate the feasibility of the runtime manipulation of the global deformation effect in relation to the change of volume as well as the orientation and the radius of influence of the interaction force.

iv) Investigate the frame rate of the proposed surface model in comparison to the volume counterpart, where the same shape and MSS complexities are employed.

The first three objectives guide the assessment of the incompressible behaviour of the model. The last objective introduces an additional assessment, where the performance of the model is compared to the VMSS. The following sections discuss these assessments based on the respective experiments established in table 5.2 and the evaluation taxonomy in figure 8.1.

8.3 Volume variations

The analysis of volume variations during simulation provides a quantitative measurement of incompressibility. The existence of minor deviations from the original volume indicates the behaviour of near-incompressibility. The assumption of incompressibility has been adopted for the simulation of soft objects such as soft tissue. However, since no material is perfectly incompressible, a minor deviation is expected.

8.3.1 Gravitational pull

The shape of the object under gravity is fundamentally influenced by the volume springs that provide the vertical support relative to the downward gravitational pull along the Y-axis. Section 7.4.1 established the association between the mass at the nodes and the coefficient of the respective volume springs, where the behaviour of the proposed surface model in figure 7.7 indicated a complementary relationship when simulated under the influence of gravity. In addition, the volume behaviour of the sphere during simulation as previously illustrated in figure 7.8 demonstrated realistic

visual reactions to the gravitational pull where the shear factor of the volume was considered. The resulting volume variation during simulation is shown in figure 8.2.

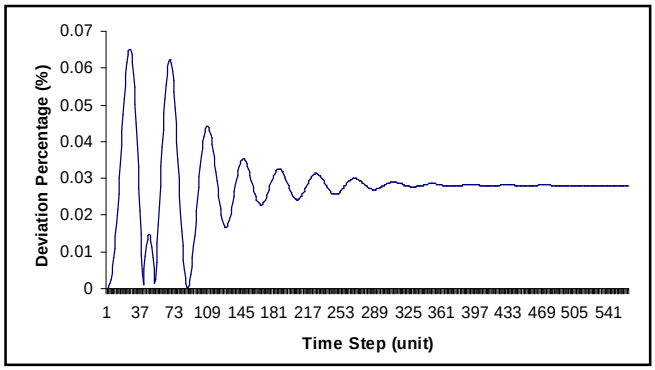

Figure 8.2: *Volume deviation (Scheme D) over time under gravity*

The initial variations were larger than the final deviation reached at equilibrium. This indicates the time taken for the MSS to catch up with the sudden change in volume at the beginning of the simulation.

The proposed model aims to emulate volume behaviour whether a closed or an open surface mesh is employed. In the next experiment, a simple breast model which was based on an open surface mesh was employed. The edge of the surface was fixed to maintain the model in a constrained environment as described in the research scope. Based on this arrangement, different positions under gravity were observed. The unloaded and loaded models in the vertical, supine and prone positions are shown in figure 8.3, where the shape and deformation respond to the weight of the breast under gravitational pull. When compared to the MR images (figure 2.8), the top views for both supine and prone positions are visually similar in terms of the shape outline. Figure 8.4 demonstrates similar shape curvatures.

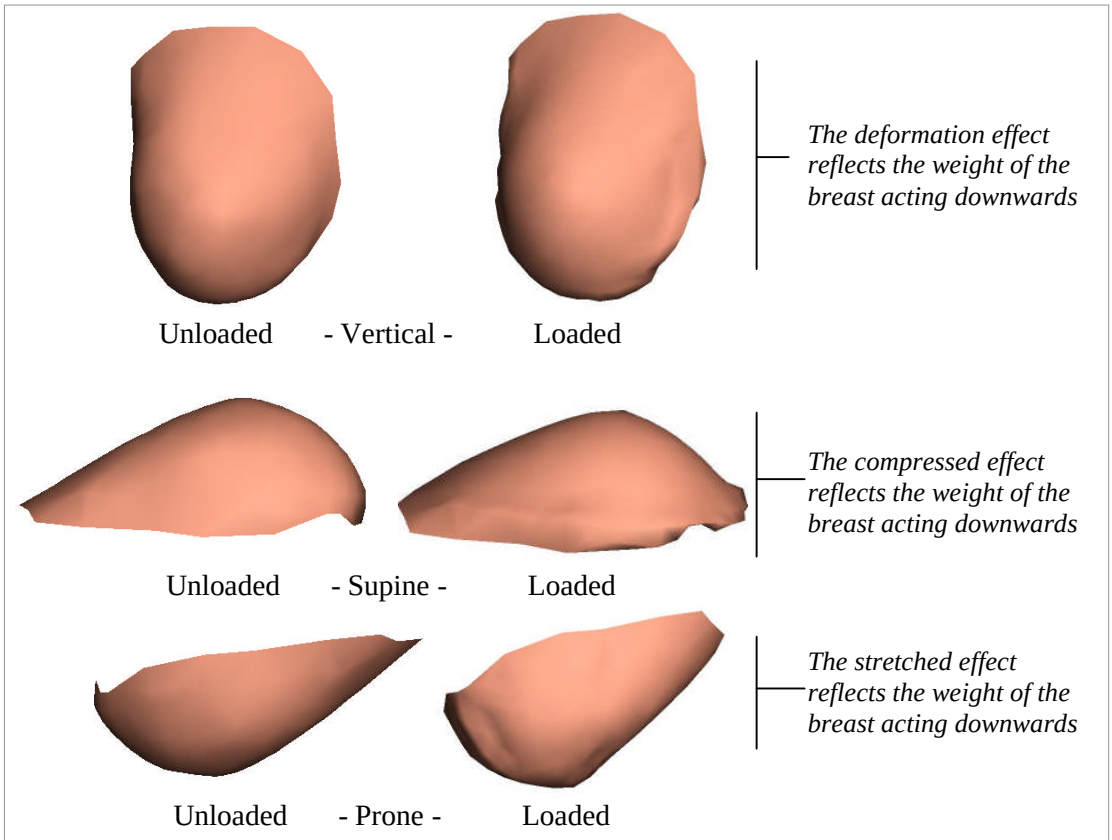

Figure 8.3: *Breast Model of Scheme D under the Unloaded and Gravity loaded conditions at the vertical, supine and prone position*

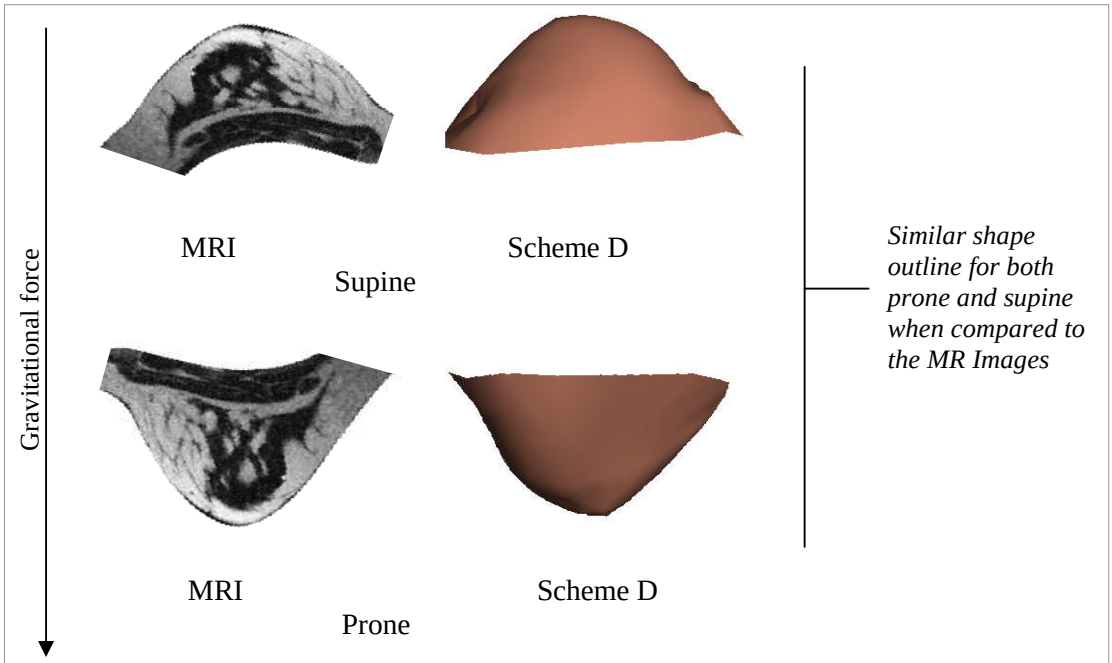

Figure 8.4: *Breast position under gravity (top supine and prone views): MR image (MRI) (Rajagopal et al. 2008) compared to Scheme D*

In reference to the volume variations illustrated in figure 8.5, the average volume deviation of the breast model at the different positions was about 3.57 percent. However, the volume preservation at the supine position was not as efficient compared to the other positions. This can be interpreted as volume loss by the open part of the surface when compressed with a supine position. This was due to the non-collision limitation of the breast against the static body such as the ribcage. On the other hand, the respective visual representations (figure 8.3 and 8.4) satisfy the global deformation effects and the shape comparison of the breast under gravitational pull.

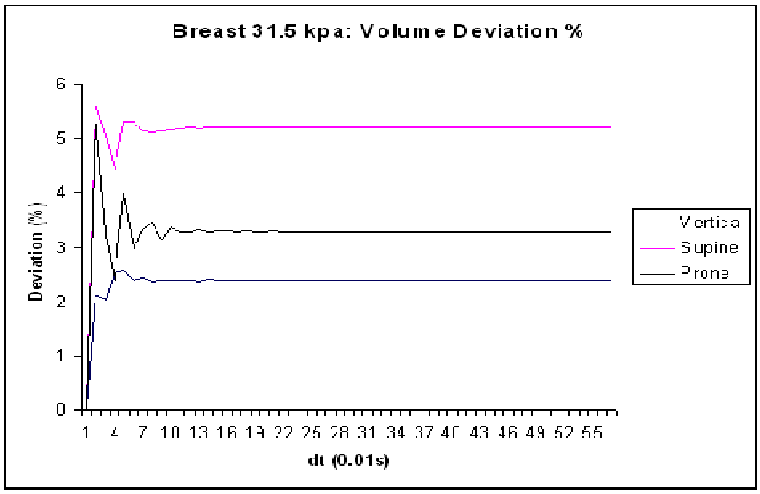

Figure 8.5: *Volume Deviation under Gravity*

The deformation of the breast model complements the impression of volume and weight concentration of the model. When in a vertical position, the weight was concentrated at the lower part of the model. Figure 8.6 illustrates the respective displacement analysis and the subsequent texture distortion for the different elasticity moduli. The movement of the breast model mostly revolved around the lower part where weight and strain mostly concentrated. The texture distortion also reflected this.

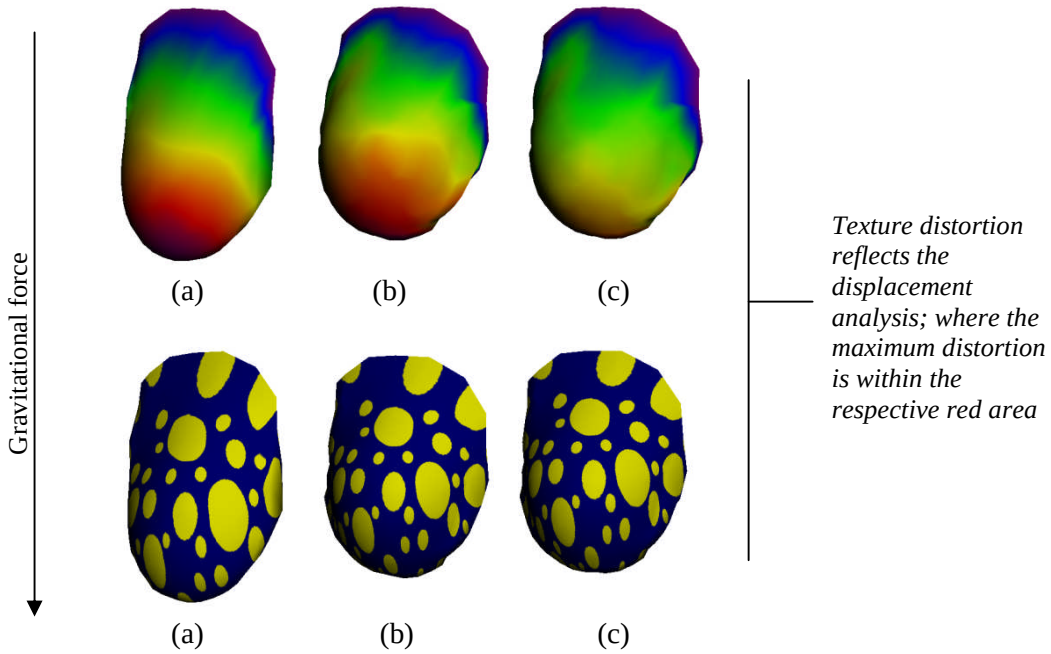

Figure 8.6: *Displacement mapping from the maximum value (red) to the minimum (blue) and the respective texture distortions (a) 3.25 kPa (b) 22.5 kPa (c) 31.5 kPa*

8.3.2 External Force Interaction

An interactive virtual simulation requires direct contact with the deformable model such as interacting with a breast model during palpation. The resultant deformation is depicted by the change in shape as a response to the interacting force. This section deals with the effects of the interaction force to volume variations during simulation.

When a constant force was imposed on the sphere surface as shown in figure 8.7, the shape consequently changed and deformed. The volume at each time step was calculated using equation 5.8. The subsequent deviation compared to the original volume was then determined.

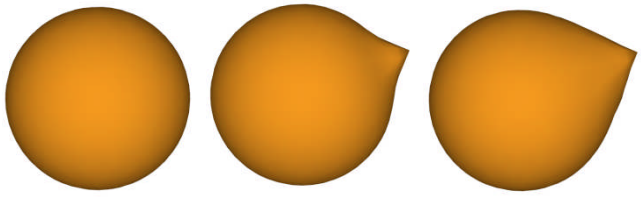

Figure 8.7: *Snapshots of object deformation under a constant force*

The analysis of these variations concludes that Scheme D preserved the object volume with the least deviation as illustrated by the comparison of the average deviation percentage in figure 8.8. This initial comparative analysis emphasises the feasibility of the proposed model to not only approximate the properties of the MSS but to also preserve the volume with the least deviation despite the absence of the actual volume data.

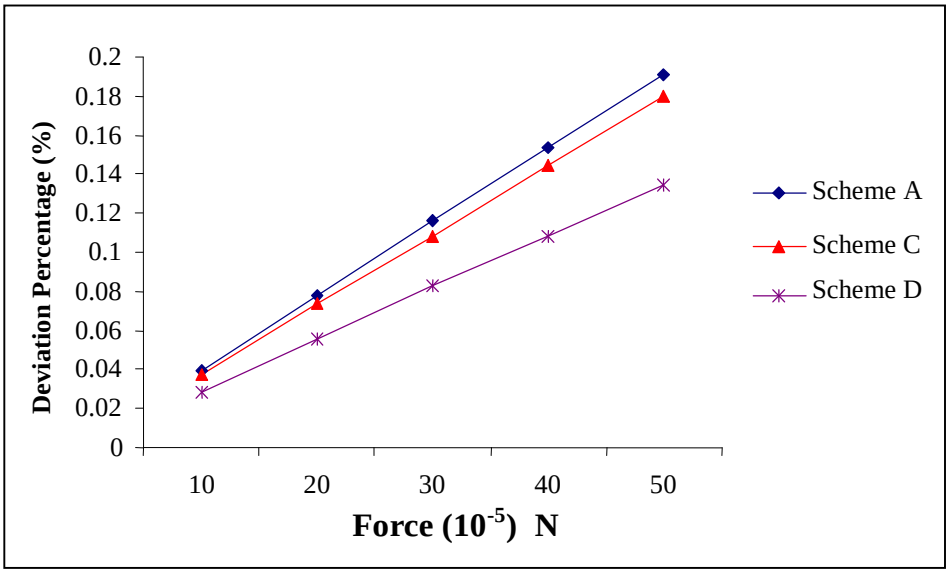

Figure 8.8: *The percentage of the average volume deviation: To compare regular method against irregular methods*

The same experiment was repeated for models of different mesh complexities, where the proposed Scheme D was compared against Scheme A, B and C. The findings, described in the next section, further establish the volume preserving characteristic of the proposed model.

8.3.2.1 Mesh Complexity

Mesh complexity can be increased to allow for a more defined visual representation of the deforming surface. The relationship of the complexity to the volume preserving capability of the deformable model has been examined by analysing three different

cubes (figure 6.4) with increasing number of nodes from Cube A to Cube C. An external force was imposed on a small part of the surface and the corresponding volume variations were noted. Based on the variations during simulation, figure 8.9 demonstrates that the proposed Scheme D preserved volume better than the other schemes for all the cubes with a deviation of less than three percent. The initial surge of volume change was due to the significant increase in velocity and displacement of the nodes imposed with the external force. The increase rate was higher than the overall volume compensation process. However, the volume stabilised at a constant value in less than a second.

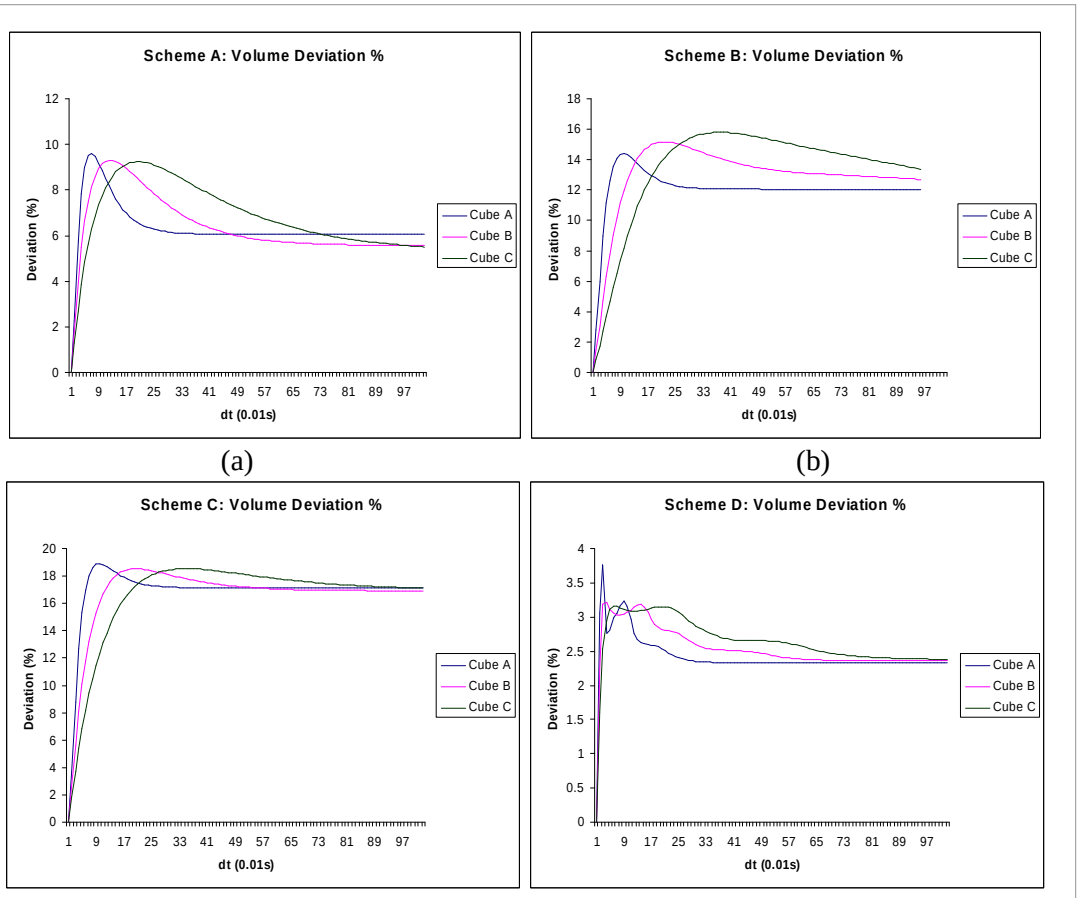

Figure 8.9: *Volume Deviation Percentage: (a) Scheme A (b) Scheme B (c) Scheme C (d) Scheme D*

For the different complexities, it was observed that a constant volume was achieved at a faster rate for the cube with the lowest number of nodes. This indicates the influence

of the mesh complexities on the preservation of volume. However, similar constant volume was achieved by all cubes at the same rate in Scheme D compared to the other schemes.

Figure 8.10 summarises the mean deviation extracted from the volume variations produced by all schemes for the different cubes. Compared to the gravity test, Scheme C failed to display a better volume preservation as the model was not influenced by the orientation of force. This concluded that it is important to support the influence of force from a single point of interaction or multiple interaction points such as imposed by the gravitational pull. Scheme D demonstrated the lowest deviation for both conditions.

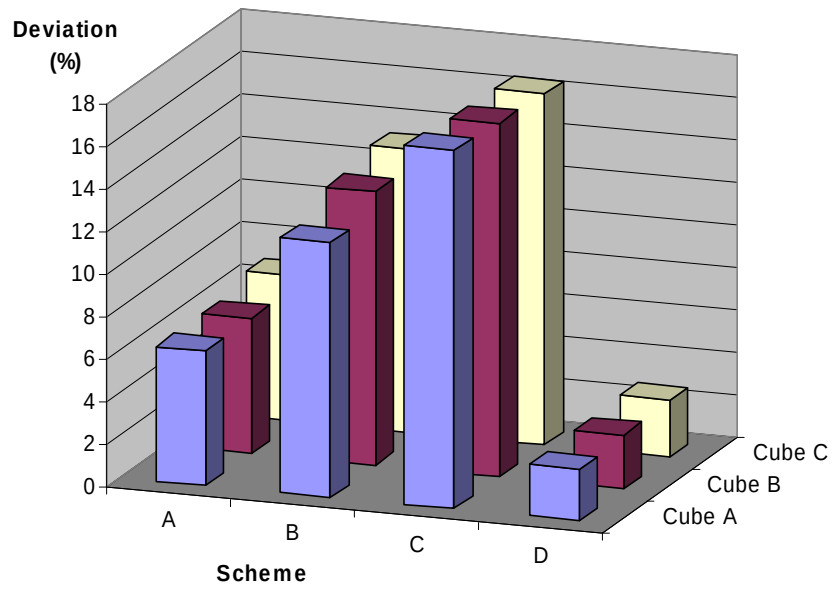

Figure 8.10: *Mean Volume Deviation Percentage*

8.3.2.2 Interacting with a Breast Model

Scheme D is further explored in this section. Forces of different magnitudes were imposed on the surface of the breast and volume was calculated at runtime. The consequent deviation of volume at runtime is illustrated by figure 8.11. As discussed

in the previous section, the initial change in volume was large due to the highly dynamic node displacement in response to the initial force before the change of volume was actually compensated by the penalty force. The increase in rate of displacement and velocity was faster than the rate of volume compensation. However, constant volume was finally maintained with minimal deviation over the following time steps.

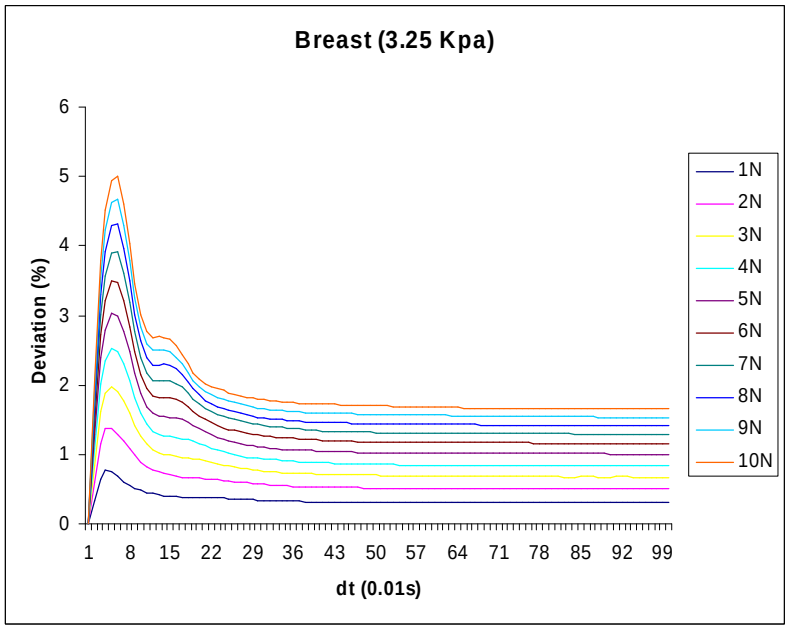

Figure 8.11: *Volume Deviation Percentage (Scheme D)*

The exercise was repeated with other elasticity moduli (22.5 and 31.5 kPa). As the elasticity modulus increased, volume was better preserved due to the increase in stiffness and incompressibility. However, the exercise showed that volume was maintained with small deviation (less than 2 percent) even when the external force was large as illustrated by figure 8.12. This further illustrates the feasibility of the proposed model to support large deformation. However, for interaction with human tissues such as breast tissue (palpation magnitudes of around 1 to 2 N), the imposed force magnitude should not be exceedingly high as it could exceed the material yield limit. Based on these palpation magnitudes, the volume deviation is minimal (less than 0.6 percent) for all three E values as summarised in figure 8.12.

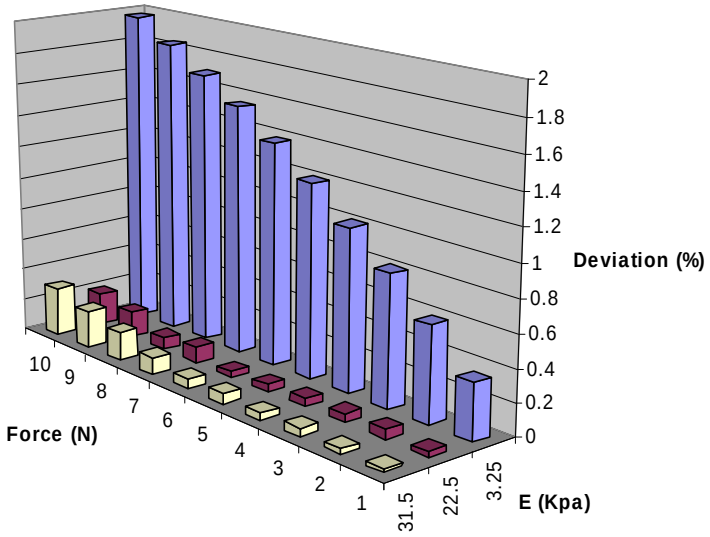

Figure 8.12: *Mean Volume Deviation Percentage (Scheme D) for the three elasticity moduli (E)*

8.3.3 Summary

The first hypothesis and the first three objectives (section 7.2) established for the evaluation in this chapter have been addressed. Volume variations for the different models were analysed at runtime. The consequent minor deviations from the original volume indicate that the model was not perfectly incompressible. On the other hand, the deviations were minimal compared to the other schemes. The preservation of volume was also reflected by the deformation in response to gravity and interaction. The important attribute of maintaining a constant volume with low deviation during simulation has been achieved

Thus the assumption of near-incompressibility is possible at runtime. This allows the global deformation effect even for hollow objects to emulate solid behaviour. The implication is the feasibility in employing this model in medical training such as the simulation of breast palpation. Not only does the influence of the gravitational pull at the various bodily positions have to be taken into account but the effect of external

force interaction has to also be supported whilst retaining volume during the simulation.

Within the range of the proposed palpation force of 1 to 2 Newton, the volume of the breast model was preserved with less than 0.6 percent deviation. A constant deviation was maintained at equilibrium and during palpation. The breast model in the supine prone and vertical positions was examined under gravitational pull. Even though the visual response of the shape of the breast reflected the influence of the gravitational pull on its weight, the volume deviation of the supine position was larger than prone and vertical. This is a limitation of employing an open surface at the supine position.

8.4 Global Deformation Effect

As discussed in chapter 2, the global deformation effect refers to the change of the object shape local to the influence of the external force imposed on its surface while maintaining the global position within a constrained environment. The resulting change in volume due to the gravitational force and the external force interaction is compensated to promote incompressibility. The parameters that govern the effect of the consequent global deformation are established as the volume variation as well as the radius and the orientation of influence of force. The resulting shape behaviour is influenced by the distribution and the concentration of volume compensation.

The next subsections discuss the deformation responses of the proposed deformable model (Scheme D) in relation to these parameters.

8.4.1 Deformation in response to volume variation

The shape of the model based on Scheme D changes in line with the concept of the relationship of true stress and true strain, where the cross-sectional area of the object

changes during simulation such as the cube in figure 7.23 and the cylinder in figure 7.24. This behaviour shows that the change in volume was compensated by the change of this area during simulation. Figure 8.13 demonstrate the responses to volume variation due to an external force on the cube.

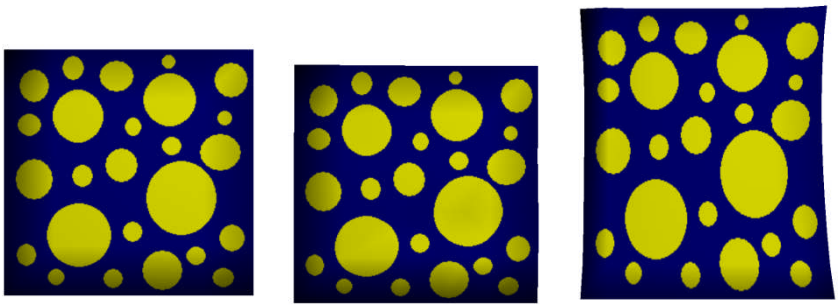

Figure 8.13: *Shape change of Scheme D due to volume variation*

A parallelogram shape (figure 8.14) was achieved by a cube model when imposed with a gravitational force with the left-most face fixed. The distortion was uniform where the degree of distortion in 8.14(a) coincided with the degree of displacement of the nodes as depicted by 8.14(b) (red to blue denotes max to minimum). This also illustrates that strain concentrated around the maximum displacement area (red), which was in between the fixed and the right-most faces.

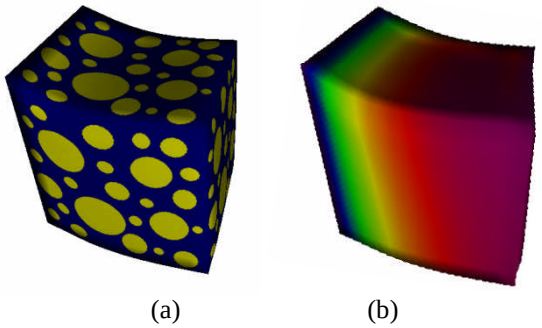

Figure 8.14: *Deformation under gravity when left-most face is fixed displaying soft solid behaviour: (a) texture distortion (b) displacement analysis*

8.4.2 Interacting with a breast model

When interacting with an incompressible object, the deformation effect should be demonstrated where pressure is internally distributed to compensate the change of volume, such as a palpation of a human breast. Figure 8.15 illustrates the visual feedback of the breast model in response to a palpating force.

The surface nodes achieved high displacement within the red area where the effect of the weight of the breast mainly concentrated under the gravitational pull. Upon interaction, the shape changed to demonstrate volume compensation, where the changes corresponded to the orientation of the palpating force represented by the point load in figure 8.15 (b).

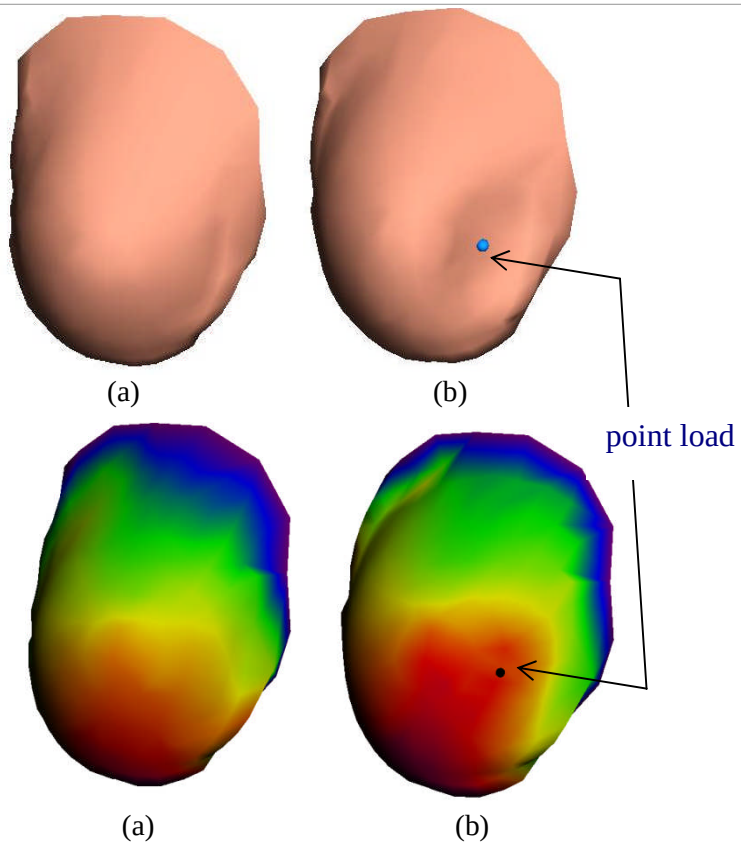

Figure 8.15: *Incompressibility is emulated (a) under the influence of gravity and (b) during interaction: The breast responding to haptic interaction and the respective displacement analysis*

Incompressibility has been attempted by methods such as discussed in Part I, where the reaction of the surface deformation responded to volume variations. For instance, the weight distribution method proposed by Hong et al. (2006) was based on fine-tuning the properties to create the visual effect, while methods such as those employed by Matyka & Ollila (2003) did not consider the influence of force orientation, where their method produced a balloon effect.

Unlike these methods, the configuration of the proposed model was parameterised by real material properties and influenced by the orientation and the radius of influence of the interaction force. Figure 8.16 further illustrates the effect of incompressibility due to volume compensation and force orientation.

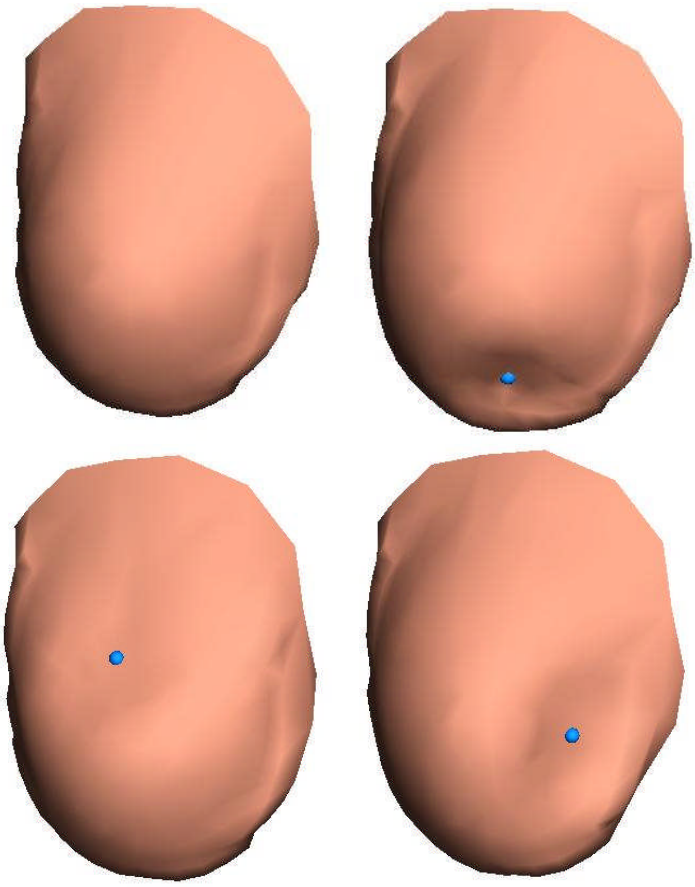

Figure 8.16: *Realistic responses to interaction where the breast surface reacts to volume variation*

8.4.3 Radius and orientation of influence

To produce a more realistic global deformation based on the radius and the orientation of influence of the interaction force, the weighted factors were manipulated at runtime. When the default weighted factors were set to 1 (figure 8.17 (a)), the global deformation effect was incorrect. The same default setting had been employed by Hong et al. (2006).

The proposed model promotes more versatility for both local and global deformation. Upon interaction, the weighted factor at each node was modified during simulation in regards to the radius and the orientation of the interaction force as described by equation 5.9. Consequently, figure 8.17 (b) shows that at runtime; the automatic factors derivation based on these parameters produced a more realistic behaviour.

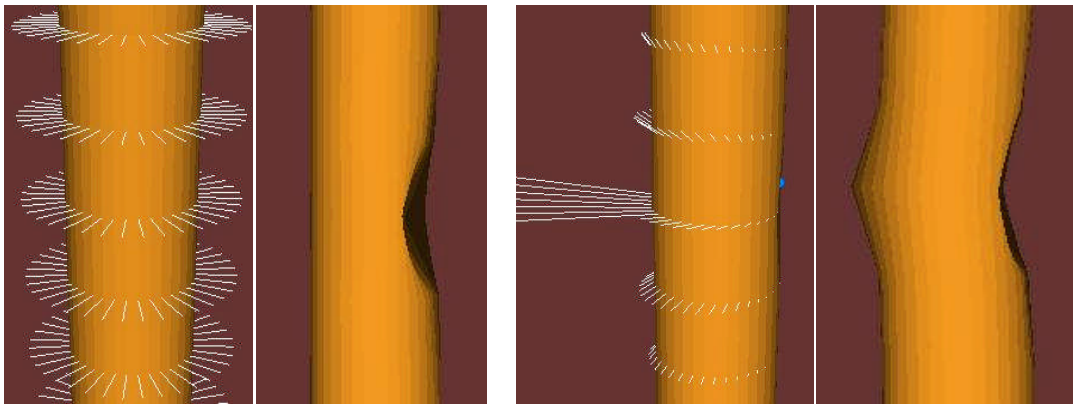

(a) (b)

Figure 8.17: *The white lines reflect the weighted factors at the nodes (a) factors are uniform (b) factors extracted at runtime*

The distribution of weights defined the area of influence of the penalty pressure to compensate volume change during simulation. When the weighted factors were dynamically modified at runtime according to the orientation threshold, the deformation distribution iteratively changed as shown in figures 8.18 and 8.19.

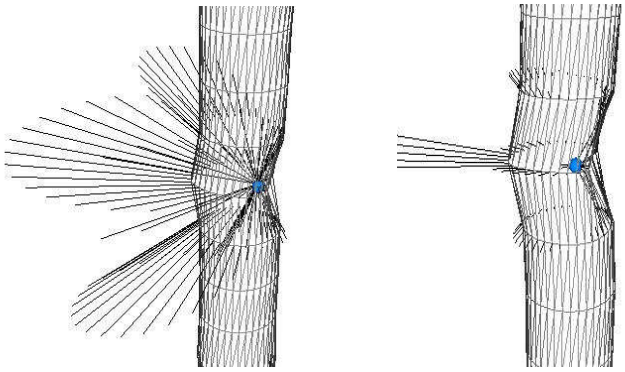

Figure 8.18: *Runtime weighted factors with a pre-defined radius of influence and orientation threshold*

Figure 8.19 demonstrates the spread in the deformation effect by the change of texture colour in response to node displacements (minimum (blue) to maximum (red)). The second state (t2) of the tube demonstrates that the nodes at the opposite side of the interaction point were displaced in response to the interaction despite the absence of the connecting medium.

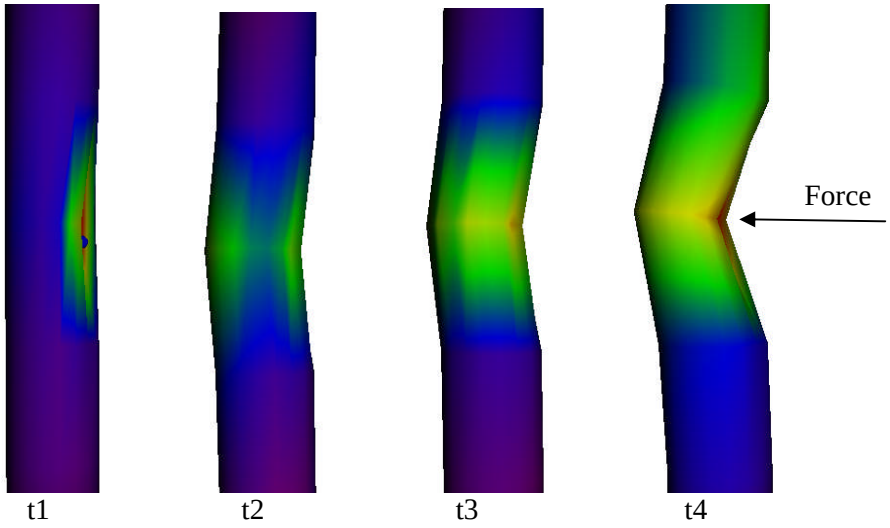

Figure 8.19: *Displacement Analysis showing a global deformation effect on the surface influenced by the interaction force radius and orientation*

This emphasises the potential of employing a surface model to emulate global deformation effect despite the non-existence of internal volume. A generalised framework is thus, provided where it can be employed in more case specific scenarios. Currently, it serves as a proof of concept, where it further emphasises the

versatility of the deformable model to emulate the changes in shape and non-linear deformation in response to the volume variations.

8.4.4 Summary

The second hypothesis established in section 6.2 for the evaluation has been addressed in this section. The second and third objectives were further explored, where the global deformation effect was observed in relation to the interaction force.

Despite the absence of an internal medium, the visual deformation effect of the surface model reflects the assumption of an incompressible volume. Surface models such as the breast model and the tube model demonstrated the respective bulging and bending effects relative to the interaction point. These visual feedbacks ultimately highlight the feasibility of the runtime manipulation of the deformation effect in relation to the change of volume as well as the orientation and the radius of influence of the interaction force.

8.5 Volume Mass Spring Systems (VMSS)

An additional experiment was carried out to evaluate the performance of the proposed model against a VMSS which incorporates radial elements and a volume penalty. The significance of this evaluation is to compare the performance of two different models with similar complexities in terms of the number of springs used. The reason why a volume mass spring model was employed is that the FEM model is known to be slow and commonly biased towards small deformation.

8.5.1 Complexity

It has been discussed in Part I that the complexity of VMSS is significantly higher than the surface alternative to represent the shape of an object. Not only can the

internal mesh of a VMSS be complicated due to the original internal mass spring network and the additional constraining springs, the computational cost is also higher.

As a control parameter for performance evaluation, the complexity of the MSS for both models should be similar to increase the degree of confidence. The significance of this approach is to allow unbiased analysis of performance. For this reason, the implemented VMSS was based on the configuration of Scheme B and the radial elements proposed by Vassilev & Spanlang (2002), where the radial elements are the internal support springs that link the surface nodes to the object centre (section 3.2.1.2). The radial discretisation provides the concentric volume penalty as proposed by Bourguignon & Cani (2000) as well as Vassilev & Spanlang (2002).

The subsequent comparison involves evaluating the computational efficiency of the proposed model (Scheme D) against the VMSS without the influence of mesh complexity, where both have the same number of springs.

8.5.2 Performance comparison

Based on this framework, a simple performance evaluation was carried out to illustrate that the surface data would reduce computational complexity even when the MSS complexity was similar. Table 8.1 shows the average frame per second (FPS) achieved by the VMSS and the proposed surface model for a real-time simulation with both visual and haptic rendering. A stretching force was imposed on the various models and the average FPS over the same duration of time was extracted.

The FPS of Scheme D exceeded the update rate of VMSS. Therefore, this shows that the proposed model achieved a better performance even when the MSS complexity was the same.

Table 8.1: *Total FPS Comparison*

Model (number of surface nodes)	Cube A (602 nodes)	Sphere (1000 nodes)	Cube B (1352 nodes)	Cube C (2402 nodes)
VMSS	77	47	37	20
Scheme D	80	77	44	25

8.6 Conclusions

Not only is it vital to include real material properties in the configuration of the deformable model, it is also important to achieve the volume effects. In reference to the analysis and summaries for both section 8.3 and 8.4, near-incompressibility has been illustrated, where a constant volume was maintained with minimal deviation irrespective of the absence of an internal MSS.

The evaluation has accomplished all the hypotheses and the objectives established for the proposed model. The findings illustrate the feasibility of employing the estimation and the volume preserving scheme to address the issues in the estimation of the properties and volume behaviour incurred by the two-dimensional surface MSS. Not only can the real material properties now be embedded, but the volume behaviour can also be demonstrated despite the absence of an internal medium. This allows the proposed framework to be easily adapted for case specific areas in the future.

The final ranking of schemes can be summarised in terms of the preservation of volume. The last column of table 7.7 can be populated with the rankings according to the comparative analysis carried out in this chapter. Table 8.2 indicates that the proposed deformable model (Scheme D) surpasses the other schemes for all parameters.

Table 8.2: *Ranking of the schemes (out of 4 stars) in reference to the key experiments*

Scheme	Stress and Strain	Topology Refinement	Volume Preservation
A	*	*	***
B	**	**	**
C	***	***	*
D	****	****	****

Despite the lowest accuracy in the elastic and homogenous behaviour, Scheme A resisted deformation more than Schemes B and C. This is due to the larger elasticity modulus compared to the original value during the stress and strain analysis (table 7.2), which indicates stiffer shape preserving springs. This further emphasises the feasibility of shape preserving springs towards emulating a solid effect. These springs are now enhanced by the proposed model, where a volume dimension amongst other considerations has been included in the configuration of the springs' coefficient.

This chapter has demonstrated the versatility of the proposed configuration in attaining a deformable volume despite the shortcomings of a surface approach.

Chapter 9
Discussion

9.1 Introduction

The evaluation has been carried out and the main findings have been documented in Chapters 7 and 8. This chapter aims to analyse and summarise these findings as well as the contributions and the implications of the research work. The structure of the discussion consists of the overview of the outcomes of the evaluation methods, the analysis of the key findings and the contributions of the proposed framework.

9.2 Overview

The proposed framework pertained to the goal (section 3.3.1) and the scope (section 4.2.2) of the deformable model, where the configuration:

- included real material properties based on the assumptions of elasticity, homogeneity and incompressibility,
- addressed the issue of the design of the mesh topology and its influence on the estimation of properties,
- established the relationship between the surface elements and volume,
- demonstrated the local and global deformation behaviour in response to external force influences regardless of the non-existence of volume.

As a proof of concept, the feasibility of this framework was empirically evaluated in reference to the hypotheses generated in chapter 6. These hypotheses were explored with consideration of the issues in estimating properties and volume behaviour as summarised in table 9.1.

Table 9.1: *The hypotheses of the evaluation*

	Hypotheses	Chapter
i)	Irrespective of the mesh topology, the resulting dynamic behaviour should reflect the assumption of homogeneity and elasticity of the real material.	7
ii)	Irrespective of topological refinement, the behaviour of the altered area should be similar, where homogeneity is still preserved despite the change.	7
iii)	For an elastic and incompressible material, the original shape at rest as well as volume during deformation should be conserved. Since materials such as soft tissues are not perfectly incompressible, minor discrepancy in volume preservation is expected.	8
iv)	Despite the absence of internal discretisation, the global deformation effect of the surface model reflects the assumption of an incompressible volume.	8
v)	As the surface method is a dimensional departure from the volume counterpart, the computational complexity is also reduced. When compared to a VMSS with similar mass-spring complexity, the proposed surface model is expected to be more efficient.	8

The hypotheses adhered to the scope of behaviour and the assumptions for real-time simulation of a deformable object. The evaluation parameters were thus, elasticity, homogeneity and incompressibility. In reference to these parameters, the objectives summarised in table 9.2 were explored and accomplished.

Additionally, the proposed configuration (Scheme D) was compared to the other schemes (section 6.4.2) based on key experiments that consist of the:

- stress and strain analysis (section 7.3.2),
- assessment of behaviour preservation in response to topological modification (section 7.4.2), and
- analysis of volume variation during simulation (section 8.3.2).

These key investigations addressed each of the evaluation parameters respectively. The resulting rankings are summarised in table 9.3, where the comparison reinforces that the proposed framework was more efficient in all three evaluations.

Table 9.2: *The status of the key evaluation objectives in relation to the material parameters (E = Elasticity, H= Homogeneity, I = Incompressibility)*

Evaluation objectives	E	H	I
Chapter 7: Properties Estimation			
i) Demonstrate the elastic behaviour of the model by observing the ability to conserve shape during simulation	√		
ii) Validate the resulting elasticity modulus of the simulated model by analysing the stress and strain relationship	√		
iii) Compare the model against a reference model of identical physical and material properties	√		
iv) Illustrate material homogeneity by analysing the relationship of the distribution of mass and spring coefficients		√	
v) Highlight the flexibility of the estimation technique in supporting topological modification while preserving the homogeneity of the deformation behaviour		√	
vi) Emphasise the material homogeneity despite the design of the topology by observing texture distortions during deformation		√	
Chapter 8: Volume Behaviour			
i) Analyse the volume variations of the model under the influence of gravitational pull and an interaction force.			√
ii) Observe the visual effect of the local and global deformation under different conditions			√
iii) Investigate the feasibility of the runtime manipulation of the global deformation effect in relation to the change of volume as well as the orientation and the radius of influence of the interaction force.			√

Table 9.3: *Ranking of the schemes (out of 4 stars) in reference to the key experiments for the evaluation parameters (elasticity, homogeneity and incompressibility respectively)*

Scheme	Stress and Strain	Topology Refinement	Volume Preservation
A	*	*	***
B	**	**	**
C	***	***	*
D	****	****	****

The following sections further emphasise the feasibility of the proposed technique according to the hypotheses and objectives. The correlations provide an overview of the contributions and the implications of the research work.

9.3 The surface approach

The feasibility of employing a surface model to emulate volume behaviour was investigated. The key issues that were addressed are properties estimation and the emulation of volume behaviour. These issues highlight the shortcomings of a surface approach, where the surface elements have no direct relationship with the actual volume.

Nevertheless, volume was discretised for the surface mesh based on the uni-axial tensile properties of a material. The proposed discretisation allows volume to be distributed to the surface elements. In the case of a MSS, the estimation of mass and the proposed volume spring coefficients are proportional to the respective volumes at the nodes.

In relation to the goal and scope of the proposed model, the consequent configuration features:

- the consideration of the design of the mesh topology,
- the initial volume discretisation based on the concept of uni-axial tension,
- the parameterisation of the coefficient of the subsequent volume springs with real material properties,
- the runtime determination of the volume spring coefficients relative to the orientation of force, and
- the runtime manipulation of the deformation effect relative to the orientation of force and volume variations.

This approach has introduced an attempt towards parameterising the properties of a surface model with real material properties. The parameterisation took into account

the assumptions (table 3.2) of material properties. The assumptions of elasticity, homogeneity and incompressibility, though generalised, are deemed feasible due to the limitation of a human's perceptual capabilities (Wall & Harwin 1997; Bordegoni et al. 2001; Wade & Swanstons 2001; Batteau et al. 2004; Sur et al. 2004; Payandeh et al. 2005; Wuillemin et al. 2005).

The proposed hypotheses based on these parameters were validated. Despite the non-existence of volume elements and regardless of the design and complexity of the original topology, the proposed model produced the same material properties with minor deviation compared to the original material values. Uniform texture distortions as well as shape and volume conservation were reproduced and demonstrated during simulation. This illustrates elasticity, homogeneity and incompressibility. Furthermore, the local dynamic behaviour was also preserved upon mesh topological modification despite the irregularity of the consequent mesh topology, compared to the less feasible approaches (Zhang et. al. 2002; Choi et al. 2005; Payandeh et al. 2005).

Regardless of the absence of an internal medium, the proposed surface MSS was able to support a global deformation effect at runtime. Shape constraint, such as introduced by Hong et al. (2006), was avoided to promote versatility. Instead, their deformation weighting method was modified and enhanced by allowing the deformation effect to be configured at runtime based on the radius and the orientation of the interaction force. Hence, the volume effect was manipulated at runtime rather than being confined by the specific and pre-defined boundary as well as shape constraints (Nedel & Thalmann 1998; Aubel & Thalmann 2000; Hong et al. 2006; Nealan et al. 2006).

Both small and large deformations were supported as illustrated by the evaluations in Chapters 7 and 8. This demonstrates the feasibility of employing the extraction formulas for the tensile modulus such as the uni-axial, shear and bulk moduli. For force magnitudes ranging from 1 to 2 Newton, the properties of the original material were consistently preserved during simulation and the degree of coincidence of the dynamic behaviour of the pre- and post-refined area was also maintained with minimal deviation. This consistently reinforces the feasibility and versatility of the proposed estimation method.

The combination of real-time computation and accuracy was improved for the surface approach towards emulating soft solid behaviour. Moreover, it was more versatile than the approaches summarised in table 3.1 in terms of the issues of properties estimation and volume behaviour. The findings in relation to these issues will be summarised in the next subsections. Furthermore, the implication in the simulation of breast is also analysed.

9.3.1 Properties estimation

The estimation technique considered the design of the mesh topology and the tensile properties related to the initial volume discretisation with the aim of promoting elasticity and homogeneity.

When the tensile analysis was carried out, the elasticity modulus was re-produced with minimal deviation relative to the original modulus. The mean accuracy percentages for small and large deformations were around 98 percent (table 7.3) and 84 percent (table 7.4) of the true value respectively. This illustrates the feasibility of employing properties such as the uni-axial, shear and bulk moduli in relation to the estimated volume for each volume springs. The implication of this is the contribution

of the configuration technique towards generating virtual models embedded with real material properties instead of employing excessive fine-tuning or random values.

Besides portraying elasticity, the behaviour of the model has to also reflect homogeneity regardless of the regularity of the mesh topology. Homogeneity was demonstrated when the uniformity of the texture distortion was preserved during deformation. To quantitatively evaluate the homogenous behaviour, the local behaviour of pre- and post-refinement within the area of interest was analysed. When compared to the other schemes (figure 7.15 and 7.17), the displacement behaviour of the point of interaction demonstrated similar behaviour over time with minimal mean and standard deviations (0.03 and 0.02 mm respectively). Upon the incidence of large force magnitudes (1 – 5N), the behaviour of the local area was still preserved with minor deviation (less than 0.02 cm combined deviation as shown in figure 7.19 and 7.20). This further highlights the feasibility of the model in supporting large deformations (by force magnitudes larger than the proposed 1 – 2 N palpation force), which was previously established by the accuracy of the extracted elasticity value of around 84 percent of the true modulus, when large stress was imposed on the model.

This demonstrates that the estimation method supported both regular and irregular topologies. This emphasises that approximating properties based on the mesh topology is more accurate compared to the general uniform properties distribution utilised by Scheme A and adapted by the existing approaches (Deussen et al. 1995; Delingette 1998; Bourguignon & Cani 2000; Brown et al. 2001; Bielser 2003; Matyka & Ollila (2003); Sundaraj 2004; Paloc et al. 2006; Lloyd et al. 2007). The findings also highlight the versatility of employing regular and irregular convex shapes with either open or closed surface mesh.

Not only is it vital to correctly configure the properties of the surface model, but the resulting dynamic behaviour of the model during simulation has to also reflect the appropriate volume effects.

9.3.2 Volume behaviour

Based on the proposed configuration of the deformable model, volume behaviour was demonstrated, where both local and global deformation effects were demonstrated at runtime. External influences such as the gravitational pull and interaction forces are important in a realistic simulation. Not only was the shape of the model preserved during simulation, but the proposed model also conserved volume during deformation in order to promote incompressibility.

The preservation of volume was validated based on the mean deviation from the original volume in response to runtime deformation. Compared to the other schemes (figure 8.9), the proposed model produced the lowest mean volume deviation when the surface models with different mesh complexities were deformed during simulation. A constant volume with minimal deviation (around 2 percent) was maintained at runtime, which indicates that non-rigid solids are not perfectly incompressible

The global shape deformation responded to the change in volume relative to the orientation and the radius of influence of the interaction force (figure 8.19). Volume variations due to these external influences were penalised to promote incompressibility. The resulting volume compensation was manipulated at runtime and the respective deformation effect was determined relative to both orientation and radius of influence. This was achieved by manipulating the weight distribution, bulk

modulus and the concept of incompressibility. The demonstrated behaviour serves as a proof of concept where the proposed technique for deformation manipulation can be further exploited to address case-specific behaviours.

9.3.3 Towards breast simulation

The breast was utilised as an instance of soft objects, based on which the scope of the deformable behaviour was established. The published material values (table 7.1) such as the elasticity modulus of 3.25 kPa, 22.5 kPa and 31.5 kPa were implemented to aid the evaluation of properties estimation in the consideration of elastic and homogeneous behaviour. The model produced a modulus with a mean accuracy within the range of 97 to 98 percent when compared to each of the moduli respectively (figure 7.4).

When imposed under different conditions such as gravitational pull or interaction forces, the global deformation effect was demonstrated (figure 8.3, 8.4, 8.6 and 8.16). Despite the open structure of the surface model, volume with minimal deviation (about 3.57 percent**)** was achieved during simulation. The implication of this is the feasibility in employing both closed and open surface models for solid simulation.

In the context of breast interaction, the yield limit of the material is not to be exceeded. Within the estimated palpation force range of 1 to 2 Newton, the volume of the breast model was preserved with less than 0.6 percent deviation (figure 8.12). When imposed with a wide range of force magnitudes (1 – 10 N), there was an increase in volume deviation (less than 2 percent) for high force, such as 10 N (figure 8.11 and 8.12). The mean volume deviation at the top force magnitude ranged from 0.4 percent to 2 percent of the original volume for the different elasticity moduli.

Irving et al. (2007) produced volume losses of 1 to 15 percent for nearly incompressible FEM (Poisson ratio in range of 0.45 to 0.499). For this reason, the findings concluded that large deformation due to large force magnitudes was also supported by the proposed model (Poisson ratio < 0.5), where the tensile analysis also indicated the average of 84 percent accuracy (table 7.5). This reinforces the feasibility of not only demonstrating a global deformation effect but also preserving volume during simulation.

The breast model at the supine position demonstrated the shape change in response to the gravitational pull (figure 8.3 and 8.4), but the volume deviation was larger than the other positions such as prone and vertical (figure 8.5). This is the shortcoming of employing an open surface at the supine position. Nevertheless, the global deformation effect based on volume compensation was demonstrated at a deviation of around 5 percent and the comparison against the MR images indicated similar shape outline at the top view (figure 8.4).

9.4 Knowledge Contributions and Implications

9.4.1 A novel extension to the configuration of a physics-based surface model

The key knowledge contribution is the feasibility of increasing the accuracy in the configuration of a deformable surface model for computer-based simulation of soft solid objects with the inclusion of real material properties. The novel extension to the surface MSS enables the tensile properties of the material to be integrated into an enhanced configuration despite its shortcomings. The benefits of the reduced

complexity of a surface model have now been correlated with the improved accuracy in the estimation of properties and volume behaviour.

The proposed deformable model presents a surface MSS parameterised with real material properties which can be employed as a template for a more specific simulation application. The novel advancements to the classic surface MSS and the ordinary shape preserving springs include:

i) The inclusion of volume preservation in the configuration of the model properties.

ii) An original approach in adopting the tensile analysis of a material in establishing the configuration of surface properties in terms of volume behaviour, which adheres to the standard practice in extracting the bio-material properties within biomechanical research (see section 4.4). This relationship has not previously been established for a discreet surface model to resolve the absence of volume for the emulation of solid behaviour.

iii) The parameterisation of the volume springs based on the quantitative measurement of bio-materials, such as the Young's, Shear and Bulk moduli (see section 5.2 and 5.3).

iv) The consideration of runtime properties of the intended material, where the stiffness of the volume springs is dependent on the elasticity and shear stiffness in response to the orientation of force (see section 5.2.3).

v) The runtime manipulation of the deformation effect to emulate solid behaviour despite the absence of volume (see section 5.3.3).

The original shape preserving springs in addition to the classic MSS (Laugier et al. 2000; Meseure & Chaillou 2000; Laugier et al. 2001; Mendoza et al. 2002; Laugier et

al. 2003; Zhang et al. 2002; Choi et al. 2005; Payandeh et. al 2005) failed to consider the influence of volume. Moreover, the inclusion of additional springs to the original MSS utilised by Bourguignon & Cani (2000) and Brown et al. (2001) resulted in stiffer material with deviation from the original properties (Hong et al. 2006). Acknowledging this, the proposed configuration has not only preserved volume with minimal deviation but also reproduced properties with high accuracy compared to the original value. Moreover, high deformation was also supported, where global deformation effect is possible.

This was achieved by the coefficients of the springs, which are now based on the tensile properties taking into account the dependency of dynamic behaviour of the surface nodes upon their respective surface normals and the imposing force orientation. These considerations have not been taken by other volume discretisation (Costa & Balaniuk 2001; Balaniuk & Salisbury 2003; Matyka & Ollila 2003; Balaniuk et. al. 2006). Additionally, this technique avoids the common assumption of regular mesh topology for properties distribution (Deussen et al. 1995; Delingette 1998; Bourguignon & Cani 2000; Brown et al. 2001; Bielser 2003; Sundaraj 2004; Paloc et al. 2006; Lloyd et al. 2007), which is impractical and is not versatile.

Previously, the benefits of a surface model were often overshadowed by the lack of accuracy in the properties estimation. The generic configuration for both properties and volume behaviour was analysed to be versatile in not only emulating incompressibility despite the absence of internal volume but also preserving homogeneity and elasticity regardless of the irregularity of the mesh topology. The advantages of a surface model over a volume model are now paired with the direct

inclusion of material properties in the configuration. The next sections further describe the main features of this configuration.

9.4.1.1 Volume discretisation

The need to embed real material properties into the configuration of the deformable model motivated the analysis of the relationship between the mesh elements to the object volume. The dependency on the two-dimensional area was extended to include volume discretisation relative to the total volume of the object.

Based on the scope of a convex or near-convex object, such as a human breast, the proposed volume discretisation is versatile in terms of supporting regular as well as irregular shapes. The previous shape preserving springs have been enhanced where they are now representing sub-volumes. The material properties of the respective volume are used to estimate the stiffness of each spring, where the tensile analysis of the resulting volume is based on the surface normal at the nodes instead of the distance vector of the radial link. This highlights the feasibility of employing the extraction of the elasticity modulus based on the stress and strain relationship. Consequently, the existing published moduli can be employed in the configuration of the model properties. Both small and large deformations can be supported in real-time, which is important for a highly deformable solid.

9.4.1.2 The estimation technique

Properties estimation is a challenge for particle systems such as the MSS. As the level of mesh complexity is reduced by one magnitude, the estimation of the consequent surface model in order to emulate a deformable solid is even more complicated. Hence, it is vital to estimate the properties such as the spring coefficients based on the

real material properties. The method bridges the gap between the surface model and the application of real material properties.

Instead of employing a single coefficient to define the spring stiffness, the volume discretisation represented by each spring has been employed to estimate the influences from the uni-axial, rigidity and incompressibility tensile properties. The respective parameters are the Young's modulus, shear modulus and bulk modulus. The feasibility of employing these parameters has been demonstrated by the elastic, homogeneous and incompressible behaviour of the deformable model at runtime. The anisotropic behaviour of the volume was also verified by the dependency of the volume springs on the orientation of force. Accordingly, the novel estimation method includes the determination of the stiffness coefficients based on the surface normal relative to the force orientation.

The flexibility in modifying the topology, such as mesh refining at runtime has also been demonstrated, where properties re-estimation was supported at runtime. Both local and global deformation behaviours were preserved within the refined area. Such flexibility promotes fast prototyping. Other methods such as off-line fine-tuning of properties and the pre-computation of boundary constraints are less flexible. The complexity is magnified by to the need to repeat the fine-tuning and pre-computation procedures in response to topological modification. Therefore, the proposed estimation supports the need for refinement within an operational area.

The proposed model provides a generalised template on which further work can be carried out. Furthermore, since the estimation is based on volume discretisation for each of the mesh nodes separately, other surface mesh elements such as square elements can be explored. Various objects with different shape and mesh complexities

can also be exploited. The implication of the findings is that soft bodies such as soft tissues can be modelled using a surface MSS and the respective material properties can be applied to define the behaviour of the surface model within the prescribed assumptions and scope.

9.4.1.3 The emulation of volume effect

The main disadvantage of a surface model is the absence of internal discretisation. However, volume discretisation was proposed which enables the extraction of the material properties of the model within the scope of an elastic, homogeneous and incompressible material. The volume behaviour can thus be emulated despite this shortcoming.

The proposed volume springs not only preserved shape during simulation in order to promote linear elasticity, but also conserved volume with minimal deviation when deformed. This has significantly enhanced the original shape preserving springs. The impression of incompressibility was made possible at runtime.

In accordance with the requirement for volume behaviour, the technical contributions include the distribution of volume compensation based on the orientation and radius of the interaction force. While promoting incompressibility, both local and global deformation effects were supported. This demonstrates the feasibility of creating a realistic deformable effect based on the external interaction.

Even though the proposed model only provides a generalised framework towards supporting case-specific shape deformations, it can be extended for future applications. This implies that the behaviour such as illustrated by the tube deformation (section 8.4.3), can be further explored for case-specific simulations.

9.4.2 Implication in the application of medical training

The issues in the deployment of medical training simulation include addressing a fine balance between the accuracy of the deformable model and maintaining real-time interactivity (Mezger et al. 2008). The existing techniques in volume-based deformable modelling have often promoted realism at the cost of computation efficiency. On the other hand, the surface approaches have often achieved the opposite. Therefore, the main motivation of the research was to investigate the feasibility of improving the accuracy of a surface model by parameterising it with real material properties.

The implication of the novel configuration of a deformable model is towards the development of a training simulation in the medical domain, where real-time interactivity is supported. The feasibility is further reinforced by the use of bio-material properties in the configuration. The properties of the model are not based on rigorous fine-tuning or pre-computations but are based on bio-material properties.

As illustrated in this thesis, the framework is suitable for breast simulation[2], where the breast is convex within a static global positional dynamism. Technologies that engage both visual and tactile perceptions have also been exploited in the implementation of the simulation framework. This can potentially provide a platform towards breast simulation for the application of breast assessment via haptic palpation for the detection of tumours. Since the organ can be based on the material properties, accuracy can be accomplished with minimal deviation as shown by the empirical evaluation.

[2] Refer to Arnab et al. (2008) in the bibliography

The modelling technique benefits future simulation endeavours, for instance the modelling of other organs for medical training, such as prostate glands and testicles, as well as the modelling of soft materials utilised in other domains such as product design and manufacturing.

9.5 Conclusions

This chapter has highlighted the significance of the proposed deformable model according to the evaluation hypotheses and objectives. The contribution in the research domain is in the deformable modelling of soft objects for a computer-based simulation. The evaluation findings reinforce the feasibility and versatility of the proposed model to demonstrate elasticity, homogeneity and incompressibility despite the shortcomings of a surface approach. The subsequent potential is in the application of real-time simulations, such as in the domain of medical training, where the consideration of real material properties and the assumptions in the estimation technique contribute towards accuracy. Consequently, the implementation of a surface MSS will not only benefit from the low computational and mesh complexity but also from the enhanced configuration.

Chapter 10
Conclusions

10.1 Summary

10.1.1 Background

The research aims to contribute to the development of real-time simulation of deformable objects. The importance of direct interaction with the objects, such as the palpation of a breast for breast assessment, emphasises the need for both computational efficiency and accuracy of the model.

The issues concerning the use of volume data in the configuration of a deformable model have been identified, where the real-time requirement for an intra-operative application overshadows the greater precision that is necessary for a scientific analysis. It has been recognised that the physics-based mass spring framework promotes the benefits of rapid prototyping, computational efficiency and the support for large deformation compared to FEM. However, the efficiency is still restricted by the intricacy of the internal volume discretisation.

This complexity issue motivates the exploitation of a surface alternative in order to benefit from the lower mesh and computational complexity. However, the issue of accuracy is prominent due to the shortcomings of a surface model such as the absence of the volume dimension. The definition of properties is thus constrained. The difficulty in parameterising the subsequent mass spring configuration with real material properties is further magnified by the lack of volume definition for the surface data.

Nevertheless, the assumptions for a real-time application that include the material parameters such as elasticity, homogeneity and incompressibility allow a reduced set of material values to be utilised in order to support the use of a surface alternative. Hence, to generate a framework for a deformable surface model, the issues of the estimation of properties and volume behaviour relative to these material parameters have been considered.

10.1.2 Aim and objectives

The aim of the research was to improve the accuracy of the configuration of a surface model towards simulating soft solid objects in terms of the properties estimation and volume behaviour as well as in reference to the material parameters: elasticity, homogeneity and incompressibility. To achieve this aim, the research objectives were addressed, where a novel extension to the configuration of a surface model was subsequently proposed and evaluated. The objectives of the thesis were as summarised in table 10.1. These objectives have been addressed and accomplished in the chapters, which are in line with the theme established for the thesis structure.

Table 10.1: *The status of the objectives of the thesis as addressed by the chapters*

Thesis Objectives	Status	Chapter
Investigate the issues related to deformable modelling and the physics-based techniques in the volume approach,	√	2
Explore the attempts in surface modelling in relation to the issues of properties estimation and volume behaviour	√	3
Propose an enhanced framework and configuration of a deformable surface model	√	4 5
Evaluate the proposed model relative to the issues of properties estimation and volume behaviour, and the material parameters that include elasticity, homogeneity and incompressibility	√	6 7 8
Discuss the evaluation findings and the consequent contributions and implications.	√	9

10.1.3 The proposed framework

In reference to the aim and objectives, the goal of the proposed framework of the deformable model was to address the following considerations:

i) The inclusion of real material properties based on the elasticity, homogeneity and incompressibility parameters in the configuration of its properties,

ii) The solution to the issues relating to the design of the mesh topology and its influence on the estimation of properties,

iii) The establishment of the relationship between the surface elements and volume,

iv) The demonstration of the local and global deformation behaviour in response to external force influences regardless of the non-existence of volume.

The outcome of the research investigation was the realisation of this goal. The proposed framework was empirically evaluated, where the feasibility of employing this model for the simulation of soft objects was highlighted. The benefits of the reduced complexity of a surface MSS have been correlated with the improved accuracy in the estimation of properties and volume behaviour.

10.1.4 The contributions

The key contributions of the proposed framework as discussed in section 9.4 are:

i) A novel extension to the configuration of a physics-based surface model that increases the accuracy of the material properties in the emulation of deformable objects (documented as Scheme D in the evaluation analysis and Discussion)

This is a potential alternative to deformable modelling of soft objects, which can be utilised in a real-time and interactive simulation. The thesis has proposed a physics-based surface model that extends the classic MSS by coupling the benefits of real-time capability with improved accuracy in the estimation of properties and volume

behaviour. The novel extension enables the tensile properties of the material to be integrated into an enhanced configuration despite the lack of volume information. The configuration of the model features key techniques in estimating the properties for the surface elements and the runtime derivation of these properties in relation to the uni-axial tensile, shear and bulk properties of the material as well as the influence of force. Despite the issues related to the surface mesh topology and the shortcomings in terms of the lack of volume, the model reflected the original material value and the preservation of volume with minimal deviations. The global deformation effect which is essential to emulate the behaviour of a real soft material upon interaction, such as the palpation of a generic breast, was also demonstrated. Therefore, the novelty of this extension features the following attributes:

- **The adoption of tensile analysis in establishing the configuration of the surface properties in terms of volume behaviour, which adheres to standard practice in extracting bio-material properties within biomechanical research.** This relationship has not previously been established for a discreet surface model to resolve the absence of volume towards the emulation of solid behaviour.
- **The parameterisation of the volume springs based on the quantitative measurement of bio-materials, such as the Young's, Shear and Bulk moduli, and the Poisson ratio.** The state-of-the-art in similar springs relies heavily on fine-tuning the properties with random values or by assuming regular topology for the assumption of uniform properties distribution. A more sophisticated method only considers a single modulus to describe the material behaviour. Hence, the novel extension provides a more accurate representation of the properties by considering more than one quantitative measurement.

- **The consideration of runtime properties of the intended material, where the stiffness of the volume springs is dependent on the elasticity and shear stiffness in response to the orientation of force.** This adheres to the real behaviour of a material under properties extraction, where both Young's and Shear moduli address the uni-axial and shear tensile respectively. Other methods fail to recognise this behaviour when a surface MSS is employed.
- **The runtime manipulation of the deformation effect to emulate solid behaviour despite the absence of volume.** Other researchers opt for pre-defined deformation effect or key-framed animation which limits the versatility of the deformation effect at runtime.

ii) Potential application in the domain of medical simulation

The feasibility of embedding real properties into the configuration of a discrete model has been demonstrated and the accuracy increases the confidence in employing a surface model to emulate non-rigid solid behaviour. The interactive manipulation of this model at runtime indicates the potential in the application of soft tissue simulation. For instance, the breast can be simulated based on its material properties. The immediate future application is in the development of a training simulator for breast assessment. Interaction with a breast model via haptic palpation can be exploited towards the detection of tumours.

10.2 Perspectives

Although the potential of the proposed framework has been demonstrated and the implication in the medical application is promising, there are several research

limitations that can be explored towards the optimisation of the deformable model. This section describes the prospective future work and improvements.

10.2.1 Breast simulation

Early detection of a breast tumour is of paramount importance as it provides patients with a greater chance of survival (Gerling et al. 2003). There is a deficiency in clinical skills in medical schools as well as in public awareness of the detection method (Saslow et al. 2004; McDonald et al. 2004). Therefore, training in breast palpation to detect anomalies requires the skills to be honed, which has an implication to the rate of detection.

Acknowledging this, a deformable breast model is an important component in the development of a training simulator for breast assessment. Since the proposed framework is based on a surface approach, models can be rapidly assimilated utilising the surface data obtained from 3D scanners under various loading conditions or positions.

The current framework does not consider the complete mechanics of a breast and the additional inhomogeneity of material to represent the existence of tumour. Nevertheless, the proposed framework provides the basis on which such behaviour can be built, where a correlation between the global surface model (breast) and the internal, yet foreign object (tumour) can be explored. The feasibility of manipulating the behaviour of the surface nodes by exploiting the properties of the volume springs at runtime demonstrates the potential of generating an effect of internal inhomogeneity.

Consistent with the proposed configuration, the material properties of both breast and tumour tissue can be utilised to provide a customisable model to support various breast conditions by modifying the embedded parameters. Moreover, the distribution of the global deformation effect can be extended with the consideration of the foreign object.

10.2.2 Algorithms

Achieving a high level of realism involves accurately integrating the measured biomechanical properties of tissues that constitute the breast and interactivity that exhibits indiscernible latency in visual and haptic response. The advancement in algorithms such as selective rendering and computation require further research in the requirements of specific applications. The proposed framework provides a platform for this to be explored in the future.

Currently, the proposed model employs the operational area to illustrate local refinement as well as the global deformation effect, where the effect was distributed based on the orientation and the radius of influence of the interaction force. The proposed radius and orientation of influence can be subjective to the specific applications or scenarios.

Optimisation techniques, such as selective rendering and computation of both visual and haptics relative to a specific operational area, can be explored. Such adaptive behaviour includes the runtime manipulation of the area in terms of computation and mesh refinement. The concept of the operational area takes advantage of the assumptions that most deformations are local, where the motions of surgical instruments are relatively slow (Brown et al. 2001). To further improve the speed of the simulation, computation intensity can be concentrated within this area. For

instance, this limits the number of springs that will be processed during a deformation. The area can be determined adaptively in response to particular interaction.

The requirement for the degree of refinement is also application specific, which was not extensively explored in this work. Nevertheless, the current model supports mesh refinement where the time step remains the same. It is consistent with the aim to provide a generalised estimation method based on a homogeneous framework that preserves not only the material properties but also the local dynamic behaviour if modification is required during simulation. Acknowledging the versatility of the proposed configuration, the refinement algorithm can be further customised to support the application-specific requirements.

Employing the same time step for multi-resolutions may cause a stiffness issue due to the differential equations solved utilising the explicit Euler method. A stiff system may occur if the surface mesh is too refined or the elasticity modulus is significantly high. Consequently, the time step will have to be modified to avoid instability, which may result in latency. Thus, a further review of the refinement needs and solutions to the stiffness issue such as other integrators can be explored in future work. However, within the scope of this thesis, highly deformable material was of interest. Therefore, producing a stiff system was unlikely. Furthermore, even though an explicit integrator was employed, the findings of the evaluation demonstrated that the proposed configuration is feasible and versatile.

10.2.3 Inter-disciplinary approach

This thesis has demonstrated the feasibility of parameterising a surface model with real material properties towards emulating the behaviour of deformable volumes,

which is crucial for interactive simulations. However, a realistic medical simulator is still far from reality.

The area of significant interest is the identification of the parameters that define the behaviour of the physical models for soft tissue simulation. Hence, collaboration with medical professionals and researchers from the biomechanical field is necessary. The existing expertise within the domain of graphics and haptics has to be correlated with the need for accuracy and realism in medical simulations. Furthermore, all sensory aspects are to be engaged in the environment to create a more realistic and immersive experience

Within this context, the increase in collaboration amongst the researchers within the inter-disciplinary research community will gradually turn the dream of a realistic and usable medical training simulation into reality in the near future. Hence, the proposed work in this thesis aims to contribute to the greater work in this field as well as in other domains that will benefit from the simulation of deformable objects.

Appendix A: Material properties

A.1 Young's modulus of tissues related to breast

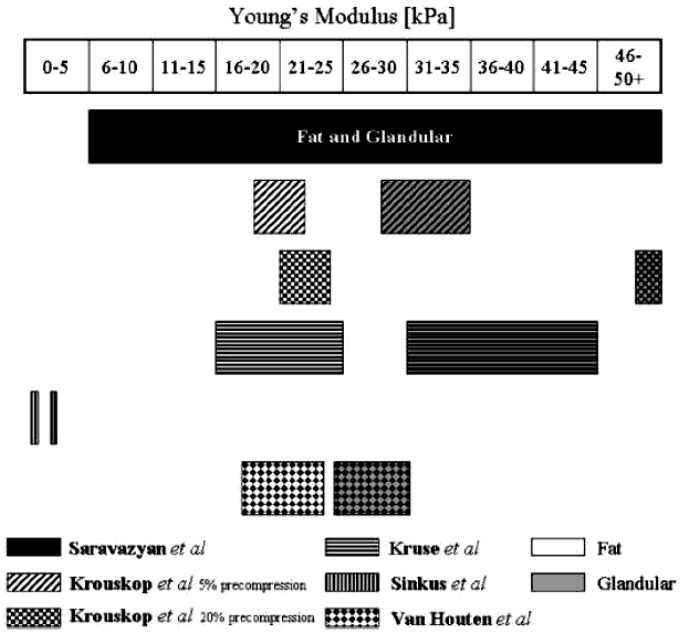

Figure A.1: *The values for normal adipose and glandular tissues compiled from various works (Van Houten et al. 2003)*

Table A.1: *The mean and standard deviation values for the Young's modulus as published by Samani et al. (2007)*

Breast tissue type	Num. of samples	Young's modulus (kPa) mean ± STD
Normal fat	71	3.25±0.91
Normal fibroglandular tissue	26	3.24±0.61
Fibroadenoma	16	6.41±2.86
Low-grade Infiltrating Ductal Carcinoma (IDC)	12	10.40±2.60
Infiltrating Lobular Carcinoma (ILC)	4	15.62±2.64
Ductal Carcinoma In Situ (DCIS)	4	16.38±1.55
Fibrocystic disease	4	17.11±7.35
Intermediate-grade IDC	21	19.99±4.2
High-grade IDC	9	42.52 ±12.47
Invasive mucinous carcinoma (IMC)	1	20.21
Fat necrosis	1	4.45

Appendix B: Haptics

B.1 Haptic rendering

Human haptics or tactile perception is prone to these attributes: texture, hardness, elasticity, shape, and thermal to describe an object in terms of tactile perception (Hespanha et al 2002). Consequently, the general attributes constantly used by developers to simulate touch are attributes such as stiffness, damping, static and dynamic friction (Temkin et al, 2000; Acosta and Temkin 2005a).

In the deformable model thread, properties such as the material parameters are employed in both haptic and visual rendering to describe the tactile feedback and the deformation effect of the model. The rendering of tactile feedback or commonly known as haptic rendering deals with two main stages (figure B.1), which are the collision detection and collision response (Basdogan & Srinivasan 2002).

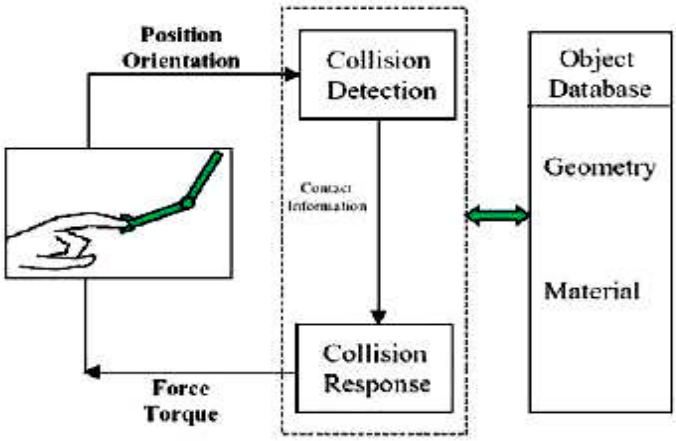

Figure B.1: *Haptic Rendering (Basdogan & Srinivasan 2002)*

Interaction with the virtual model is determined by the collision detection algorithm and the consequent collision response determines the force feedback and the resulting object deformation. Both haptics and visual data demand an update.

B.2 Haptics data structure

Cai et al. (1999) employed a haptic data structure (figure B.2) that supports a general hierarchical structure based on the arrays of triangle structures (array of vertex's coordinates) produced by the three dimensional data structures (wavefront, Open Inventor, VRML, etc) of the object model. This approach deals with converting the existing 3D data structure by simply attaching the appropriate haptic material attributes to the list of vertices. This produces a simple mapping of haptic data to the geometry.

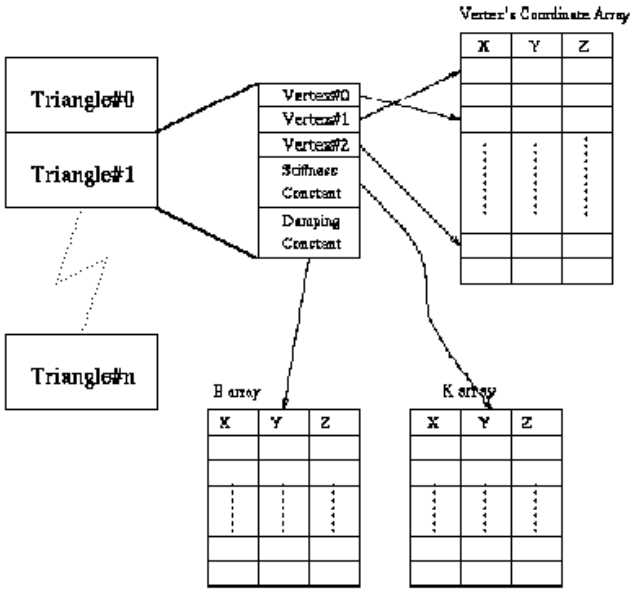

Figure B.2: *3D Geometric and material property data structure (Cai et al. 1999)*

Although this approach only creates a simple lookup table that combines the vertex's coordinate array and the material arrays of simple polygonal mesh, the concept inspires the possibility of addressing the organisation of not only material data for the polygonal mesh, but also the deformation equations, force calculation as well as the operational area based on the current interaction with the model. The availability of such data structures for polygonal datasets assists in the organisation of properties for the deformable model and its dynamic behaviour at runtime.

Appendix C: The proposed framework

C.1 The initialisation and runtime structure

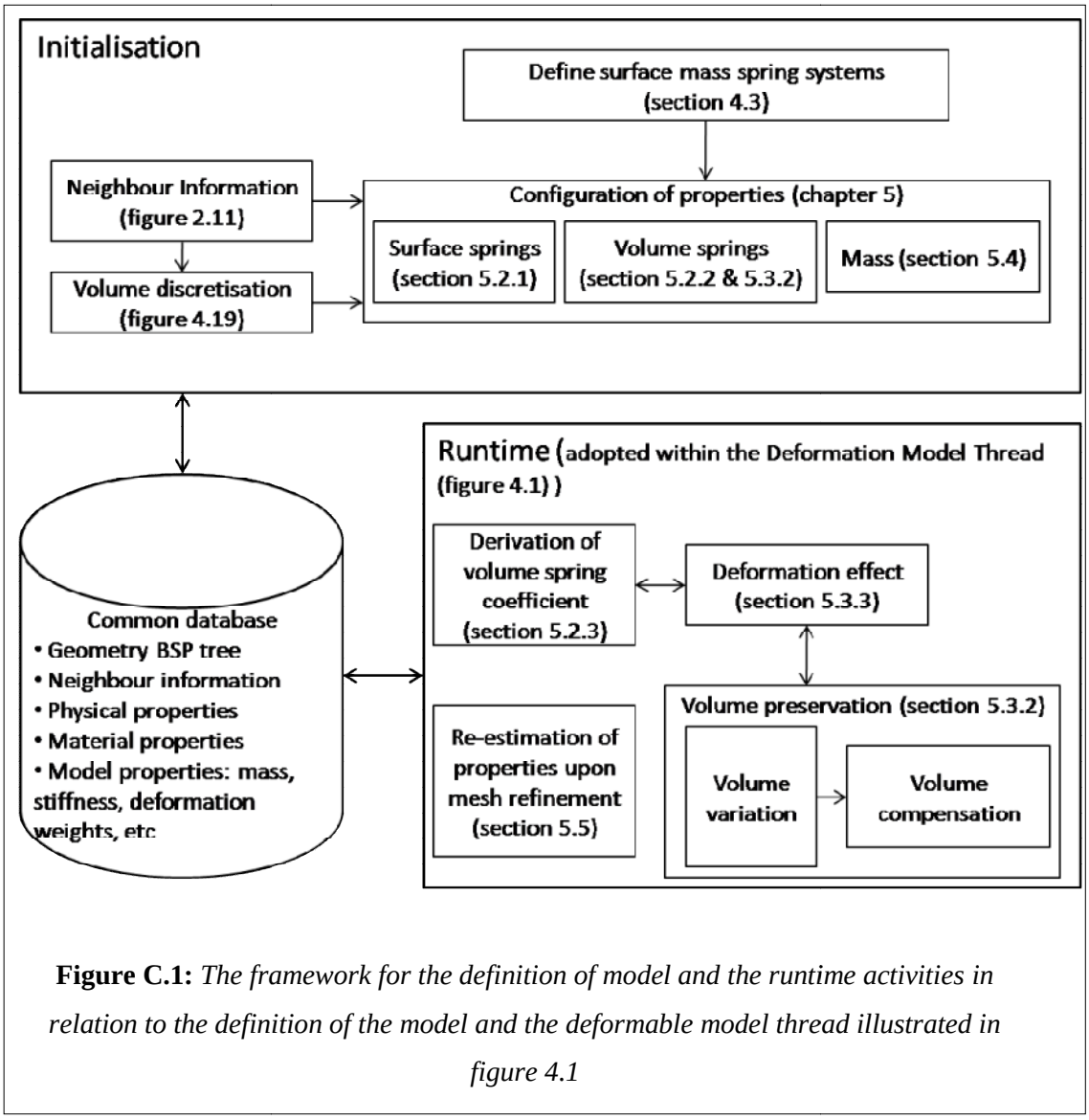

Figure C.1: *The framework for the definition of model and the runtime activities in relation to the definition of the model and the deformable model thread illustrated in figure 4.1*

References

Acosta, E. & Temkin, B. (2005a) Graphics-to-Haptics: A Tool for Developing Haptics Virtual Environments, In Proceedings of *the First Joint Eurohaptics Conference and Symposium on Haptic Interfaces for Virtual Environment and Teleoperator Systems*, IEEE.

Acosta, E. & Temkin, B. (2005b). Dynamic Generation of Surgery Specific – a Feasibility Study, In James F. Westwood et al. (eds.), *Medicine Meets Virtual Reality* 13, IOS Press, pp. 1 – 8.

Adams, B., Ovsjanikov, M., Wand, M., Seidel, H.-P., G Uibas, L. (2008). Meshless modeling of deformable shapes and their motion. *ACM SIGGRAPH Symposium on Computer Animation*.

Al-Khalifah, A., & Roberts, D. (2004). Survey of modelling approaches for medical simulators. In Proceedings of *the 5th Intl Conf. Disability, Virtual Reality and Assoc. Tech.*, Oxford, UK.

Astley, O.R. & Hayward, V. (1998). Design Constraints for Haptic Surgery Simulation. In Proceedings of *ICRA 2000*, pp. 2446-2451.

Aubel, A., & Thalmann, D. (2000). Realistic Deformation of Human Body Shapes, In Proceedings of *Computer Animation and Simulation 2000*, Interlaken, August 2000, pp. 125-135.

Azar, F., Metaxas, D., Schnall, A. M. (2001). Deformable finite element model of the breast for predicting mechanical deformations under external perturbations, *J. Acad. Radiol*., 8, pp. 965–75.

Balaniuk, R. & Salisbury, K. (2003). Soft Tissue Simulation using the Radial Element Method, In Proceedings of *IS4TM-International Symposium on Surgery Simulation and Soft Tissue Modelling*, France, June 12-13.

Balaniuk, R., Costa, I., Melo, J. (2006). Cosmetic breast surgery simulation, *VIII Symposium on Virtual Reality (SVR2006)*, Belem-Pa.

Baraff, D. and Witkin, A. (1998). Large steps in cloth simulation. In Proceedings of *the 25th Annual Conference on Computer Graphics and interactive Techniques* SIGGRAPH '98. ACM, New York, NY, pp. 43-54.

Bartels, R. H., Beatty, J. C., and Barsky, B. A. (1987). *An Introduction to Splines for Use in Computer Graphics and Geometric Modeling*. *Morgan Kaufmann Publishers Inc*.

Basdogan, C. & Srinivasan, M.A. (2002), Haptic Rendering in Virtual Environments, *Handbook of Virtual Environments*. K. Stanney. London, Lawrence Earlbaum, Inc., Chapter 6, pp. 117-134.

Basdogan, C., De, S, Kim, J., Muniyandi, M., Kim, H., Srinivasan, M.A. (2004). Haptics in Minimally Invasive Surgical Simulation and Training, *IEEE Computer Graphics and Applications*, 24(2), pp. 56–64.

Bathe, K.J. (1996). *Finite Element Procedures*. Prentice-Hall, New Jersey.

Batteau, L.M., Liu, A., Maintz, J.B.A., Bhasin, Y. & Bowyer, M.D. (2004). A study on the perception of haptics in surgery simulation. In S. Cotin & D.N. Metaxas (Eds.), *ISMS'04* (pp. 185-192).

Baudet, V., Beuve, M., Jaillet, F., Shariat, B., Zara, F. (2007). Integrating tensile parameters in 3d mass-spring system. In Proceedings of *Surgetica*.

Berkley, J., Weghorst, Gladstone, H., S., Raugi, G., Berg, D., Ganter, M., (2004) Banded matrix approach to Finite Element modelling for soft tissue simulation, *Virtual Reality*, 4(3), pp. 203-212.

Bianchi, G., Solenthaler, B., Szekely, G., Harders, M. (2004) Simultaneous Topology and Stiffness Identification for Mass-Spring Models on FEM Reference Deformations, In Proceedings of *MICCAI 2004*, Saint-Malo, France, Volume LCNS 3217, pp. 293-301.

Bielser, D. (2003). *A Framework for Open Surgery Simulation*, Doctor of Technical Sciences Thesis, Swiss Federal Institute of Technology, ETH, Zurich.

Bordegoni, M., Cugini, U., Mussio, P. (2001). Issues in the Combination of Visual and Haptic Interaction, In Proceedings of *1st International Conference on Universal Access in Human-Computer Interaction*, New Orleans.

Botsch, M., Pauly, M., Wicke, M., Gross, M.H. (2007). Adaptive Space Deformations Based on Rigid Cells, *Comput. Graph. Forum*, 26(3), pp. 339-348.

Bourguignon, D., & Cani, M.P. (2000). Controlling Anisotropy in Mass-Spring Systems, In Proceedings *of Computer Animation and Simulation*, pp. 113-123.

Bro-Nielsen, M. & Cotin, S., (1996). Real-time volumetric deformable models for surgery simulation using finite elements and condensation, In Proceedings of *Eurographics'96, Computer Graphics Forum*, 15, pp. 57-66.

Brown, J., Sorkin, S., Bruyns, C., Latombe J.C. (2001). Real Time Simulation of Deformable Objects: Tools and Application, *Comp. Animation*.

Bruyns, C., Ottensmeyer, M. (2002). Measurements of soft-tissue mechanical properties to support development of a physically based virtual animal model. In *MICCAI 2002*, pp. 282–289.

Burdea, G., Patounakis, G., Popescu, V., Weiss, R. E. (1998). Virtual Reality Training for the Diagnosis of Prostate Cancer, In Proceedings of *the IEEE International Symposium on Virtual Reality Applications (VRAIS '98)*, pp. 190–198.

Cacciola, F. (2007) *Triangulated Surface Mesh Simplification*, Chapter 38, CGAL, Computational Geometry Algorithms Library, CGAL Open Source Project, Release 3.3.1. 25 August 2008. [Online] Available from: http://www.cgal.org [Accessed 14th November 2008].

Cai, Z., Dill, J., Payandeh, S. (1999). Haptic Rendering: Practical Modeling & Collision Detection, In Proceedings of *the ASME, Virtual Environment and Tele-operator System symposium*, Nashville.

Carignan, M., Yang, Y., Thalmann, N.M., Thalmann, D. (1992). Dressing animated synthetic actors with complex deformable clothes. *SIGGRAPH 1992*, pp. 99-104.

Chen, H., Sun, H., Jin, X., (2007), Interactive soft-touch dynamic deformations: Research Articles, In *Comput. Animat. Virtual Worlds* 18, 3 (Jul. 2007), pp. 153-163.

Chen, D. & Zeltzer, D. (1992). Pump it up: a biomechanically based model of muscle using the finite element method, *SIGGRAPH Comput. Graph*., 26(2), pp. 89-98.

Choi, Y., Hong, M., Choi, M., Kim, M. (2005). Adaptive Surface-deformable Model with Shape-preserving Spring, *Journals of Computer Animation and Virtual Worlds*, *Comp. Anim. Virtual Worlds 2005*, 16, pp. 69-83.

Chui, C., Kobayashi, E., Chen, X., Hisada, T., Sakuma, I. (2007). Transversely isotropic properties of porcine liver tissue: experiments and constitutive modelling. *Med Biol.Eng Comput*. 45(1), pp. 99-106.

Cignoni, P., Ganovelli, F., Scopigno, R. (1999). Introducing Multiresolution Representation in Deformable Object Modeling, In Proceedings of *SCCG'99*, Buderice, Slovakia, 28 April – 1 May 1999, pp. 149-158.

Costa, I.F. & Balaniuk, R. (2001). LEM - An Approach for Real Time Physically Based Soft Tissue Simulation. *ICRA 2001*, pp. 2337-2343.

Cotin, S., Delingette, H., Ayache, N. (1998). *Real-time elastic deformations of soft tissues for surgery simulation*, INRIA.Technical Report RR-3511.

Cotin, S., Delingette, H., Ayache, N. (1999). Real-Time Elastic Deformations of Soft Tissues for Surgery Simulation, *IEEE Transactions on Visualization and Computer Graphics*, 5(1), pp. 62-73.

Cotin, S., Delingette, H., Ayache, N. (2000). A hybrid elastic model for real-time cutting, deformations, and force feedback for surgery training and simulation, *The Visual Computer*, 16(8), 437-452.

Cavusoglu, M.C., Goktekin, T.G., Tendick, F., Sastry, S.S. (2004). GiPSi: An Open Source/Open Architecture Software Development Framework for Surgical Simulation. In Proceedings of *Medicine Meets Virtual Reality XII (MMVR 2004*), Newport Beach, CA, January 14-17, 2004, pp.46-48.

Dachille, F., Qin, H., Kaufman, A. (2001). A nover haptics-based interface and sculpting system for physics-based geometric design, *Computer-aided Design*, 33, pp.403-420, Elsevier.

Debunne, G., Desbrun, M., Barr, A., Cani, M.P. (1999). Interactive multiresolution animation of deformable models. In Proceedings of *10th Eurographics Workshop on Computer Animation and Simulation*, Milano, 1999.

Debunne, G., Desbrun, M., Cani, M.P., Barr, A. (2001). Dynamic Real-Time Deformations using Space and Time Adaptive Sampling, *Computer Graphics (ACM SIGGRAPH).*

Delingette, H. (1998). Towards Realistic Soft Tissue Modeling in Medical Simulation, In Proceedings of the *IEEE: Special Issue on Surgery Simulation*, pp. 512-523.

Delingette, H. & Ayache, N. (2004). Soft tissue modeling for surgery simulation. In N. Ayache, (Ed.), *Computational Models for the Human Body: Handbook of Numerical Analysis*, Elsevier.

Deussen, O., Kobbelt., Tucke, P. (1995). Using Simulated Annealing to Obtain Good Nodal Approximations of Deformable Objects, *Computer Animation and Simulation '95*, Springer-Verlag.

DiMaio, S. P. & Salcudean, S. E. (2005). Interactive simulation of needle insertion models, *IEEE Trans. Biomed. Eng*.

Dinsmore, M., Langrana, N., Burdea, G., Ladeji, J. (1997). Virtual Reality Simulation for Palpation of Subsurface Tumors, In Proceedings of *the IEEE Virtual Reality Annual International Symposium*.

Eischen, J.W. & Bigliani, R. (2000). Continuum versus particle representations, *Cloth modeling and animation*, August 2000, A. K. Peters, Ltd.

Etzmuss, O., Gross, J., Strasser, W. (2003). Deriving a Particle System from Continuum Mechanics for the Animation of Deformable Objects, *IEEE Trans. Visualization and Computer Graphics*, vol. 9, 538-550.

Fuhrmann, A., Grob, C., Luckas, V. (2003). Interactive animation of cloth including self collision detection. In Proceedings of *Winter School of Computer Graphics (WSCG 2003)*, pp. 203-208.

García, M., Mendoza, C., Pastor, L., and Rodríguez, A. (2006). Optimized linear FEM for modeling deformable objects: Research Articles. *Comput. Animat. Virtual Worlds* 17, pp. 393-402.

Gibson, S. (1997). 3d chainmail: a fast algorithm for deforming volumetric objects, *Symposium on Interactive 3D Graphics*, Providence, Rhode Island, 1997, pp. 149–154.

Gibson, S. & Mirtich, B. (1997). A survey of deformable modelling in computer graphics, *TR-97-19*, Mitsubishi Electric Research Laboratory, Cambridge, MA, USA.

Gerling, G.J., Weissman, A.M., Thomas, G.W., Dove, E.L. (2003). Effectiveness of a dynamic breast examination training model to improve clinical breast examination (CBE) skills, *Cancer Detection and Prevention*, 27 (6): 451-456.

Girod, B., Keeve, E., Girod, S. (1996). Craniofacial surgery simulation, *In Proceedings of the 4th International Conference on Visualization in Biomedical Computing VBC'96*, Hamburg, Germany, September 1996, pp. 541-546.

Grantcharov, T.P., Kristiansen, V.B., Bendix, J., Bardram, L., Rosenberg, J., Funch-Jensen, P. (2004). Randomized clinical trial of virtual reality simulation for laparoscopic skills training. *British Journal of Surgery, 91*(2), pp. 146-150.

Heng, P., Cheng, C., Wong, T., Wu, W., Xu, Y., Xie, Y., Chui, Y., Chan, K., Leung, K. (2006). Virtual Reality Techniques, *Journal of Clinical Orthopedics and Related Research*, Lippicott Williams & Wilkins, 442, pp. 5-12.

Hespanha, J., McLaughlin, M., Sukhatme, G. (2002). Introduction to Haptics: How Devices can emulate touch, *Touch in Virtual Environment: Haptics and the Design of Interactive Systems*, Prentice Hall PTR, Sep 6 2002.

Holbrey, R.P. (2004) *Virtual Suturing for Training in Vascular Surgery*, PhD thesis, University of Leeds.

Hong Zhu, Q., Chen, Y., Kaufman. A. (2001). Real-time biomechanically-based muscle volume deformation using FEM. Computer Graphics Forum, 17(3), pp. 275-284.

Hong, M., Jung, S., Choi, M.H., Welch, S.J. (2006) Fast Volume Preservation for a Mass-Spring System, *IEEE Computer Graphics and Applications*, September/ October 2006, IEEE Computer Society.

Hoppe, H., DeRose, T., DuChamp, T., McDonald, J., Steutze, W. (1993) Mesh Optimisation, In Proceedings of *SIGGRAPH '93*, ACM Press, pp. 19-26.

Hu, J., Chang, C.Y., Tardella, N., Pratt, J., English, J. (2005). Effectiveness of Haptic Feedback in Open Surgery Simulation and Training Systems. Medicine Meets Virtual Reality 14: *Accelerating Change in Healthcare: Next Medical Toolkit,* Studies in Health Technology and Informatics, 119, pp. 213-218.

Hutchinson, D., Preston, M., Hewitt, W. (1996). Adaptive Refinement for Mass-Spring Simulations. In Proceedings of *7th Eurographics Workshop Animation and Simulation,* Springer-Verlag, pp. 31–45.

Immersion (2008). *Medical and Surgical Simulators - Realistic, Safe, Cost-effective*, [Online] Available from: http://www.immersion.com/medical/ [Accessed 26 November 2008].

Irving, G., Schroeder, C., Fedkiw, R. (2007). Volume conserving finite element simulations of deformable models. *ACM Trans. Graph*., 26(3).

James, D.L. & Pai, D.K. (1999) Artdefo: accurate real time deformable objects. *In Proceedings of the 26th annual conference on Computer Graphics and Interactive Techniques* (SIGGRAPH), pp. 65-72.

Jansson, J. & Vergeest, M. (2002) A Discrete Mechanics Model For Deformable Bodies, *Computer-Aided Design*, Amsterdam.

Joukhadar, F. Garat, and C. Laugier, (1997). Parameter identification for dynamic simulation, In Proceedings of *IEEE Int. Conf. Robotics and Automation* , Albuquerque, NM, 3, pp. 1928-1933.

Karlsuhe. (1997). *The 'Karlsruhe Endoscopic Surgery Trainer'*. [Online] Available from: http://www-kismet.iai.fzk.de/TRAINER/mic_trainer1.html [Accessed 26 February 2009].

Keeve, E., Girod S., Pfeife, P., Girod, B. (1996). Anatomy-based facial tissue modeling using the finite element method. In Proceedings of *IEEE Visualization '96*, pp. 21-28.

Koch, R.M., Roth, S.H.M., Gross, M.H. Zinnermann, A.P., Sailer, H.F.R. (2002). A Framework for Facial Surgery Simulation. In Proceedings of *ACM SCCG 2002*, Spring Conference on Computer Graphics 2002, Budmerice, Czech Republic, Apr 24-27, 2002.

Krouskop, T. A., Wheeler, T. M., Kallel, F., Garra, B. S., Hall, T. (1998). Elastic moduli of breast and prostate tissues undercompression, *Ultrason. Imaging*, 20, pp. 260–74.

Kruse, S. A., Smith, J. A., Lawrence, A. J., Dresner, M. A., Manduca, A., Greenleaf, J. F., Ehman, R. L. (2000). Tissue characterization using magnetic resonance elastography: preliminary results, *Phys. Med. Biol*. 45, pp. 1579–1590.

Kuehnapfel, U., Cakmak, H.K., Maa, H. (1999). 3D modeling for endoscopic surgery. In Proceedings of *IEEE Symposium on Simulation*, IEEE, Delft University, Delft, NL, Oct 1999, pp. 22-32.

Kühnapfel U., Çakmak H.K., Maass H., Waldhausen, S. (2001). Models for simulating instrumenttissue interactions. In Proceedings of *9th Medicine Meets Virtual Reality 2001 (MMVR 2001)*, Newport Beach, CA, USA, Jan. 23–27, 2001.

Kuroda, Y., Nakao, M., Kuroda, T., Oyama, H., Yoshihara, H. (2005). MVL: Medical VR Simulation Library, In Proceedings of *13th Medicine Meets Virtual Reality Conference*, pp.273-276, January 24-27, 2005.

Lafleur, B., Magnenat-Thalmann, N., and Thalmann, D. (1991). Cloth animation with self-collision detection. In Proceedings of the *Conf. on Modeling in Comp. Graphics*, Springer, pp. 179--188.

Langrana, N. A., Burdea, G., Lange, K., Gomez, D., Deshpande, S. (1994). Dynamic Force Feedback in a Virtual Knee Palpation, In Proceedings of *Artificial Intelligence in Medicine*, pp. 321–333.

Lasky, H., Pasch, J., Kenneth, A. (2000). *Method and Apparatus Tissue Imaging*, Wo/2000/071023, World Intellectual Property Organization.

Laugier, C., d'Aulignac, D., Boux de Casson, F. (2000). Modeling human tissues for medical simulators. In Proceedings of *the IEEE-RSJ International Conference on Intelligent Robots and Systems*.

Laugier, C., Mendoza, C., Sundaraj, K. (2003) Towards a Realistic Medical Simulator using Virtual Environments and Haptic Interaction, *Robotics Research: The Tenth International Symposium*, Springer Tracts in Advanced Robotics, 6.

Lee,Y.C., Terzopoulos, D., Walters, K. (1995). Realistic modeling for facial animation. In Proceedings of *SIGGRAPH '95: the 22nd annual conference on Computer graphics and interactive techniques*, pp. 55-62, New York, NY, USA. ACM Press.

Leskovsky, P., Harders, M., Szekely, G., Talbi, N., Joli, P., Kheddar, A., Esen, H., Buss, M., Rossi, D., Bicchi, A. (2005). *Report on Soft Tissue Demonstrators, TOUCH-HapSys Towards a Touching Presense: High-definition Haptic Systems*, Information Society Technologies.

Levental, I., Georges, P.C., Janmey, P.A. (2007). Soft biological materials and their impact on cell function, *Journal of Soft Matter*, 3, pp.299.

Lloyd, B.A., Szekely, G., Harders, M. (2007). Identification of Spring parameters for Deformable Object Simulation, *IEEE Transactions on Visualisation and Computer Graphics*, 13(5), Sept/Oct 2008.

Maciel, A., Boulic, R., Thalmann, D. (2003) Towards a Parameterization Method for Virtual Soft Tissues Based on Properties of Biological Tissue, *In Proceedings of 5th IFAC 2003 Symposium on Modelling and Control in Biomedical Systems (including Biological Systems)*, Melbourne, Australia. pp. 235-240. Elsevier Ltd., Oxford.

Maciel, A. (2005). *A biomechanics-based articulation model for medical applications*, PhD Thesis, Virtual Reality Lab (VRLab), Swiss Federal Institute of Technology (EPFL).

Marchal, M., Promayon, E., Troccaz, J. (2005). Simulating Complex Organ Interactions: Evaluation of a Soft Tissue Discrete Model, In Proceedings of *SVC 2005*, LNCS 3804, pp. 175-182, © Springer-Verlag Berlin Heidelberg 2005.

Matyka, M. & Ollila, M. (2003). A pressure model for soft body simulation, In Proceedings of *Sigrad*, Umea, November 2003.

McCreery, G. L. Trejos, A. L. Naish, M. D. Patel, R. V. Malthaner, R. A. (2008). Feasibility of locating tumours in lung via kinaesthetic feedback, *International Journal Of Medical Robotics And Computer Assisted Surgery*, 4(1), pp. 58-68, John Wiley and Sons Ltd.

McDonald, S., Saslow, D., Alciati, MH. (2004) Performance and reporting of clinical breast examination: a review of the literature. *CA Cancer J Clin* 2004; 54 (6), pp. 345-61.

Mendoza, C., Sundaraj, K., Laugier, C. (2002) Issues in Deformable Virtual Objects Simulation with Force Feedback, *International Advanced Robotics Program (IARP): International Workshop on Human Robot Interfaces*, Rome - Italy, 2002.

Mendoza, C., & Laugier, C. (2003). Tissue Cutting Using Finite Elements and Force Feedback, *International Symposium in Surgery Simulation and Soft Tissue Modeling (IS4TM)*, Juan-les-Pins, France, June 2003.

Mentice (2008). [Online] Available from: http://www.mentice.com [Accessed 25 February 2009].

Mezger, J., Thomaszewski, B., Pabst, S., and Straßer, W. (2008). Interactive physically-based shape editing. In Proceedings of the *2008 ACM Symposium on Solid and Physical Modeling* (Stony Brook, New York, June 02 - 04, 2008). SPM '08. ACM, New York, NY, pp. 79-89.

Meseure, P. & Chaillou, C. (2000). A deformable body model for surgical simulation, *The Journal of Visualization and Computer Animation*, 11, pp. 197-208, John Wiley & Sons, Ltd.

Mollemans, W., Schutyser, F., Cleynenbreugel, J., Suetens. P. (2003). Tetrahedral mass spring model for fast soft tissue deformation. In *International Symposium on Surgery Simulation and Soft Tissue Modeling*, pp. 145-154.

Morris, D. (2006). *Haptics and Physical Simulation for Virtual Bone Surgery*. PhD thesis, Department of Computer Science, Stanford University.

Nave, C. (2006). HyperPhysics (© C.R. Nave, 2006), Merlot Classic Award winner for 2005. [Online] Available from: http://hyperphysics.phy-astr.gsu.edu/Hbase/cm.html#cmp [Accessed 14 November 2008].

The National Library of Medicine (NLM) (2001). *The Visible Human Project*, [Online] Available from: http://www.nlm.nih.gov/research/visible/vhpconf2000/AUTHORS/SULLIVAN/FIGURE1.HTM [Accessed 25 February 2009].

The National Library of Medicine (NLM) (2003). *The Visible Human Project*, [Online] Available from: http://www.nlm.nih.gov/research/visible/visible_human.html. [Accessed 25 February 2009].

Nealan, A., Muller, M., Keiser, R., Boxerman, E; Carlson, M. (2006). Physically based deformable models in computer graphics. *Computer Graphics Forum*, 25(4). (December 2006), pp. 809-836.

Nedel, L.P., & Thalmann, D. (1998). Real Time Muscle Deformation using Mass-Spring Systems, *Computer Graphics International*, IEEE Press, Hannover, pp.156-165.

Origlio, V. (2008). *Stochastic*, From MathWorld--A Wolfram Web Resource, created by Eric W. Weisstein. [Online] Available from: http://mathworld.wolfram.com/Stochastic.html [Accessed 26 November 2008].

Paloc, C., Bello, F., Kitney, R., Darzi, A. (2002). Multiresolution Volumetric Mass Spring System for Real Time Soft Tissue Deformation. *In Proceedings of* MICCAI. pp. 219 – 226.

Paloc, C., Faraci, A., Bello, F. (2006). Local Mesh Adaptation for Soft Tissue Simulation. *ISBMS*, pp. 206-214.

Parke, F.I. & Waters, K. (1996). *Computer Facial Animation*, A. K. Peters Wellesley.

Patkin, M. (1998). *Breast lumps-examination, self-examination, description, and a method of recording*, Presentation at the Breast Surgery Group Flinders Medical Centre, 22 June 1998. [Online] Available from: http://www.mpatkin.org/surgery_clinical/brestlumps.htm [Accessed 25 February 2009].

Payandeh, S., Dill, J., Zhang, J. (2005). A study of level-of-detail in haptic rendering. *ACM Trans. Appl. Percept.* 2(1), pp. 15-34.

Pezzementi, Z., Ursu, D., Misra, S., Okamura, A.M. (2008). Modeling Realistic Tool-Tissue Interactions with Haptic Feedback: A Learning-based Method, In Proceedings of *Symposium on Haptic Interfaces for Virtual Environments and Teleoperator Systems 2008*, 13-14 March, Reno, Nevada, USA, pp. 209-215.

Picinbono, G., Delingette, H., Ayache, N. (2001). Non-linear and anisotropic Elastic Soft Tissue Models for Medical Simulation, In Proceedings of *the International Conference on Robotics and Automation*, Seoul, South Korea, May 2001, pp. 1371-1376.

Promayon, E., Baconnier, P., Puech, C. (1996) Physically-based Deformations Constrained in Displacements and Volume, In Proceedings of *Eurographics '96*, Blackwell Publishers, Sept. 1996, pp. 155-164.

Provot, X. (1995). Deformation constraints in a mass-spring model to describe rigid cloth behavior. In *Graphics Interface*, pp. 147-154.

Radetzky, A. & Nurnberger, A. (2002). Visualization and simulation techniques for surgical simulators using actual patient's data, *Artificial Intelligence in Medicine*, 26, pp. 255-279.

Rajagopal, V., Nash, M.P., Highnam, R.P., Nielsen, P.M.F. (2008). The breast biomechanics reference state for multi-modal image analysis, *Lecture Notes in Computer Science* 5116, pp. 385-392.

Roan, E. & Vemaganti, K. (2007) The Nonlinear Material Properties of Liver Tissue Determined From No-Slip Uniaxial Compression Experiments, *J. Biomech. Eng.*, June 2007, 129 (3), pp. 450-456.

Roose, L., Maerteleire, W., Mollemans, W. (2005). Validation of Different Soft Tissue Simulation Methods for Breast Augmentation, *Computer Assisted Radiology and Surgery 2005*, 1281, pp. 485-490.

Ruiter N.V., Stotzka, R., Müller T.O., Gemmeke, H., Reichenbach, J.R., Werner, A. (2006). Model-Based Registration of X-Ray Mammograms and MR Images of the Female Breast Kaiser, *IEEE transactions on nuclear science*, 53(1), pp: 204-211, February 2006.

Russell, O.G., & Ziewacz, J.T. (1995). Pressures in a simulated breast subjected to compression forces comparable to those of mammography, *R**a**diology*, 194, pp. 383-387, R**a**diologic**a**l Society of North **A**meric**a.**

Salisbury, K., Brock, D., Massie, T., Swarup, N., and Zilles, C. (1995). Haptic rendering: programming touch interaction with virtual objects. In Proceedings of *the 1995 Symposium on interactive 3D Graphics.*

Samani, J. Z., Zubovits, J., Plewes, D. (2007). Elastic Moduli of Normal and *Pathological* Human Breast Tissues: An Inversion-technique-based Investigation of 169 Samples, *Phys. Med. Biol*. 52, pp. 1565-1576.

Sarvazyan, A., Goukassian, D., Maevsky, E., Oranskaja, G. (1994). Elasticity imaging as a new modality of medical imaging for cancer detection. *In Proc. Int. Workshop on Interaction of Ultrasound with Biological Media*, pp 69–81.

Saslow, D., Hannan, J., Osuch, J., et al. (2004). Clinical breast examination: practical recommendations for optimizing performance and reporting. CA Cancer J Clin 2004, 54, pp. 327–344.

Senderberg, T.W, & Parry, S.R. (1986). Free-form deformation of solid geometric models, *Computer Graphics*, 26(2), pp. 151-160.

Shinar, T., Schroeder, C. and Fedkiw, R. (2008). Two-way Coupling of Rigid and Deformable Bodies, In James, D. & Markus, G (Eds.), *ACM SIGGRAPH Eurographics Symposium on Computer Animation (SCA)*, pp. 95-103.

Sifakis, E., Shinar, T., Irving, G., Fedkiw, R. (2007). Hybrid simulation of deformable solids. In *Proceedings of the 2007 ACM Siggraph/Eurographics Symposium on Computer Animation* (San Diego, California, August 02 - 04, 2007). Symposium on Computer Animation. Eurographics Association, Aire-la-Ville, Switzerland, pp. 81-90.

Simple3D. (2006). *3D Scanners, Digitizers, and Software for making 3D Models and 3D Measurements*. [Online] Available from : http://www.simple3d.com/ [Accessed 28 February 2009].

Sinkus, A., Tanter, M,. Xydeas, T., Catheline, S., Bercoff, J., Fink, M. (2005). Viscoelastic shear properties of in vivo breast lesions measured by MR elastography, *Magn. Reson. Imaging*, 23, pp. 159–65.

Sharp, B. (2000). Subdivision Surface Theory, *Game Developer*, January 2000.

Shinya, M. (2005). Theories for Mass-Spring Simulation in Computer Graphics: Stability, Costs and Improvements, *IEICE Transaction of Information and Systems*,

Volume E88, The Institute of Electronics, Information and Communication Engineers, April 2005.

Sundaraj, K. (2004). *Real-Time Dynamic Simulation and 3D Interaction of Biological Tissue : Application to Medical Simulators*, PhD Thesis, Institut National Polytechnique De Grenoble, France.

Sur, H., Faraci, A., Bello. F. (2004). Validation of soft tissue properties in surgical simulation with haptic feedback. In Westwood, J.D., Haluck R.S., Hofman, H.M., Mogel, G.T., Phillips, R., & Robb, R.A., (Eds), In Proceedings of *Medicine Meets Virtual Reality 12, Building a Better You: The Next Tools for Medical Education, Diagnosis and Care*, Studies in Health Technology and Informatics, 98, IOS Press, 2004, pp. 382-384.

Surgical Science. (2008). *LapSim Gothenburg, Sweden*, [Online] Available from: http://www.surgical-science.com/index.cfm/en/products/lapsim_gyn_/ [Accessed 25 February 2009].

Szekely, G., Brechbuhler, C., Hutter, R., Rhomberg, A., Ironmonger, N., Schmid, P. (2000). Modelling of soft tissue deformation for laparoscopic surgery simulation. *Medical Image Analysis*.

Tanguy, L.F., Tomayo, O.A., Lucas, A., Haigron, P. (2007). Angioplasty simulation using ChainMail method, *In Proceedings of SPIE Medical Imaging 2007: Visualization and Image-Guided Procedures*, 6509.

Tanner, C., Degenhard, A., Schnabel, J. A., Hayes, C., Sonoda, L. I., Leach, M. O., Hose, D. R., Hill, D. L. G., Hawkes, D. J. (2001). A method for the comparison of biomechanical breast models. In Proceedings of *IEEE Workshop on Mathematical Methods in Biomedical Image Analysis* (MMBIA 2001), IEEE, pp. 11-18, Kauai, Hawaii, USA, 9-10 December 2001.

Temkin, B., Stephens, B., Acosta, E., Wei, B., Hatfield, P. (2000). Virtual Body Structures, *In Proceedings of The Third Visible Human Project Conference*, October 5 and 6, 2000, National Institutes of Health, Bethesda, Maryland USA.

Terzopoulos, D. (2003). Deformable Models: Classic, Topology-Adaptive and Generalized Formulations, In S. Osher, N. Paragios (eds.), *Geometric Level Set Methods in Imaging, Vision, and Graphics*, Springer-Verlag, New York, 2003, Ch. 2, pp. 21–40.

Terzopoulos, D., Platt, J., Barr, A., Fleischer, K. (1987). Elastically deformable models. In *Proceedings of the 14th Annual Conference on Computer Graphics and interactive Techniques* M. C. Stone, Ed. SIGGRAPH '88. ACM, New York, NY, pp. 205-214.

Teschner, M., Girod, S., Girod, B. (2000). Direct Computation of Nonlinear Soft-Tissue Deformation. *VMV 2000*, pp. 383-390.

Teschner, M., Heidelberger, B., Müller, M., Gross, M.H. (2004). A Versatile and Robust Model for Geometrically Complex Deformable Solids. *Computer Graphics International*, pp. 312-319.

Tobler, R.F. & Maierhofer, S. (2006). A mesh data structure for rendering and subdivision. *In Proceedings of 14th International Conference in Central Europe on Computer Graphics,* Visualization and Computer Vision (WSCG 2006), January 2006.

Van Gelder, A. (1998). Approximate Simulation of Elastic Membranes by Triangulated Spring Meshes, *Journal of Graphics Tools 1998*, 3(2), pp. 21-42.

Van Gelder, A. & Wilhelms, J. (1997). Simulation of elastic membranes and soft tissue with triangulated spring meshes. *Technical Report*. UMI Order Number: UCSC-CRL-97-12., University of California at Santa Cruz.

Van Houten, E. W., Doyley, M. M., Kennedy, F. E., Weaver, J. B., Paulsen, K. D. (2003). Initial in vivo experience with steady-state subzone-based MR elastography of the human breast, *J. Magn. Reson. Imaging*, (17), pp. 72–85.

Vassilev, T., Spanlang, B., Chrysanthou, Y. (2001). Fast Cloth Animation on Walking Avatars. *Comput. Graph. Forum*, 20(3).

Vassilev, T., & Spanlang, B. (2002). A Mass-Spring Model for Real Time Deformable Solids, *In Proceedings of East-West Vision 2002*, Graz, Austria, September 12-13, 2002, pp. 149-154.

Villard, J., Borouchaki, H. (2002). Adaptive Meshing for Cloth Animation, *In Proceedings of 11th International Meshing Roundmation*, Ithaca, NY, 15-18 September 2002.

Volino, P., Courchesne, M., Thalmann, N.M. (1995). Versatile and efficient techniques for simulating cloth and other deformable objects, In Proceedings of *the 22nd annual conference on Computer graphics and interactive techniques*, p.137-144.

Volino, P., Cordier, F., Thalmann, N.M. (2005). From early virtual garment simulation to interactive fashion design. *Computer-Aided Design*, 37(6), pp. 593-608.

Wade, N.J & Swanston, M.T. (2001). *Visual Perception: An Introduction*, 2nd Edition.

Wall, S.A. & Harwin, W.S., (2000). Interaction of Visual and Haptic Information in Simulated Environments: Texture Perception, In Proceedings of *1st Workshop on Haptic Human Computer Interaction*, 31st August - 1st September, Glasgow, Scotland, pp. 39-44.

Williams, C., KakadarisK, I.A., Ravi-Chandar, K., Miller, M.J., Patrick. C. W. (2003). Simulation studies for predicting surgical outcomes in breast reconstructive surgery. *Lecture Notes in Computer Science*, 2878, pp. 9–16.

Wuillemin, D., van Doorn, G., Richardson, B., Symmons, M. (2005). Haptic and Visual Size Judgements in Virtual and Real Environments. In *Proceedings of the First Joint Eurohaptics Conference and Symposium on Haptic interfaces For Virtual Environment and Teleoperator Systems* (March 18 - 20, 2005). WHC. IEEE Computer Society, Washington, DC, pp. 86-89.

Zhang, J., Payandeh, S., Dill, J. (2002). Haptic Subdivision: an Approach to Defining Level-of-Detail in Haptic Rendering, In Proceedings of *the 10th Symposium on*

Haptic Interfaces for Virtual Environment and Teleoperator Systems, Orlando, FL, March, 2002, pp. 201-208.

Zhang, Y., Qiu, Y., Goldgof, D. B., Sarkar, S., and Li, L. (2007). 3D Finite Element Modeling of Nonrigid Breast Deformation for Feature Registration in -ray and MR Images. In Proceedings of *the Eighth IEEE Workshop on Applications of Computer Vision* (February 21 - 22, 2007). WACV. IEEE Computer Society, Washington, DC, 38.

Zhuang, Y. & Canny, J. (1995). Real-time Simulation of Physically Realistic Global Deformation. *In Proceedings of the IEEE Vis'99 Late Breaking Hot Topics*. San Francisco, California. October 24-29, 1999.

Bibliography

Arnab, S. & Raja, V. (2007). Irregular Surface Mesh Topology for Volumetric Deformable Model, *International Conference and Workshop*, 4-5 October 2007, Athens, Greece.

Arnab, S. & Raja, V. (2008). A Deformable Surface Model for Soft Volume Simulation, *22nd EUROPEAN Modelling & Simulation*, Nicosia, Cyprus, 3 - 6 June 2008, IEEE Germany Section.

Arnab, S. & Raja, V. (2008). A Deformable Surface Model with Volume Preserving Springs. In *Proceedings of the 5th international Conference on Articulated Motion and Deformable Objects* (Port d'andratx, Mallorca, Spain, July 09 - 11, 2008). F. J. Perales & R. B. Fisher, Eds. Lecture Notes in Computer Science, vol. 5098. Springer-Verlag, Berlin, Heidelberg, pp. 259-268.

Arnab, S. & Raja, V. (2008). Chapter 4: Simulating a Deformable Object Using a Surface Mass Spring System. In *Proceedings of the 2008 3rd international Conference on Geometric Modeling and Imaging - Volume 00* (July 09 - 11, 2008). GMAI. IEEE Computer Society, Washington.

Arnab, S., Solanki, M., Raja, V. (2008). A Deformable Surface Model for Breast Simulation, 20th International Conference of the Society for Medical Innovation and Technology, Vienna, Austria 28 - 30 August, 2008.

Basdogan, C., Ho, C.H., Srinivasan, M.A. (1997). A Ray-Based Haptic Rendering Technique for Displaying Shape and Texture, Proceedings of the dynamic System and Control Division, DSC-Vol.61, ASME, pp.77-84.

Berkley, J., Turkiyyah, G., Berg, D., Ganter, M., Weghorst, S. (2004). Real-time Finite Element Modeling for Surgery Simulation: An application to virtual suturing. In *IEEE Transactions on Visualization & Computer Graphics*, 10, May/June 2004, pp. 1- 12.

Chen, H., Wu, W., Sun, H., Heng, P. (2007). Dynamic touch-enabled virtual palpation, *Comput. Animat. Virtual Worlds* 18, 4-5 (Sep. 2007), pp. 339-348.

Cosman, P.H., Cregan, P.C., Martin, C.J., Cartmill, J.A. (2002). Virtual Reality Simulators: Current Status In Acquisition and Assessment of Surgical skills, *ANZ J. Surg.2002*, pp 30 -34.

Delingette, H. (1998). Towards realistic soft tissue modeling in medical simulations, INRIA Technical Report RR-3506.

Delingete, H, Ayache, N. (2005). Hepatic Surgery Simulation, Communications of the ACM February 2005, Vol. 48, No 2, pp 31-36.

Enderle, J., Blanchard, S., Bronzino, J. (2005). *Introduction to Biomedical Engineering*, Second Edition, Elsevier Academic Press.

Fung, Y.C. (1993). *Biomechanics: Mechanical Properties of Living Tissues* (New York: Springer).

Gain, J. & Bechmann, D. (2008). A survey of spatial deformation from a user-centered perspective. *ACM Trans. Graph*. 27(4), pp. 1-21.

Greenleaf, W.J. & Piantanida, T. (2000). Medical applications of virtual reality technologies, In Bronzino, J.D. (eds.), *The Biomedical Engineering Handbook*, 2nd edition, Volume (1), CRC Press , IEEE Press, pp. 69.

Hunter, P., Robbins, P., Noble, D. (2002). The IUPS Human Physiome Project, Invited Review, *Pflugers-Eur J Physiol* (2002), Springer-Verlag 2002.

Irving, G., Teran, J., Fedkiw, R. (2004). Invertible Finite Elements for robust simulation of large deformation, In Boulic, R. & Pai, D.K. (Eds), *Eurographic/ACM Siggraph Symposium on Computer Animation.*

Irving, G., Schroeder, C., Fedkiw, R. (2007). Volume conserving finite element simulations of deformable models. *ACM Trans. Graph*., 26(3), pp. 13.

Kuroda, Y., Nako, M., Kuroda, T., Oyama, H., Yoshihara, H. (2005). MVL: Medical VR Simulation Library, In James F. Westwood et al. (eds.), *Medicine Meets Virtual Reality 13*, IOS Press, 2005, pp. 273-276.

Kondo, R. and Anjyo, K. (2008). Directable animation of elastic bodies with point-constraints. *Comput. Animat. Virtual Worlds*, 19(3-4), (Sep. 2008), pp.165-173.

Liu, A., Tendick, F., Cleary, K., Kaufmann, C. (2003). A survey of surgical simulation: applications, technology, and education, *Presence*, 12(6), Dec 2003, MIT Press.

Liu, A. (2005). Solid Mechanics of Homogeneous Materials, Chapter 1, Mechanics and Mechanisms of Fracture: An Introduction. ASM Internationals. pp. 1-39.

Marchal, M., Allard, J., Duriez, C., Cotin, S. (2008). Towards a Framework for Assessing Deformable Models in Medical Simulation. In F. Bello and P. J. Edwards, (Eds), *The 4th International Symposium on Biomedical Simulation* (London, UK, July 07 - 08, 2008). Lecture Notes In Computer Science, 5104. Springer-Verlag, Berlin, Heidelberg, pp. 176-184.

Montgomery, K., Bruyns, C., Brown, J., Sorkin, S., Mazzella, F., Thonier, G., Tellier, A., Lerman, B., Menon, A. (2002). Spring: A general framework for collaborative, real-time surgical simulation. In J. D. Westwood et al. (Eds.), *Medicine meets virtual reality* (pp. 296-303). Amsterdam: IOS Press.

Nealen, A., Sorkine, O., Alexa, M., Cohen-Or, D. (2005). A sketch-based interface for detail-preserving mesh editing. ACM Trans. Graph. 24(3), pp. 1142–1148.

Pascale, M.D., Pascale, G. D., Prattichizzo, D. (2004). Haptic and Graphic Rendering of Deformable Objects. In Proceedings of *IEEE Int. Workshop on Multimedia Signal Processing*, pp. 267-270.

Petrie, M. & Thomas, G. (2007). Mechanical properties of the haptic signals indicative of a breast cancer tumor, *In the proceedings of Systems, Man and Cybernetics, 2007, ISIC,* IEEE International Conference, 7-10 Oct. 2007 pp. 2233-2238.

Radetzky, A., Nurnberger, A., Pretchner, D.P. (2000). Elastodynamic shape modeler: A Tool for Defining the Deformation Behaviour of Virtual Tissues, Radiographics, 20, pp. 865-881.

Rubbelke, D. (1999). *Tissues of the Human Body: An Introduction*, The McGraw-Hill Companies, [Online] Available from: http://www.mhhe.com/biosci/ap/histology_mh/tismodov.html#overview [Accessed 25 February 2009].

Salisbury, K., Conti, F., Barbagli, F. (2004). Haptic Rendering: Introductory Concepts. *IEEE Comput. Graph. Appl.* 24(2), pp. 24-32.

Sifakis, E. & Fedkiw, R. (2005). Facial Muscle Activations from Motion Capture, *Video Proceedings of the 2005 Computer Vision and Pattern Recognition Conference (CVPR)*, 2005.

Sinkus, A., Tanter, M., Xydeas, T., Catheline, S., Bercoff, J., Fink, M. (2005). Viscoelastic shear properties of in vivo breast lesions measured by MR elastography, *Magn. Reson. Imaging*, 23, pp. 159–65.

Suvranu, D., Jung, K., Yi-Je, L., Mandayan, S. (2005). The Point Collocation-Based Method of Finite Spheres (PCMFS) for Real Time Surgery Simulation, *Computer and Structures*, Science Direct, Elsevier.

Von Georgi, R., Thele, F., Münstedt, K. (2005). Breast self examination: Instruction videos and palpation aids improve the tumor recognition? *Journal of Clinical Oncology, 2005 ASCO Annual Meeting Proceedings*. 23(16S).

Yang, W., Feng, J., Jin, X. (2008). Shape deformation with tunable stiffness, *The Visual Computer*, 24(7-9), Springer Berlin / Heidelberg.

Zerbato, D. Galvan, S. Fiorini, P. (2007). Calibration of mass spring models for organ simulations, Intelligent Robots and Systems, 2008. IROS 2008. IEEE/RSJ International Conference, pp. 370-375